Investigating the role and regulation of the AMPK-related kinase NUAK1

Duncan Richard Bull

A thesis submitted to Imperial College London

for the degree of Doctor of Philosophy
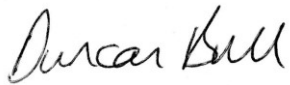
October 2013

Cellular Stress Group

Medical Research Council, Clinical Sciences Centre

Imperial College London

Declaration of Originality

I hereby certify that I am the sole author of this thesis and that no original part of this thesis has been published previously. I declare that any material or information from the work of others that is included in my thesis, published or otherwise, is fully acknowledged in the text and in the list of references. I confirm that this thesis has not been submitted for a higher degree to any other university or institution.

Signed: *Duncan Bull*   Date: 2nd October 2013

Copyright Declaration

Abstract

AMP-activated protein kinase (AMPK) is a well characterised central regulator of energy homeostasis with many downstream substrates and potential therapeutic targets. Recently several kinases related to AMPK have been identified which are activated by the same upstream kinase, LKB1, and share significant sequence homology with the catalytic α subunit of AMPK. Previous studies have implicated NUAK1, one of these related kinases, in cell cycle regulation and other studies have identified various partner proteins but as yet there is no consensus model of its regulation or physiological role. This aim of this study was to investigate the regulation and interactions of NUAK1 using an *in vitro* system and also use an *in vivo* tissue specific mouse knockout system to investigate its function in two different tissues.

The results of these studies reveal new insights into the regulation of NUAK1 *in vitro* and suggest that the kinase is capable of activation by autophosphorylation, in the absence of LKB1. NUAK1 is shown to interact with 14-3-3 proteins and evidence that this interaction may be important for the function of the kinase is presented. Cell based studies in mouse embryonic fibroblasts (MEFs) lacking NUAK1 show that it is involved in proliferation and there are suggestions of pathways involved in regulating this effect.

NUAK1 liver-specific knockout mice were generated and extensive metabolic phenotyping analyses were carried out. In young animals deletion of NUAK1 in liver did not lead to any obvious changes in whole body metabolism. However, preliminary studies revealed a possible role for NUAK1 in metabolic regulation in older mice and in response to liver damage. Mice with heart-specific deletion of NUAK1 were generated and these mice were found to have a cardiac hypertrophy phenotype in response to angiotensin II treatment. Potential signalling pathways downstream of NUAK1 in the heart were then investigated in this model.

Acknowledgments

I would like to thank my supervisors Dave Carling and Naveenan Navaratnam for all their help and guidance throughout my project, especially Nav for watching over me in the lab and giving me some invaluable support! Thanks to David Carmena for his assistance and his early work on this project. Thank you also to everyone else in the Cell Stress group, past and present, for all their help and for making my time in the lab so fun.

Many thanks to Phill Muckett for his incredible help with the animal work and to Zoe Webster and the Transgenic Facility for re-deriving the mouse lines. Thanks to Anna Slaviero and Olga Boruc for their assistance with the CLAMS and echocardiography. Thanks to Mahrokh Nohadani for her work with the histology. Thanks to Luke Boulter and the group in Edinburgh for their work on the panCK staining.

I acknowledge the financial support of the Medical Research Council which allowed me to carry out my PhD.

Finally, thanks to my parents for supporting me for twenty-seven years and to everyone who has kept me sane throughout the past four years, especially those who helped drag me across the finishing line!

Abbreviations

ACC	Acetyl-Coenzyme-A carboxylase
ACE	Angiotensin converting enzyme
ACTH	Adrenocorticotropic hormone
ADP	5'adenosine diphosphate
AICAR	5-aminoimidazole-4-carboximide ribonucleoside
AID	Autoinhibitory domain
ALT	Alanine aminotransferase
AMARA	Synthetic peptide, AMARAASAAALARRR
AMP	5'adenosine monophosphate
AMPK	5'adenosine monophosphate-activated protein kinase
aPKC	Atypical protein kinase C
AST	Aspartate aminotransferase
ATP	5'adenosine triphosphate
AUC	Area under curve
BK	Bradykinin
BRSK	Brain-specific kinase
BSA	Bovine serum albumin
BSEP	Bile salt export pump
C. elegans	*Caenorhabditis elegans*
CaM	Calmodulin
CaMKK	Ca^{2+}/calmodulin-dependent protein kinase kinase
CAPS	3-[cyclohexylamino]-1-propanesulfonic acid
CBM	Carbohydrate binding module
CBS	Cystathionine β-synthase
CDE	Choline-deficient ethionine supplemented diet
CK	Cytokeratin
CK2	Casein kinase 2
CLAMS	Comprehensive Laboratory Animal Monitoring System
Cox6b	Cytochrome c oxidase subunit VIb
CREB	cAMP-response element binding protein
CRTC2	CREB-regulated transcription co-activator 2
CV	Calorific value
DAK	Death-associated kinase
DDC	Diethyl 1,4-dihydro-2,4,6,-trimethyl-3,5-pyridinedicarboxylate
DMEM	Dulbecco's Modified Eagle's Medium
DMSO	Dimethyl Sulphoxide
DTT	Dithiothreitol
E. coli	*Escherichia coli*
ECAR	Extracellular acidification rate
ERK	Extracellular-signal regulated kinase
et al.	*et alia*
FAS	Fatty acid synthase
g	Acceleration due to gravity
GAPDH	Glyceraldehyde 3-phosphate dehydrogenase

GLUT	Glucose transporter
GSK-3β	Glycogen synthase kinase-3β
GTP	Guanosine triphosphate
H&E	Haematoxylin & Eosin
HCC	Hepatocellular carcinoma
HDL	High density lipoprotein
HEPES	4-(2-hydroxyethyl)-1-piperazineethanesulfonic acid
ILK	Integrin-linked kinase
IP3	Inositol trisphosphate
ipGTT	Intra-peritoneal glucose tolerance test
IPTG	Isopropyl-1-thio-b-D-galactopyranoside
IRS	Insulin receptor substrate
IVC	Individually ventilated cage
KO	Knockout
KOMP	Knockout Mouse Project
KSR1	Kinase suppressor of Raf-1
LATS	Large tumour suppressor
LB	Luria broth
LDL	Low density lipoprotein
LKB1	Liver kinase B1/serine threonine kinase 11
LNR	Synthetic peptide, KKLNRTLSFAEPG
MAP	Microtubule associated protein
MAPK	Mitogen-activated protein kinase
MARK	Microtubule affinity-regulating kinase
MCK	Muscle creatine kinase
MEF	Mouse embryonic fibroblast
MELK	Maternal embryonic leucine zipper kinase
MHC	Myosin heavy chain
MLC	Myosin regulatory light chain
MLCK	Myosin light chain kinase
MO25	Mouse protein 25
MRCK	Myotonic dystrophy protein kinase-related cdc42-binding kinase
mTOR	Mammalian target of rapamycin
MYPT	Myosin phosphatase targeting
NDR	Nuclear Dbf2-Related Kinase
Ndufs4	NADH dehydrogenase protein 4
NMR	Nuclear magnetic resonance
NUAK	Nua (novel) kinase
OCR	Oxygen consumption rate
PAGE	Polyacrylamide gel electrophoresis
PAK	p21-activated protein kinase
PAR	Partitioning defective mutant
PAS	Periodic Acid Schiff
PBS	Phosphate-buffered saline
PCR	Polymerase chain reaction
PFA	Paraformaldehyde
PFKFB	6-phosphofructo-2-kinase/fructose-2,6-biphosphatase

PGC1α	Peroxisome proliferator-activated receptor-γ co-activator 1α
PI3K	Phosphoinositide 3-kinase
PJS	Peutz-Jeghers syndrome
PKA	Cyclic AMP-dependent protein kinase
PKC	Protein kinase C
PMSF	Phenylmethylsulphonyl fluoride
PP1C	Protein phosphatase 1C
PVDF	Polyvinylidene difluoride
qPCR	Quantitative polymerase chain reaction
RAB-GAP	RAB family GTPase activating protein
RAPTOR	Regulatory-associated protein of mTOR
RER	Respiratory exchange ratio
RHEB	RAS homologue enriched in brain
ROCK	Rho-associated protein kinase
ROS	Reactive oxygen species
S.E.M	Standard error of the mean
SAD	Synapses of the amphid defective
SAMS	Synthetic peptide, HMRSAMSGLHLVKRR
SDS	Sodium lauryl sulfate
SIK	Salt-inducible kinase
SILAC	Stable Isotope Labelling by Amino Acids in Cell Culture
SNF1	Sucrose non-fermenting protein 1
SREBP1C	Phosphorylate sterol regulatory element-binding protein 1C
STRAD	STE20-related adaptor protein
TAB	TGFβ-activated kinase binding protein
TAE	Tris-acetate-EDTA buffer
TAK1	Transforming growth factor-β activated kinase-1
TAZ	Transcriptional coactivator with PDZ-binding motif
TBS-T	Tris buffered saline with Tween
TCEP	Tris(2-carboxyethyl)phosphine
TGFβ	Transforming growth factor-β
UBA	Ubiquitin associated domain
USP9X	Ubiquitin-specific protease 9X

Table of Contents

List of Figures

List of Appendices

1 Introduction

AMP-activated protein kinase (AMPK) is an important enzyme involved in metabolism and energy regulation (Carling, 2004; Hardie, 2008). The structural composition, signalling pathways and effects of AMPK have been well studied. It is involved in many clinical and pathological conditions leading to great interest in the therapeutic potential of AMPK (Zhang et al., 2009; Zhou et al., 2009). Recently twelve kinases related to AMPK that are regulated by the same upstream kinase, LKB1, have been identified (Lizcano et al., 2004). LKB1 is a heterotrimeric kinase, requiring partner proteins STRAD and MO25 for optimal activity (Alessi et al., 2006; Lizcano et al., 2004; Manning et al., 2002). Eleven of these related kinases contain a conserved regulatory threonine residue which is phosphorylated by LKB1 and they appear to have many diverse functions including regulation of cell polarity, cell growth, differentiation and control of cellular energy (Alessi et al., 2006). It is thought that LKB1 is constitutively active but there is little information to suggest how this affects the regulation of the AMPK-related kinases (Bright et al., 2009). The AMPK signalling network has been well studied and the upstream kinases and downstream targets have been well characterised (Boudeau et al., 2004; Inoki et al., 2003; Woods et al., 2005). However currently there is relatively little known about the function and regulation of the AMPK-related kinases.

This thesis represents a study of the role and regulation of NUAK1. In this chapter, the background of the regulation and function of AMPK is given as an introduction to the field of AMPK-related kinases. The existing understanding of the role of NUAK1 and some of the other AMPK-related kinases is reviewed. The role of LKB1 and other kinases linked to NUAK1 are also discussed and the current understanding of pathological processes investigated within the project are outlined.

1.1 AMPK

AMPK is a highly conserved serine-threonine kinase with a varied range of intracellular and whole body functions. As its name would suggest, it is activated by AMP which is formed mainly by the action of adenylate kinase converting 2ADP > ATP + AMP. Recent data has also shown that AMPK is activated by ADP (Xiao et al., 2011). The activation by AMP and ADP is a

useful way of measuring the energy consumption by the cell and because it is capable of sensing the ADP:ATP and AMP:ATP ratios, AMPK has a crucial role in controlling cellular energy homeostasis. If the cell is subjected to any form of stress that interferes with ATP synthesis (e.g. hypoxia or lack of nutrients), the ADP:ATP and AMP:ATP ratios will increase. There are also pharmacological AMPK activators, such as metformin that reduces ATP synthesis by inhibiting complex I of the respiratory chain (Owen et al., 2000). This reduction in ATP levels will also increase the ADP:ATP and AMP:ATP ratios, thereby activating AMPK. Similarly any cellular stresses that increase ATP consumption, such as muscle contraction, will likewise activate AMPK by changing the ADP:ATP and AMP:ATP ratios. Because ATP levels are so important to maintaining cell integrity, AMPK has a fundamental role in switching off anabolic (ATP consuming) pathways and switching on catabolic (ATP producing) pathways during periods of energy limitation.

As would be expected from such a key cell signalling protein, the essential role of AMPK is preserved in orthologues from almost every eukaryotic organism for which the genome has been sequenced (Hardie et al., 2012). The yeast orthologue of AMPK from *Saccharomyces cerevisiae,* SNF1, has been widely studied and has provided many insights into downstream pathways and the broader function of AMPK (Hardie, 2007). Other studies have identified ways in which AMPK is regulated by cytokines and hormones that are known to regulate whole-body metabolism (Kahn et al., 2005). Various pharmacological compounds, including anti-diabetic drugs metformin and phenformin, are known to activate AMPK probably by interfering with ATP synthesis (Hardie, 2008). These data, and other indications, show that AMPK may play a crucial role in diseases such as obesity, diabetes and the metabolic syndrome.

Although a huge amount is known about AMPK and its upstream and downstream pathways, there are still many questions concerning nuances of the way its activity is regulated and the effect of attenuating its actions. Major outstanding issues include the identity of protein phosphatases responsible for dephosphorylating AMPK and ways of investigating non-canonical mechanisms of activation. The eventual aim of this field of research is to identify novel therapeutic drugs and, with such wide-ranging effects, it will be crucial to elucidate the

exact changes involved in activating or inhibiting AMPK activity in different cell types and organs.

1.1.1 AMPK structure and regulation

AMPK is a heterotrimeric kinase and over the past 10 years a great deal of work has been undertaken to clarify the individual roles of each of the different subunits. AMPK is formed of a catalytic α subunit and regulatory β and γ subunits (Figure 1.1). The α-subunit contains the kinase activity and the binding of AMP or ADP to the γ subunit has been reported to promote phosphorylation of a conserved threonine residue within the kinase domain (referred to as Thr172 as it was originally identified in rat AMPK (Davies et al., 1995; Oakhill et al., 2011). The phosphorylation of this residue has been shown to be essential for activity (Hawley et al., 1996). Early data also showed that AMP binding protects against the dephosphorylation of the α subunit, providing another mechanism to further increase the activity of the kinase (Davies et al., 1995). The binding of AMP, but not ADP, to the γ subunit also allosterically activates the enzyme and collectively these two effects cause over a 1000-fold increase in AMPK activity (Sanders et al., 2007; Suter et al., 2006).

Interestingly, recent data has suggested that the protection against dephosphorylation may be the more physiologically relevant mechanism of AMPK regulation (Sanders et al., 2007). In addition, new data has emerged that shows ADP can also produce the same protection against dephosphorylation and provides new insight into how the balance of the adenine nucleotides could affect the activation of AMPK in a cellular environment (Xiao et al., 2011). This report indicates that AMP or ADP can change the equilibrium between structures of AMPK that are sensitive or insensitive to dephosphorylation, thereby attenuating the reduction in activity caused by protein phosphatases. However, a consensus on the mechanism of AMPK activation is still proving elusive, as another group have recently shown that these conclusions based on bacterially expressed recombinant AMPK may not be physiologically relevant (Gowans et al., 2013). Using purified rat liver AMPK, their observations suggested that AMP, rather than ADP, would be the most important physiological regulator. These inconsistencies may prove to be an artefact of experimental conditions or a genuine difference in the mechanism of activation under different conditions.
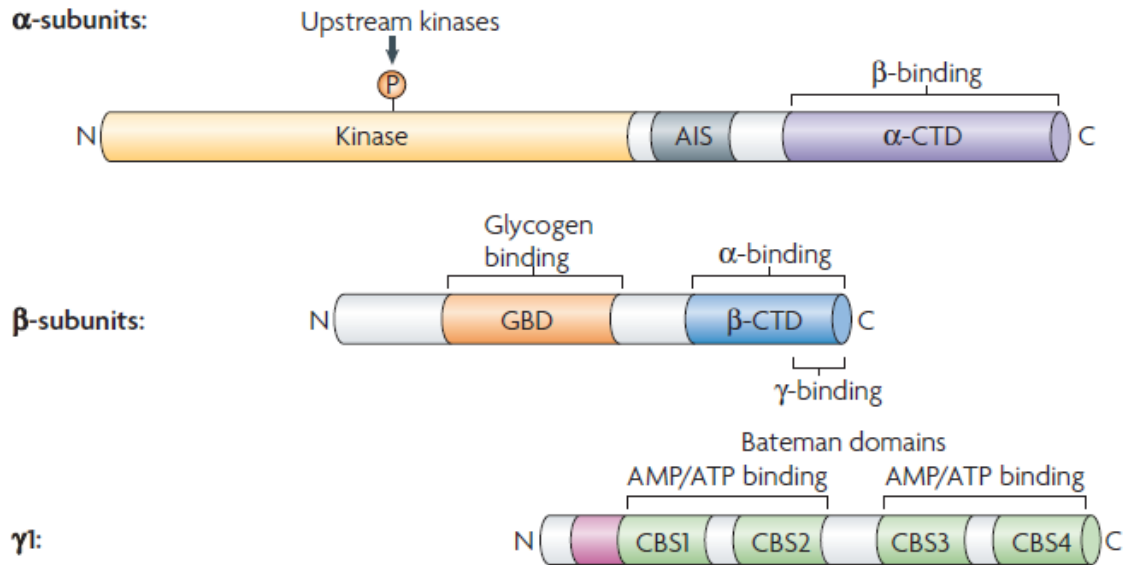
Figure 1.1 Domain structure of AMPK subunits (from Hardie, 2007)

The catalytic α subunits have a C-terminal domain (α-CTD) that is required for binding the β and γ subunits and an autoinhibitory domain (AID) that inhibits the activity of the catalytic domain. The β subunit contains a carbohydrate binding module (CBM) but the exact function of this in the active kinase is unclear. The regulatory γ subunits (of which there are three in mammalian systems) contain four cystathionine β-synthase (CBS) domains which form the interface for binding adenine nucleotides. The kinase domain also contains the T-loop with the critical threonine residue that must be phosphorylated for activity.

1.1.2 Upstream kinases of AMPK

AMPK requires phosphorylation of T172 in the activation loop of the catalytic α subunit by an upstream kinase in order to be active (Davies et al., 1995; Hawley et al., 1996). To date, three kinases upstream of AMPK that are capable of activating the critical threonine residue have been identified. The first of these kinases to be described was the tumour suppressor liver kinase B1 (LKB1) (Hawley et al., 2003; Woods et al., 2003). In order to be active, LKB1 requires the binding of two subunits, STE20-related adaptor (STRAD) and mouse protein 25 (MO25). Numerous studies have looked at the role of LKB1 as it has been identified as a tumour suppressor involved in the hereditary cancer predisposition syndrome, Peutz-Jeghers. LKB1 appears to be ubiquitously expressed and constitutively active (Boudeau et al., 2003). Recent data has indicated that the binding of AMP or ADP to AMPK plays a crucial role in its activation

despite LKB1 being constitutively active (Oakhill et al., 2011). The binding of AMP or ADP can protect AMPK against the dephosphorylation of T172 by protein phosphatases thereby allowing it to be maintained in its active conformation (Sanders et al., 2007; Suter et al., 2006; Xiao et al., 2011). The regulation of this cycle of phosphorylation and dephosphorylation seems likely to play an important role in the tissue specific function of AMPK.

LKB1 is considered a "master" kinase which has been implicated in numerous important and clinically relevant processes from cell cycle regulation in haematopoietic stem cells (Nakada et al., 2010) to cell polarity in liver development (Woods et al., 2011). Also, early studies that showed LKB1 activating the AMPK-related kinases measured an increase in activity in the presence of LKB1 expression without taking into consideration other potential upstream kinases (Lizcano et al., 2004). Although this study provided various convincing pieces of data to show LKB1 activates the AMPK-related kinases, it did not conclusively show that phosphorylation by LKB1 is the only activating mechanism.

Ca^{2+}/calmodulin-dependent protein kinase kinase α and β (CaMKKα/β) are also capable of phosphorylating the key threonine residue on AMPK (Hawley et al., 2005; Hurley et al., 2005; Woods et al., 2005). CaMKKβ has been the focus of more attention in this area and is activated in response to a rise in intracellular calcium levels which in turn leads to an increase in AMPK activity. This means that AMPK is capable of responding to a change in cytosolic calcium as well as nucleotide levels. CaMKKβ is expressed mainly in neuronal cells but is also present in thymus, testis and T cells (Anderson and Kane, 1998). In cell types where both LKB1 and CaMKKβ are expressed, different stimuli may activate AMPK through different pathways (Stahmann et al., 2006; Tamas et al., 2006).

The third upstream kinase for AMPK that has been reported is transforming growth factor-β (TGFβ)-activated kinase-1 (TAK1). This was identified using a screen for kinases that phosphorylate and activate the AMPK homologue sucrose non-fermenting protein 1 (SNF1) in yeast (Momcilovic et al., 2006). TAK1 has also been shown to activate AMPK in heart via an LKB1-dependent pathway (Xie et al., 2006). TAK1 has been researched from many different angles and appears to have a role in many different pathways. TAK1 has been shown to be involved in inflammatory response pathways (Sato et al., 2005) and similar to LKB1, TAK1

requires binding partners called TGFβ-activated kinase binding proteins 1-3 (TAB1-3) for its activation (Singhirunnusorn et al., 2005). The exact *in vivo* role of TAK1 activating AMPK is currently disputed despite several reports on this area (Chen et al., 2013b; Wang et al., 2013).

1.1.3 AMPK and metabolism

AMPK is generally activated by any metabolic stress that changes the AMP:ATP and ADP:ATP ratios, either by inhibiting ATP production or increasing ATP consumption. AMPK can also be activated by a number of extrinsic hormones and cytokines that can also influence cellular and whole body metabolism. AMPK was originally identified as an inhibitor of acetyl-CoA carboxylase 1 (ACC1) in rat liver (Carling et al., 1989). The effect of ACC1 inhibition is a reduction in the synthesis of fatty acids, a key ATP consuming biosynthetic pathway, and much of the research in the field since has focussed on the role of AMPK in metabolic pathways. Many studies, especially since the widespread use of animal models, have made observations about the involvement of AMPK in metabolic processes but in some cases the exact signalling pathway has yet to be clarified. Broadly, AMPK exerts its effect of switching off anabolic pathways by two mechanisms. Firstly it can directly phosphorylate and regulate the activity of key enzymes and co-factors involved in biosynthetic pathways such as glycogen synthase (Carling and Hardie, 1989; Jorgensen et al., 2004), regulatory-associated protein of mTOR (RAPTOR) (Gwinn et al., 2008) and 3-hydroxy-3-methylglutaryl CoA reductase (Clarke and Hardie, 1990). Through these and other pathways AMPK can directly reduce lipid, protein and carbohydrate synthesis, thereby reducing ATP consumption on a fairly immediate timescale to exert short-term control. However, AMPK can also exert a degree of long-term control by regulating the expression of proteins involved in these pathways over a longer time period. The exact transcriptional effect of AMPK is unclear but it is known to phosphorylate sterol regulatory element-binding protein 1C (SREBP1C) and inhibit its activity as a transcription factor (Li et al., 2011). AMPK can also regulate transcription directly by phosphorylation of CREB-regulated transcription co-activator 2 (CRTC2) (Koo et al., 2005) and indirectly via control of the localisation of the class IIa histone deacetylases, which in turn can control other transcription factors (Mihaylova and Shaw, 2011).

Reducing the activity of anabolic pathways is one half of the role of AMPK and the other downstream effect is to increase catabolic pathways with the objective of increasing the ATP concentration in the cell back to a stable level. One way in which AMPK achieves this is by increasing glucose uptake during periods of stress such as muscle contraction. AMPK can mediate the same pathway as insulin by causing the translocation of glucose transporter 4 (GLUT4) channels to the plasma membrane which increases glucose uptake. The key difference to insulin stimulated glucose uptake is that during times of stress, glucose is oxidised to make ATP rather than incorporated into glycogen, which is an anabolic process and would appear to defeat the purpose of activating AMPK to conserve ATP. The translocation of GLUT4 proteins involves signalling through several pathways including RAB family GTPase activating proteins (RAB-GAPs) such as TBC1D1, which AMPK can phosphorylate to promote the translocation of GLUT4 vesicles to the plasma membrane. Akt, a key kinase in the insulin signalling pathway can also phosphorylate RAB-GAPs (Treebak et al., 2009) and the distinct roles of these two pathways are currently unclear. Recent animal models have confirmed the role of AMPK in contraction stimulated glucose uptake, however there may be other downstream effectors besides the RAB-GAP family (O'Neill et al., 2011). AMPK also has the ability to regulate translocation of the transporter CD36, thereby increasing uptake of fatty acids which can be oxidised to produce ATP (Habets et al., 2009). AMPK also seems able to increase glucose uptake in cell types which express only glucose transporter 1 (GLUT1) by activating channels that are already part of the plasma membrane (Barnes et al., 2002). Not only can AMPK promote the uptake of molecules for ATP production, it can also stimulate glycolysis and the β-oxidation pathway via phosphorylation of 6-phosphofructo-2-kinase/fructose-2,6-biphosphatase 2 (PFKFB2) in heart and acetyl-CoA carboxylase 2 (ACC2) in skeletal muscle respectively (Marsin et al., 2000; Merrill et al., 1997).

Mitochondria are a key site of metabolism and it has been shown that AMPK can promote mitochondrial biogenesis to increase the cellular capacity for oxidative production of ATP. Treating rats with a known pharmacological activator of AMPK, 5-aminoimidazole-4-carboxamide ribonucleoside (AICAR), produced an upregulation of mitochondrial genes in skeletal muscle (Winder et al., 2000). It has been suggested that AMPK regulates this response by targeting a central mitochondrial control gene, peroxisome proliferator-activated receptor-γ co-activator 1α (PGC1α). Studies have suggested that AMPK is capable of directly

activating PGC1α by phosphorylation (Jager et al., 2007) or indirectly by changing the concentration of NAD^+, which is required for the deacetylation of PGC1α (Canto and Auwerx, 2010). Recent reports suggest that AMPK not only plays a role in the formation of new mitochondria, but is also involved in the removal of defective mitochondria by a process called mitophagy; a particular form of autophagy. This has been proposed on the basis that AMPK can phosphorylate and activate the mammalian orthologues of kinases responsible for autophagy in yeast (Egan et al., 2011).

The key downstream targets and the metabolic processes that can be regulated by AMPK are summarised in Figure 1.2. The diversity of these target processes show how important AMPK is to maintaining cellular energy levels. By influencing systems to recruit energy sources to the cell, switch on ATP producing pathways, produce more mitochondria and remove faulty mitochondria it allows the cell to maintain ATP-generating capacity under conditions of stress.

Another idea which has developed in recent years is the possibility that AMPK plays a key role in the whole body regulation of metabolism by affecting the arcuate nucleus feeding centre in the brain. Hormones known to stimulate or prevent feeding, such as grehlin and leptin, can activate or inhibit AMPK in key subsets of neurons (Andersson et al., 2004; Minokoshi et al., 2004). While the exact downstream effect exerted by AMPK is unclear, indications that direct activation of AMPK can increase feeding (Andersson et al., 2004) would suggest that it does play a role in signalling pathways in the brain in response to hormonal cues. AMPK also appears to have a key function in a different set of neurons upstream of the feeding centre, which suggests that the role of AMPK in the brain may be much broader than originally thought (Yang et al., 2011).
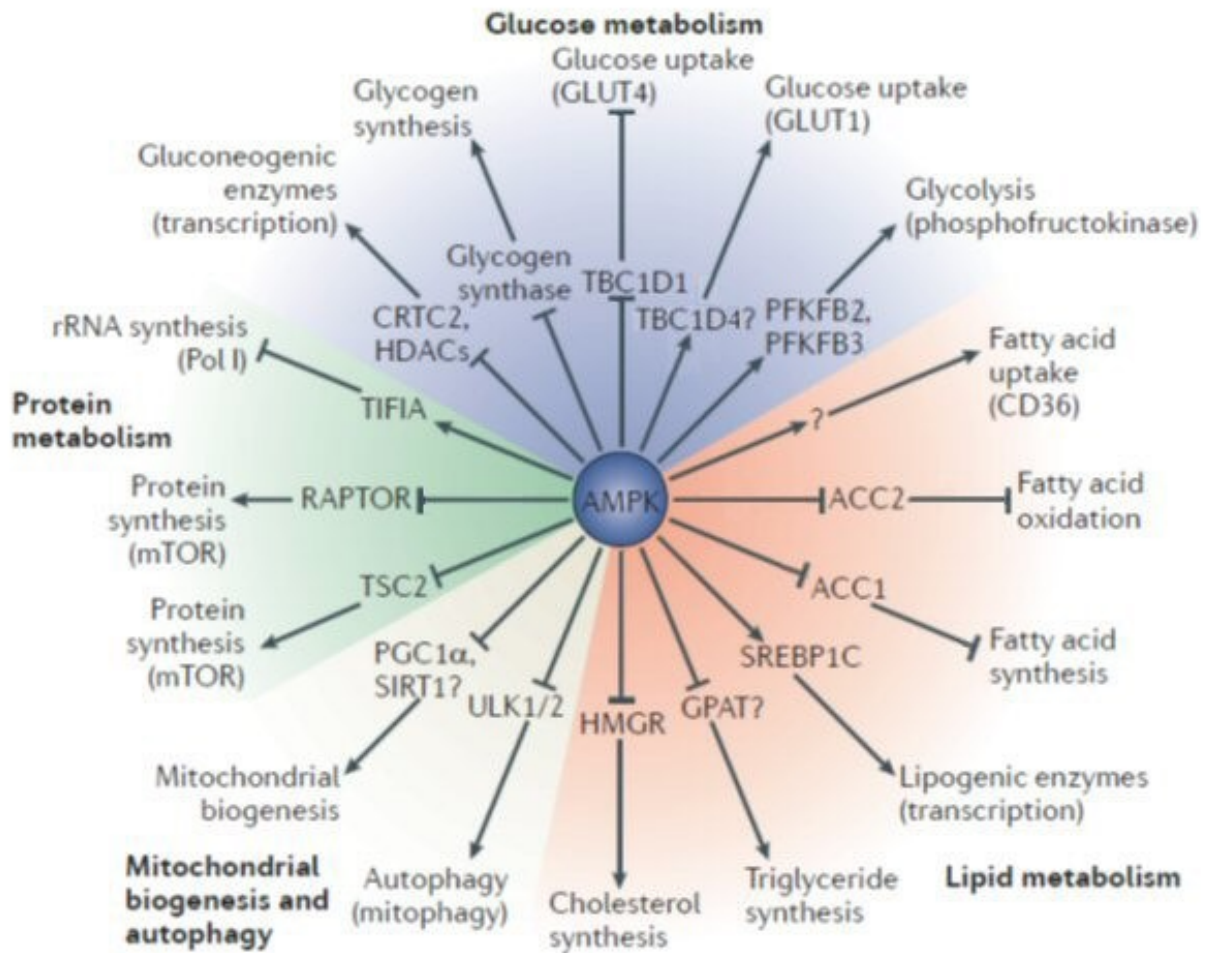
Figure 1.2 Downstream targets of AMPK in metabolism (modified from Hardie et al., 2012)

AMPK has a diverse range of downstream targets involved in cell metabolism. The action of AMPK is broadly focussed around inhibiting anabolic pathways, such as fatty acid synthesis through ACC1 and activating catabolic pathways such as glycolysis through PFK. The exact interactions and pathways may vary between cell types but the pathways listed here are widely accepted as being affected by AMPK. Red indicates pathways involved in lipid metabolism, blue indicates pathways involved in glucose metabolism, green indicates pathways involved in protein metabolism and white for processes involved in mitochondrial biogenesis.

1.1.4 AMPK, cell proliferation and cancer

With such wide ranging effects in cell metabolism, it is not surprising to find that changes in AMPK signalling can have significant effects on cell proliferation with implications for the treatment of cancers. LKB1 is well characterised as a bona fide tumour suppressor in humans (Hemminki et al., 1998) but it is also known to be upstream of the AMPK-related kinases (Lizcano et al., 2004), making it unclear exactly which other kinases are involved in mediating the tumour suppressor functions of LKB1. This is a short background just on the role of AMPK in cell proliferation.

Because AMPK is such a ubiquitous and important signalling protein there have been a lot of conflicting reports regarding its function in either promoting or inhibiting cell growth and division. Many of these studies suggest that activating AMPK would reduce cell growth and proliferation, which is consistent with the role of the protein kinase in switching off anabolic pathways. Firstly, as most tumours have a high energy demand, it would be predicted that under conditions of limited energy availability, such as in tumour hypoxia, AMPK activation would reduce cell growth. However, to understand the wider effects of AMPK in this field it is important to consider other intracellular signalling pathways that regulate cell growth, particularly the mammalian target of rapamycin complex 1 (mTORC1) pathway.

The mTORC1 pathway has been well characterised and, in its entirety, is incredibly complex and a recent attempt to map the whole pathway highlighted over 700 different interactions (Caron et al., 2010). To understand the involvement of AMPK I will focus on the key parts of the pathway highlighted in Figure 1.3.
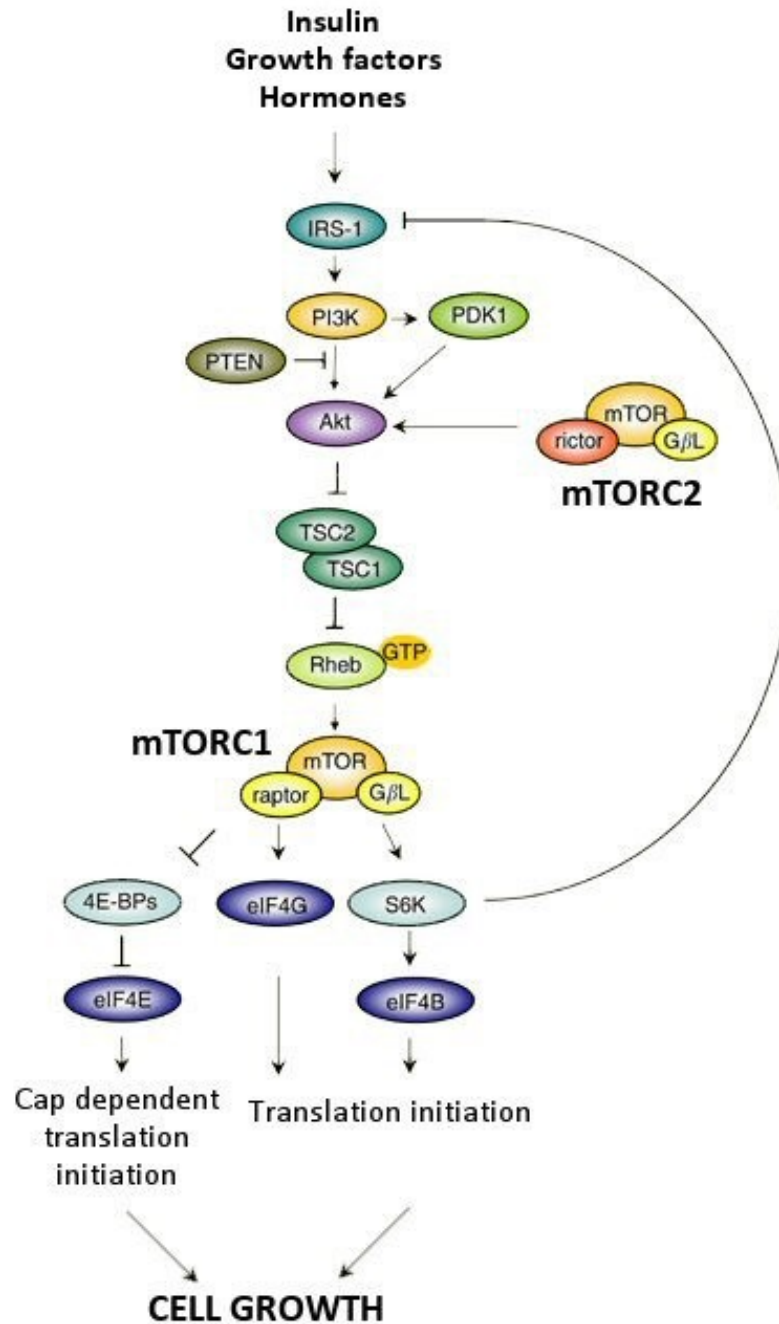
Figure 1.3 The mTOR pathway (adapted from Petroulakis et al., 2006)

mTOR exists in two functionally different complexes, mTORC1 and mTORC2. The mTOR pathway is capable of integrating inputs from several different systems, including insulin and hormone signalling via the phosphoinositide 3-kinase (PI3K) pathway. This and the mitogen-activated protein kinase (MAPK)/extracellular-signal regulated kinase (ERK) signalling pathway both act on the tuberous sclerosis 1 (TSC1)/tuberous sclerosis 2 (TSC2) complex. This behaves as a GTPase-activating protein (GAP), which can inhibit the function of the small GTPase RAS homologue enriched in brain (RHEB). This leads to an increase in the GTP-bound form of RHEB, which activates mTORC1, leading to a series of downstream effects which are generally pro-cell growth and proliferation.

The regulation of cell growth and proliferation is highly dependent on the metabolic status of the cell, so it would be logical for there to be a mechanism for integrating the energy sensing signal from AMPK into one of the key pathways for controlling cell growth. As an energy dependent process, cell division and growth should only occur under conditions of efficient energy availability. This means that the activity of the mTORC1 is opposite to that of AMPK, so that mTORC1 is active during times of nutrient availability compared to AMPK which is active during times of stress and energy depletion. Therefore, it would be expected that AMPK activation would inhibit mTORC1 to reinforce this control. AMPK can phosphorylate the mTOR partner protein RAPTOR, which reduces mTORC1 activity by promoting the binding of 14-3-3 proteins (Gwinn et al., 2008). AMPK is also capable of directly phosphorylating mTOR which antagonises activation by Akt (Cheng et al., 2004). Finally, AMPK can signal to other components of the pathway, for example, by phosphorylating TSC2 leading to lower RHEB activity and consequently reduced mTORC1 activity (Inoki et al., 2003) (Figure 1.4A).

Several cancers display high levels of *de novo* fatty acid synthesis and there are beneficial anti-tumourigenic effects of inhibiting fatty acid synthase (FAS), which is a crucial enzyme in this process (Pizer et al., 1998). It has been established that AMPK activation can inhibit fatty acid synthesis, both indirectly via regulating FAS expression through SREBP1 and directly via ACC1 inactivation (Chajes et al., 2006; Foretz et al., 1998) (Figure 1.4A). Consistent with this AMPK activators can inhibit fatty acid synthesis in cancer cell lines leading to reduced cell growth and increased apoptosis (Chajes et al., 2006; Xiang et al., 2004).

The anti-cancer role of AMPK activation leading to inhibition of cell growth and proliferation would seem the most logical role of the kinase given the wider knowledge about how the pathways interact. However, recent data has suggested that the opposite may be the case, such that inhibition of AMPK could lead to reduced cell growth. Various screening studies have indicated that AMPK activity, and that of its upstream kinase CaMKKβ, is increased in prostate cancer cell lines (Frigo et al., 2011; Massie et al., 2011). Another study showed that a known AMPK inhibitor can reduce cancer cell proliferation (Park et al., 2009). AMPK may have a positive effect on cell growth simply by activating catabolic pathways such as glycolysis to produce more energy, as discussed previously (Figure 1.4B), but this may only be part of the story. Some other data has emerged recently, via novel screening techniques, to suggest

how AMPK may exert this pro-proliferative effect by targeting components of the myosin phosphorylation pathway (see section 1.5).

A
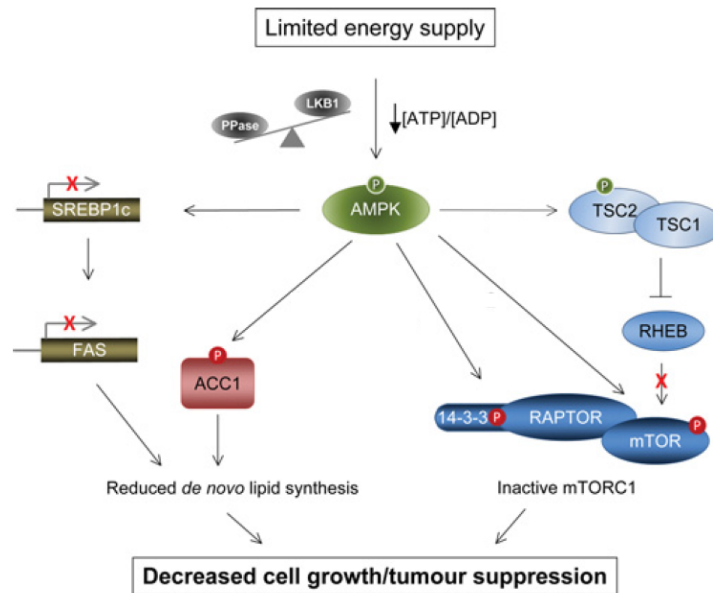
B
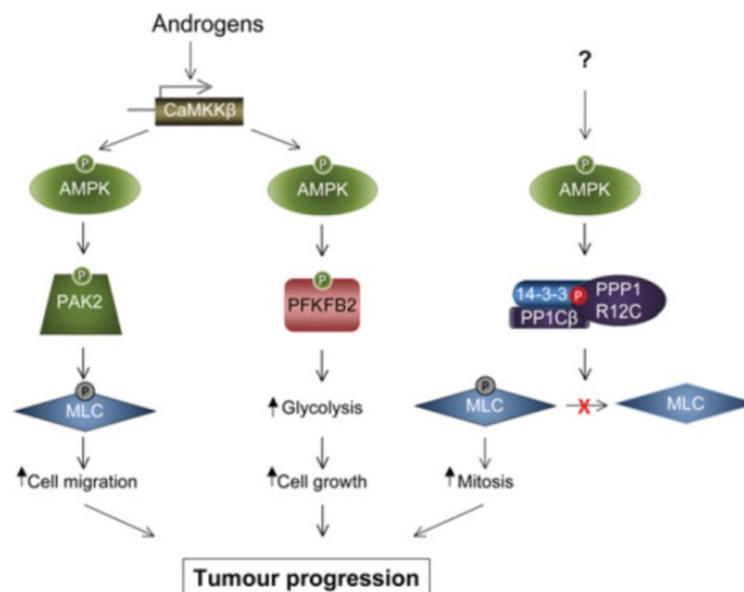
Figure 1.4 Actions of AMPK in cell proliferation and cancer (from Carling et al., 2012)

Activating and inhibitory phosphorylation are shown in green and red respectively

Various pathways which involve AMPK are highlighted as having either **(A)** an anti-proliferative effect or **(B)** a pro-proliferative effect. In both cases AMPK could be activated by a variety of pathways, but specific activating mechanisms such as a change in the AMP:ATP or ADP:ATP ratios or increased expression of the upstream kinase CaMKKβ are proposed to be involved in certain conditions.

The potential anti-proliferative effects of AMPK could be mediated through several pathways. Activating phosphorylation of TSC2 inhibits RHEB, leading to inhibition of mTORC1. Direct phosphorylation of mTOR or phosphorylation of RAPTOR, thereby increasing 14-3-3 binding also both decrease mTORC1 activity. Also AMPK is known to down regulate *de novo* fatty acid synthesis by two mechanisms – firstly by directly phosphorylating and inhibiting ACC1 activity and secondly by suppressing SREBP1c expression leading to reduction in other genes involved in fatty acid synthesis (Figure 1.4). Similarly, the potential pro-proliferative effects of AMPK could involve two mechanisms. Firstly AMPK increases glycolysis by directly activating PFKFB2 and PFKFB3, which would provide more energy for faster cell growth. Secondly, AMPK activation can lead to increased MLC phosphorylation, which leads to increased mitosis and cell migration (Figure 1.4, section 1.5).

Currently the overall role of AMPK and its related pathways in cancer cell growth and proliferation is unclear and there are conflicting reports in the literature which are difficult to reconcile. Further investigation of the downstream targets and other proteins involved in signalling cascades may reveal cell-type specific roles or other mechanisms that allow differential control of AMPK activity in response to different conditions. It is possible that AMPK only influences mitosis in certain cells as there are several isoforms of the MYPT subunits and previous studies have shown that AMPK does not target all of the isoforms (Zagorska et al., 2010). There is also a possible role for related proteins involved in other signalling cascades to control separate parts of these pathways.

1.2 AMPK-related kinases

Data from the sequencing of the human kinome revealed a family of twelve protein kinases that are closely related to AMPK and share significant sequence homology within the catalytic α subunit (Manning et al., 2002) (Figure 1.5A). All the kinases listed are highly conserved and also show a high degree of homology across their mouse orthologues (Figure 1.5B). There are also eight other kinases that contain the same conserved threonine site within their T-loop sequence but do not have the same overall sequence homology with the other AMPK-related kinases (Jaleel et al., 2005). In this thesis, references made to "AMPK-related kinases" are consistent with the definition used in Manning et al. (2002).

Critical
threonine
residue

↓

A

```
AMPKα1     163  HRDLKPENVLLDAHMNAKIADFGLSNMMSD--GEFLRTSCGSPNYAAPEVISGRLYAGPE
AMPKα2     137  HRDLKPENVLLDAHMNAKIADFGLSNMMSD--GEFLRTSCGSPNYAAPEVISGRLYAGPE
NUAK1      176  HRDLKLENILLDDNCNIKIADFGLSNLYQK--DKFLQTFCGSPLYASPEIVNGRPYRGPE
NUAK2      173  HRDLKLENILLDANGNIKIADFGLSNLYHQ--GKFLQTFCGSPLYASPEIVNGKPYTGPE
MARK1      180  HRDLKAENLLLDGDMNIKIADFGFSNEFTV--GNKLDTFCGSPPYAAPELFQGKKYDGPE
MARK2      140  HRDLKAENLLLDADMNIKIADFGFSNEFTF--GNKLDTFCGSPPYAAPELFQGKKYDGPE
MARK3      176  HRDLKAENLLLDADMNIKIADFGFSNEFTV--GGKLDTFCGSPPYAAPELFQGKKYDGPE
MARK4      179  HRDLKAENLLLDAEANIKIADFGFSNEFTL--GSKLDTFCGSPPYAAPELFQGKKYDGPE
BRSK1      154  HRDLKPENLLLDEKNNIRIADFGMASLQVG--DSLLETSCGSPHYACPEVIKGEKYDGRR
BRSK2      139  HRDLKPENLLLDEKNNIRIADFGMASLQVG--DSLLETSCGSPHYACPEVIRGEKYDGRK
SIK1       147  HRDLKTENLLLDGNMDIKLADFGFGNFYKS--GEPLSTWCGSPPYAAPEVFEGKEYEGPQ
SIK2       140  HRDLKAENLLLDNNMNIKIADFGFGNFFKS--GELLATWCGSPPYAAPEVFEGQQYEGPQ
SIK3       128  HRDLKAENLLLDANLNIKIADFGFSNLFTP--GQLLKTWCGSPPYAAPELFEGKEYDGPK
MELK       130  HRDLKPENLLFDEYHKLKLIDFGLCAKPKGNKDYHLQTCCGSLAYAAPELIQGKSYLGSE
consensus  199  ***** **.*.*. .......***...... . * *.***..**.**....*. *.*..
```

B

```
AMPKα1     137  HRDLKPENVLLDAHMNAKIADFGLSNMMSD--GEFLRTSCGSPNYAAPEVISGRLYAGPE
AMPKα2     137  HRDLKPENVLLDAQMNAKIADFGLSNMMSD--GEFLRTSCGSPNYAAPEVISGRLYAGPE
NUAK1      177  HRDLKLENILLDDNCNIKIADFGLSNLYQK--DKFLQTFCGSPLYASPEIVNGRPYRGPE
NUAK2      185  HRDLKLENILLDANGNIKIADFGLSNLYHK--GKFLQTFCGSPLYASPEIVNGKPYVGPE
MARK1      180  HRDLKAENLLLDADMNIKIADFGFSNEFTV--GNKLDTFCGSPPYAAPELFQGKKYDGPE
MARK2      173  HRDLKAENLLLDADMNIKIADFGFSNEFTF--GNKLDTFCGSPPYAAPELFQGKKYDGPE
MARK3      176  HRDLKAENLLLDADMNIKIADFGFSNEFTV--GSKLDTFCGSPPYAAPELFQGKKYDGPE
MARK4      179  HRDLKAENLLLDAEANIKIADFGFSNEFTL--GSKLDTFCGSPPYAAPELFQGKKYDGPE
BRSK1      154  HRDLKPENLLLDEKNNIRIADFGMASLQVG--DSLLETSCGSPHYACPEVIKGEKYDGRR
BRSK2      140  HRDLKPENLLLDERNNIRIADFGMASLQVG--DSLLETSCGSPHYACPEVIRGEKYDGRK
SIK1       147  HRDLKTENLLLDSNMDIKLADFGFGNFYKP--GEPLSTWCGSPPYAAPEVFEGKEYEGPQ
SIK2       140  HRDLKAENLLLDNNMNIKIADFGFGNFFKT--GELLATWCGSPPYAAPEVFEGQQYEGPQ
SIK3       187  HRDLKAENLLLDANLNIKIADFGFSNLFTP--GQLLKTWCGSPPYAAPELFEGKEYDGPK
MELK       130  HRDLKPENLLFDENHKLKLIDFGLCAKPKGNKDYHLQTCCGSLAYAAPELIQGKSYLGSE
consensus  207  ***** **.*.*........***...... . * *.***..**.**....*. *.*..
```

Figure 1.5 Sequence homology of the AMPK-related kinases

(A) Alignment of the sequences of the human kinases with the critical threonine residue highlighted. **(B)** A sequence alignment of the kinases using sequences from the mouse reference genome. The homology within the kinase domain is clearly very high and also the homology between the human and mouse forms of the kinases is very evident.
AMPK = AMP-activated protein kinase, NUAK1/2 = Nua (novel) kinase 1 and 2, MARK1-4 = Microtubule affinity-regulating kinases 1-4, BRSK1/2 = Brain-specific kinases 1 and 2, SIK1-3 = Salt-inducible kinases 1-3, MELK = Maternal embryonic leucine zipper kinase

1.2.1 Regulation of AMPK-related kinases by upstream kinases

As described earlier there are three kinases (LKB1, CaMKKβ and TAK1) that have been well characterised as being upstream activators of AMPK. When they were first discovered, one of the defining features of the AMPK related kinases (with the exception of MELK) was that they share a common upstream kinase, LKB1 (Lizcano et al., 2004). The function of LKB1 has already been well defined in the literature as an activator of AMPK (Hawley et al., 2003; Woods et al., 2003) and certain known activators of AMPK such as metformin have been shown to act through phosphorylation by LKB1 (Shaw et al., 2005). No study since the original identification of the AMPK-related kinases has looked at all of them simultaneously but some data suggests that that the other AMPK upstream kinases may not activate the related kinases. Conflicting reports exist as to whether CaMKKβ can phosphorylate and activate brain-specific kinases 1 and 2 (BRSK1 and BRSK2) (Bright et al., 2008; Fujimoto et al., 2008). Additionally these reports dispute the role of cyclic AMP-dependent protein kinase (PKA) upstream of the BRSKs, but other studies have indicated a role for PKA upstream of salt inducible kinase 1 (SIK1) (Takemori et al., 2002). Some studies into the function of the AMPK-related kinases have also suggested that they can be regulated by other pathways and that there may be similarities in the activation of sub-families of the related kinases (Bright et al., 2009). The microtubule affinity-regulating kinase (MARK) group of kinases have been shown to be regulated by the TAO1 kinase (Hutchison et al., 1998) and glycogen synthase kinase-3β (GSK-3β) (Timm et al., 2008). There is also evidence that the SIK sub-family can be regulated by Akt2, leading to transcriptional control through degradation of CREB regulated transcription coactivator 2 (CRTC2) (Dentin et al., 2007) and by Ca^{2+}/calmodulin-dependent kinase (CaMK) (Sjostrom et al., 2007).

As with AMPK, it is probable that the balance between phosphorylation and dephosphorylation is a key determinant of AMPK-related kinase activity which would suggest that the regulation of inactivating phosphatases may also play an important role. This is particularly interesting as several studies have shown that members of the related kinase family have substrates that are part of protein phosphatase complexes (Sjostrom et al., 2007; Yamamoto et al., 2008; Zagorska et al., 2010) which raises the possibility of regulatory feedback loops.

1.2.2 Regulation of AMPK-related kinases by ubiquitination

There have been reports that some members of the AMPK-related kinase family interact with, and may be regulated by, ubiquitin specific proteases USP9X and USP11 (Al-Hakim et al., 2008; Jaleel et al., 2006). The AMPK-related kinases are distinctive within the human kinome because most of them contain an ubiquitin associated (UBA) domain (Katajisto et al., 2007; Manning et al., 2002). Notably, the two related kinases that do not contain UBA domains are NUAK1 and NUAK2, meaning there could be key mechanisms of regulation linked to the absence of this domain (Figure 1.6).
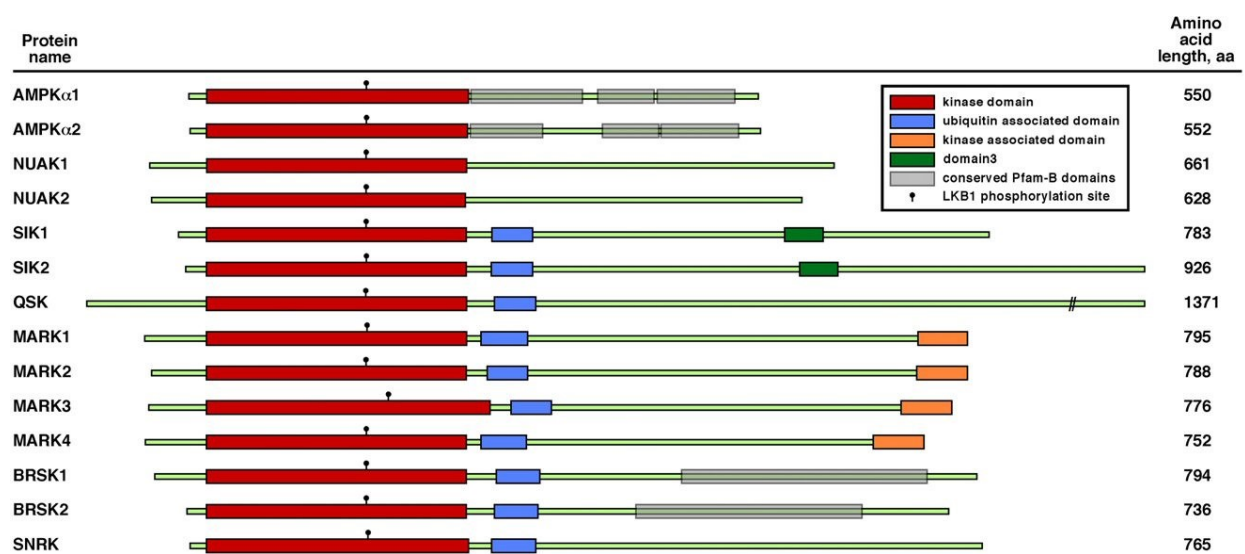
Figure 1.6 Domain comparison of AMPK-related kinases (from Katajisto et al., 2007)

The domain structure of the human AMPK-related kinases is compared, aligned to the N-terminal end of the kinase domain. The LKB1 phosphorylation site of a conserved threonine residue is highlighted in the kinase domain which is shown in red. Ubiquitin-associated domains (UBA) are shown in blue. Kinase associated domains, which are part of the MARK family and are of unknown function, are highlighted in orange. Domains which were identified in the SIK proteins contain an inhibitory PKA-phosphorylation site and can regulate subcellular localisation. Pfam-B domains conserved in human, *Drosophila* and *C. elegans* genomes are highlighted in grey.

The UBA domains appear to be essential for activation, as a specific mutation within this region can prevent phosphorylation by LKB1 (Bright et al., 2008; Jaleel et al., 2006). Ubiquitination is a very important cellular process which can target proteins to various parts of the cell or mark them for degradation. The exact purpose of the ubiquitination of the AMPK-related kinases is not yet known, but may have an important role in controlling stability

or activation by upstream kinases. Although domain identification programs do not detect a UBA in NUAK1 or NUAK2, sequence alignments show there is some homology between this region and the UBA domains on other AMPK-related kinases (Figure 1.7, (Jaleel et al., 2006). There is evidence that polyubiquitination may play a role in inhibiting NUAK1, as non-ubiquitin specific protease 9X (USP9X) binding mutants were found to be hyperubiquitinated and inactive (Al-Hakim et al., 2008). MARK4 and NUAK2 have been shown to interact with USP9X and the binding site was identified as a tryptophan residue that is conserved in all the AMPK-related kinases. However, none of the other kinases showed any interaction with USP9X (Al-Hakim et al., 2008).

```
AMPKα1    311  STMIDDEALKEVCEKFEC--S------EEEVISCIYNRNHQDPIAVAYHLIIDNRRIMNE
AMPKα2    285  ANVIDDEAVKEVCEKFEC--T------ESEVMNSIYSGDPQDQIAVAYHLIIDNRRIMNQ
NUAK1     324  ESPL----IARIIDWHHR--STGLQADTEAKVKGIAKP------TT-SEVMLERQRSLKK
NUAK2     321  GHPGSDSARASMADWLRR--SSRPLLENGAKVCSFFKQH-APGGGS-TTPGLERQHSLKK
MARK1     327  DPDFNDTKRIDIMVTMGF--A------RDEINDALINQK-YDEVMATYILIGRKPPEFEG
MARK2     287  LPDYKDPRRTELMVSMGY--T------REEIQDSIVGQR-YNEVMATYLLIGYKSSELEG
MARK3     323  ELDISDQKRIDIMVGMGY--S------QEEIQESISKMK-YDEITATYLLIGRKSSELDA
MARK4     326  EEDFGDTKRIEVMVGMGY--T------REEIKESITSQK-YNEVTATYLLIGRKTEEGGD
BRSK1     311  SNGELDPDVLESMASIGCFRD------RERIHREIRSEE-ENQEKMIYYLILDRKERYPS
BRSK2     294  SLEDIDPDVLDSMHSIGCFRD------RNKLIQDILSEE-ENQEKMIYFLLLDRKERYPS
SIK1      300  NLGDYDEQALGIMQTIGV--D------RQRTVESIQNSS-YNHFAAIYYLLLERLKEYRN
SIK2      292  SIGEFNEQVIRIMHSIGI--D------QQKTIESIQNKS-YNHFAAIYFLLVERLKSHRS
SIK3      283  QVDPLNEDVILAMEDVGL--D------KEQTIQSIRSDA-YDHYSAIYSLICDRHKRHKT
MELK      279  FIHLDDDCVTEISVHHRN--N------RQTVEDLISLWQ-YDHITATYLLLIAKKARGKP
consensus 361       .  .....  ..  .      ..  ..... . . . ..... . . ....... .
```

Figure 1.7 Sequence alignment of UBA domains in AMPK-related kinases

Alignment of the sequences of the human kinases across the UBA domains. The variation across this region within NUAK1 and NUAK2 is very evident. AMPK = AMP-activated protein kinase, NUAK1/2 = Nua (novel) kinase 1 and 2, MARK1-4 = Microtubule affinity-regulating kinases 1-4, BRSK1/2 = Brain-specific kinases 1 and 2, SIK1-3 = Salt-inducible kinases 1-3, MELK = Maternal embryonic leucine zipper kinase

MELK, which is known to autophosphorylate, does not have a particularly high degree of homology across the UBA domain compared to the other related kinases. It shares some homology with NUAK1 across this region but this is unlikely to indicate that NUAK1 would share functional similarities with MELK (Figure 1.7). Polyubiquitination of NUAK1 prevented activation by LKB1 *in vitro* (Al-Hakim et al., 2008). A report investigating ubiquitination of AMPK-related kinases proposed a system of regulation based on the conformation of different domains within the protein. It was suggested that the kinase domain and Lys^{29}/Lys^{33} polyubiquitin chains compete for binding to the UBA domain (Al-Hakim et al., 2008). This

system of regulation also relates to previous data suggesting that the kinase domain binding to the UBA domain is important for LKB1 activation of other related kinases (Jaleel et al., 2006). As identified by these previous studies, there are several other ways in which ubiquitination could affect kinase activity such as steric shielding of the critical threonine residue or other sites interacting with upstream kinases. Similarly, the presence of ubiquitin chains could promote dephosphorylation by phosphoprotein phosphatases (Al-Hakim et al., 2008). The exact function of the UBA domain may vary depending on other factors, since ubiquitination is normally used as a method of targeting proteins for degradation but ubiquitination of NUAK1 does not seem to affect its stability (Al-Hakim et al., 2008). Another study on the UBA domain of MARK3 discovered it has intrinsic conformational instability which can cause it to unfold, affecting interactions with other proteins, which could in turn affect its activity (Murphy et al., 2007).

1.2.3 AMPK-related kinases and 14-3-3 proteins

14-3-3 proteins are small regulatory molecules which have been shown to bind to various AMPK-related kinases (Al-Hakim et al., 2005). The 14-3-3 protein family consists of 30 kDa acidic proteins which are widely expressed in most tissues. There are five major isoforms (which are named α – η). 14-3-3 proteins are functional dimers that can regulate interactions between other proteins. Over 200 known interacting partners exist and 14-3-3 proteins have been shown to be involved in a number of cellular processes, particularly trafficking, cytoskeletal structure, cell cycle progression and subcellular localisation (Aitken, 2006; Al-Hakim et al., 2005; Morrison, 2009). The protein family is highly conserved across most mammalian species and all the isoforms are typically identical, but contain a few loci of variation. 14-3-3 homologues have been identified in a broad range of eukaryotic organisms. In terms of the AMPK-related kinases there is some contention over whether 14-3-3 proteins interact directly with the kinase or via another partner protein and whether they can directly affect the kinase activity. There could be a huge range of possibilities, including different partner proteins in different tissues and redundancy within the 14-3-3 isoforms. SIK1 and SIK3 are known to interact with 14-3-3s after phosphorylation by LKB1 and in the case of the SIK kinases, the binding of 14-3-3s localises them to the cytoplasm and increases their catalytic activity (Al-Hakim et al., 2005). 14-3-3 proteins are known to interact with the PAR-1/MARK

enzymes (Brajenovic et al., 2004) and some data suggests phosphorylation of PAR-1/MARK by atypical protein kinase C (aPKC) favours 14-3-3 binding and can cause changes in subcellular localisation (Hurov et al., 2004; Kusakabe and Nishida, 2004; Suzuki et al., 2004b). Another study showed that this interaction with 14-3-3s is mediated by several phosphorylation sites (Goransson et al., 2006), but it has no apparent effect on catalytic activity (Al-Hakim et al., 2005).

1.2.4 AMPK-related kinases and other signalling pathways

Due to the interest in LKB1 and its downstream functions, recent effort has focussed on understanding the regulation of the AMPK-related kinases and other signalling pathways in which they are involved. Although research in this area is not as extensive as the work on AMPK itself, there are still some interesting indications of the function of the AMPK-related kinases and potential crosstalk with other well characterised pathways (Bright et al., 2009). There are broadly four subfamilies of kinases within the AMPK-related kinases (MARKs, BRSKs, SIKs and NUAKs) and of these, the MARKs have been studied most extensively.

1.2.5 MARK/PAR family

Microtubule affinity-regulating kinases (MARKs) were originally identified in the brain and so named because they are able to regulate the interaction of microtubule associated proteins (MAPs) and microtubules (Drewes et al., 1997). In particular, MARK phosphorylation of a well characterised microtubule organising protein tau causes dissociation from microtubules and destabilisation of the whole microtubule network (Stoothoff and Johnson, 2005). Tau is also known to have a role in controlling transport along the microtubule network by blocking interactions with motor proteins (Stamer et al., 2002). There is also an increasing body of evidence that tau plays a role in the development of neural pathologies such as Alzheimer's disease and that dysregulation of associated pathways may be responsible for further neural damage (Weiner, 2013). In *Drosophila,* the neurotoxic effects of tau can be reduced by expressing tau protein mutated at two serine residues. These residues lie in the domain responsible for microtubule association and are phosphorylated by the *Drosophila* homologue of the MARK proteins, partitioning defective mutant 1 (PAR-1) (Nishimura et al.,

2004). These mutations also prevented hyperphosphorylation of tau at different residues by other kinases and it has been suggested that phosphorylated tau may be cleaved and can then aggregate to form filaments and insoluble neurofibrillary tangles seen in neuropathies such as Alzheimer's disease (Gamblin et al., 2003).

Studies investigating the MARK homologues in the PAR family of kinases in other model organisms such as *Drosophila* and *C. elegans* have revealed some additional functions. The family was originally identified as a regulator of embryonic polarity and partitioning in *C. elegans* (Kemphues et al., 1988). The PAR family have also been shown to be required for the establishment of cell polarity in a series of other model organisms (reviewed in Marx et al., 2010). PAR proteins have been implicated in neuron growth, as overexpression of MARK2 inhibits axon formation and polarization of neurones (Chen et al., 2006). Another study has provided links to calcium-dependent pathways as Ca^{2+}/calmodulin dependent kinase I (CaMKI) is known to phosphorylate MARK2 and promote neurite outgrowth (Uboha et al., 2007). Conflicting reports in different organisms have shown the PAR family interacting and controlling elements of the Wnt signalling pathways, thereby influencing cell growth and proliferation (Figure 1.8) (Kusakabe and Nishida, 2004; Sun et al., 2001). Some reports suggest that different isoforms of PAR-1 (i.e. MARK1 – 4 in mammals) may control different parts of the Wnt signalling pathways (Mamidi et al., 2012; Ossipova et al., 2005).

MARK1 might be involved in synaptic plasticity because potassium chloride-induced depolarization of neurons and neurotrophic factors increase MARK1 activity (Jeon et al., 2005). MARK2 knockout mice models indicated a variety of functions such as fertility, metabolic processes and regulation of the immune system (Bessone et al., 1999; Hurov and Piwnica-Worms, 2007; Hurov et al., 2001). MARK3 has been shown to inactivate Cdc25 phosphatase, important for the control of the cell cycle, which prevents activation of the Cdc2/cyclin B complex by dephosphorylation, which is required for entry into mitosis (Peng et al., 1998). MARK3 is also known to be downstream of Pim-1, regulating the same Cdc25 signal at the G2/M cell cycle checkpoint (Bachmann et al., 2004). MARK3 has also been shown to interact with the Ras-MAPK pathway via the kinase suppressor of Raf-1 (KSR1) (Muller et al., 2001). One isoform of MARK4 is highly expressed in hepatocellular carcinomas (Beghini et

al., 2003; Kato et al., 2001), which suggests that it may play a role in tumour progression (Figure 1.8).

1.2.6 BRSK family

The BRSKs have the most tightly controlled expression of all the AMPK-related kinases as they are almost exclusively expressed in the brain, with a low level of expression detected in the testis and pancreas (Bright et al., 2008; Hezel et al., 2008; Inoue et al., 2006; Kishi et al., 2005). Homologues have been identified in *Drosophila* and *C. elegans* as Synapses of the Amphid Defective (SAD kinases) and shown to be regulators of neuronal polarity (Crump et al., 2001). Research into the area of SAD kinases in other model organisms (SAD-A = BRSK2, SAD-B = BRSK1) have revealed more information about the way they are regulated, but some recent studies have investigated BRSK proteins in mammalian systems. Mice with each kinase deleted individually were healthy, but double mutants showed poor responsiveness to physical stimulation and died shortly after birth, indicating that neuronal function was severely impaired and suggesting there may be redundancy within the BRSK family (Kishi et al., 2005). Double knockout mice have thinner cortices and individual neurones lack distinct neural outgrowths, possibly regulated by tau phosphorylation (Kishi et al., 2005). Interestingly, pyramidal neuron-specific LKB1 knockout mice showed a similar phenotype to the BRSK double knockout mice, indicating that the AMPK-related kinases probably play a role in regulating the tissue-specificity of the downstream functions of LKB1 (Barnes et al., 2007).

Recent evidence has indicated a function for these kinases outside the brain, as BRSK2 has been shown to be a downstream mediator of mTOR signalling in the pancreas (Nie et al., 2013). BRSK2 deletion leads to reduced glucose-stimulated insulin secretion from isolated β-cells, similar to the phenotype of deletion of S6 kinase 1, a downstream target of mTORC1 (Nie et al., 2013). BRSK2 expression can be stimulated by glucose and inhibited by rapamycin, implicating mTOR signalling and potential interaction with other metabolic processes (Figure 1.3 and Figure 1.4).

1.2.7 SIK family

The salt-inducible kinases (SIK) family of proteins were first identified from the adrenal glands of rats fed a high-salt diet, suggesting its involvement in gene expression after stimulation by the steroid adrenocorticotropic hormone (ACTH) (Wang et al., 1999). As the name would suggest, rises in intracellular sodium can increase expression of SIK1, which activates the Na^+/K^+ ATPase that in turn regulates various essential cell functions (Popov et al., 2011; Sjostrom et al., 2007). High sodium levels also increase calcium levels in the cell because ion pumps exchange sodium and calcium and the high calcium concentration activates CaMK which is thought to be able to phosphorylate and activate SIK1 (Sjostrom et al., 2007). There are thus multiple potential upstream kinases and the AMPK-related kinases may be involved in pathways decoding many extrinsic signals. SIK2 appears to be ubiquitously expressed (Xia et al., 2000) but particularly high expression has been shown in adipose tissue where it can phosphorylate insulin receptor substrate-1 (IRS1) (Horike et al., 2003). This phosphorylation is at the same site that is phosphorylated by AMPK (Jakobsen et al., 2001), which suggests SIK2 may be involved in insulin signal transduction and there could be some convergence between the AMPK and the AMPK-related kinase pathways (Figure 1.8). SIK2 also crosses over into other AMPK targets by phosphorylating CRTC2 at the AMPK site and preventing CREB-activated transcription (Figure 1.4) (Screaton et al., 2004). SIK3 may interact with pathways regulating cell proliferation, as mitotic defects have been observed following knockdown of the *Drosophila* homologue, QSK (Bettencourt-Dias et al., 2004).
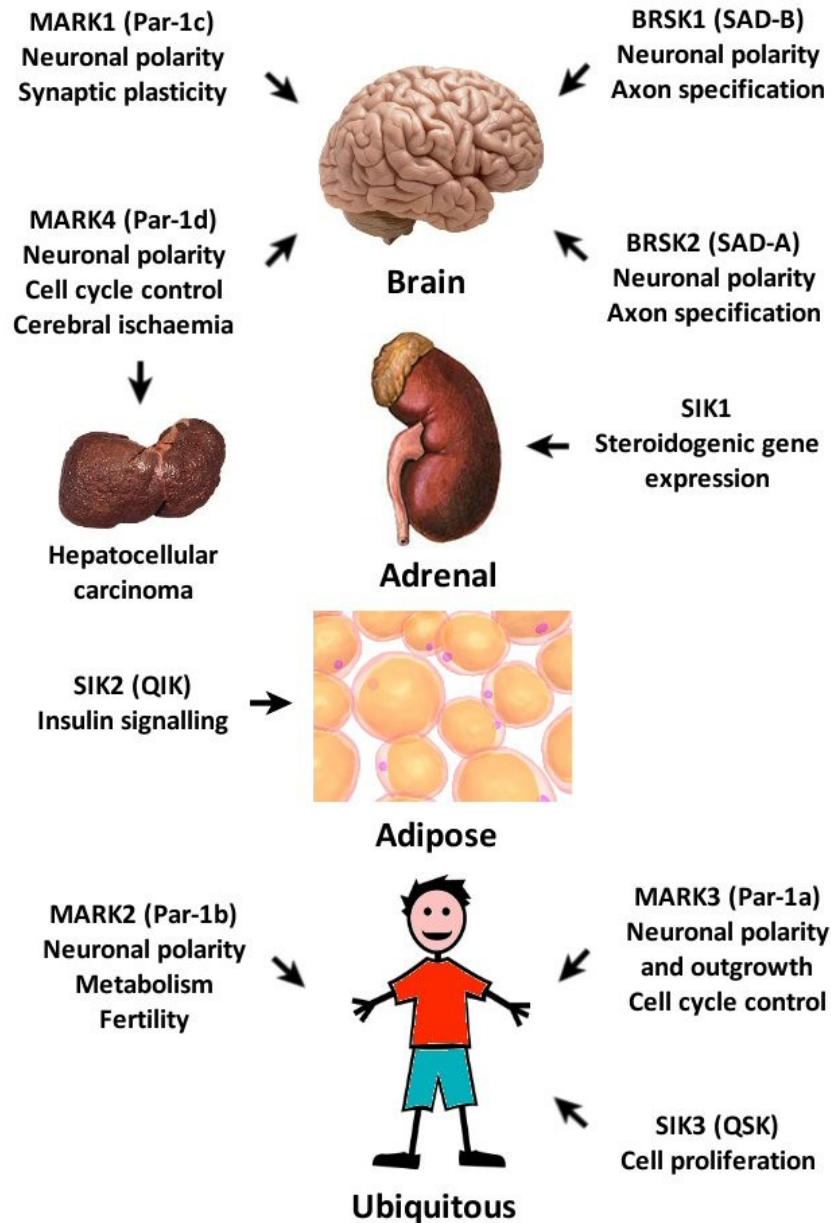
Figure 1.8 Functional roles and tissue specificity of AMPK-related kinases (adapted from Bright et al., 2009)

The various roles of AMPK-related kinases (with homologue names in brackets) are shown alongside the predominant site of expression. The exact expression profile of some of the kinases is unclear and there is likely to be lower expression in other tissues. The broad range of functions of the AMPK-related kinases suggest their involvement in many signalling pathways.

1.3 NUAK1

Nua (novel) kinase 1 (NUAK1) (also known as AMPK-related kinase 5, ARK5) is of particular interest, as various reports in the literature have indicated that it is involved tumour progression and senescence (Humbert et al., 2010; Kusakai et al., 2004a; Suzuki et al., 2003a; Suzuki et al., 2003b). Previous studies have suggested many interesting biological functions for NUAK1, however none of these observations provide coherent evidence for its function and regulation and there is little evidence for its role in cellular functions *in vivo*.

1.3.1 NUAK1 homology, expression, structure and regulation

The human NUAK1 protein is comprised of 661 amino acids (MW ≈ 76 kDa) and mouse NUAK1 has 658 amino acids and 100% homology across the kinase domain compared to human NUAK1 (Figure 1.5 and Figure 1.9) with various orthologues identified in other species (Figure 1.9). In a study to assess the global NUAK1 mouse knockout, expression was assessed by βgal inserted into the NUAK1 gene and by *in situ* hybridisation to look at mRNA levels (Hirano et al., 2006). The two methods correlated well, showing that mRNA levels should be an accurate indicator of protein expression in adult tissues. At embryonic day 9.5 βGal expression was found throughout the undifferentiated neuroectoderm and was ubiquitous in the epidermis but particularly highly expressed in the ventral body wall. At E14.5 and E18.5 βGal expression was only seen in differentiated areas of the cortex but not in other brain areas and was maintained in the epidermis of the whole body.

An early study on NUAK1 activation in rat skeletal muscle investigated the expression profile in adult tissues and found mRNA present in heart, kidney, brain, liver, and skeletal muscle (Fisher et al., 2005).

A

B
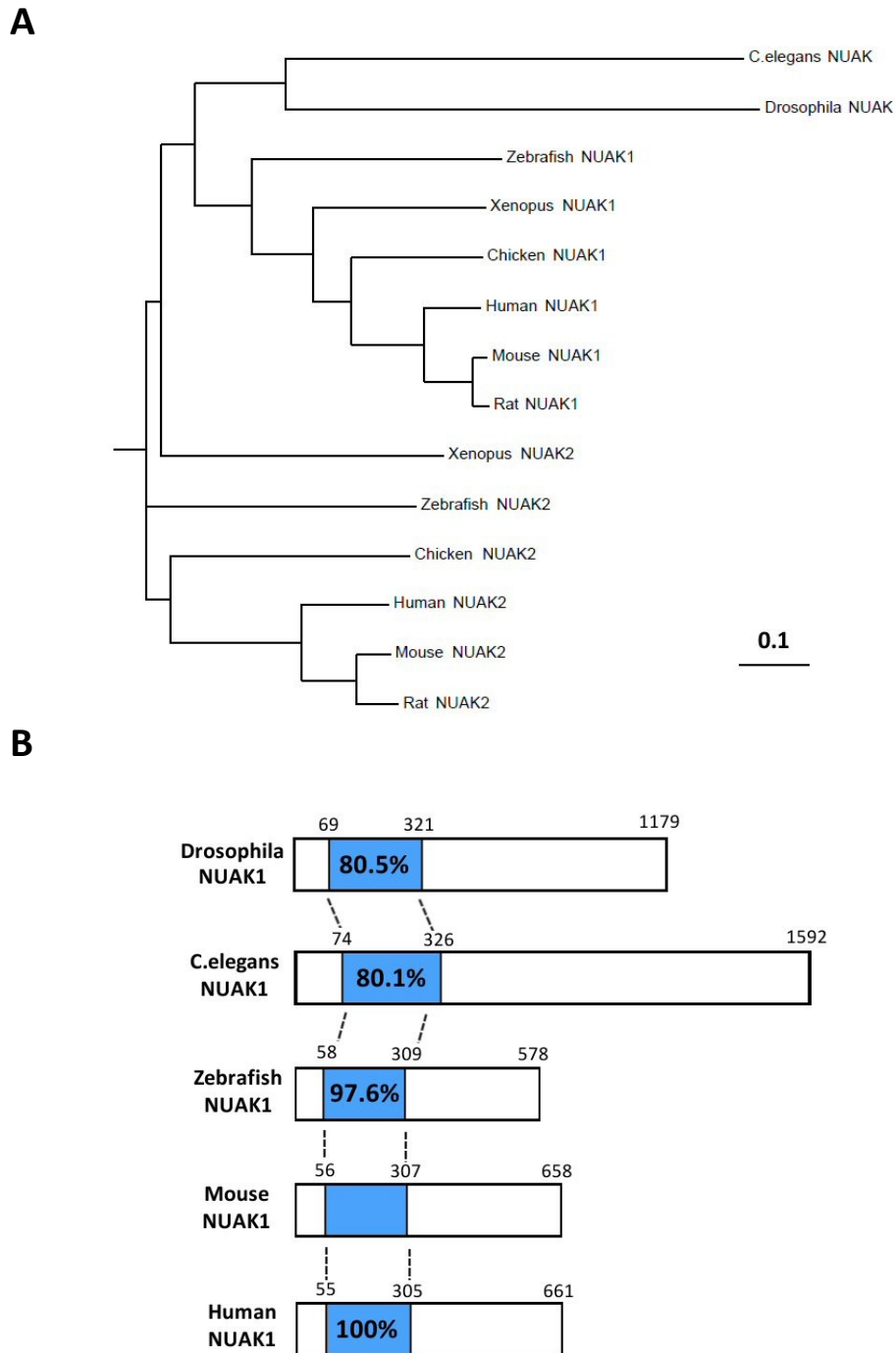
Figure 1.9 Homology of NUAK1 in various species (adapted from Hirano et al., 2006)

(A) A phylogenetic tree of NUAK1 and NUAK2 orthologues from various species are shown, displaying the genetic divergence between the two NUAK family kinases and the distant relationship of the vertebrate orthologues to the *C. elegans* and *Drosophila* proteins. **(B)** The domain structure of various NUAK1 orthologues and the kinase domains are highlighted. The percentage figures show the level of homology to the mouse NUAK1 kinase domain and the numbers indicate the relevant residues within the protein.

Like all the AMPK-related kinases, NUAK1 has a highly conserved T loop and a critical threonine residue in the catalytic domain (Figure 1.5). The conserved threonine (residue 211 in human NUAK1) can be phosphorylated and activated by LKB1 (Lizcano et al., 2004) and other reports have suggested that NUAK1 can be activated by phosphorylation on serine 600 by Akt (Suzuki et al., 2004b).

Initially, only a few laboratories studied the role of NUAK1 and various reports emerged from Hiroyasu Esumi's group in Japan, including an initial report identifying NUAK1 by homology to the previously discovered NUAK2 (Suzuki et al., 2003b). However much of the biochemical analyses in these studies were carried out by observing cross-reaction with an antibody generated against a peptide from human NUAK2 (KKPRQRESGYYSSPEPS, residues 450 - 467). The group were interested in studying the connection of the AMPK family to metabolic processes in cancer cells, particularly the Akt pathway (Suzuki et al., 2003b). NUAK1 was an attractive candidate for this as it contains a conserved Akt consensus sequence (residues 595 – 600), but there are concerns that the methods used would not conclusively rule out a role for other AMPK-related kinases (Suzuki et al., 2003b). Another report from the same group identified Nuclear Dbf2-Related Kinase 2 (NDR2) as a novel upstream kinase of NUAK1, capable of phosphorylating it on the critical T211 residue (Suzuki et al., 2006). NDR2 was identified by sequence homology to AMPK upstream kinases LKB1 and CaMKKβ but the confirmation of the role *in vitro* and the biochemical methods used are unclear, leading to concerns about the conclusions. Similarly reports that NUAK1 phosphorylation is stimulated by muscle contraction, insulin and AICAR have related issues with the methods, as much of the blotting data uses the same cross-reacting antibody and no significant difference in NUAK1 activity was measured (Fisher et al., 2005).

Other reports in the literature have described a possible role for NUAK1 in controlling cell adhesion through regulating the phosphorylation of MYPT1 which, in a complex with PP1β, can dephosphorylate MLC (Zagorska et al., 2010). The proposed model involves 14-3-3 binding to MYPT1 and reducing phosphatase activity but there may be many other aspects such as interaction with other partner proteins or other kinases affecting the system. This study also identified a conserved motif (Gly-Ile-Leu-Lys or GILK motif) that mediates the binding of NUAK1 to PP1β (Zagorska et al., 2010). Interestingly, NUAK2, which likewise

contains a GILK motif, has also been implicated in the phosphorylation of MYPT1 (Yamamoto et al., 2008). Taken together, there may be redundancy between these two protein kinases as the latter study confirmed that NUAK2 can interact with PP1β. NUAK1 and NUAK2 are the only AMPK-related kinases that contain GILK motifs and so this mechanism of myosin phosphatase regulation may be specific to them. Consistently, the involvement of the *C. elegans* homologue of the NUAK family (unc-82) in myosin organisation during development has been described (Hoppe et al., 2010). Another piece of supporting data from a large scale screen identified NUAK1 as one of two candidate loci for the determination of muscle strength, indicating an involvement in muscle development and myosin organisation (Windelinckx et al., 2011).

It is currently unclear if NUAK1 requires dimerization or partner proteins for activity, like AMPK, but recent data regarding the structure and activation of members of the MARK/PAR family indicate that they are capable of autoactivation (Marx et al., 2010), and this may be true of other related kinases. Another AMPK-related kinase, MELK, has intrinsic activity and is capable of autophosphorylation with no involvement of LKB1 for activation (Lizcano et al., 2004).

Very recent data has emerged showing that NUAK1 may have other functions in different tissues, such as controlling axon branching by interfering with mitochondrial transport (Courchet et al., 2013). NUAK1 can be regulated by microRNAs, specifically miR-211 (Bell et al., 2013). The downregulation of NUAK1 by miR-211 led to increased cell adhesion in melanoma cells and provides another clue to the role of NUAK1. Importantly, all these data may link with the myosin organisation phenotype seen in *C. elegans* and may be modulated by components of the same pathways, meaning downstream effects of NUAK may converge on MYPT and PP1β (see section 1.5).

All of the other information gathered to date regarding the function and regulation of NUAK1 has come from screens looking at cancer progression and cell proliferation. Some of these data may link with the pathways identified above but more work will be required to confirm the functional relevance of NUAK1 in these pathways.

1.3.2 NUAK1 in cancer, cell proliferation and senescence

Most of the earliest reports that NUAK1 is involved in regulating cell proliferation and possible cancer phenotypes also came from Hiroyasu Esumi's group and they all suggested that NUAK1 was pro-proliferative (Kusakai et al., 2004a; Kusakai et al., 2004b; Suzuki et al., 2005). Increased NUAK1 mRNA was detected in human cancer biopsies and cell lines. However, there was no evidence of increased NUAK1 kinase activity. The only suggested downstream mechanism for how NUAK1 promoted cell proliferation and invasion was by regulation of caspase-6, indicated by coincident expression in colorectal cancer cells (Suzuki et al., 2004a). While this is a possible mechanism, NUAK1 is a protein kinase whose downstream targets would not be regulated by changes in their expression but by changes in their phosphorylation.

Contrary to these reports, data emerged from our laboratory, in collaboration with others, that downregulation of NUAK1 leads to an increase in replicative lifespan and a reduction in senescence (Humbert et al., 2010). This report also showed a requirement for LKB1 activation of NUAK1, consistent with previous reports that this is an upstream kinase for NUAK1 (Lizcano et al., 2004). The mechanism proposed for the effect on senescence was regulation of large tumour suppressor kinase 1 (LATS1) as NUAK1 was shown to phosphorylate it directly and a dominant-negative version had the same phenotypic effect as NUAK1 knockdown (Humbert et al., 2010). Another report investigating cancer models with deregulated MYC expression found that NUAK1 depletion prolonged cell survival by maintaining metabolic homeostasis (Liu et al., 2012). However, the mechanism proposed for this was partly via direct phosphorylation and regulation of AMPK and mTORC1 (Figure 1.3), which has not been reported by any other group despite numerous studies on AMPK activation (Hardie, 2008).
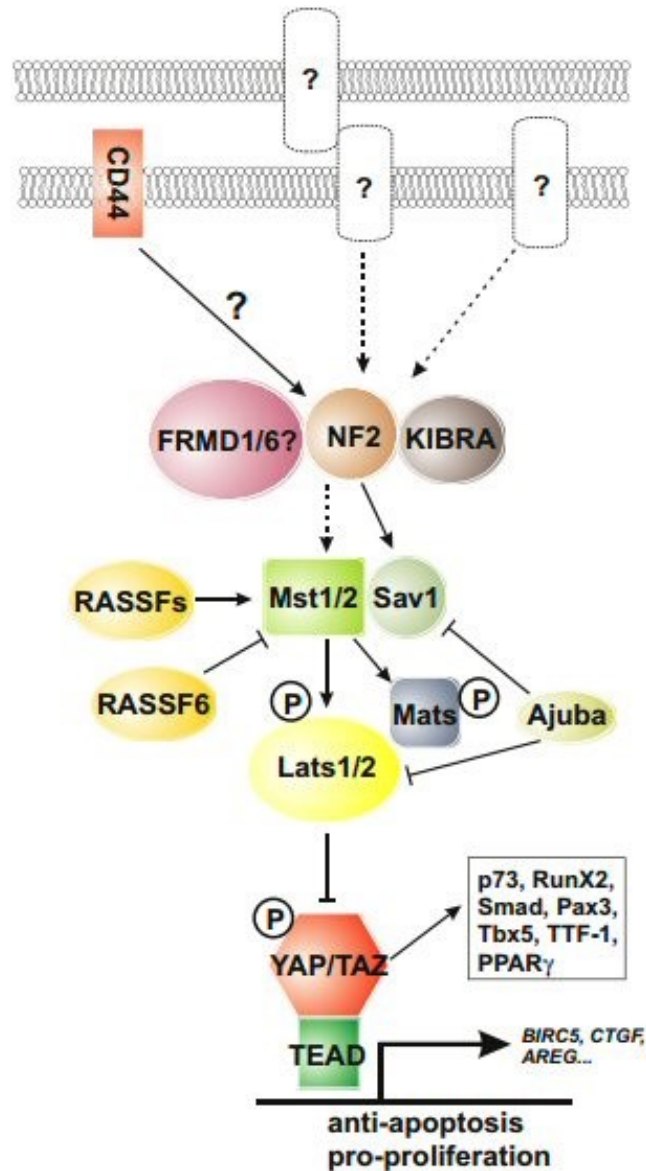
Figure 1.10 The Hippo pathway (from Pan, 2010)

The Hippo pathway is a growth regulating signalling pathway first identified in *Drosophila* but the components of the cascade are highly conserved in mammals. Known direct interactions are shown by solid lines or as proteins in direct contact with each other. Dashed lines indicate potential interactions identified by homology from the *Drosophila* pathway but for which there is currently no evidence.

The finding that NUAK1 can phosphorylate and activate LATS1 links it to a highly conserved growth regulating signalling pathway, Hippo, known to be involved in the control of organ size (Pan, 2010). The main end target of the Hippo pathway is the inactivation of transcriptional coactivators Yes-associated protein (YAP) and transcriptional coactivator with PDZ-binding motif (TAZ), which in turn regulate the expression of a number of genes as shown in Figure

1.10. Overexpression of YAP is capable of mimicking loss of Hippo signalling and producing vastly oversized organs, also leading to hepatocellular carcinoma when overexpressed in mouse liver (Dong et al., 2007). Reports that NUAK1 can phosphorylate and reduce expression of LATS1 would suggest that it can control the Hippo pathway to activate YAP/TAZ, leading to an increase in proliferation and organ size. This suggests that the presence of NUAK1 would be pro-proliferative but other studies in human cell lines have suggested that LATS1 downregulation causes irreversible cell cycle arrest in normal human cells, implicating an anti-proliferative role for NUAK1 (Humbert et al., 2010; Takahashi et al., 2006).

To further complicate the situation, several other reports have appeared in the past two years supporting the initial hypothesis that NUAK1 activity promotes proliferation, at least in certain cancer models including breast (Chang et al., 2012), glioma (Lu et al., 2013), non-small cell lung cancer (Chen et al., 2013a) and hepatocellular carcinoma (Cui et al., 2013). An isolated study also reported that NUAK1 was capable of directly phosphorylating and regulating p53, leading to cell cycle arrest (Hou et al., 2011). However, no such mechanism has since been reported despite many other validated upstream kinases of p53 and numerous reports studying its role in cell proliferation (Carvajal and Manfredi, 2013). NUAK1 can regulate adhesion in melanoma cells and may function to control the balance between tumour growth and metastasis, but it is unclear if it has a direct pro or anti-proliferative effect (Bell et al., 2013).

1.3.3 NUAK1 global knockout and omphalocele

Efforts to identify novel genes involved in brain development in mice led to the creation of a global NUAK1 knockout, then termed omphalocele kinase 1 (Omphk1), due to the phenotype created by the deletion of the gene (Hirano et al., 2006). Despite the interest in the gene due to its expression in the brain, the main phenotype was in the ventral body wall. The knockout was generated by inserting the *lacZ* gene just after the translation initiation site to investigate expression by *βgal* staining and knockout was confirmed by RT-PCR. No live NUAK1 knockout embryos were born and the embryos displayed an omphalocele phenotype by embryonic day 14.5, showing it much more markedly by day 18.5 (Hirano et al., 2006). NUAK1 was expressed in both sternal and abdominal bands, but the latter failed to fuse properly across the central

abdomen. Prior to embryonic day 12.5, the knockout embryos were normal and the area covered by the primary body wall was shown to express NUAK1 (Hirano et al., 2006). The pathways involved in mediating this phenotype were not investigated and it was highlighted that several screening studies previously showed other kinases are expressed in the ventral body wall (Carninci et al., 2005; Okazaki et al., 2002; Stopka and Skoultchi, 2003).

An omphalocele phenotype is an abdominal wall defect, where various internal organs remain outside the abdomen surrounded by a membrane because of a defect in the closure of the abdominal wall. These sorts of malformations are one of the primary forms of physical human birth defects and are present in about 1 in every 2000 – 4000 live births (Brewer and Williams, 2004a). In humans there is a high rate of mortality (25%) and often other associated pathologies such as neural tube defects. In a small proportion of human cases, chromosomal abnormalities have been detected but the exact pathways involved in this phenotype are unclear (Brewer and Williams, 2004a). Some cases have been linked to trisomy 18 (Kanagawa et al., 2002) and trisomy 13 (Yatsenko et al., 2003). NUAK1 is located on human chromosome 12 (12q23.3) and therefore is unlikely that the omphalocele phenotype has the same underlying cause that produces the effect in NUAK1 knockout mice. Recent data from mouse knockouts have also provided some clues as to the pathways involved, as the following transgenic models all display ventral body wall defects: AP-2α (Brewer and Williams, 2004b), Hoxb2/b4 double mutant (Manley et al., 2001), Tgfβ2/β3 double mutant (Dunker and Krieglstein, 2002), Mab21l2 (Yamada et al., 2004) and ROCK-I/ROCK-II double knockout (Thumkeo et al., 2005).

Recent data from Shinichi Aizawa's laboratory has shown the mouse global knockout of NUAK1 and NUAK2 displays similar embryonic lethality due to exencephaly, facial clefting, and spina bifida in addition to failure of the ventral body wall to close (Ohmura et al., 2012). The report showed changes in the accumulation of various cytoskeletal components including phosphorylated MLC, F-actin, and cortactin in the developing neural plate, indicating possible downstream targets (Ohmura et al., 2012).

1.3.4 NUAK1 muscle specific knockout

Due to the embryonic lethality of NUAK1 global knockout mice, it has been impossible to assess the physiological role of the kinase in adult tissues so studies have been conducted using conditional tissue-specific deletions. Only one report to date has shown a skeletal muscle-specific knockout of NUAK1 by deleting the kinase using cre-recombinase under the control of the muscle creatine kinase (MCK) promoter (Inazuka et al., 2012). The choice of skeletal muscle as a target tissue was based on previous expression data from the same group (Fisher et al., 2005). No basal phenotype was observed, suggesting that there is no significant developmental effect of deleting NUAK1 in muscle. However, on a high fat diet, muscle-specific NUAK1 knockout mice had lower fasting blood glucose levels, improved glucose tolerance and increased muscle glycogen (Inazuka et al., 2012). The suggested mechanism for this was by controlling phosphorylation of insulin receptor substrate 1 (IRS1), although no direct interaction was shown, only evidence for increased phosphorylation in knockouts. These data, combined with previous inconsistent reports from the same laboratory (Fisher et al., 2005) could suggest that NUAK1 is affecting IRS1 phosphorylation via activation or inhibition of other pathways, rather than by any direct binding to the substrate.

1.4 LKB1

1.4.1 LKB1 structure and regulation

LKB1 was first identified after looking for the genetic determinant of the human cancer pre-disposition condition called Peutz-Jeghers syndrome (PJS). The gene or genes responsible were first narrowed down to a locus on chromosome 19 (Hemminki et al., 1997). After various attempts to identify mutations in genes from this region that were linked to PJS it was narrowed down to a kinase that had previously been identified as part of a genetic screen (Hemminki et al., 1998; Su et al., 1996). A parallel study also identified mutations that correlated with PJS and termed the kinase serine threonine kinase 11 (STK11) (Jenne et al., 1998). The initial screen that identified LKB1 showed that it has a high degree of homology with XEEK1 which is known to be expressed in early *Xenopus* embryos and is phosphorylated by PKA (Su et al., 1996).

A systematic study of the entire human kinome after the publication of the human genome showed that there is only one LKB1 gene in humans, which is composed of ten exons (nine coding exons) and spans 23kb. Recent data has shown that there are two LKB1 splice variants, termed LKB1 long (LKB1L) and LKB1 short (LKB1S) (Denison et al., 2009; Towler et al., 2008). The short form of LKB1 has restricted tissue distribution and appears to be predominantly expressed in the testis, whereas the LKB1L form appears to be expressed ubiquitously (Alessi et al., 2006; Denison et al., 2009). The only function that has been described for LKB1S is a role in spermatogenesis (Denison et al., 2011; Towler et al., 2008) and although there is not yet any evidence for it, this variant could play a role in regulating the AMPK-related kinases.

Human LKB1 consists of 433 residues and the catalytic domain (residues 49–309) shares some sequence identity with AMPK and its related kinases (Figure 1.11C) (Manning et al., 2002; Zeqiraj et al., 2009). The non-catalytic regions of the kinase do not seem to share homology with any other proteins and do not contain any known functional domains, although there is a farnesylation site at the C-terminus of the long form. Expression analyses show that it appears to be ubiquitously expressed across all the adult and foetal tissues that were examined (Hemminki et al., 1998). Various biochemical studies since the initial discovery have determined that LKB1 forms a complex in mammalian cells with two other proteins called STE20-related adaptor (STRAD) and mouse protein 25 (MO25) (Figure 1.11). Both these partner proteins are required for maximal LKB1 activity and STRAD has been identified as a pseudokinase, which may be a vestigial upstream kinase that evolved to become a scaffold. Also, various cell based studies have shown that changes in STRAD and MO25 expression can influence the binding and sub cellular localisation of LKB1 (Boudeau et al., 2003). Numerous studies have showed that LKB1 is constitutively active in all the cell types it has been found in, by immunoprecipitation of LKB1 complexes from tissue and cell extracts and through observing no change in LKB1 activity under conditions known to activate its downstream target AMPK (Sakamoto et al., 2004; Woods et al., 2003).

A
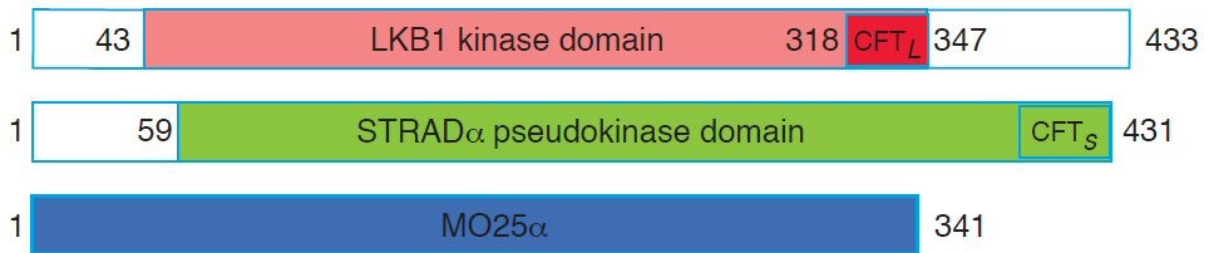
B
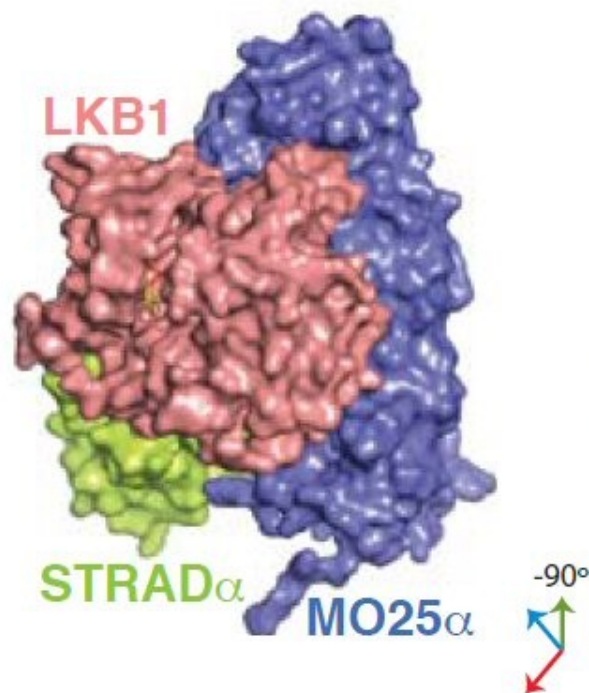
C

T172 in AMPK equivalent

```
LKB1       173 VHKDIKPGNILLTTGGTLKISDLGVAEALHPFAADDTCRTSQGSPAFQPPEIANGLDTESG
AMPKα1     162 VHRDLKPENVLLDAHMNAKIADFGLSNM---MSDGEFLRTSCGSPNYAAPEVISGR-LYAG
NUAK1      175 VHRDLKLENILLDDNCNIKIADFGLSNL---YQKDKFLQTFCGSPLYASPEIVNGR-PYRG
consensus  198 VHrDlKpeNlLLd   nlKIaDfGlsnm    f  ddflrTscGSP ya PEiinGr  y G
```

Figure 1.11 Structure and sequence homology of the LKB1 complex (adapted from Zeqiraj et al., 2009)

(A) Domain structure of LKB1, STRADα and MO25α **(B)** Surface representation of the three dimensional crystal structure of the LKB1 complex, showing a potential function of MO25 in holding the complex together. **(C)** Sequence alignment of the human kinase domains of LKB1 (the catalytic part of the LKB1 complex), AMPKα1 and NUAK1 showing the sequence similarity between the three kinases.

51

1.4.2 LKB1 as a tumour suppressor

Early biochemical studies of the role of LKB1 quickly suggested that it may have a key role in cell cycle progression and cell proliferation, because overexpression of active LKB1 in cell lines known not to express LKB1 endogenously, such as HeLa, caused a G1 cell cycle arrest (Tiainen et al., 1999). In the same study catalytically inactive mutants, including known PJS mutations, were found not to arrest the cell cycle despite similar over expression.

Before tissue specific knockouts of LKB1 were developed there were studies using heterozygous germ line deletions of LKB1 investigating the effect of partial loss of activity *in vivo.* Given the involvement of LKB1 in PJS and potential tumour suppressor effects, much of the focus was on the incidence of cancer within this model. The most striking observation was the high level of hepatocellular carcinomas (HCC), particularly in male mice (Nakau et al., 2002). In terms of LKB1 activity, conflicting reports have been made about whether total or partial loss of LKB1 can lead to formation of polyps and tumours. Various groups showed that LKB1 expression in polyps from PJS patients was approximately half the normal level, suggesting that the heterozygosity gene dosage effect was enough to form tumours (Jishage et al., 2002; Miyoshi et al., 2002; Rossi et al., 2002). A parallel report also showed that many polyps isolated from heterozygous LKB1 mice showed total loss of LKB1 expression, either through gene inactivation or loss of the wild-type allele (Bardeesy et al., 2002). These studies did not look at the biochemical basis for this effect, but it suggests that loss or lower activity of LKB1 and pathways downstream of it may be responsible for the increased incidence of polyps and hepatocellular carcinomas.

1.4.3 LKB1 heart-specific mouse knockout

Due to the role of LKB1 as a tumour suppressor and being upstream of AMPK there has been significant interest in studying the *in vivo* role of the kinase using mouse knockout models. Early attempts to use gene targeting to delete the gene throughout the entire body caused embryonic lethality in mid-gestation due to death of mesenchymal cells, defects in vascular development and malformations of the neural tube (Ylikorkala et al., 2001). In recent years it

has become more feasible to use conditional gene targeting technology such as FLP recombinase and tissue specific expression of cre recombinase to alter the expression of genes in individual tissues. This allows much more detailed analysis of the physiological role within certain cell types and provides a mechanism to study the role of genes, such as LKB1, that cause embryonic lethality when knocked out in the entire organism.

A recent study used cre recombinase under the control of the α myosin heavy chain (αMHC) promoter to delete LKB1 specifically in cardiac myocytes (Ikeda et al., 2009). Previous models to study cardiac-specific deletion of LKB1 had used cre recombinase under the control of the muscle creatine kinase (MCK) promoter but other work has highlighted various issues with incomplete gene deletion using the MCK-cre strategy (Sakamoto et al., 2006; Shield et al., 1996).

Cardiac-specific LKB1 knockout mice showed cardiac dysfunction characterised by atrial enlargement and fibrillation in younger mice. Left ventricular hypertrophy was seen in older mice but not in younger mice and the cardiac dysfunction led to death within 6 months of birth (Ikeda et al., 2009). This study also looked at effectors downstream of LKB1 to determine the pathways involved in mediating this effect. Collagen I and III mRNA levels were higher, along with an increase in atrial fibrosis while phosphorylation of AMPK was reduced. However, mTOR and p70S6 kinase phosphorylation were both higher (Ikeda et al., 2009). While this indicates that AMPK and mTOR pathways discussed earlier may be involved in this effect, it does not rule out the involvement of other effectors downstream of LKB1.

As one of the main downstream signalling targets of LKB1, the role of AMPK in the heart has been extensively studied using mouse knockouts. A study investigating the deletion of AMPKα2, the predominant catalytic subunit in the heart, showed it does not cause any basal functional or morphological adaptations, but impairs glucose uptake and consequently glycogen production (Carvajal et al., 2007). Also, overexpression of a dominant-negative form of AMPKα2 was shown to cause a decrease in basal cardiac contractility (Li et al., 2004). Conflicting reports highlight the difficulty of interpreting results and the inherent problems with using different background strains and experimental conditions (Viollet et al., 2009). Also, various mutations in the AMPKγ subunit are known to increase glycogen storage and

cause a cardiomyopathy called Wolff-Parkinson-White (WPW) syndrome. Transgenic mouse models of these mutations in the heart have been thoroughly characterised and show the importance of these signalling pathways in cardiac development and metabolism (Dyck and Lopaschuk, 2006).

The contrast between the phenotype of the LKB1 heart knockout and the absence of a basal contractility phenotype in the AMPKα2 heart knockout indicate that there may be a significant role for other pathways influenced by LKB1, such as the AMPK-related kinases.

1.4.4 LKB1 liver-specific mouse knockout

Given the strong association with AMPK and the key role of AMPK in metabolism, various studies have investigated the role of LKB1 in the liver. The liver plays a key role in several metabolic functions including bile production and regulation of glucose and lipid levels. Deletion of LKB1 in the liver of adult mice caused an almost complete loss of AMPK activity, indicating that LKB1 is the major pathway for AMPK activation in this organ (Shaw et al., 2005). The functional effect was severe hyperglycaemia and an increase in expression of genes involved in glucose and lipid synthesis. Another interesting metabolic effect was the dephosphorylation of CRTC2, increasing the expression of PGC-1α, which plays a key role in increasing gluconeogenesis (Shaw et al., 2005). Another important finding in this report was that the action of metformin, a pharmacological activator of AMPK, requires the presence of LKB1 *in vivo* (Shaw et al., 2005). This suggests that metformin acts via LKB1 and therefore may affect other downstream pathways. However the effect of metformin could be due to ATP depletion and therefore be specific to AMPK.

Other functional effects of the loss of LKB1 in the liver, particularly with reference to cellular processes not directly linked to AMPK, have been investigated. A role for LKB1 in sub cellular organisation and targeting proteins to the cell membrane has been highlighted (Fu et al., 2010). A similar LKB1 liver-specific knockout mouse model displayed malformed bile ducts and canaliculi, which results in poor bile acid clearance and build-up of bile acids in the liver and serum (Woods et al., 2011). The basis for this effect is the mis-localisation of a key membrane transporter bile salt export pump (BSEP). The observation that LKB1 is involved in

establishing cell polarity is backed up by other reports (Baas et al., 2004) and indicates that there may be other mechanisms downstream of LKB1 controlling this effect.

1.5 Myosin organisation and regulation in cell division

Cellular myosin II is a key component of the cytoskeleton and plays an important role in cell division. The regulation of myosin contractility is therefore important for controlling proliferation and cell growth. Functionally, myosin II is made up of heavy and light chains and is activated by phosphorylation of the regulatory light chain (MLC) at either T18 or S19 (Moussavi et al., 1993). The phosphorylation of these residues promotes interaction with actin to form an actomyosin complex, thereby increasing contraction. The activation of MLC by phosphorylation also promotes the formation of myosin filaments which are important in the formation of filopodia and lamellipodia (Ikebe et al., 1988; Scholey et al., 1980).

Several kinases are known to phosphorylate MLC at the activating residues *in vitro* or *in vivo* (Figure 1.12). All of these kinases are themselves part of wider regulatory networks and can be controlled by various upstream proteins or external signalling molecules. This range of activators of MLC seems to be important for the spatial subcellular control of MLC activation. In the case of MLCK and ROCK, phosphorylation of MLC occurs in different parts of the cell (Totsukawa et al., 2000).

The processes controlling dephosphorylation of MLC are equally important for regulating its activity. The primary myosin phosphatase consists of three subunits: a large regulatory subunit called PPP1R12A (MYPT1), a catalytic subunit which is an isoform of PP1C and another smaller subunit whose role is unclear (Hartshorne et al., 2004). MYPT1 acts as a partner protein and helps to target the catalytic subunit of PP1C to the myosin (Alessi et al., 1992). It is important to bear in mind that several of the upstream activators which cause MLC phosphorylation can also exert an effect on the phosphatase (Figure 1.12).

AMPK can target PAK2, an upstream kinase of MLC, which plays a crucial role in regulating cytoskeletal organisation. An inactivating mutation of the AMPK target site on PAK2 led to decreased phosphorylation of MLC in response to AMPK activation (Banko et al., 2011). The

same study also showed AMPK can phosphorylate PPP1R12C, another of the myosin phosphatase targeting (MYPT) family. This subunit forms an active complex with PP1Cβ and 14-3-3 proteins. Mutation of the AMPK site abolished interaction with 14-3-3 but did not change the interaction with PP1Cβ (Banko et al., 2011). Another study reported phosphorylation of MYPT1 by NUAK1 (Zagorska et al., 2010). This study by Zagorska and colleagues suggested that binding of 14-3-3s to the MYPT1–PP1β complex reduced its ability to dephosphorylate MLC *in vitro.* Their data showed that although AMPK could phosphorylate the same MYPT1 residues as NUAK1 *in vitro,* regulation by AMPK was not physiologically important *in vivo.* Although no direct evidence was shown, the action of AMPK on PPP1R12C could inhibit phosphoprotein phosphatase PP1β, leading to a further increase in phosphorylated MLC (Figure 1.4B). Therefore, AMPK activation can affect MLC phosphorylation from two angles, both by increasing the activity of an upstream kinase, PAK2, and by inhibiting dephosphorylation, suggesting that AMPK has some role in the control of mitosis (Carling et al., 2012). This is supported by a study showing that AMPK-knockout *Drosophila* embryos had defects in polarity and cell division (Lee et al., 2007).

The activity of myosin phosphatase can be inhibited by phosphorylation of MYPT1 at a critical threonine residue (T695) by kinases including ROCK (Kimura et al., 1996) and other kinases listed in the diagram. ROCK can also have another activating effect by phosphorylating MYPT1 at T850 causing myosin to dissociate from the phosphatase complex.
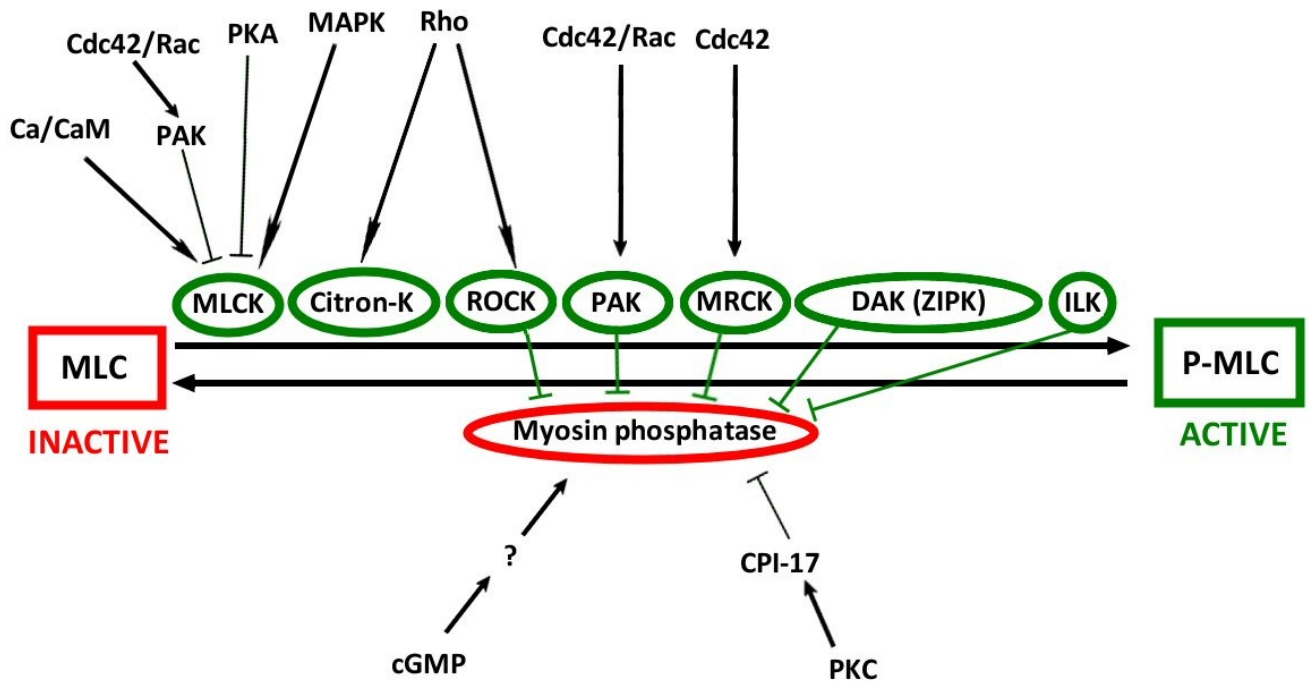
Figure 1.12 Control of MLC phosphorylation (adapted from Matsumura et al., 2005)

Positive regulatory mechanisms are shown in green and negative effects are shown in red.

There are various kinases that are known to phosphorylate and activate MLC and these can be regulated by a series of upstream molecules. Several of the positive regulators of MLC phosphorylation cause this effect by inhibiting the myosin phosphatase complex.
MLCK = Myosin light chain kinase, ROCK = Rho-associated protein kinase, Citron-K = citron kinase, PAK = p21-activated protein kinase, MRCK = myotonic dystrophy protein kinase-related cdc42-binding kinase, DAK = death-associated kinase, ILK = integrin-linked kinase, ZIPK = ZIP-like kinase, CaM = calmodulin, MAPK = mitogen-activated protein kinase, PKA = protein kinase A, PKC = protein kinase C, CPI-17 = inhibitory phosphoprotein of smooth muscle myosin phosphatase.

Cell detachment can increase NUAK1 activity, which phosphorylates MYPT1, thereby inhibiting myosin phosphatase and leading to enhanced phosphorylation of MLC (Zagorska et al., 2010). NUAK1 could therefore be a novel regulator of MLC phosphorylation and some of the associated cellular functions and pathologies.

1.6 Liver damage and hepatocellular carcinoma

Hepatocellular carcinoma (HCC) is a major disease burden across the whole world and has been rising in several Western countries in recent years (El-Serag, 2011; El-Serag and Mason, 1999). The occurrence of HCC is higher in the Middle East and North Africa, as the incidence

of hepatitis B and C is higher in these regions and can play a role in the development of the cancer (El-Serag, 2004). Patients with pre-existing liver problems, primarily cirrhosis, are more likely to develop HCC. Several studies in Western countries showed that up to 40% of patients being treated for HCC did not have chronic infection with hepatitis B or C which demonstrates that there must be other underlying causes. Some of these patients did show signs of having a fatty liver, consistent with some of them being obese and other studies have shown an increased risk of HCC in type II diabetic patients (Calle et al., 2003; El-Serag et al., 2006). There are certain rarer causes of HCC, but the majority of cases can be accounted for by cirrhosis, hepatitis B or C infection, or adaptations caused by obesity and development of a fatty liver. The common factor in all these cases is that they cause chronic liver damage. It is known that mature hepatocytes can upregulate growth factor signalling in response to various forms of liver damage (including the Ras-Raf-MEK-ERK and PI3K-Akt-mTOR pathways). If the damage is chronic then this upregulation will carry on, leading to continual activation of such pathways, which could play a key role in uncontrolled cell growth (Minguez et al., 2009; Villanueva et al., 2007).

For many years, models of chronic liver damage in rodents have been studied and various diets have been developed that recapitulate various forms of human liver disease. The first of these is chronic feeding of diethyl 1,4-dihydro-2,4,6,-trimethyl-3,5-pyridinedicarboxylate (DDC) (Magnus et al., 1969) and also a choline deficient ethionine supplemented diet (CDE) (Shinozuka et al., 1978). Both these models have been analysed in more detail and are known to produce liver progenitor cells, known as "oval" cells, which play a key role in liver regeneration (Akhurst et al., 2001; Fickert et al., 2007). These oval cells are produced in response to cholestasis, cholangitis and biliary fibrosis (Fickert et al., 2007). Recently more evidence has shown that the proliferation of oval cells plays a role in the development of HCC and pathways involved in the growth of these cells may provide novel therapeutic targets (Shen and Cao, 2012).

1.7 Cardiac hypertrophy and the renin-angiotensin system

Cardiac hypertrophy is a physiological response to changes in the cardiovascular system that requires the heart to pump harder, thereby inducing growth of cardiac myocytes and thickening of the cardiac muscle (Kohli et al., 2011). Cardiac hypertrophy can occur in response to normal stimuli such as exercise or pregnancy (Zaidi and Sharma, 2013), but is more commonly associated with various pathological states. It is often a secondary pathology induced by stresses such as hypertension, myocardial infarction, or imbalances in hormonal systems. There are also various known genetic variations that can cause congenital cardiomyopathies that result in hypertrophy (Tousoulis et al., 2013). Pathological cardiac hypertrophy leads to an increase in muscle mass without increasing its pumping ability, which can cause fibrosis and scarring of the cardiac tissue (Moreno-Moral et al., 2013).

There are several interlinked regulatory systems that maintain healthy blood pressure and normal cardiac function. One key hormonal regulator is the renin-angiotensin system of hormonal feedback. Angiotensin is a peptide hormone that has wide ranging effects causing a rise in blood pressure. When blood pressure is low, the kidneys secrete an enzyme called renin into the bloodstream which converts the liver-derived hormone precursor angiotensinogen into angiotensin I. Angiotensin I is then converted to angiotensin II by the angiotensin converting enzyme (ACE) expressed by pulmonary endothelial cells (Nguyen Dinh Cat and Touyz, 2011). Angiotensin II is the major active component of the system and triggers mechanisms to increase blood pressure such as vasoconstriction and secretion of the hormone aldosterone from the adrenal cortex. Aldosterone causes the kidneys to reabsorb more sodium and water, thereby increasing the volume of fluid in the bloodstream, which also raises blood pressure (Nguyen Dinh Cat and Touyz, 2011). In addition to producing angiotensin II, ACE also converts bradykinin (BK), a known vasodilator into various inactive metabolites, further increasing its effect to raise blood pressure (Carey and Siragy, 2003). The effects of angiotensin II are mediated by two receptors, type 1 and type 2 (AT1 and AT2) that appear to cause opposite effects. The main receptor is AT1 and causes the production of second messengers such as inositol trisphosphate (IP3) and activation of various protein kinases such as MAPK, p70S6K and PKC (Higuchi et al., 2007). Most of the downstream effects of angiotensin II are mediated through AT1 receptors, including vasoconstriction, aldosterone

secretion and cardiovascular inflammation, fibrosis and hypertrophy (Figure 1.13) (Nguyen Dinh Cat and Touyz, 2011; Savoia et al., 2011). The AT2 receptor has partial homology (34%) with the AT1 receptor and is the main angiotensin II signalling mechanism in the foetus (Grady et al., 1991). It is only expressed at low levels in adult tissues, but acts to partially antagonise the effects of the AT1 receptor (Horiuchi et al., 1999). The AT2 receptor stimulates vasodilation, anti-inflammatory mechanisms and inhibition of cell growth via activation of protein phosphatases and generation of nitric oxide (Figure 1.13) (Lemarie and Schiffrin, 2010; Savoia et al., 2011). Recent insights into the renin-angiotensin system have revealed a homologue of the angiotensin converting enzyme, ACE2 which can breakdown angiotensin I and II to produce other peptides Ang-(1-9) and Ang-(1-7), which represent fragments of the original decapeptide, angiotensin I. These peptides also contribute to effects antagonising the primary effect of the AT1 receptor via the G protein-coupled receptor Mas (Figure 1.13) (Dantas and Sandberg, 2005; Ferrario, 2011; Santos et al., 2003).
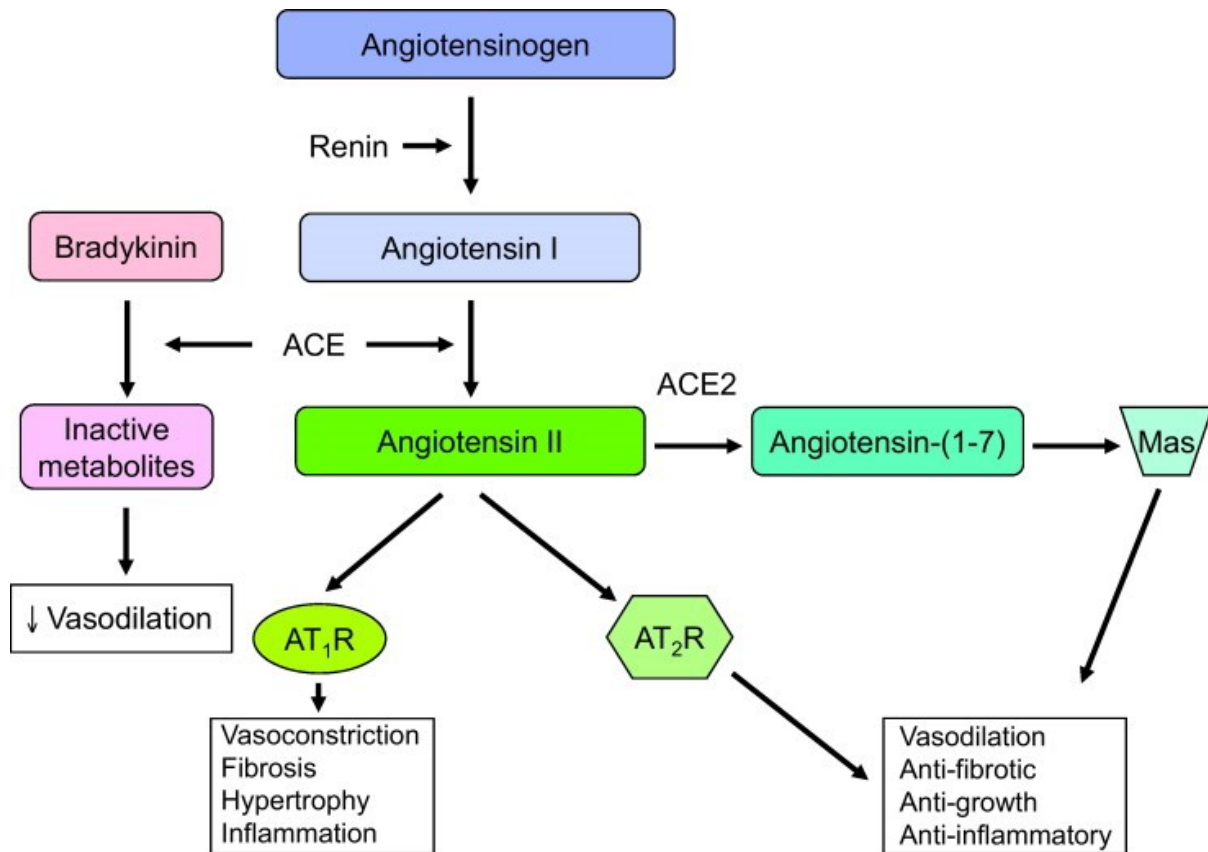
Figure 1.13 The renin-angiotensin system (from Nguyen Dinh Cat and Touyz, 2011)

Liver-derived angiotensinogen is broken down to angiotensin I by the enzyme renin which is secreted from the kidney. Angiotensin II and other related peptides are then formed by the angiotensin converting enzymes (ACE and ACE2). These angiotensin derived peptides then have a series of antagonising downstream effects via the AT1 and AT2 receptors. ACE can also inactivate bradykinin which reduces its effect on vasodilation, thereby helping to increase blood pressure.

Angiotensin II has been widely studied in a variety of clinical settings, animal models and transgenic rodent systems to assess effects on vascular and cardiac processes. Administration of purified angiotensin II peptide via intravenous injection or a subcutaneous pump is commonly used as a way of inducing hypertension to create a generic cardiovascular stress which induces physiological changes in blood vessels and the heart (Horiuchi et al., 2012; Qin, 2008). Angiotensin II has been proposed to elicit some of its effect on hypertrophy by increasing the production of reactive oxygen species (ROS) in mitochondria (Dai and Rabinovitch, 2011). The exact role of the mitochondrial ROS in causing hypertrophy is unclear, but protein kinases such as ERK are sensitive to activation by ROS and may be involved. Angiotensin II is often used in animals to exacerbate small differences in a cardiac phenotype

61

or induce hypertrophy in transgenic models and observe effects of genetic alterations (McDermott-Roe et al., 2011).

1.8 Summary and Aims

This project seeks to further the investigation of NUAK1 within the wider context of AMPK regulation and provide answers to some of the questions raised by previous studies. The functions of NUAK1 are not fully understood and indications that NUAK1 may be a potential therapeutic target for the treatment of cancer and metabolic disorders need further validation using *in vivo* models.

This study aims to increase the understanding of NUAK1 regulation by upstream kinases and binding proteins, such as 14-3-3s. Another objective of this study is to use mass spectrometry approaches to identify novel interaction partners and possible links to other signalling pathways.

Prior to this project there was very little data from *in vivo* models regarding the role of NUAK1 and this study aims to investigate the role of NUAK1 in liver and heart using transgenic mouse models. The data from these studies will seek to clarify the physiological function of NUAK1 and the biochemical mechanisms involved. The *in vivo* data will aim to further understand the role of NUAK1 in pathological conditions and provide more information to interpret its possible therapeutic potential.

Observations from this study also aim to contribute more knowledge to the wider field of LKB1 signalling and AMPK-related kinases. This research will contribute to a currently disparate set of evidence of NUAK1 function and regulation, while providing a summary and aiming to explain some of the inconsistencies in the existing knowledge.

2 Materials and Methods

2.1 Materials

2.1.1 General reagents

Adenosine monophosphate (AMP), Adenosine triphosphate (ATP), 4-(2-hydroxyethyl)-1-piperazineethanesulfonic acid (HEPES), Tris(hydroxymethyl)aminomethane (Tris), ammonium persulphate (APS), magnesium chloride ($MgCl_2$), sodium fluoride (NaF), sodium pyrophosphate ($Na_4P_2O_7$), dithiothreitol (DTT), N,N,N',N'-tetramethylethylenedamine (TEMED), protein A/G-sepharose, β-mercaptoethanol, agarose, N-cyclohexyl-3-aminopropanesulfonic acid (CAPS), Taq DNA polymerase, ampicillin, Dimethyl sulfoxide (DMSO), Triton X-100, phenylmethylsulphonyl fluoride (PMSF) and trypan blue dye were obtained from Sigma (Poole, UK). Glucose oxidase kit and BSA protein standards were obtained from Thermo Fisher Scientific (Leicestershire, UK). 10x Tris/Glycine/SDS buffer, ProtoGel bisacrylamide and Ecoscint scintillant were purchased from National Diagnostics (Yorkshire, UK). Polyvinylidene difluoride (PVDF) membrane was from Millipore (Watford, UK). Primers were generated by Sigma-Genosys (Haverhill, UK). Cal Phos transfection kit was from Clontech (Saint-Germain-en-Laye, France). NaOH, sodium lauryl sulfate (SDS), NaCl, Tween 20, glycerol, ethylenediaminetetraacetic acid (EDTA), ethanol, methanol, KCl, KH_2PO_4, chloroform and glucose were from VWR (West Sussex, UK). Plasmid miniprep, maxiprep and gel purification kits, QIAquick gel extraction kit, RNeasy column and GelPilot DNA Loading Dye were from Qiagen (Crawley, UK). 3MM chromatography paper and P81 phosphocellulose paper were obtained from Whatman (Maidstone, UK). DMEM, Penicillin/Streptomycin and sodium pyruvate were from Gibco (Paisley, UK). Complete EDTA free protease inhibitor cocktail was from Roche (Burgess Hill, UK). TRIzol was from Invitrogen (Paisley, UK). PageRuler Plus Prestained protein marker was from Fermentas (York, UK). DC Protein assay kit was from Bio-Rad (Hertfordshire, UK). LNR, LATS, SAMS and AMARA peptides were synthesised in house by the peptide synthesis facility (Clinical Sciences Centre). [γ-^{32}P]ATP (6000 Ci/mmol) was obtained from Perkin Elmer (Amersham, UK).

2.1.2 Buffers

SDS-PAGE buffer – 50mM Tris-HCl, pH8.4, 400mM glycine, 0.1% (w/v) SDS

TBS-T (Tris buffered saline with Tween) buffer – 20mM Tris-HCl, pH7.4, 0.5M NaCl, 0.5% (v/v) Tween20.

Protein binding buffer – 50 M HEPES, pH7.4, 300mM NaCl, 10mM Imidazole.

Protein washing buffer - 50mM HEPES, pH7.4, 300mM NaCl, 25mM Imidazole.

Protein elution buffer – 50mM HEPES, pH 7.4, 300mM NaCl, 250mM Imidazole.

Gel filtration buffer – 50mM HEPES, pH 7.4, 300mM NaCl and 1mM Tris(2-carboxyethyl) phosphine hydrochloride (TCEP).

HGE – 50mM HEPES, pH 7.4, 10% (v/v) glycerol, 1mM EDTA.

Cell Lysis Buffer – 50mM HEPES, pH7.4, 10% (v/v) glycerol, 1mM EDTA, 1mM benzamidine, 0.1mM PMSF and 4μg/ml trypsin inhibitor, 0.5% (v/v) Triton.

Homogenisation Buffer - 50mM Tris, pH 7.4, 50mM NaF, 5mM $Na_4P_2O_7$, 1mM EDTA, 250mM sucrose, 1mM dithiothreitol, 4μg/ml trypsin inhibitor, 0.1mM phenylmethylsulfonyl fluoride, 1mM benzamidine.

Western blot buffer – 10mM N-Cyclohexyl-3-aminopropanesulfonic acid (CAPS), pH 11, 10% methanol.

Phosphate-buffered Saline (PBS-A) – 137mM NaCl, 2.7mM KCl, 4.3mM Na_2HPO_4, 1.4mM KH_2PO_4, pH 7.4

Perfusion buffer - 138mM NaCl, 50mM HEPES, 5.56mM glucose, 0.5mM EGTA, 5.4mM KCl, 0.338mM Na_2PO_4, 0.44mM KH_2PO_4, 4.17mM $NaHCO_3$, carboxygenated, pH 7.4

TAE (Tris, acetic acid, EDTA) – 40mM Tris, 20mM acetic acid, 1mM EDTA, pH 8.0.

Luria broth (LB) – 1% (w/v) tryptone, 0.5% yeast extract, 0.5% (w/v) NaCl

SOC media – 2% (w/v) tryptone, 0.5% yeast extract, 0.05% (w/v) NaCl, 20mM glucose

10% buffered formalin – 4% (v/v) formaldehyde in PBS-A

Methacarn fixative – 60% (v/v) methanol, 30% (v/v) chloroform, 10% (v/v) glacial acetic acid

2.1.3 Bacterial strains

***E. coli* strain JM109** (*end*A1, *rec*A1, *gyr*A96, *thi*, *hsd*R17 (rk⁻, mk⁺), *rel*A1, *sup*E44, Δ(*lac-pro*AB), [F' *tra*D36, *pro*AB, *laq*IqZΔM15]) competent cells were obtained from Promega (Sussex, UK). These were used for the transformation and amplification of plasmid DNA. The (*end*A) endonuclease deficiency allows high quality plasmid DNA to be produced and the (*rec*A)

recombinase deficiency improves insert stability. The *hsd*R mutation prevents cleavage of the plasmid DNA by the *Eco*K endonucleases system.

***E. coli* strain BL21-Codon-Plus (DE3)-RIL** (B F-, ompT, hsdS(r_B^- m_B^-), dcm$^+$, Tet^r, gal λ(DE3), endA, Hte [argU ileY leuW Cam^r]) competent cells from Agilent (Waldbronn, Germany) were used for expression of recombinant proteins and grown in LB supplemented with appropriate antibiotics. These cells are naturally deficient in the Lon protease and are engineered to be deficient in the ompT protease, reducing the risk of degradation of expressed proteins. The DE3 designation means the strains contain the λ DE3 lysogen and carries the gene for T7 RNA polymerase under the control of the *lac*UV5 promoter allowing high levels of protein expression following induction with isopropyl-1-thio-b-D-galactopyranoside (IPTG). The RIL strain of cells also contains plasmids encoding extra copies of the *argU*, *ileY* and *leuW* tRNA genes which are rare in *E. coli*, the lack of which can lead to the formation of truncated and degraded protein products.

2.1.4 Mammalian cells

CCL13 cells (Human liver epithelial cells), HEK293T cells (Human embryonic kidney cells carrying the large T antigen) and COS7 (African Green Monkey SV40-transformed kidney fibroblasts) were obtained from American Cell Type Culture Collection (Middlesex, UK) and maintained at 37°C, 5% CO_2 in Dulbecco's Modified Eagle's Medium (DMEM with sodium pyruvate, 4500mg/L glucose and pyridoxine) (Invitrogen) supplemented with 10% (v/v) foetal calf serum, 2mM N-glutamine and 0.5mg/ml penicillin-streptomycin. Cells were passaged before reaching confluency using trypsin-EDTA (Invitrogen).

Wild-type and NUAK1 knockout primary Mouse Embryonic Fibroblasts (MEFs) were isolated under the supervision of Dr Naveenan Navaratnam (MRC Clinical Sciences Centre), see section 2.2.12 . Primary mouse hepatocytes were isolated with the assistance of Dr Alicia Garcia (MRC Clinical Sciences Centre), see section 2.2.17 .

2.1.5 Proteins

Recombinant AMPK complex (α1β1γ1) was expressed in *Escherichia coli* and purified by Dr David Carmena (Clinical Sciences Centre) as previously described (Sanders et al., 2007). Recombinant CaMKKβ and LKB1 complex, obtained by the co-expression of human His-LKB1, STRADα and MO25α, were expressed in *Escherichia coli* and purified by Dr David Carmena. Recombinant human his-tagged PP2Cα protein was expressed and purified by Dr David Carmena.

2.1.6 Antibodies

T211 phosphorylation was determined using rabbit monoclonal antibodies raised against AMPK phospho-T172 from Cell Signalling (#2535). His-tagged proteins were detected using mouse monoclonal anti-His antibodies from Qiagen (34660). Anti-FLAG tag antibodies were from Cell Signalling (Rabbit, #2368) or Sigma (Mouse, F1804). Anti-FLAG M2 affinity gel was from Sigma (A2220). Anti-pan 14-3-3 rabbit antibody was from Santa Cruz Biotechnology (K-19). Anti-α/β-tubulin rabbit antibody was from Cell Signalling (#2148). Anti-NUAK1 rabbit antibody was sourced from Cell Signalling (#4458). Anti-phospho-(Ser/Thr) casein kinase 2 substrate (P-S/T3-100) rabbit monoclonal antibody was from Cell Signalling (#8738). A pan-AMPK β subunit rabbit antibody (Sip2) was raised in house against a β-GST fusion protein (lacking the N-terminal 68 amino acids).

Secondary antibodies for use with the LI-COR scanner were used for all immunodetection of western blots. IRDye800 goat anti-mouse and goat anti-rabbit were from LI-COR Biosciences UK Ltd (Cambridge, UK). AlexaFluor 680 goat anti-mouse and goat anti-rabbit antibodies were from Invitrogen.

2.1.7 Plasmids

pET15b (Novagen) plasmid containing the full length wild-type human NUAK1 cDNA and pRSF-Duet1 plasmid containing full length wild-type human 14-3-3ε were kindly provided by Dr Naveenan Navaratnam. pcDNA3.1/V5-His-TOPO® vector was from Invitrogen (K4900-01).

2.2 Methods

2.2.1 Animals

Embryonic stem cells (ES) carrying a transgenic construct for NUAK1 (CSD Knockout First, promoter driven) were generated by the trans-NIH Knock-Out Mouse Project (KOMP) and obtained from the KOMP Repository (www.komp.org). NIH grants to Velocigene at Regeneron Inc. (U01HG004085) and the CSD Consortium (U01HG004080) funded the generation of gene-targeted ES cells for 8500 genes in the KOMP Program and archived and distributed by the KOMP Repository at UC Davis and CHORI (U42RR024244).

Mice carrying this construct were re-derived on a C57-Bl6 background by Zoe Webster (Clinical Sciences Centre, Transgenic Facility). To produce the appropriate conditional knockouts, the animals were crossed with transgenic mice carrying the FLP recombinase (Jackson Laboratory), cre recombinase under the control of the albumin promoter (Jackson Laboratory) and cre recombinase under the control of the α myosin heavy chain (αMHC) (a gift of Prof. Michael Schneider, National Heart and Lung Institute).

2.2.1.1 Housing conditions

All mice were bred and maintained by myself and Phillip Muckett according to Home Office regulations as defined by the Animal (Scientific Procedures) Act, 1986. Mice were stocked at a maximum density of 7 animals per cage, or 4 animals per cage over 30g bodyweight, in Allentown XJ individually ventilated cages (IVCs). Environmental conditions were maintained within strict limits; temperature 21°C ± 2°C, humidity 55% ± 10% and light conditions were

kept on 12hour light/12 hour dark cycles. Unless otherwise stated mice were fed on Special Diet Services (SDS) Rat and Mouse No.3 Breeding diet.

2.2.1.2 Genotyping

Ear clipping was used to identify individual mice and to obtain tissue for genetic identification. DNA was purified from ear clips by heating at $100^{\circ}C$ for 20 minutes in 50µl of 200mM NaOH with occasional vortexing. This was then neutralised with 25µl of 1M Tris pH8. The resulting solution was used in polymerase chain reaction (PCR) experiments to determine the genotype of the animal. Reddymix PCR mix (Thermo Scientific, #AB-0575/DC/LD/A) or MyTaq™ HS Red Mix (Bioline, BIO-25047) were used according to the manufacturer's instructions with the relevant primers listed in the appendix. Tail tips were taken for post mortem genotyping and DNA was extracted in the same way for use in PCR reactions to confirm the identity and genotype of animals used in each experiment.

2.2.1.3 Echo-MRI

Body composition of animals at the age indicated in the figure was determined by a trained, genotype-blinded operator using an EchoMRI-100V machine. This instrument calculates body composition by using nuclear magnetic resonance (NMR) to create contrast between soft tissues based on the differences in relaxation times of the hydrogen proton spins in water in different environments. The method does not require the animals to be anaesthetised, which reduces the risk of harm to the mice.

2.2.1.4 Intra-peritoneal glucose tolerance test (ipGTT)

Mice were fasted overnight prior to administration of glucose by intra-peritoneal injection (1g/kg of body weight). Blood samples from the tail were taken at 0, +15, +30, +60, +120 minutes after glucose dosing. Blood glucose levels were measured with an Accu-Chek Compact Plus glucometer.

2.2.1.5 Comprehensive Laboratory Animal Monitoring System (CLAMS)

Mice were housed individually for at least a week prior to going into the CLAMS system to allow for acclimatisation to single housing. Experiments were limited to 5 days to ensure that animals were never left unattended for more than an overnight period thereby reducing any possible harm.

The CLAMS system is a monitoring system that allows multi parameter assessment of many animals simultaneously. Cohorts of 12 – 16 mice were placed in the system which measures oxygen consumption, carbon dioxide production and food and water intake. The calorimetric data is then calculated indirectly from the gases flowing in and out of the animal chamber. Heat is derived by looking at the exchange of oxygen for carbon dioxide that occurs during the metabolism of an energy source. The relationship between the volume of oxygen consumed and the amount of carbon dioxide produced reveals the energy content of the energy source the animal is using. This calorific value is then linked with the volume of gases exchanged to compute heat.

Animals were monitored several times daily by a trained, genotype-blinded operator and experiments were terminated early if they were having an adverse effect on the animal.

2.2.1.6 Echocardiography

Mice were anaesthetised with 4% (v/v) isoflurane and arranged in a supine position on a bench-mounted heat pad. The chest wall was shaved to allow application of pre-warmed ultrasound gel and anaesthesia was maintained with 1.5% (v/v) isoflurane in 100% oxygen administered via a mask. Echocardiography images were taken using a Vevo 770 Imaging System (VisualSonics) and analysed without prior knowledge of the genotype. Parameters were measured using VisualSonics EKV software and then raw data exported to Microsoft Excel and GraphPad Prism for analysis. Mice were euthanised after echocardiography and appropriate tissues harvested for analysis.

2.2.1.7 Angiotensin II treatment

Mice were dosed with angiotensin II peptide (Sigma) dissolved in 0.9% (w/v) sterile saline solution. The concentration of the peptide solution was calculated based on body weights taken the day prior to the start of the experiment such that each mouse would receive 1.2mg/kg/day of angiotensin II. Delivery was by micro-osmotic minipumps (Azlet, model 1002). Surgery was carried out under sterile conditions, according to Home Office guidance. Mice were anaesthetised with 4% isoflurane and maintained with 1.5% (v/v) isoflurane in 100% oxygen administered via a mask. Baseline measurements of body weight, food intake and water intake were recorded for at least a week prior to the diet change and during the course of the experiment. Any animals that lost more than 20% of their body weight were immediately euthanised to prevent suffering.

2.2.1.8 Tissue harvesting

Mice of the age and sex specified in the figure were culled by cervical dislocation. Tissues were harvested and immediately frozen in liquid nitrogen. Prior to analysis, tissues were roughly chopped in two volumes of ice-cold homogenisation buffer and then briefly homogenized with a rotor-stator homogenizer. The homogenates were then centrifuged at 16000 x g for 15 min to remove insoluble material.

2.2.1.9 Serum metabolite analysis

Mice of the age and sex indicated in the figure were culled by decapitation and whole blood was drained into heparinised collection tubes (Sarstedt). Blood was immediately centrifuged at 2000 x *g* for 10 min to separate red cells and clotting factors. Serum was then drawn off and stored at -80ºC until analysis. Samples were then sent to the Core Biochemical Assay Laboratory, Cambridge University for analysis.

2.2.1.10 CDE Diet and panCK staining

Mice of the age and sex indicated in the figure were maintained on a normal chow diet and changed to a choline deficient, ethionine supplemented (CDE) diet for a maximum of three weeks before being culled by cervical dislocation. Diet was from Harlan Laboratories (Teklad TD.90262). DL-Ethionine (Sigma) was dissolved in drinking water at a concentration of 0.15% (w/v) and supplemented with 10% (v/v) Robinson's Sugar Free Orange Squash to make it more palatable. Baseline measurements of body weight, food intake and water intake were recorded for at least a week prior to the diet change and during the course of the experiment. Any animals that lost more than 20% of their body weight were immediately euthanised to prevent suffering.

Livers were harvested immediately following cervical dislocation and lobes were fixed in 10% (v/v) buffered formalin or methacarn overnight. Liver lobes were then dehydrated through a series of alcohol grades (see section 2.2.2) before wax embedding. The wax embedded samples were then sent to our collaborators at Edinburgh University (Prof. Stuart Forbes et al.) for sectioning, staining and imaging.

2.2.2 Histology

Samples were immediately fixed after harvesting in 10% (v/v) formalin, methacarn or 4% (v/v) paraformaldehyde depending on the tissue and staining protocol in question. The tissue was left in the fixative overnight at 4°C and was then transferred into 70% (v/v) ethanol. The tissues were then put through a series of dehydration steps before immersion in clearing agent and wax:

- 90% (v/v) Ethanol – 1 hour
- 95% (v/v) Ethanol – 1 hour
- 100% (v/v) Ethanol – 1 hour
- 100% (v/v) Ethanol – 1 hour
- Histo-clear II – 1 hour
- Histo-clear II – 1 hour
- Molten paraffin wax – 1 hour

Samples were then embedded on histology cassettes using a Leica EG1160 embedder.

All sectioning and staining was conducted by Mahrokh Nohadani (C & C Laboratory Services Ltd.).

2.2.2.1 Haematoxylin & Eosin staining (H&E)

Briefly, sections were deparaffinised by washing in xylene and rehydrated in descending dilutions of alcohol. Sections were then stained with haematoxylin solution for 8 – 10 minutes. Sections were washed with water before being counterstained in eosin solution for 30 seconds to 1 minute. Sections were then dehydrated through ascending alcohol dilutions before being mounted on slides.

2.2.2.2 Periodic Acid Schiff staining (PAS)

Briefly, sections were deparaffinised by washing in xylene and rehydrated in descending dilutions of alcohol. Sections were then oxidised in 0.5% (w/v) periodic acid solution for 5 minutes. Sections were washed in distilled water before being stained with Schiff reagent for 15 minutes. Sections were then counterstained in haematoxylin for 1 minute before being dehydrated through ascending alcohol dilutions and mounted on slides.

2.2.2.3 Sirius red staining

Briefly, sections were deparaffinised by washing in xylene and rehydrated in descending dilutions of alcohol. Nuclei were then stained with haematoxylin for 8 – 10 minutes. Sections were washed in distilled water before being stained with picro-sirius red (1% (w/v) solution of Sirius red in saturated picric acid) for 1 hour. Sections were then washed with acidified water before being dehydrated through ascending alcohol dilutions and mounted on slides.

2.2.3 Cloning

Site-specific point mutations were generated using the QuikChange® site-directed mutagenesis kit (Stratagene) according to the manufacturer's protocol. This method was performed using Phusion DNA polymerase which replicates both plasmid strands with high fidelity without displacing the mutant oligonucleotide primers. Briefly, the procedure uses a vector DNA with the insert of interest and two synthetic oligonucleotide primers containing the desired mutation. Primers used in this project were synthesised by Sigma Genosys and are listed in the appendix. PCR extension occurs from the annealed primers resulting in the generation of new plasmids containing the mutated codon. Mutagenesis was carried out in a 50μl reaction volume containing: 50ng plasmid DNA, 10ng of forward and reverse primer, 0.2mM dNTPs, 1% (v/v) DMSO, and Pfu Ultra buffer containing 2mM $MgCl_2$, and 1 unit of Pfu Ultra enzyme. A polymerase chain reaction (PCR) was programmed for an initial heating step of 1 min at 95°C followed by 20 cycles of denaturation step at 95°C for 1 min, annealing step at 60°C for 1 min and extension step at 68°C for 7 min and then a final extension step of 68°C for 10 min. Following PCR, 10μl of the reaction was incubated in another 50μl reaction with 2 units of *DpnI* endonuclease (specific for methylated DNA) at 37°C for 1h to digest the original DNA. This relies on the fact that the template DNA, having been purified from bacteria, is methylated whereas the mutated products of the PCR reaction are unmethylated. The product vector DNA incorporating the desired mutations was then transformed into *E. coli* JM-109 competent cells and the DNA was prepared from small-scale cultures from isolated colonies using either the plasmid mini-prep or maxi-prep kit (Qiagen). The introduction of the desired mutations, and confirmation of no unwanted changes, was verified by sequencing performed by the Sequencing Service, MRC Clinical Sciences Centre using vector primers.

2.2.4 Plasmid DNA purification

Plasmid DNA was purified from 5 ml or 250 ml bacterial cultures using a Qiagen miniprep or maxiprep kit following the manufacturer's instructions. Briefly, cells were centrifuged and the cell pellet was lysed using appropriate lysis buffer. Proteins and genomic DNA were precipitated using the buffers in the kit. Following centrifugation, the supernatant containing plasmid DNA was passed through the appropriate column and then washed with buffer.

Plasmid DNA was eluted and precipitated with isopropanol. Following centrifugation at 15000 x *g* for 40 minutes the supernatant was discarded and the DNA pellet was washed with 70% (v/v) ethanol. After further centrifugation, plasmid DNA was resuspended in an appropriate volume of distilled water. DNA concentration was measured on an Amersham Biosciences Ultrospec 2100pro. Sequencing was performed by the Sequencing Service at MRC Clinical Sciences Centre using vector primers.

2.2.5 Agarose gel electrophoresis

DNA samples were diluted in Qiagen GelPilot DNA Loading Dye and analysed by electrophoresis at 120V for 1 hour on a 2% (w/v) agarose gel. Bands were visualised by UV exposure on Syngene Gene Genius transilluminator.

2.2.6 Bacterial transformations and culture

Competent JM109 cells were thawed on ice. Cells were mixed gently with DNA and incubated on ice for 30 min before undergoing heat shock for 50 seconds at 42°C. Transformation reactions were cooled on ice for 2 minutes before addition of 900µl SOB media (2% (w/v) tryptone, 0.5% (w/v) Yeast extract, 10mM NaCl, 2.5mM KCl) and incubation at 37°C for 1 hour. Cells were pelleted by centrifugation and resuspended in Luria broth (LB) (1% (w/v) tryptone, 0.5% (w/v) yeast extract, 0.05% (w/v) NaCl) and plated on LB plates (LB broth with 1.5% (w/v) agar) with appropriate antibiotic (100µg/ml ampicillin or 50µg/ml kanamycin). Plates were incubated overnight at 37°C and single colonies were used to inoculate liquid cultures.

2.2.7 Protein expression

Recombinant NUAK1 was expressed and purified from *E. coli.* Briefly, BL21-Codon-Plus (DE3)-RIL competent cells were transformed with the plasmid of interest and colonies selected by growth on agar plates supplemented with the appropriate antibiotic. A single clone was selected and grown in LB containing the appropriate antibiotic overnight at 37°C in a shaking

incubator. This overnight culture was used to inoculate a larger culture (4 x 500ml) in LB medium and grown at 37°C until an optical density at 600nm of 1.0 was reached. Subsequently, the culture was transferred to a shaking incubator at room temperature and protein expression was induced with a final concentration of 0.4mM IPTG for an additional 16 hours. Cells were harvested by centrifugation and lysed by sonication in lysis buffer (50mM HEPES, 300mM NaCl, 10mM imidazole, pH 8.0). His-tagged proteins were isolated from the lysate using nickel affinity chromatography on an AKTApurifier system (GE Healthcare). After elution the appropriate fractions containing useable protein (assessed by SDS-PAGE) were pooled and concentrated using centrifugal VivaSpin 20 concentrators (30000 MWCO) (Millipore). Concentrated protein was then size separated on a Sepharose column (Superdex 200, GE Healthcare) using an AKTA purifier system and appropriate fractions concentrated to produce the final protein solution. Quality of the concentrated protein was assessed by SDS-PAGE.

2.2.8 Protein determination

Protein assays were carried out using the Bio-Rad DC kit according to the manufacturer's instructions, against BSA protein standards (Thermo Scientific). Absorbance at 750nm was read using the Spectromax 340pc plate reader.

2.2.9 Western blotting

Samples for SDS-PAGE were denatured for 5 minutes at 95°C in sample buffer (250mM Tris, pH6.8, 8% (w/v) SDS, 30% (v/v) glycerol, 10% (v/v) β-mercaptoethanol, 0.04% (w/v) bromophenol blue) before loading into a 10% (w/v) polyacrylamide gel and run for 1 hour at 200 V in Tris-Glycine buffer (25mM Tris, 192mM glycine, 0.1% (w/v) SDS). Proteins were transferred to a polyvinylidene difluoride (PVDF) membrane in transfer buffer (5mM CAPS, pH 11, 10% (v/v) methanol) at 60 V for 4 hours. Membranes were blocked in 5% (w/v) milk powder (CoffeeMate) in TBS-T (20mM Tris pH 8, 150mM NaCl, 0.5% (v/v) Tween 20) before incubation with primary antibody at an appropriate dilution for a minimum of 2 hours. Following three washes in TBS-T, membranes were incubated for an hour with the

appropriate fluorescently conjugated secondary antibody at a dilution of 1:10,000. Membranes were then washed three times with TBS-T before detecting on the LICOR Odyssey scanner using 700nm and 800nm wavelengths to detect the fluorescent dyes.

2.2.10 Radiolabelling kinase assays

AMPK was assayed as previously described (Davies et al., 1989). A similar technique and buffer was used to measure NUAK1 activity. Details are shown in the results (Figure 3.4) regarding the peptide substrate specificity of NUAK1. The specific activity of the radioactive ATP was measured during each set of assays.

2.2.10.1 AMPK assays

Recombinant AMPK or immunoprecipitated protein bound to resin was incubated at 37°C whilst shaking for 20 minutes with 200μM AMP, 200μM SAMS peptide (HMRSAMSGLHLVKRR), 10mM HEPES, 0.2% (v/v) Triton X-100, and 200μM [γ-^{32}P]ATP in a total volume of 25μl. The reaction mix (20μl) was spotted onto a P81 paper and washed thoroughly in 1% (v/v) orthophosphoric acid to remove radioactive ATP. Samples were submerged in EcoScint fluid and counted in a TriCarb 2800TR scintillation counter.

2.2.10.2 NUAK1 assays

Recombinant NUAK1 or immunoprecipitated protein bound to resin was incubated at 37°C whilst shaking for 20 minutes with 5mM MgCl$_2$, 200μM ATP, 200μM of the indicated peptide, 10mM HEPES, 0.2% (v/v) Triton X-100 and 200μM [γ-^{32}P]ATP in a total volume of 25μl. The reaction mix (20μl) was spotted onto a P81 paper and washed thoroughly in 1% (v/v) orthophosphoric acid to remove radioactive ATP. Samples were submerged in EcoScint fluid and counted in a TriCarb 2800TR scintillation counter.

2.2.11 Mammalian cell transfection

The day before transfection, cells were seeded at an appropriate level to be 60% confluent on the day of transfection. Transfection was carried out using the CalPhos mammalian transfection kit (Clontech) according to the manufacturer's instructions. Briefly, 30µg DNA was combined with 0.124M $CaCl_2$ and HEPES-buffered saline and was incubated for 30 minutes at room temperature before adding drop-wise to the cell culture medium. The cell culture medium was changed the following morning. Cells were harvested 48 hours post-transfection or as described in the figure legends.

2.2.12 Mouse Embryonic Fibroblast (MEF) isolation

Isolation of wild-type and NUAK1 null MEFs was performed at embryonic days 11.5 - 13.5. The embryos were removed from the uterus and thoroughly washed with PBS. The head, spleen and liver were removed and the rest of the embryo was chopped and digested for an hour with trypsin before passing through a 70µM cell sieve. The cells were thoroughly resuspended and cultured in DMEM supplemented with 10% (v/v) FCS and penicillin/streptomycin.

2.2.12.1 Cell counting

Cells were counted for the purposes of plating density for transfections and for determining the number of cells present at different stages of growth. Cells were detached from the culture plate or flask by treatment with trypsin-EDTA (Invitrogen). Detachment was confirmed by observing the remaining attached cells using a light microscope. Cells were then centrifuged at 1300 x *g* and the supernatant discarded. The cells were resuspended in an appropriate volume of DMEM and an aliquot was diluted at an appropriate ratio with more DMEM and finally at a 1:1 ratio with trypan blue dye (Sigma). Cells were counted using a Neubauer Improved haemocytometer on a light microscope and multiplied by the appropriate ratios to establish the cell density.

2.2.13 Cell lysis

Cells were washed with PBS and immediately scraped into lysis buffer (10mM HEPES, 100mM NaCl, 2.5mM $MgCl_2$, 1mM dithiothreitol (DTT), 5mM $Na_2P_2O_7$, 50mM NaF, 0.5% (v/v) Triton X-100, complete protease inhibitor cocktail). Samples were incubated for 15 minutes on ice before centrifugation at 21000 x *g* at 4°C. Supernatants were stored at -80°C until further use.

2.2.14 Immunoprecipitation

Proteins were immunoprecipitated from cell lysates for kinase assays or western blotting. Equal amounts of protein were made up to a volume of 100µl with lysis buffer and incubated at 4°C for at least 2 hours with 15µl of 50% (v/v) protein A/G Sepharose slurry and 0.5µl of the appropriate antibody as described in the figure legends. The immunoprecipitates were then washed 3 times with HEPES buffer A (50mM HEPES, 1mM EDTA, 10% (v/v) glycerol, 1mM DTT, 1% (v/v) Triton X-100, protease inhibitor cocktail).

2.2.15 RNA extraction

Cells were washed thoroughly with PBS and scraped into 500µl TRIzol and incubated for 5 minutes at room temperature before addition of 100µl chloroform. For tissue RNA extraction 100mg of material was homogenised in 500µl of TRIzol and then treated in the same way. After adding chloroform, samples were inverted for 15 seconds before a further three minute incubation. Samples were centrifuged at 12000 x *g* for 15 minutes to separate the RNA fraction in the upper aqueous phase. 0.53% (v/v) ethanol was added before loading onto an RNeasy column. The column was washed with Buffers RW1 and PPE and RNA was eluted in RNase-free water. RNA concentration was measured by absorbance at 260 nm in an Amersham Biosciences Ultrospec 2100pro and samples were stored at -80°C.

2.2.16 Quantitative PCR (qPCR)

mRNA was isolated from cells or tissues as described in 2.2.15. cDNA was then produced from this material using SuperScript® II Reverse Transcriptase (Invitrogen, 18064-014) according to the manufacturer's instructions. cDNA concentration was determined by absorbance at 260nm using a NanoDrop® ND-1000 UV-Vis spectrophotometer. qPCR reactions were carried out on the Opticon DNA engine 2 using the Qiagen SYBR Green kit according to the manufacturer's instructions. 10ng of total cDNA was incubated with SYBR green RT-PCR master mix, RT mix and appropriate primers and put through 40 cycles of extension. All cDNA expression values are shown as cDNA expression relative to a house keeping gene as described in the figure legends and all primers were tested to show they gave linear results before being used.

2.2.17 Mouse primary hepatocyte isolation

Primary hepatocyte isolation was carried out as previously described (Foretz et al., 1998) with some amendments. Perfusions were carried out by Dr Alicia Garcia. Mice were anaesthetised with 200µl/100g of body weight using a solution of 0.286% (w/v) xylazine (Rompun®) and 42.9mg/ml ketamine (Ketaset®) in distilled water. Mice were canulated in the inferior vena cava and the liver was perfused with perfusion buffer at 37°C (138mM NaCl, 50mM HEPES, 5.56mM glucose, 0.5mM EGTA, 5.4mM KCl, 0.338mM Na_2PO_4, 0.44mM KH_2PO_4, 4.17mM $NaHCO_3$, carboxygenated, pH 7.4). After washing with perfusion buffer for 15 minutes the liver was digested with collagenase buffer (perfusion buffer minus EGTA, 5mM $CaCl_2$ with 0.025% (w/v) collagenase H). Digested livers were removed and hepatocytes were released and filtered, and washed twice with ice cold perfusion buffer followed by washing with ice cold M199. Cells were plated onto collagen coated plates in plating medium (M199, Penicillin/Streptomycin, 10% (v/v) bovine serum albumin (BSA), Ultrosero G, 100nM T_3, 100nM dexamethasone, 100nM insulin). Plating medium was removed 4 hours later and replaced with overnight medium (M199, Penicillin/Streptomycin, 100nM dexamethasone, 1nM insulin) and cells were cultured for at least 16 hours in this medium. The following day, the medium was changed to M199 supplemented only with penicillin and streptomycin at least 2 hours before treatment or harvesting.

2.2.18 Hepatic glucose production

Mouse hepatocytes were treated on the day following isolation as described in the figure legends. Following the required treatment time, media were removed and cells were washed twice with PBS before addition of 1 ml Hepatic Glucose Production medium per 6 well plate well (DMEM minus phenol red, supplemented with 2mM sodium pyruvate, 20mM sodium lactate). Samples of the culture media were taken 2 hours, 4 hours and 6 hours following the medium change. Glucose concentration was read in a 96 well plate using the TRACE DMA glucose oxidase kit compared to glucose standards read on the Spectromax 340pc at 490 nm.

2.2.19 Extracellular flux analysis (Seahorse)

Wild-type and NUAK1 knockout hepatocytes were seeded onto XF24 Cell Culture Microplates at the same density (2×10^5 cells per well) after harvesting and analysed the following day (see section 2.2.17). The cells were analysed on a XF24 Extracellular Flux Analyser (Seahorse Biosciences) by Dr Alicia Garcia. This machine takes real-time measurements of oxygen consumption rate (OCR) and extracellular acidification rate (ECAR). OCR is an indicator of mitochondrial respiration, and ECAR can be used to indicate glycolytic capacity. The cells were subjected to treatment with drugs in the XF Mito Stress Kit according to the manufacturer's instructions. The different drugs allow the measurement of four key parameters of mitochondrial function: basal respiration, ATP turnover, proton leak, and maximal respiration.

2.2.20 Immunofluorescence

For immunofluorescence analysis, 10-20000 cells were seeded on poly-lysine coated glass cover slips overnight and transfected with appropriate plasmids, as listed in the figure legends. After 36-48 hours, the cells were fixed with methanol or 4% (v/v) paraformaldehyde (PFA) for 10min. PFA fixed cells were permeabilised with 0.2-0.5% (w/v) Triton in PBS for 2-3 min and washed 3 times, 10 minutes each, with PBS at room temperature. Washed cells were blocked with 0.5% (w/v) fish gelatine in PBS for 2-3 hours and incubated with the primary

antibody (1:100-1:300 dilution) overnight. After overnight incubation, coverslips were washed with PBS as before and incubated with appropriate fluorescently conjugated secondary antibody (1:200 dilution) for 30 min. Secondary antibody was removed and cells were washed 3 times in PBS and mounted on glass coverslips using Vectashield with DAPI and imaged using a Leica SP5 microscope. Images were captured with Leica LAS AF and further analysed using Metamorph software.

2.2.21 Mass spectrometry methods

2.2.21.1 Stable Isotope Labelling by Amino Acids in Cell Culture (SILAC)

This experiment was kindly conducted by Dr Naveenan Navaratnam (Clinical Sciences Centre). Stable isotope labelling by amino acids in cell culture (SILAC) is a method for *in vivo* incorporation of a label into proteins for quantitative mass spectrometry proteomics. SILAC relies on incorporation of a so called 'light' or 'heavy' form of an amino acid into proteins in a cell which can then be distinguished by mass spectrometry analysis. Wild-type MEFs were grown on 'light' DMEM media lacking arginine and lysine and specifically supplemented with 'normal' arginine and lysine and dialysed foetal bovine serum. NUAK1 knockout MEFs were grown on 'heavy' media containing ^{13}C arginine and ^{15}N lysine.

Equal quantities of cells were harvested and lysed in the same way (see 2.2.13). The lysates were normalised to ensure the same amount of total protein was used and then the mixed lysates were digested with trypsin for analysis by mass spectrometry using an LTQ Orbitrap XL machine.

2.2.21.2 Neuronal phosphoscreen

This experiment was kindly conducted by Dr Nicola Bright (Clinical Sciences Centre). Lysate from wild-type primary embryonic mouse cortical neurons were harvested and equal quantities were incubated with varying amounts of active recombinant NUAK1 or AMPK (0µg, 1µg and 5µg) for different times. The method relies on a high specific activity recombinant

kinase phosphorylating downstream targets in the lysate in a time-dependent manner. Phosphopeptides were generated by trypsin digestion and concentrated on a titanium dioxide column and the resulting material was analysed by mass spectrometry. By comparing the rate of phosphorylation, this method can identify specific phosphopeptides phosphorylated by the recombinant kinase. The method has been used in published reports (Casado et al., 2013).

2.2.21.3 FLAG tagged SILAC immunoprecipitation

This experiment was kindly conducted by Dr Naveenan Navaratnam (Clinical Sciences Centre). FLAG-tagged full-length NUAK1 was over expressed in HEK293T cells and grown on 'heavy' SILAC media as before. Control cells with vector only transfection were grown under similar conditions on 'light' SILAC media. Cells were harvested and NUAK1 protein immunoprecipitated using an anti-FLAG resin and eluted with flag peptide. The resulting material from transfected and un-transfected cells was then mixed, separated by SDS-PAGE and analysed by mass spectrometry to identify any proteins that co-immunoprecipitated with NUAK1.

2.2.21.4 Mass spectrometry analysis

Data was generated from the different mass spectrometry screens in the form of lists of proteins, ordered either by hierarchy of quantity of the peptide detected or the degree of change compared to the relevant control sample. Some data was compared using peptide fingerprints but where this was not available, protein data was converted into consistent gene acronyms using the Database for Annotation, Visualization and Integrated Discovery (DAVID) (http://david.abcc.ncifcrf.gov). By comparing the consistent index of gene acronyms, a list of all the proteins that appeared in at least two of the different methods was determined. These lists were then analysed using the gene ontology search resources provided by the Lewis-Sigler Institute for Integrative Genomics, Princeton University (http://go.princeton.edu/).

2.2.22 Statistical analysis

Data are expressed as the mean ± standard error of the mean (S.E.M.). The Student's t-test or an ANOVA followed by an appropriate *posthoc* test was used to determine statistical significance. The means were considered to be significantly different if a value of $p<0.05$ was obtained.

3 *In vitro* and cellular characterisation of NUAK1

3.1 Introduction

Previous studies investigating the role of NUAK1 have only looked at very specific aspects of the activation and control of the kinase (Lizcano et al., 2004) or have identified the kinase as part of wider screens looking at a specific pathology or role of another kinase (Suzuki et al., 2004b). The first study to take an overall view of the field of AMPK-related kinases identified LKB1 as a common upstream kinase and other consistent features such as their lack of activation by AICAR (Lizcano et al., 2004). However, given that LKB1 has previously been suggested to be constitutively active (Alessi et al., 2006) this raised further questions about how the activity of the related kinases are controlled. Another study from the same group identified the presence of a conserved UBA domain and linked this to the regulation of AMPK-related kinase phosphorylation by LKB1 (Jaleel et al., 2006). Aside from these data, there have been only a few other studies that have indicated potential mechanisms of NUAK1 regulation and many of these have provided contradictory evidence. Part of this study seeks to identify and clarify regulatory features of NUAK1 *in vitro* which may be linked to the functional role of the kinase *in vivo.* Reports have linked NUAK1 to a several pathways, but a consistent appraisal of its function remains elusive.

In this chapter, recombinant protein and over-expression in cell lines are used to study the control and activation of NUAK1. Mass spectrometry screens have also been undertaken to provide a larger scale insight into possible pathways and interaction partners of NUAK1. Previous studies (unpublished) in our laboratory have shown that NUAK1 interacts with 14-3-3 (Appendix 3) and this interaction is explored further.

3.2 Results

3.2.1 Recombinant NUAK1 expression

Only one previous study to date has used recombinant NUAK1 to investigate its function (Lizcano et al., 2004). This previous report used the human NUAK1 sequence cloned from a brain cDNA library and expressed the protein in a pGEX constructs with a GST-HA tag. BL21 *E.*

coli cells were used for expression but it is not stated exactly which cells were used. This study reported that recombinant NUAK1 required activation by the LKB1 complex. To confirm these findings a similar strategy was used.

A
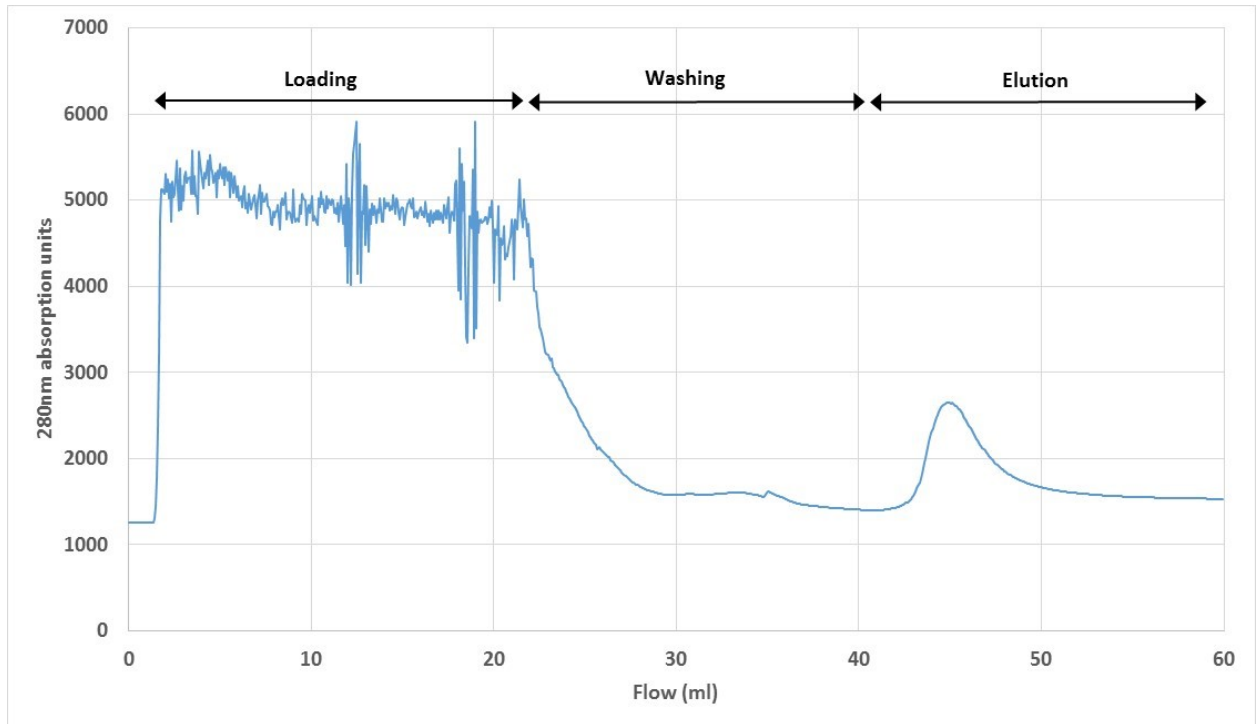
B
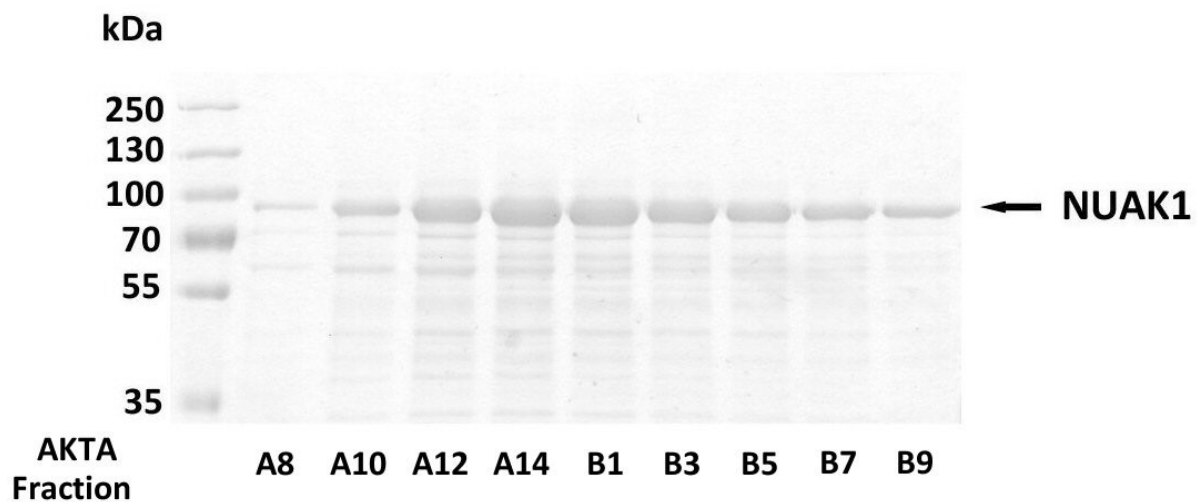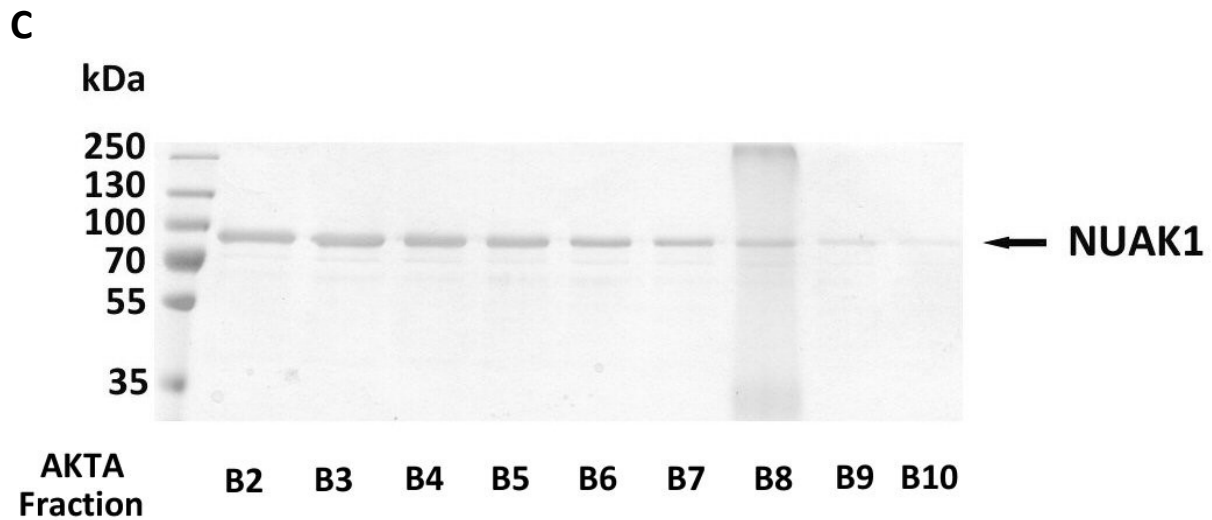
Figure 3.1 Purification of recombinant NUAK1

(A) Recombinant NUAK1 was purified from whole cell extract of *E. coli* competent cells transformed with pRSF-Duet1 vector containing His/FLAG tagged human NUAK1 and induced overnight with 0.4mM IPTG. The protein was purified by Ni^{2+}-Sepharose affinity chromatography. The purification was carried out on an AKTApurifier (GE Healthcare) and eluted protein was monitored by absorption at 280nm. The different stages of purification – loading, washing and elution are shown in panel A. The peak of purified protein is eluted between 40 and 50ml. **(B)** Purified protein was collected in 1ml fractions during the elution phase and resolved on a 10% SDS-PAGE Tris-Glycine gel and stained with SimplyBlue stain. **(C)** Peak fractions were then pooled and concentrated before further purification by size exclusion on a gel-filtration column (Superdex 200, GE Healthcare) and 1ml fractions were collected. These fractions were then resolved on a 10% SDS-PAGE Tris-Glycine gel and stained as before.

Recombinant human NUAK1 expressed well in *E. coli* and was purified in reasonable quantities (approximately 1mg per litre of bacterial culture) (Figure 3.1). Therefore, various manipulations were made to NUAK1 to investigate how changes in the sequence would affect the expression and activity. Mutations were made in key residues to investigate the role of previously identified aspects of kinase regulation. Firstly, the conserved threonine residue in the activation loop (T211 in human NUAK1), previously identified by other studies of the AMPK-related kinases (Lizcano et al., 2004; Manning et al., 2002) was mutated to alanine, which should ablate activity. NUAK1 also contains the highly conserved DFG motif, common to many kinases, immediately N-terminal to the activation loop. Crucially, two residues, an aspartic acid (D196 in human NUAK1) and a lysine (K84 in human NUAK1) are required for binding the Mg^{2+} ion that co-ordinates β and γ phosphates of Mg^{2+}-ATP in the active site. By mutating these residues to alanine, this prevents the binding of Mg^{2+}-ATP rendering the kinase inactive. These are well characterised mutations that have been shown to eliminate activity in many kinases, including AMPK (Johnson et al., 1996) and have previously been used in studies of NUAK1 (Humbert et al., 2010). This is because the kinase domain and active site of many kinases is highly conserved (Figure 1.6). Also, as several previous reports have indicated that various members of the AMPK-related kinase family interact with 14-3-3 proteins (Al-Hakim et al., 2005; Brajenovic et al., 2004), NUAK1 was co-expressed with 14-3-3ε in the same recombinant system. The 14-3-3ε isoform was chosen, as our previous data (Appendix 3) and another report had suggested that this was the most likely to interact with NUAK1 (Ballif et al., 2006).

A

B
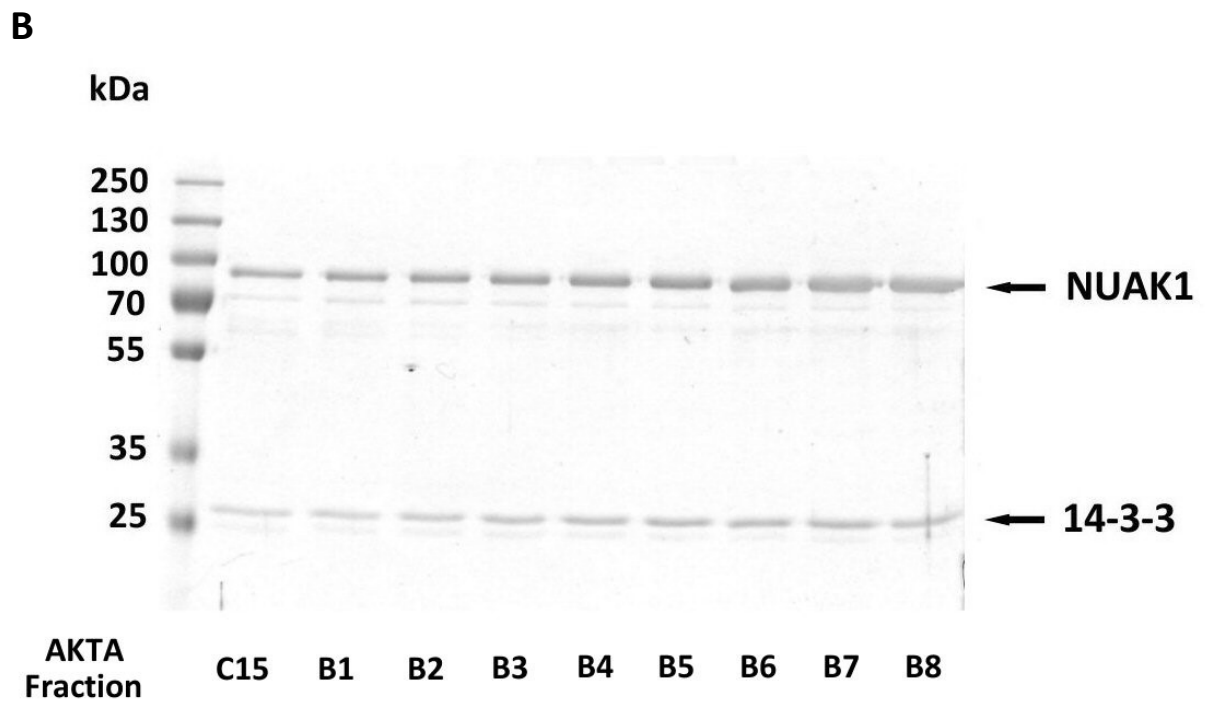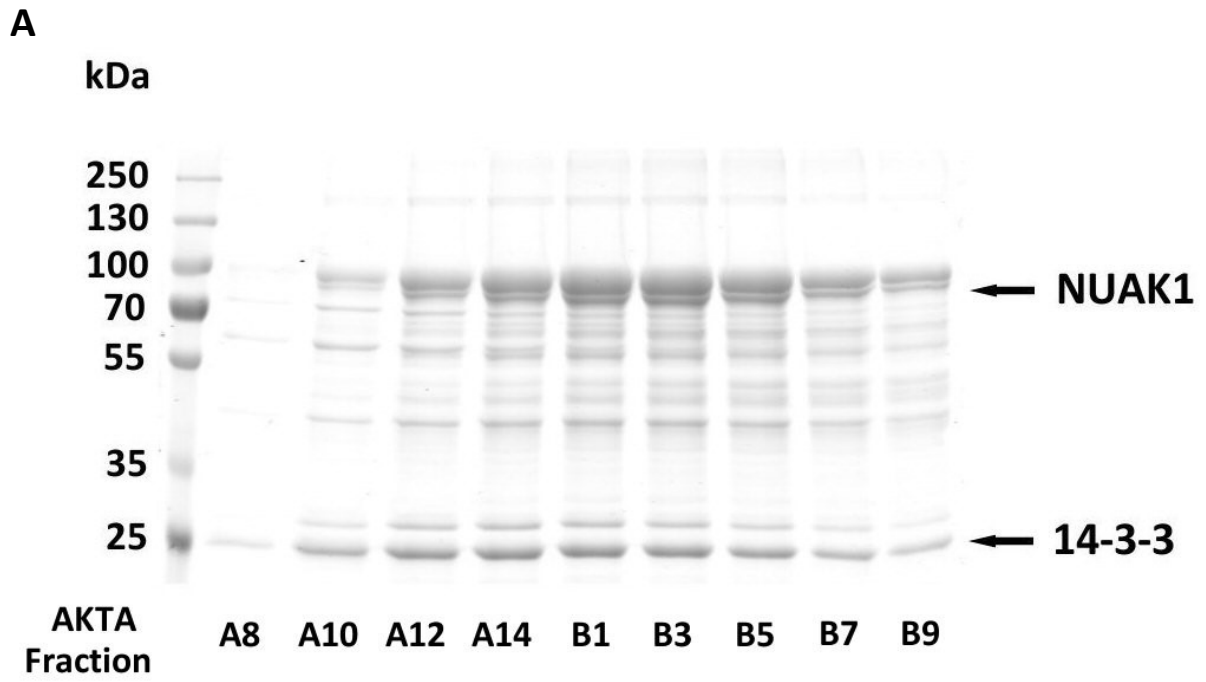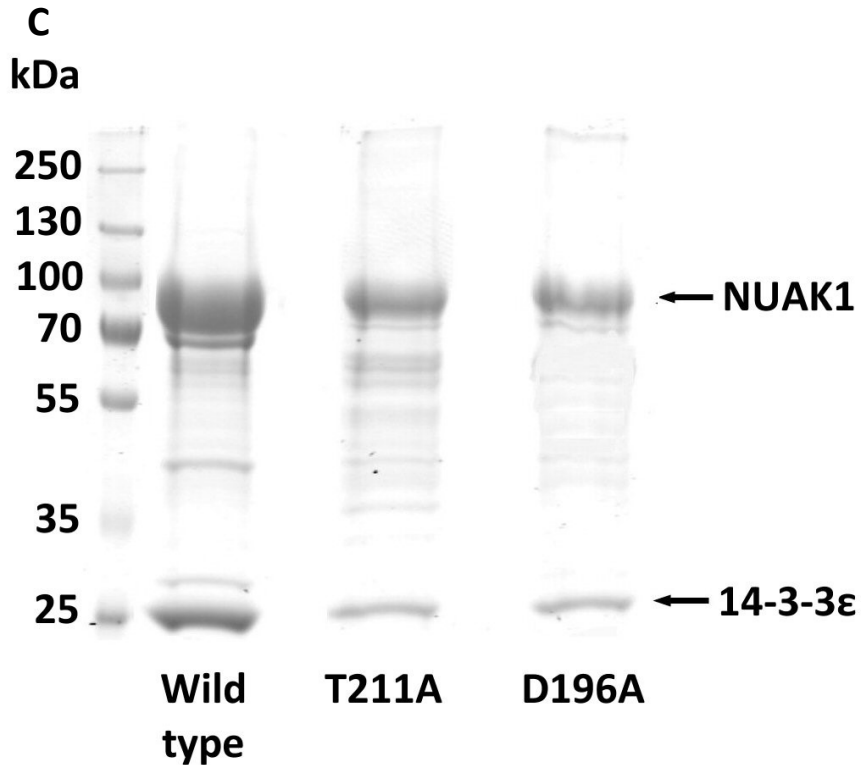
Figure 3.2 Expression of recombinant NUAK1 with 14-3-3ε

Recombinant NUAK1 was purified from whole cell extract of *E. coli* cells transformed with pRSF-Duet1 vector containing His/FLAG tagged NUAK1 and untagged 14-3-3ε controlled by a separate promoter and induced overnight with 0.4mM IPTG. Protein was purified in the same way as in Figure 3.1 using an AKTApurifier. **(A)** Purified protein was collected in 1ml fractions during the elution phase and resolved on a 10% SDS-PAGE Tris-Glycine gel and stained as before. **(B)** The protein was then concentrated and further purified by gel-filtration on a Superdex column and 1ml fractions collected. These fractions were then resolved on a 10% SDS-PAGE Tris-Glycine gel and stained as before. **(C)** Several mutant forms of NUAK1 were produced by site directed mutagenesis and purified in the same way using the pRSF-Duet1 vector system. Concentrated protein was resolved on a 10% SDS-PAGE Tris-Glycine gel and stained as before. The molecular weight markers are indicated on the left (kDa) and the identity of the bands is indicated on the right.

Recombinant NUAK1 could be co-expressed with 14-3-3ε and clearly formed a strong enough complex to survive purification (Figure 3.2B). The 14-3-3ε was untagged so could only be purified by Ni^{2+}-sepharose affinity chromatography by associating with the his-tagged NUAK1. Mutant forms of NUAK1 (T211A and D196A) could both be expressed and both still associated with 14-3-3ε (Figure 3.2C). During expression of both mutants the protein yield was substantially lower but sufficient quantities of protein were obtained for further experiments. The NUAK1 mutant proteins gave around half the yield of the wild-type, approximately 0.5mg per litre of bacterial culture.

3.2.2 Recombinant NUAK1 activity

A previous report (Lizcano et al., 2004) had used a modified version of the AMPK radiolabeling kinase assay (Davies et al., 1989) to measure the activity of recombinant NUAK1. A similar assay was optimised in our laboratory (see section 2.2.10.2 and used to assess the activity of the various forms of recombinant protein.
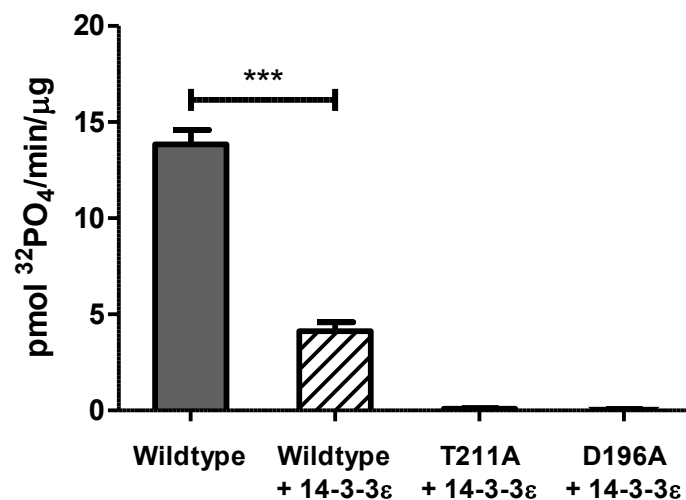
Figure 3.3 Activity of recombinant NUAK1

Recombinant wild-type NUAK1, mutated NUAK1 and NUAK1 co-expressed with 14-3-3ε was assayed by incubation with $\gamma^{32}P$-ATP and synthetic AMARA peptide substrate. Activities are shown as mean ± S.E.M. from three independent experiments and are plotted as specific activity (picomoles of phosphate incorporated per minute per microgram of protein, pmol/min/µg).

Interestingly, the wild-type full length protein as expressed in *E. coli* clearly had some basal activity without the need for incubation with LKB1 (Figure 3.3), which contradicts previous reports (Lizcano et al., 2004). The wild-type protein co-expressed with 14-3-3ε also had some activity but significantly lower than NUAK1 expressed alone. As expected, the T211A and D196A mutants showed no activity (Figure 3.3).

The radiolabelling peptide assay was adapted from the AMPK assay in which the AMARA peptide was the substrate, based on optimum recognition motifs of known downstream targets for AMPK (Dale et al., 1995). The AMARA peptide has been shown to work as a synthetic substrate for many kinases but there is no way to predict the optimum substrate for NUAK1, as very few downstream targets have been verified. In order to test the activity of NUAK1 towards different peptides, a series of previously identified substrates were tested to see if NUAK1 could phosphorylate them *in vitro.* In addition to the AMARA peptide, LNR peptide was tested, as it is known to be a suitable substrate for activity measurements of several serine/threonine-specific kinases (Ross et al., 2002). The SAMS peptide was tested as it is the original peptide substrate for AMPK (Davies et al., 1989) and a novel LATS_N1 peptide, based on the sequence of human LATS1 protein, was tested as it was shown to be phosphorylated by NUAK1 (Humbert et al., 2010).

A

B

C

AMARA	AMARAASAAALARRR
LNR	KKLNRTLSFAEPG
SAMS	HMRSAMSGLHLVKRR
LATS1_N1	PNIPVRSNSFNNPLGPRRR
LATS1_N2	PNIPVRANSFNNPLGPRRR
LATS1_N3	PNIPVRSNAFNNPLGPRRR
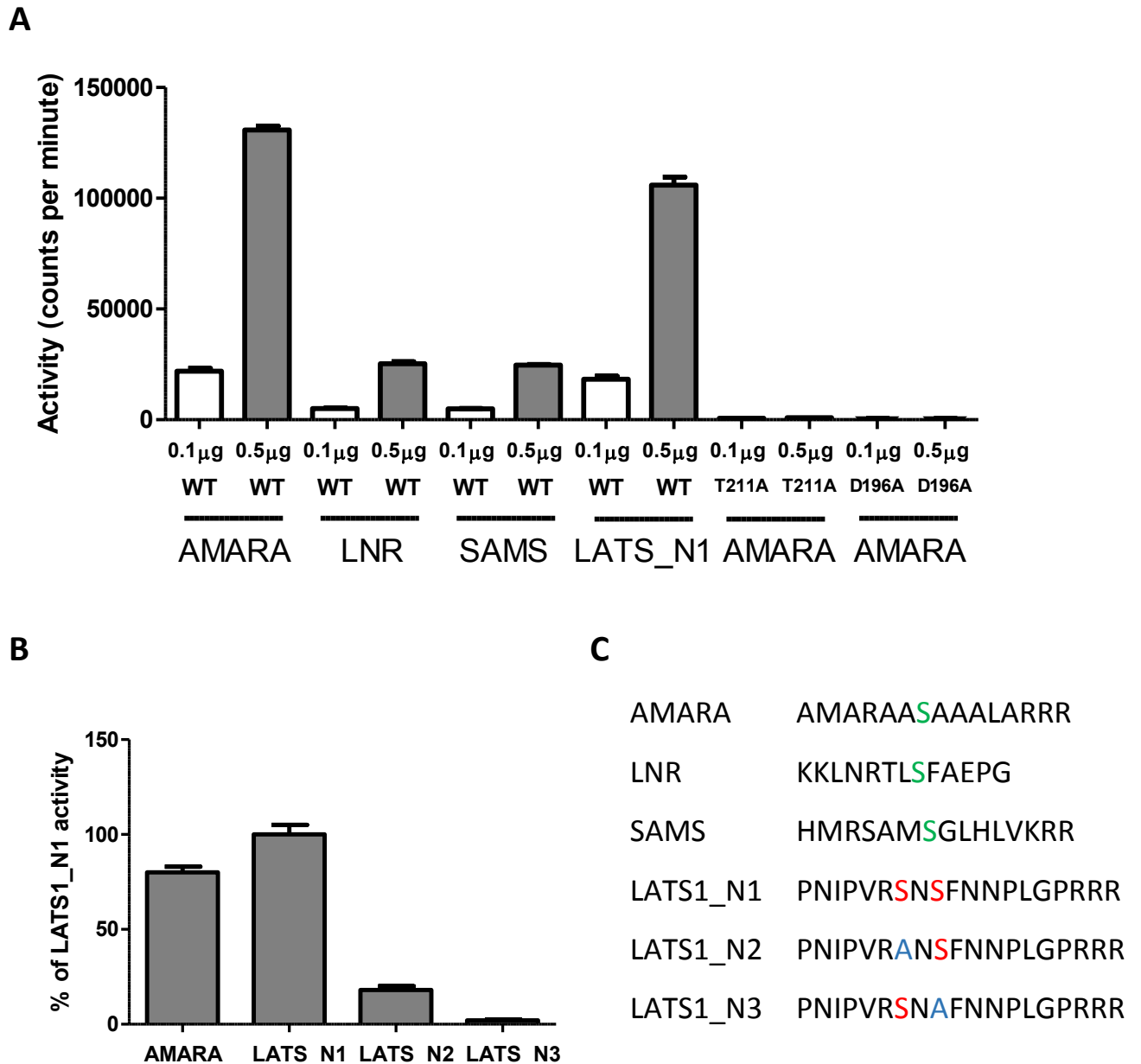
Figure 3.4 Substrate specificity of recombinant NUAK1

(A) 0.1 or 0.5µg of wild-type recombinant NUAK1 expressed without 14-3-3ε was incubated with the indicated peptide substrate and γ^{32}P-ATP in identical reaction buffers to detect any variation in substrate specificity. T211A and D196A mutated NUAK1 are shown as negative controls. **(B)** Various mutations in the LATS1 peptide as shown are incubated with equal amounts of recombinant NUAK1 in the same radiolabelling buffers and activities are shown as a percentage of the LATS_N1 peptide which is based on the N-terminal sequence of wild-type human LATS1 protein. Activities are shown as mean ± S.E.M. from three independent experiments. **(C)** The sequence of the peptides used are shown with key residues highlighted.

This demonstrated that NUAK1 shows maximal activity when assayed using the AMARA peptide with very little activity towards the SAMS peptide, as previosuly reported (Lizcano et al., 2004). This previous study of recombinant NUAK1 activity also reported it preferentially phosphortylating the LNR peptide but this does not seem to be the case in my experiment (Figure 3.4). LATS_N1 peptide showed similar levels of activity as the AMARA peptide but as LATS1 protein was a known downstream target of NUAK1 *in vivo* (Humbert et al., 2010), it was possible to mutate the targeted serine residues to assess possible variations in substrate specificity. Figure 3.4B clearly shows similar activity levels towards AMARA and LATS_N1 from equal amounts of protein but mutation of either of the serine residues to alanine in the LATS peptide reduces this activity significantly.
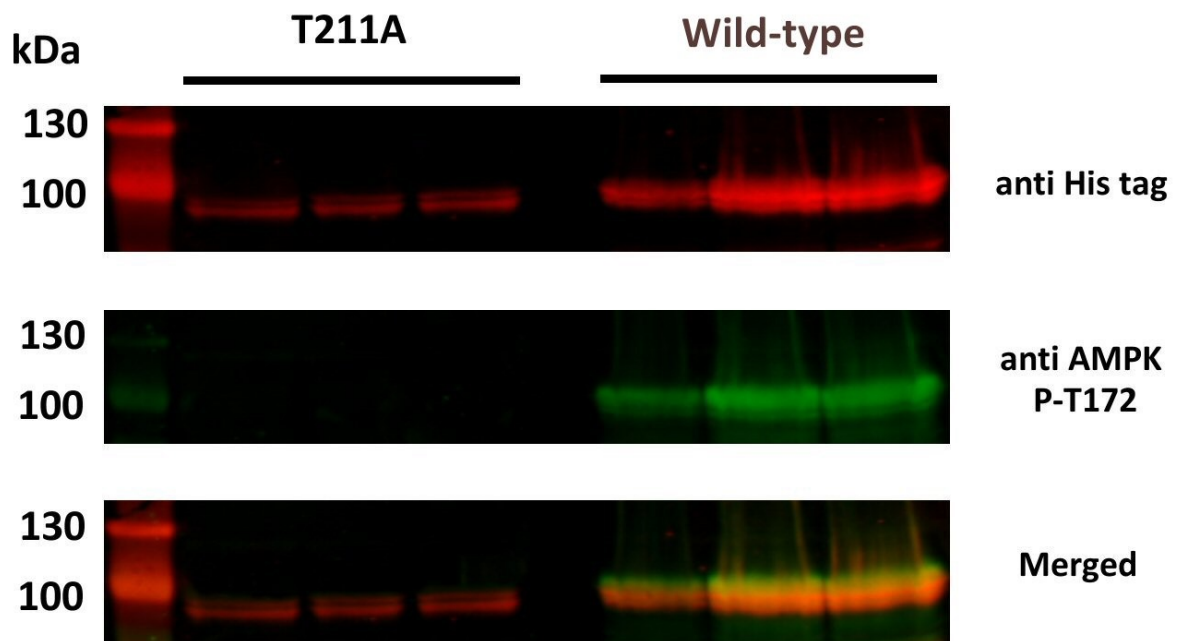
Figure 3.5 Western blot detection of recombinant NUAK1 and phosphorylation status of the T-loop

Equal volumes of eluate from bacterially expressed recombinant wild-type and T211A mutated NUAK1 was resolved on a 10% SDS-PAGE Tris-Glycine gel and transferred to Immobilon FL PVDF membrane for immunodetection. The membrane was incubated with the indicated primary antibodies followed by fluorescence conjugated secondary antibodies for multiplex detection. The membrane was scanned using a LI-COR Odyssey scanner.

As the conserved threonine residue (T211 in human NUAK1) has been shown to be critical for activity of the kinase, it is useful to determine if this phosphorylation can be detected by western blotting for further analysis of the protein *in vivo*. As shown in Figure 3.5, the recombinant protein, as expressed in *E. coli* without LKB1, can be detected on a western blot using an antibody against the His-tag. The phosphorylation status can also be detected by cross-reaction with the AMPK phospho-T172 antibody, which is the equivalent residue to T211 in NUAK1. This cross-reaction has been reported previously and provides a useful reagent for assessing the phosphorylation status of NUAK1. As expected, Figure 3.5 shows that no phosphorylation of the T211A mutant is detectable and that the expression level seems to be lower for equivalent *E. coli* culture volumes, approximately half that of the wild-type protein.

3.2.3 Cell based expression, activity and regulation of NUAK1

Assessing the activity of a kinase *in vitro* with purified recombinant protein is clearly a very artificial method that does not permit the complexities of other signalling pathways that may impact on the activity occurring *in vivo* or in cells. By expressing NUAK1 in mammalian cells it is possible to assess the activity of the kinase in a more physiologically relevant system. The same His/FLAG tagged NUAK1 construct and the T211A mutant used for bacterial expression were cloned into pCDNA3.1 vectors for transfection into mammalian cell lines. Initially COS7 cells were used as they are a readily transfectable cell line that have been shown to express LKB1.

A

B
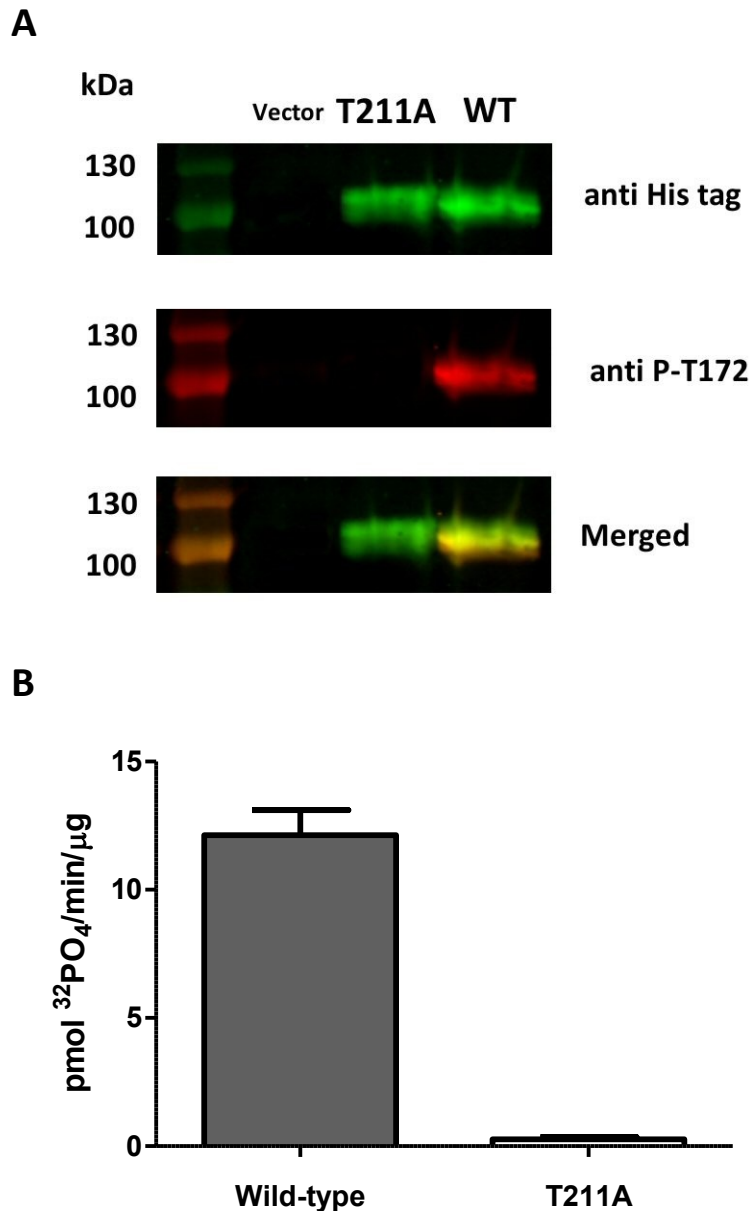
Figure 3.6 Overexpression and activity in COS7 cells

(A) Wild-type and T211A mutated NUAK1 was cloned into a pcDNA3.1 vector and transfected into COS7 cells using calcium phosphate precipitation. Cells were rapidly lysed and crude lysates were resolved on a 10% SDS-PAGE Tris-Glycine gel and transferred to Immobilon FL PVDF membrane for immunodetection. The membrane was incubated with the indicated primary antibodies followed by fluorescence conjugated secondary antibodies for multiplex detection. **(B)** Expressed protein from COS7 cells was purified using FLAG-affinity resin and activity was detected by incubation with γ^{32}P-ATP and synthetic AMARA peptide substrate. Activities are shown as mean ± S.E.M. from three independent experiments and are plotted as specific activity.

NUAK1 protein can clearly be overexpressed in COS7 cells and mutated T211A protein clearly shows as similar degree of expression but no phosphorylation of the threonine residue, as expected (Figure 3.6). Protein from cells transfected with either wild-type or T211A mutated NUAK1 was then purified using FLAG affinity resin in order to be able to assess the activity of the protein expressed in mammalian cells. As shown in Figure 3.6B, the phosphorylation status of T211 correlates with the activity of the protein, as expected and as shown in a recombinant system in Figure 3.3 and Figure 3.5. The immunoprecipitated wild-type protein displayed similar NUAK activity to bacterially expressed recombinant protein, but COS7 cells express endogenous LKB1 and it is not clear if this basal activity is a result of phosphorylation by LKB1.

As a mammalian cell expression system provides a more physiologically relevant context for regulation, it is a good opportunity to test some point mutations to better understand previous reports regarding the regulation of NUAK1. A previous study reported that NUAK1 was phosphorylated on S600 by Akt and that this resulted in activation of NUAK1 (Suzuki et al., 2004b). By mutating this and other residues it is possible to assess their effect on NUAK1 activity.

A

1 = Wild-type
2 = K84R
3 = T211A
4 = T211D
5 = S600A

B
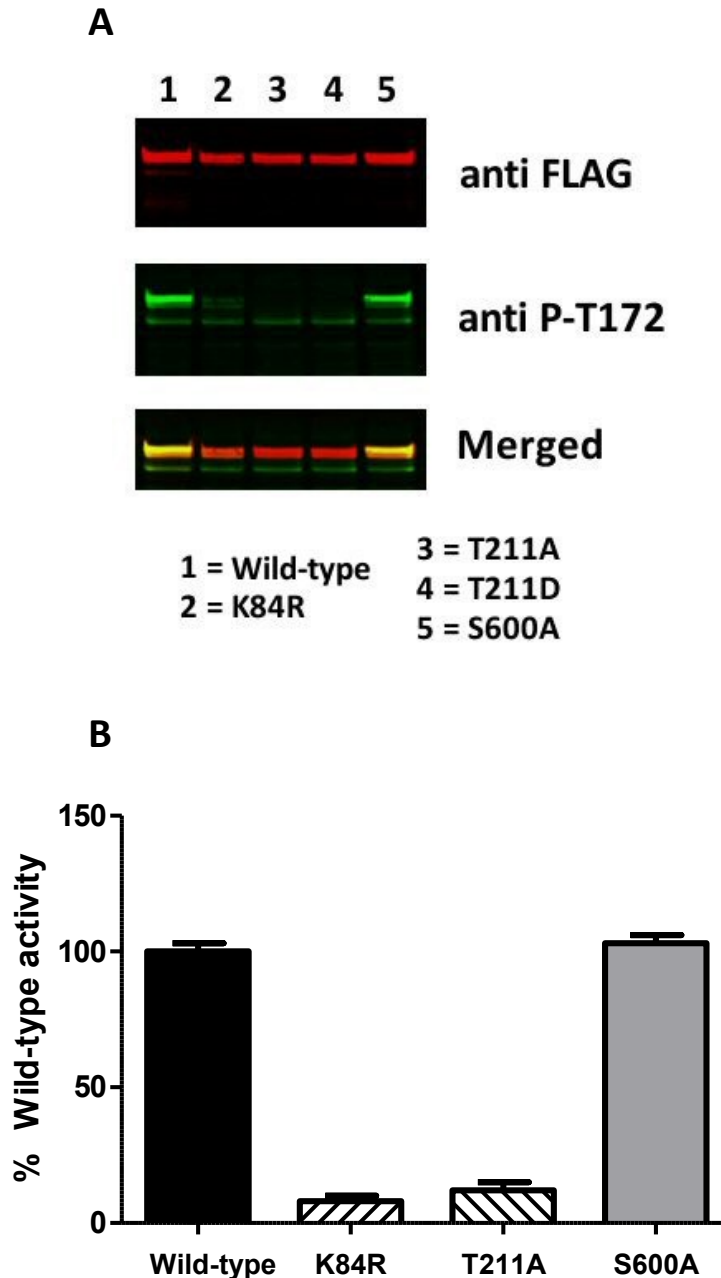
Figure 3.7 Effect of point mutations on recombinant NUAK1 activity

Point mutations of key residues in NUAK1 were created by site-directed mutagenesis and confirmed by sequencing. The protein was expressed by transfecting the relevant vector into HEK-293T cells and purified using a FLAG affinity resin. **(A)** The protein was eluted off the resin by competition with a FLAG peptide and resolved on a 10% SDS-PAGE Tris-Glycine gel and transferred to Immobilon FL PVDF membrane for immunodetection with the indicated antibodies, as before. **(B)** The activity of recombinant protein carrying the indicated mutation was determined by incubation with γ^{32}P-ATP and synthetic AMARA peptide substrate.

Wild-type NUAK1 and various mutants can also be expressed in HEK293T cells and as before the phosphorylation status of T211 correlates with the activity. Consistent with the results obtained previously in COS7 cells, the T211A mutant has very low activity (Figure 3.6 and Figure 3.7). The K84R mutant is another form of kinase-inactive NUAK1 that has been used previously (Humbert et al., 2010) and shows almost no activity. Importantly, the activity of NUAK1 harbouring the S600A mutation was similar to that of the wild-type, suggesting that Akt signalling may not play a role in NUAK1 activity, at least in HEK cells.

To assess if the over-expression of LKB1 and 14-3-3ε have any effect on NUAK1 activity in cells, these were both cloned into pcDNA3 vectors for co-expression in the same cell lines. For LKB1, three different vectors were used to co-express LKB1, STRADα (both carrying FLAG-tags) and MO25 (with a myc-tag). 14-3-3ε was expressed carrying a V5 tag.

A

1 = NUAK1
2 = NUAK1 + LKB1 + (STRADα + MO25)
3 = NUAK1 + 14-3-3
4 = NUAK1 + LKB1 + (STRADα + MO25) + 14-3-3

Red = anti-FLAG
Green = anti-14-3-3

B
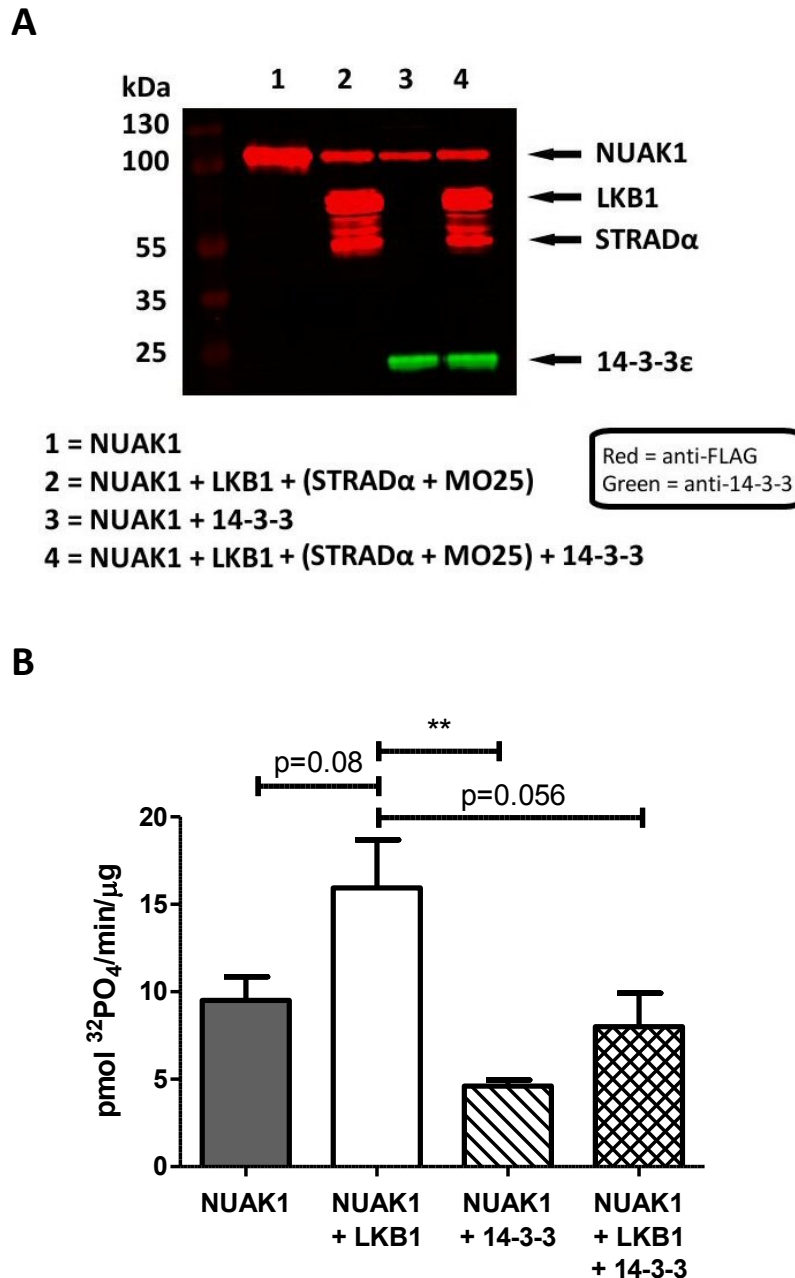
Figure 3.8 Co-expression of NUAK1 with LKB1 and 14-3-3 in cells

NUAK1 was co-expressed in COS7 cells with either full-length human LKB1 (along with MO25 and STRADα in separate vectors to ensure activity) or 14-3-3ε. **(A)** FLAG affinity purified protein was resolved on a 10% SDS-PAGE Tris-Glycine gel and transferred to Immobilon FL PVDF membrane for immunodetection. The membrane was incubated with the indicated primary antibodies followed by fluorescence conjugated secondary antibodies for multiplex detection. **(B)** Protein was purified using FLAG-affinity resin and activity of the immunocomplex was detected by incubation with γ^{32}P-ATP and synthetic AMARA peptide substrate. Activities are shown as mean ± S.E.M. from three independent experiments and are plotted as specific activity. LKB1 was also FLAG-tagged but has negligible activity towards the AMARA peptide (data not shown).

NUAK1 can clearly be overexpressed alongside LKB1 and 14-3-3ε in cells and these proteins can be purified using FLAG affinity resin. 14-3-3ε was expressed with a V5 tag and therefore must have co-purified with either NUAK1 or LKB1 (Figure 3.8). Similar to the recombinant system, LKB1 does seem capable of increasing NUAK1 activity slightly and co-expression with 14-3-3ε does seem to reduce activity to around half of the basal level (Figure 3.3 and Figure 3.8B). Interestingly, co-expression with both 14-3-3ε and LKB1 appears to restore the NUAK1 activity to around basal levels, suggesting they may have antagonistic effects.

3.2.4 Role of upstream kinases

To clarify the role of LKB1 and determine if there was any additional role of the upstream kinase in the activation of NUAK1, various activity measurements were performed using bacterially expressed recombinant proteins.
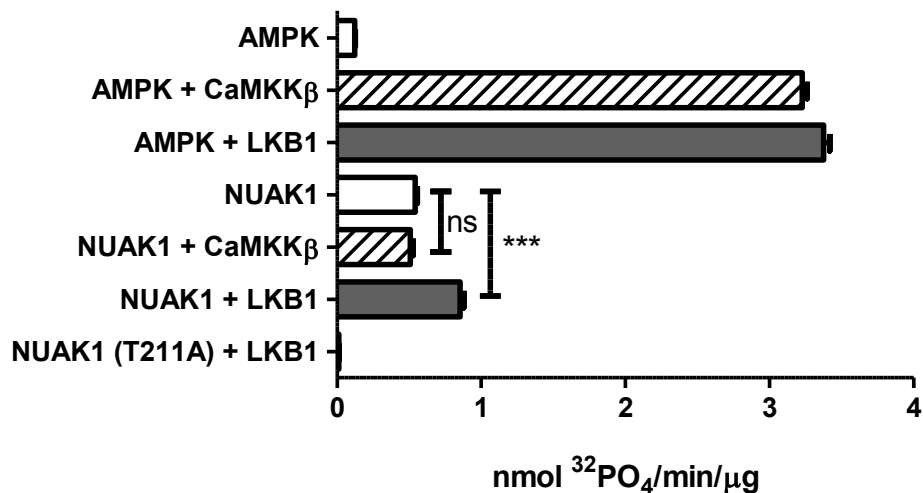
Figure 3.9 Partial activation by LKB1 but no activation by CaMKKβ of recombinant NUAK1

Recombinant NUAK1 and AMPK activity was measured using a radioactive kinase assay by incubation with γ^{32}P-ATP and synthetic AMARA peptide substrate. Bacterial recombinant NUAK1 expressed without 14-3-3 was incubated in the presence of LKB1 or CaMKKβ and MgATP to detect any effect on NUAK1 activity. Recombinant AMPK was used as a control to detect activity of recombinant LKB1 and CaMKKβ (kindly provided by Dr David Carmena). Activities are shown as mean ± S.E.M. from three independent experiments and are plotted as specific activity.

LKB1 or CaMKKβ alone have negligible activity on the AMARA peptide so the readout is solely for NUAK1. Recombinant LKB1 was expressed as an active complex with STRADα and MO25 in *E. coli* and its activity was demonstrated by activation of the human wild-type AMPK complex (α1β1γ1) as previously reported (Neumann et al., 2003). Similarly, active CaMKKβ was expressed in *E. coli* and activity was confirmed by activation of wild-type AMPK. Based on their activation of AMPK, the same amounts of active LKB1 and CaMKKβ were then incubated with recombinant NUAK1 for an assay with the AMARA peptide. CaMKKβ caused no change in activity but incubation with LKB1 caused a modest, but significant, increase in activity, around 80% more than the basal activity (Figure 3.9). T211A, the T-loop mutant of NUAK1 was used as a negative control and clearly shows no activity when incubated with LKB1.

The variation in activity of wild-type NUAK1 observed between different experiments (Figure 3.3, 3.6 and 3.9) may be attributed to differences in the degree of autophosphorylation during the purification, or to unknown differences in cellular conditions that affect the activity of the kinase.

Only one previous report has indicated any compounds or endogenous molecules that may activate or inhibit NUAK1 activity (Fisher et al., 2005). This report suggests that insulin and a known AMPK activator, AICAR, can activate NUAK1 based on immunoprecipitating NUAK1 from incubated rat muscles. To examine whether any other molecules may have an effect on NUAK1, recombinant and cell-based assays were conducted to try and modulate the activity of the kinase with known activators of other AMPK-related kinases, specifically salt and AMP. Salt has been shown to activate the SIK family kinases and AMP is a well-known allosteric activator of AMPK. To test the effect of known AMPK family activators, bacterially expressed recombinant NUAK1 was incubated with 0.2mM AMP and COS7 cells overexpressing NUAK1 were incubated with 0.5M sodium chloride

A

B

C

D
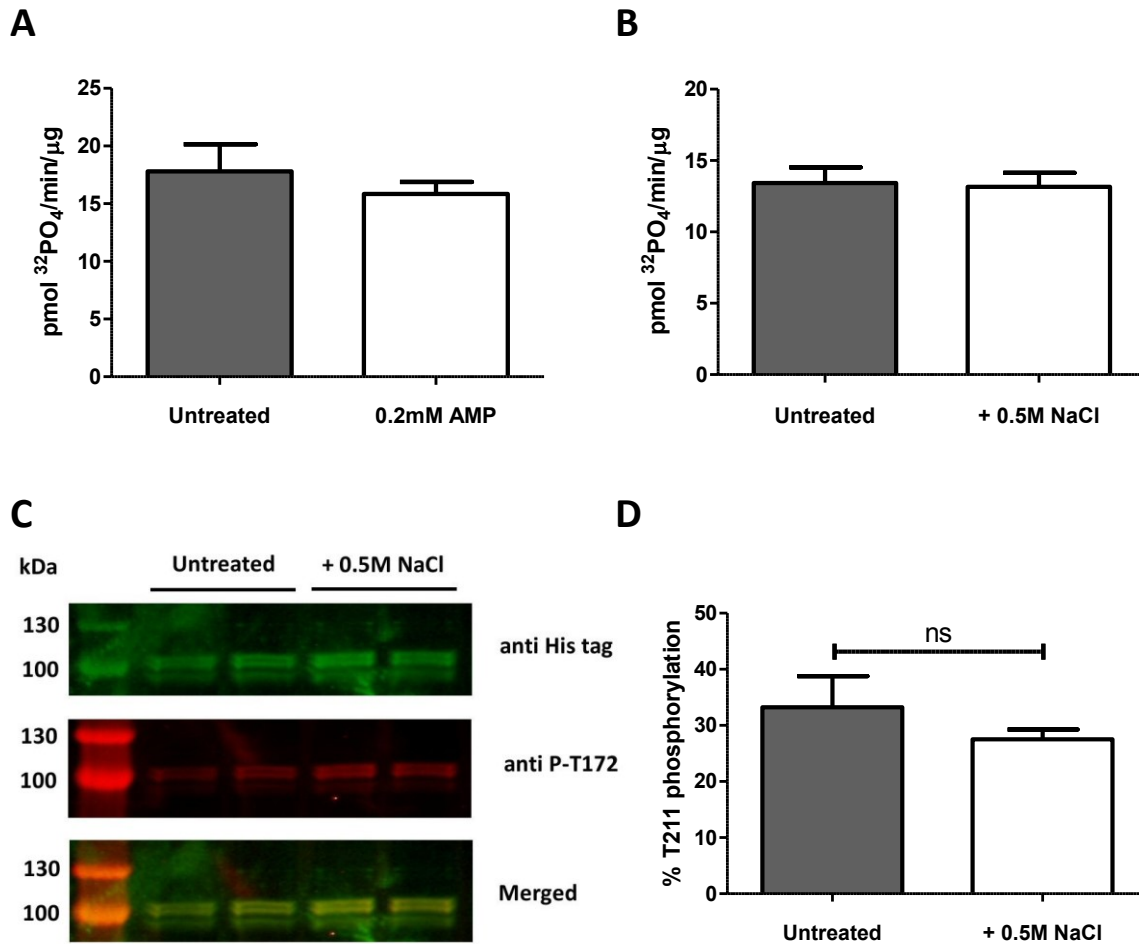
Figure 3.10 No activation of NUAK1 by known AMPK allosteric activator AMP or salt

(A) Recombinant NUAK1 expressed without 14-3-3ε was incubated with 0.2mM AMP during a kinase assay and compared to activity of the untreated protein determined by incubation with γ^{32}P-ATP and synthetic AMARA peptide substrate. **(B)** COS7 cells expressing His-tagged NUAK1 were treated with 0.5M sodium chloride, added to the culture medium for 10 minutes before rapid lysis. The activity of the protein was determined by immunoprecipitation using an anti-His antibody followed by incubation with γ^{32}P-ATP and synthetic AMARA peptide substrate. **(C) and (D)** Lysates from the treated cells were resolved on a 10% SDS-PAGE Tris-Glycine gel and transferred to Immobilon FL PVDF membrane for immunodetection, as before. The percentage of phosphorylated protein was determined using the LI-COR Image Studio software.

Clearly neither salt (in cells) nor AMP (direct addition to the kinase assay) have any significant effect on the activity of NUAK1 (Figure 3.10), suggesting there must be several different mechanisms of regulation within the AMPK-related kinase family. As before, the phosphorylation status of T211 broadly correlates with activity and using densitometry on the western blot, it is possible to establish that under basal conditions only around 35% of NUAK1 in cells is phosphorylated and active. This shows that there is a pool of unphosphorylated protein that could be activated by upstream signals.

3.2.5 Autophosphorylation of NUAK1

The fact that basal levels of activity can be detected in recombinant protein expressed in bacteria without the presence of LKB1 suggests that there must be other activating mechanisms. One possibility is that NUAK1 is capable of activation by autophosphorylation, a mechanisms previously described for another AMPK-related kinase, MELK (Lizcano et al., 2004). Autophosphorylated MELK was maximally active and unable to be further phosphorylated by LKB1. Also, some members of the MARK/PAR family may be capable of autoactivation (Marx et al., 2010). Therefore, there may be conserved mechanisms of activation by autophosphorylation amongst AMPK-related kinase family members.

Many kinase systems are a balance between phosphorylation and dephosphorylation, which is controlled by a series of phosphatases. Some kinases are constitutively active, but many respond to activation by phosphorylation, often as part of signal transduction pathways. While several well characterised kinases, notably AMPK, do not have a clearly defined phosphatase, it is crucial for the regulation of most systems to have a robust mechanism of dephosphorylation. The identity of the *in vivo* phosphatase of NUAK1 is unknown but recombinant protein phosphatase 2C (PP2C) can be used as a generic phosphatase and is capable of dephosphorylating a number of kinases. It is routinely used in *in vitro* AMPK dephosphorylation assays (Sanders et al., 2007).

A

B
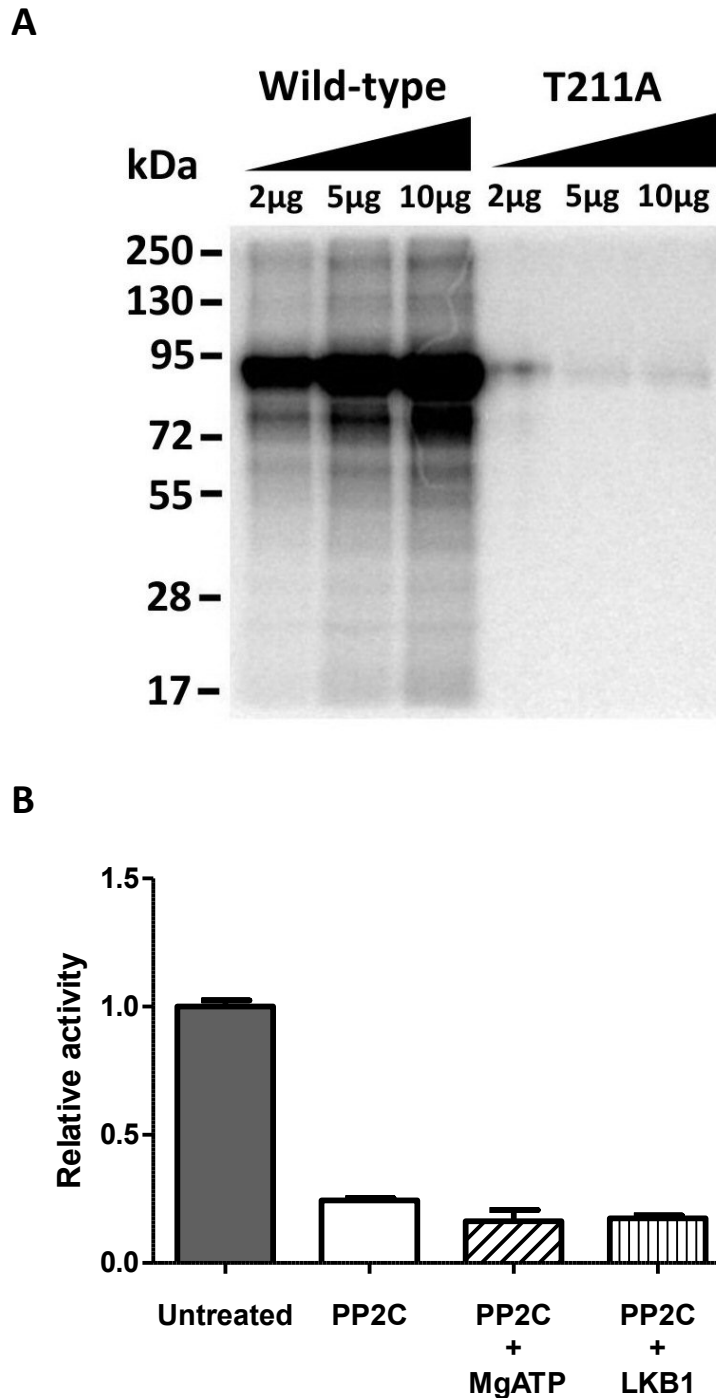
Figure 3.11 Autophosphorylation and dephosphorylation of recombinant NUAK1

(A) Various amounts of wild-type and T211A mutated bacterially expressed recombinant NUAK1 were incubated with γ^{32}P-ATP in an appropriate buffer and resolved on a 10% SDS-PAGE Tris-Glycine gel. The gel was exposed to a phosphorimager plate and imaged using a Fuji FLA-9000 phosphorimager. **(B)** Wild-type bacterially expressed recombinant NUAK1 was bound to FLAG-affinity resin and incubated with recombinant PP2C (non-FLAG tagged) and the activity determined by incubation with γ^{32}P-ATP and synthetic AMARA peptide substrate. Equal amounts of the PP2C treated protein bound to resin was also washed and treated with either MgATP or recombinant LKB1 and MgATP and used in the same radioactive kinase assay as before.

The fact that wild-type protein but not the non-activateable form (T211A) can incorporate $^{32}PO_4$ clearly shows that NUAK1 can autophosphorylate (Figure 3.11A). The T211A mutant renders the kinase inactive, therefore eliminating its ability to autophosphorylate but it is possible that active NUAK1 can autophosphorylate on other residues and this may play a role in its regulation or interaction with other proteins.

This autophosphorylation is likely to be the reason for the basal level of activity observed in the bacterially expressed recombinant protein. To analyse if the activity can be reduced by dephosphorylation, active NUAK1 was treated with recombinant PP2C and showed a significant drop in activity to around 30% of the basal level (Figure 3.11B). Because NUAK1 is capable of autophosphorylation, it was of interest to see if, when PP2C was removed from the assay and the protein bound to the FLAG resin was reincubated with MgATP, the protein could reactivate. The recombinant PP2C was not FLAG tagged so could be washed out, leaving just the NUAK1 bound to the resin. After incubation with MgATP no increase in activity was observed. Dephosphorylated NUAK1 bound to the FLAG resin was also reincubated with active recombinant LKB1, but no increase in activity was observed (Figure 3.11B).

3.2.6 Subcellular localisation of NUAK1

The data described above suggest that while LKB1 may have some role in determining the activity of NUAK1, there is likely to be some basal level of autoactivation, potentially meaning the kinase is constitutively active. If there is a constitutive level of activity then the function of the kinase may be controlled by subcellular localisation. To investigate this, immunofluoresence experiments were carried out using tagged forms of NUAK1.

A
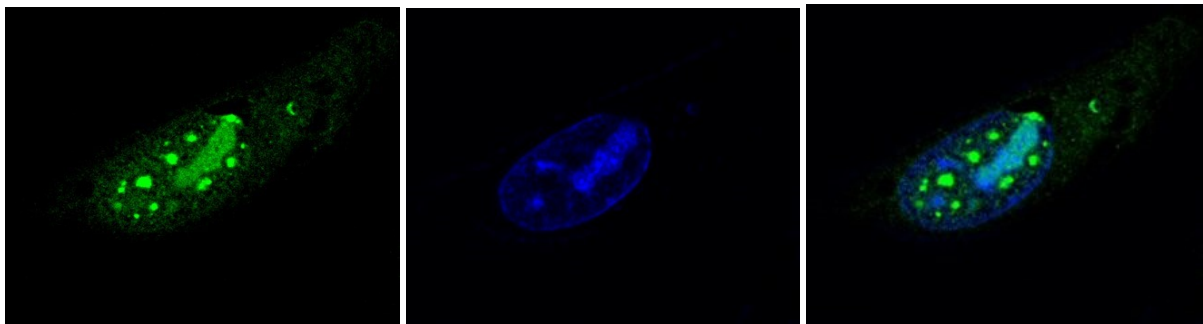
| GFP-NUAK1 | DAPI | Merged |

B

| GFP-NUAK1 | DAPI | Merged |

C

NUAK1

Tubulin
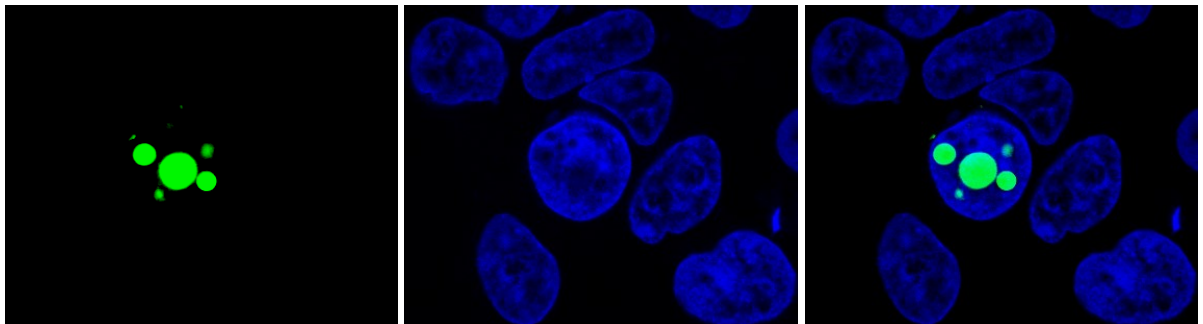
DAPI

Merged
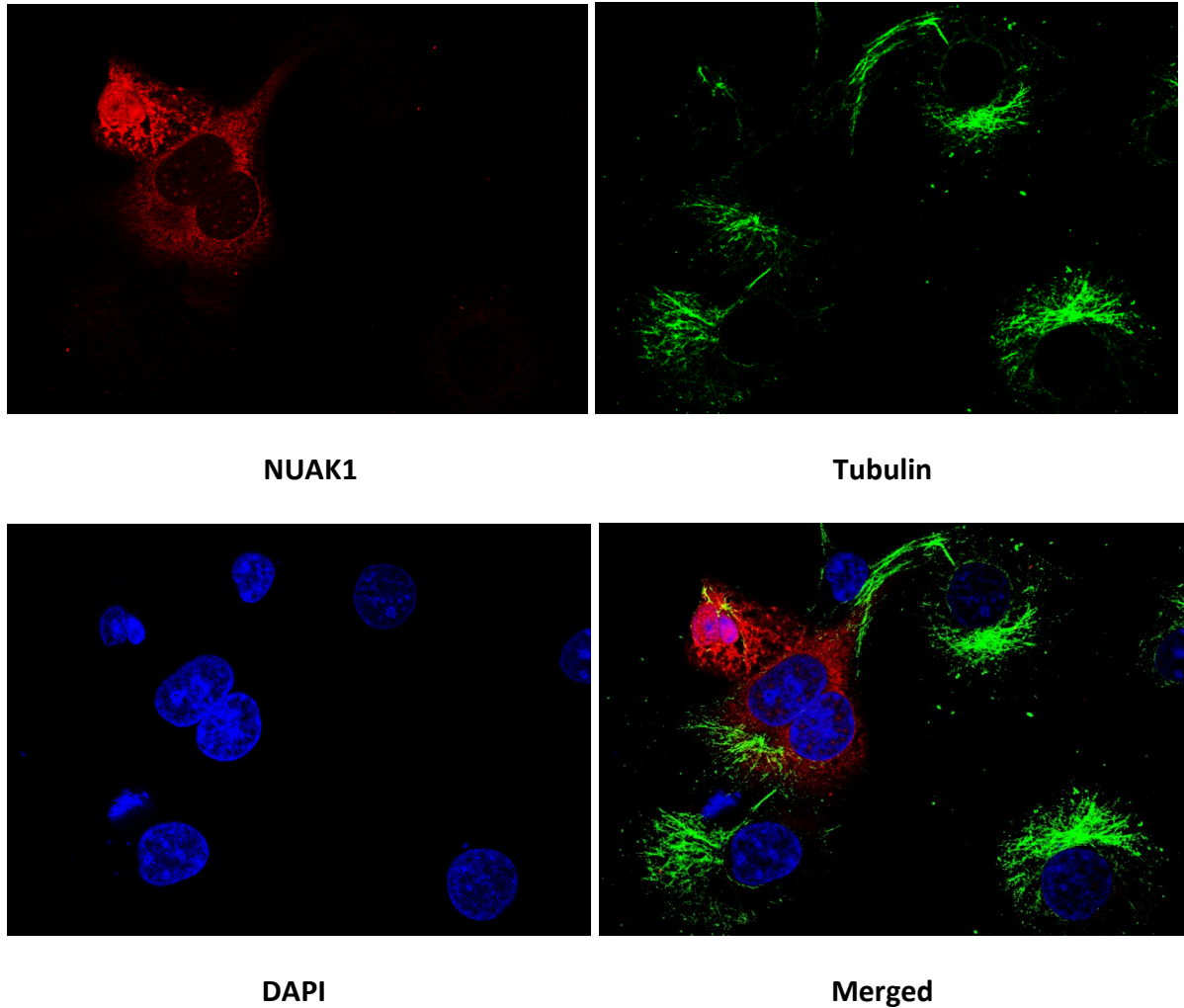
Figure 3.12 Subcellular localisation of NUAK1 in LKB1 expressing cells

(A) and (B) NUAK1 tagged with green fluorescent protein was expressed in HEK293T cells and fixed for fluorescence microscopy. Images are shown of DAPI stained transfected cells and the merged image for confirmation of subcellular localisation. **(C)** COS7 cells transfected with FLAG-tagged NUAK1 were fixed and stained with immunofluorescence antibodies against FLAG and tubulin. The DAPI stained and merged image are shown for confirmation of subcellular localisation.

GFP-NUAK1   **DAPI**   **Merged**
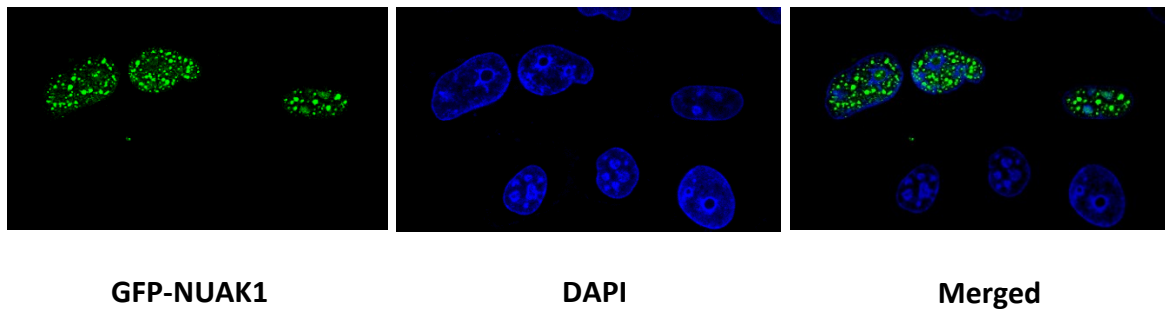
Figure 3.13 Subcellular localisation of NUAK1 in LKB1 null cells

NUAK1 tagged with green fluorescent protein was expressed in HeLa cells and fixed for fluorescence microscopy. Images are shown of DAPI stained transfected cells and the merged image for confirmation of subcellular localisation.

The subcellular localisation of NUAK1 is clearly highly regulated as some of the images show punctate regions of NUAK1 localisation in the nucleus (Figure 3.12A and B), whereas panel C shows NUAK1 to be localised entirely in the nucleus. It is possible that the subcellular localisation varies during different parts of the cell cycle as the cell in Figure 3.12C has just divided and all the NUAK1 appears to be localised in the cytoplasm. Also, Figure 3.12A and B both show HEK293T cells with different patterns of expression, possibly at different stages of the cell cycle. Interestingly, the cells in Figure 3.13 are HeLa cells, which lack LKB1 expression, yet the subcellular localisation of NUAK1 is similar to that shown in HEK293T cells in Figure 3.12A. This suggests that any role LKB1 plays in the activation of NUAK1 may not affect its subcellular localisation. Although NUAK1 clearly can translocate into the nucleus, the function of the kinase in nuclear signalling is unclear, although previous reports have linked NUAK1 to senescence and cell cycle control (Humbert et al., 2010). The nuclear role of NUAK1 may be linked to its function of phosphorylating LATS1 as part of the Hippo pathway (Figure 1.10), however it is not currently clear where this phosphorylation takes place.

3.2.7 NUAK1 knockout mouse embryonic fibroblasts (MEFs)

Later on in this project, as part of the knockout mouse breeding strategy (Figure 4.1 and Figure 4.2), NUAK1 knockout mouse embryonic fibroblasts (MEFs) became available, providing a very useful resource for analysing the potential role of the kinase as well as providing a useful negative control.

A

B

C
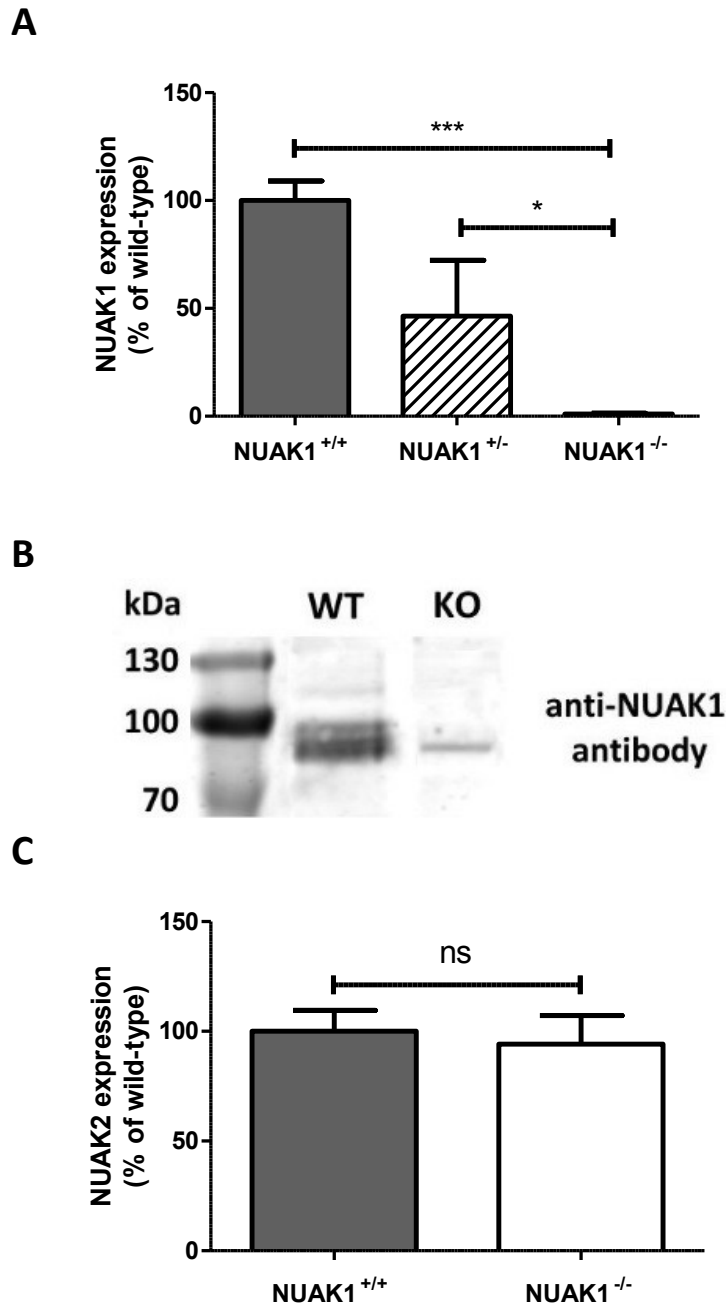
Figure 3.14 Establishment of MEFs and confirmation of NUAK1 knockout

(A) Embryonic fibroblasts were established from wild-type, heterozygous and homozygous NUAK1 knockout mouse embryos (Figure 4.1 and
Figure 4.2). mRNA was purified from wild-type and homozygous NUAK1 knockout cells and used to make cDNA. The expression level of NUAK1 was confirmed by quantitative PCR and is shown as a percentage of the wild-type MEF expression. **(B)** Total lysates from wild-type and knockout MEFs were resolved on a 10% SDS-PAGE Tris-Glycine gel and transferred to Immobilon FL PVDF membrane for immunodetection with anti-NUAK1 antibody (Cell Signalling). **(C)** NUAK2 expression levels were tested by quantitative RT-PCR to confirm that the knockout was specific and expression of similar proteins was unaffected. All qPCR figures are normalised to the expression of glyceraldehyde 3-phosphate dehydrogenase (GAPDH).

MEFs were established from wild-type, heterozygous and homozygous global NUAK1 knockout embryo littermates. NUAK1 deletion was confirmed by quantitative PCR and western blotting with the best available commercial NUAK1 antibody (see Figure 4.5), showing total deletion in the knockout MEFs (Figure 3.14). Also, the heterozygous global NUAK1 knockout MEFs showed approximately 50% of the wild-type expression levels, as expected. To ensure the knockout was specific, quantitative PCR was performed using specific primers designed against NUAK2, the closest homologous protein to NUAK1. As shown in Figure 3.14C there was no change in NUAK2 mRNA levels, suggesting the NUAK1 knockout strategy is specific.

Although there have been relatively few studies into the function of NUAK1, one obvious inconsistency in the literature is whether NUAK1 is pro or anti-proliferative. Several reports from Hiroyasu Esumi's group and others have suggested that the presence or over-expression of NUAK1 is pro-proliferative (Chang et al., 2012; Kusakai et al., 2004a; Suzuki et al., 2004b). However, a report from our laboratory and others recently showed that NUAK1 knockdown in cells was pro-proliferative (Humbert et al., 2010), contradicting these previous reports. Knockout and wild-type MEFs provide an ideal experimental system for investigating the role of NUAK1 in cell proliferation.

A

B
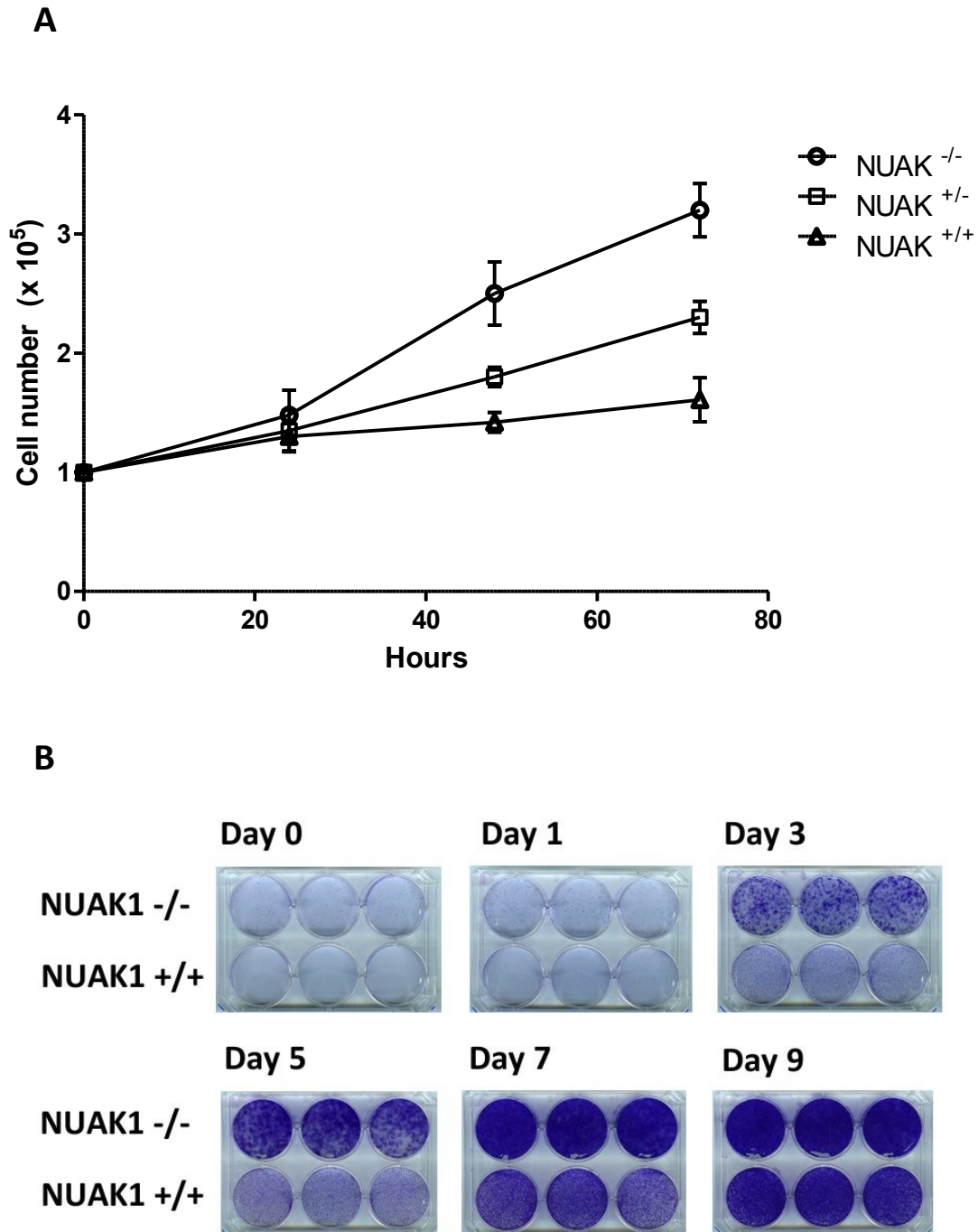
Figure 3.15 Increased growth rate in NUAK1 knockout MEFs

(A) Equal numbers (1 x 10^5 cells) of MEFs of each genotype were seeded onto 10cm tissue culture plates and grown in identical culture medium. Plates were harvested every 24 hours and total cell number was calculated from an average of three replicate plates. **(B)** Equal numbers of cells from wild-type and homozygous NUAK1 knockout MEFs were seeded on 6 well plates and grown for the indicated number of days before being fixed with 4% paraformaldehyde and stained with crystal violet.

Using two different methods it is clear that NUAK1 null MEFs grow faster than their wild-type equivalents (Figure 3.15). Interestingly, the heterozygous NUAK1 MEFs showed an intermediate growth phenotype indicating that partial loss of NUAK1 activity may affect whichever pathways mediate this phenotype. This supports the idea that NUAK1 has an anti-proliferative role or may control some mechanism in the cell cycle which contributes towards senescence. This observation could be confirmed by investigating ^{3}H thymidine incorporation to accurately quantify any increase in cell proliferation. Anecdotal evidence from handling NUAK1 knockout MEF cultures also suggests that they are more adherant, although no data is shown as a suitable assay was not performed. This is consistent with recent evidence showing NUAK1 can phosphorylate MYPT1 and regulate myosin light chain (MLC) phosphorylation, leading to cells being more adherant (Zagorska et al., 2010).

Part of the initial hypothesis behind investigating the role of NUAK1 was that it could be involved in aspects of metabolic regulation, given the important role AMPK and its downstream pathways play in metabolism. Given the higher growth rate of the NUAK1 null MEFs it was possible that there could be an upregulation of metabolic processes to provide the energy to drive cell proliferation. Changes in AMPK subunit mRNA levels and two key mitochondrial genes, cytochrome c oxidase subunit VIb (Cox6b) and NADH dehydrogenase protein 4 (Ndufs4) were assessed by quantitative PCR.

A AMPK α1

B AMPK α2

C AMPK β1

D AMPK γ1

E Cox6b

F Ndufs4
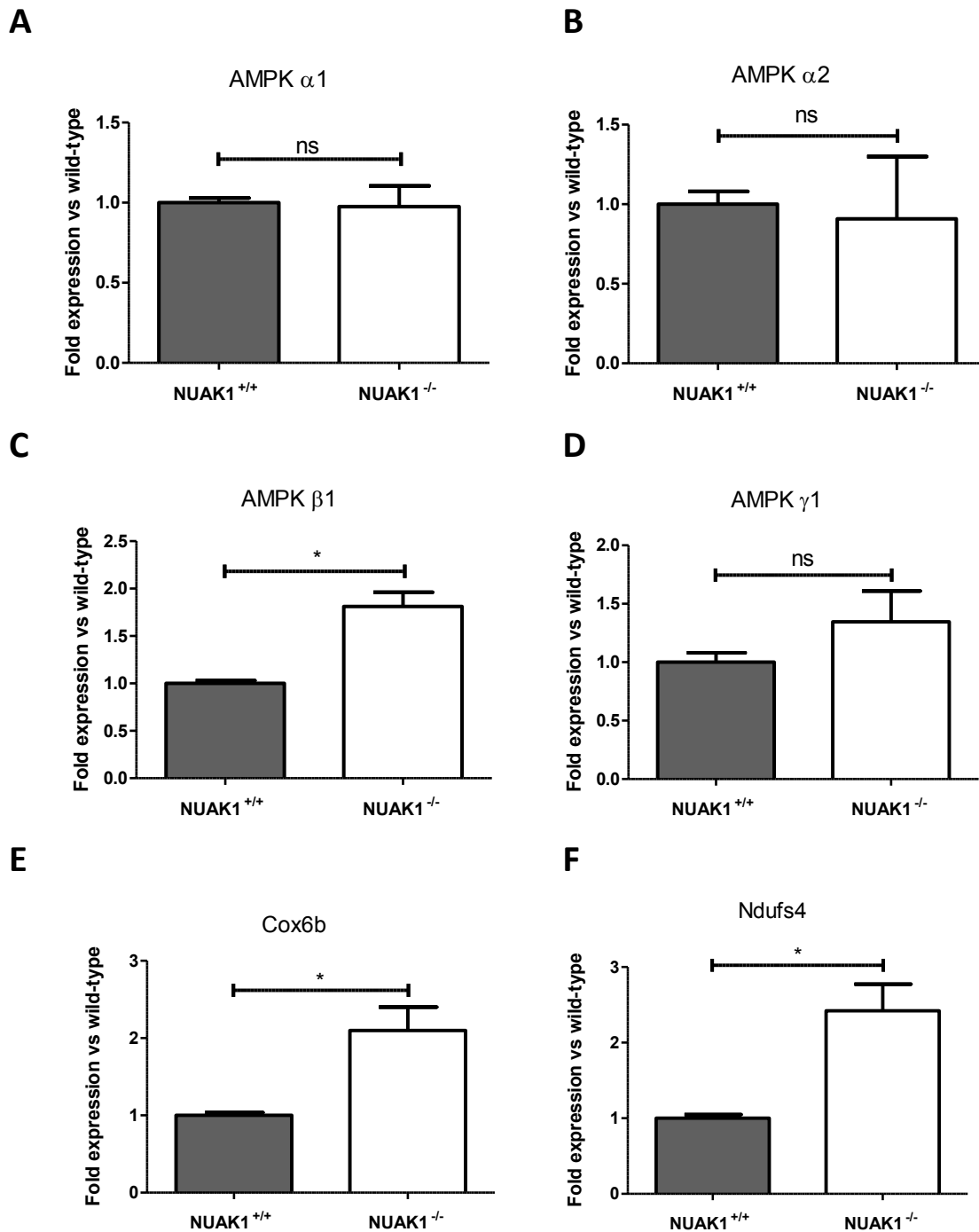
Figure 3.16 Quantitative PCR of NUAK1 knockout MEFs

mRNA purified from wild-type and homozygous NUAK1 knockout MEFs was converted to cDNA and used to determine the expression of AMPK subunits and two important mitochondrial genes. The values are shown as a fold change against the wild-type values and are an average of at least three biological replicates. **(A)** AMPK α1 subunit, **(B)** AMPK α2 subunit**, (C)** AMPK β1 subunit, **(D)** AMPK γ1 subunit, **(E)** Cox6b **(F)** Ndufs4 All figures are normalised to the expression of glyceraldehyde 3-phosphate dehydrogenase (GAPDH). Significance was analysed using the student's t-test and indicated on the graph (* = $p < 0.05$).

No changes were observed in AMPK α or γ subunit levels but a significant increase in β subunit levels was seen. This increase would not affect AMPK activity levels as the 1:1:1 stoichoimetric ratio of subunits would mean that the number of active AMPK complexes in the cell would be determined by the lowest common denominator, which would be the α or γ subunit levels, which are unchanged (Figure 3.16). Interestingly, there was a significant increase in the mRNA levels of both Cox6b and Ndufs4, suggesting that mitochondrial genes may be upregulated as a result of reduced NUAK1 activity (Figure 3.16).
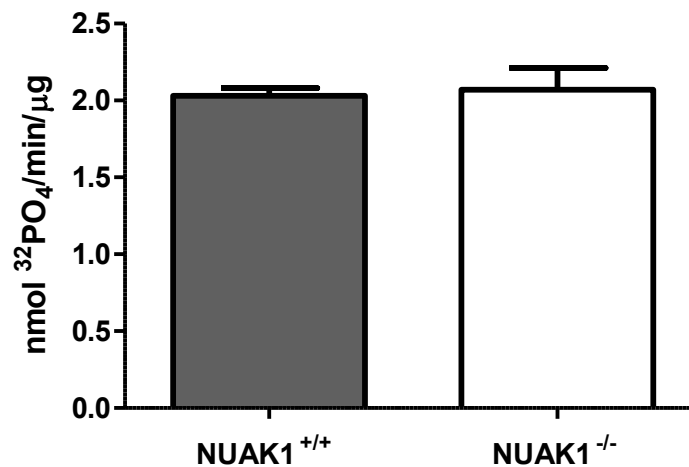
Figure 3.17 AMPK activity is unchanged in NUAK1 knockout MEFs

Endogenous AMPK complexes were immunoprecipitated from both wild-type and homozygous NUAK1 knockout MEFs using a pan-AMPKβ antibody. The activity of AMPK in the immune complex was determined by incubation with γ^{32}P-ATP and synthetic AMARA peptide substrate. No significant difference (p>0.05) was observed between wild-type and knockout MEFs when analysed using the student's t-test.

As expected from the qPCR data, there is no change in the activity of AMPK in NUAK1 knockout MEFs compared to their wild-type equivalents (Figure 3.17). This is another piece of evidence that the NUAK1 knockout is specific and is not having off target effects on other components of the AMPK-related kinase family.

3.2.8 NUAK1 mass spectrometry studies

Given the great experimental potential of having NUAK1 knockout MEFs and without any clear indication of what processes or pathways the kinase may be targeting, it was useful to take a wider approach and use an un-biased, large scale method to identify possible downstream targets. The most efficient method available for looking at changes in expression and phosphorylation of proteins on a large scale is mass spectrometry. Given the high possibility of getting false positive results, a decision was made to use three different methods and compare the results to minimise the number of false positives. The experimental basis for each method is explained in Figure 3.18A.

A
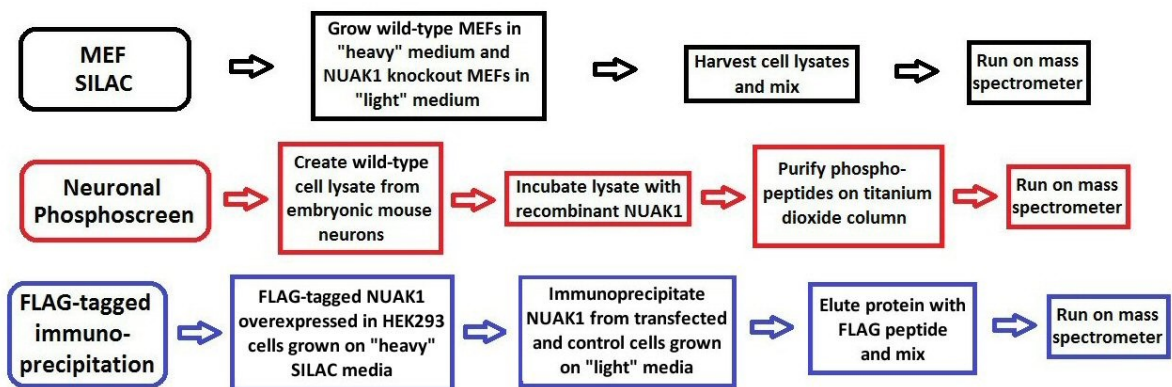
B

Gene Ontology term	Cluster frequency	Genome frequency	Corrected P-value	FDR	False Positives	Genes annotated to the term
Transcytosis	2 of 4 genes, 50.0%	9 of 25496 genes, 0.0%	5.64e-05	0.00%	0.00	USO1, SRC
Positive regulation of protein complex assembly	2 of 4 genes, 50.0%	102 of 25496 genes, 0.4%	0.00804	9.00%	0.18	CHIP, SRC

C

Gene Ontology term	Cluster frequency	Genome frequency	Corrected P-value	FDR	False Positives	Genes annotated to the term
Organelle organization	11 of 20 genes, 55.0%	2183 of 25496 genes, 8.6%	3.58e-05	0.00%	0.00	CLIP1, NSUN2, MAP1S, NUDC, MAP2, STMN1, RTN4, CRK, USO1, HUWE1, SRC
Microtubule bundle formation	3 of 20 genes, 15.0%	33 of 25496 genes, 0.1%	0.00055	0.00%	0.00	CLIP1, MAP1S, MAP2
Cellular component organization	12 of 20 genes, 60.0%	3853 of 25496 genes, 15.1%	0.00133	0.00%	0.00	CLIP1, NSUN2, MAP1S, CHIP, NUDC, MAP2, STMN1, RTN4, CRK, USO1, HUWE1, SRC
Cellular component organization or biogenesis	12 of 20 genes, 60.0%	3983 of 25496 genes, 15.6%	0.00190	0.00%	0.00	CLIP1, NSUN2, MAP1S, CHIP, NUDC, MAP2, STMN1, RTN4, CRK, USO1, HUWE1, SRC
Regulation of protein complex assembly	4 of 20 genes, 20.0%	210 of 25496 genes, 0.8%	0.00488	0.80%	0.04	CLIP1, STMN1, CHIP, SRC
Transcytosis	2 of 20 genes, 10.0%	9 of 25496 genes, 0.0%	0.00524	1.00%	0.06	USO1, SRC

D

Gene Ontology term	Cluster frequency	Genome frequency	Corrected P-value	FDR	False Positives	Genes annotated to the term
Nuclear division	5 of 25 genes, 20.0%	326 of 25496 genes, 1.3%	0.00440	0.00%	0.00	**MYPT1**, AKAP8, CDC16, KIF2A, USP9X
Mitosis	5 of 25 genes, 20.0%	326 of 25496 genes, 1.3%	0.00440	0.00%	0.00	**MYPT1**, AKAP8, CDC16, KIF2A, USP9X
Organelle fission	5 of 25 genes, 20.0%	354 of 25496 genes, 1.4%	0.00655	0.00%	0.00	**MYPT1**, AKAP8, CDC16, KIF2A, USP9X
Cellular component organization or biogenesis	13 of 25 genes, 52.0%	3983 of 25496 genes, 15.6%	0.00807	0.00%	0.00	**MYPT1**, AP3D1, CDC16, KIF2A, HNRPK, CHIP, NOP56, AKAP8, MYH9, USO1, USP9X, SRC, MARK2

E

Gene Ontology term	Cluster frequency	Genome frequency	Corrected P-value	FDR	False Positives	Genes annotated to the term
Unannotated	15 of 59 genes, 25.4%	716 of 25496 genes, 2.8%	4.02e-08	0.00%	0.00	**MRLC2**, FOR, NCBP, ADE2, SEC61, TPM3, RAB, CAB, DNAJ, DSH, FKBP59, AKAP, FAR, UAP56, NATA
Cellular protein metabolic process	22 of 59 genes, 37.3%	2981 of 25496 genes, 11.7%	0.00023	0.00%	0.00	FMR1, RIG, MMS2, FYN, FAT, RHO, NEDD8, IQGAP1, HSP40, FGFR2, RAS, HSPB1, EIF3, FGR, MAK, RAD50, ACP1, FKBP4, CAND1, UBC12, PP1, LYN
Protein metabolic process	23 of 59 genes, 39.0%	3720 of 25496 genes, 14.6%	0.00261	0.00%	0.00	PAI1, FMR1, RIG, MMS2, FYN, FAT, RHO, NEDD8, IQGAP1, HSP40, FGFR2, RAS, HSPB1, EIF3, FGR, MAK, RAD50, ACP1, FKBP4, CAND1, UBC12, PP1, LYN
Protein auto-phosphorylation	6 of 59 genes, 10.2%	185 of 25496 genes, 0.7%	0.00303	0.00%	0.00	FGR, MAK, FGFR2, RAD50, LYN, FYN

Gene Ontology term	Cluster frequency	Genome frequency	Corrected P-value	FDR	False Positives	Genes annotated to the term
Cellular protein modification process	17 of 59 genes, 28.8%	2302 of 25496 genes, 9.0%	0.00793	0.40%	0.02	FYN, FAT, RHO, NEDD8, IQGAP1, FGFR2, RAS, HSPB1, FGR, MAK, RAD50, ACP1, FKBP4, CAND1, UBC12, PP1, LYN
Protein modification process	17 of 59 genes, 28.8%	2302 of 25496 genes, 9.0%	0.00793	0.33%	0.02	FYN, FAT, RHO, NEDD8, IQGAP1, FGFR2, RAS, HSPB1, FGR, MAK, RAD50, ACP1, FKBP4, CAND1, UBC12, PP1, LYN

Figure 3.18 Summary of NUAK1 mass spectrometry screens

Various mass spectrometry screens were used to identify possible interaction partners for NUAK1 with the assistance of the CSC Mass Spectrometry Facility (Bram Snidjers and Pedro Rodriguez Cutillas). **(A)** An explanatory flowchart explains what different methods were used. For further information see section 2.2.21. By using the Database for Annotation, Visualization and Integrated Discovery (DAVID) comparisons were made between the results for each different screen. In each case Gene Ontology searches were carried out on those genes that were found in more than one screen. **(B)** This table shows the gene ontology for genes found in all three sets of results. **(C)** This table shows the gene ontology for genes found in both the MEF SILAC and neuronal phosphoscreen experiments. **(D)** This table shows the gene ontology for genes found in both the neuronal phosphoscreen and the FLAG-tagged immunoprecipitation experiments. **(E)** This table shows the gene ontology for genes found in both the FLAG-tagged immunoprecipitation and MEF SILAC experiments.
The False Discovery Rate (FDR) is a value for how often a p-value generated from random data is as good as or better than a p-value generated from the real data for that ontology term. p-value<0.01 was chosen as the cutoff and the false positives column is an indication of the expected number of false positive results that would appear, if that particular ontology term was chosen as the cutoff.

The three different mass spectrometry screens generated a huge amount of data and crucially provided some confirmation of previously reported proteins that interact with NUAK1, specifically USP9X and MYPT1 (Figure 3.18D) (Al-Hakim et al., 2008; Zagorska et al., 2010). The data shows that the proteins interacting with NUAK1 and those that show changes in phosphorylation between NUAK1 knockout and wild-type MEFs are involved in various processes including microtubule organisation, mitosis and metabolism. These data provide possible links to the downstream pathways that are controlling the increased proliferation in NUAK1 null MEFs and increase in metabolic gene expression.

Gene Ontology term	Cluster frequency	Genome frequency	Corrected P-value	FDR	False Positives	Genes annotated to the term
Microtubule cytoskeleton organization	5 of 11 genes, 45.5%	286 of 25496 genes, 1.1%	1.24e-05	0.00%	0.00	Map4, Map1b, Map1s, Mapt, Map2
Microtubule bundle formation	3 of 11 genes, 27.3%	33 of 25496 genes, 0.1%	5.37e-05	0.00%	0.00	Map1b, Map1s, Map2
Microtubule-based process	5 of 11 genes, 45.5%	418 of 25496 genes, 1.6%	8.17e-05	0.00%	0.00	Map4, Map1b, Map1s, Mapt, Map2
Establishment of mitochondrion localization, microtubule-mediated	2 of 11 genes, 18.2%	5 of 25496 genes, 0.0%	0.00028	0.00%	0.00	Map1b, Mapt
Mitochondrion transport along microtubule	2 of 11 genes, 18.2%	5 of 25496 genes, 0.0%	0.00028	0.00%	0.00	Map1b, Mapt
Establishment of mitochondrion localization	2 of 11 genes, 18.2%	7 of 25496 genes, 0.0%	0.00058	0.00%	0.00	Map1b, Mapt
Cytoskeleton organization	5 of 11 genes, 45.5%	771 of 25496 genes, 3.0%	0.00164	0.00%	0.00	Map4, Map1b, Map1s, Mapt, Map2
Positive regulation of microtubule polymerization	2 of 11 genes, 18.2%	14 of 25496 genes, 0.1%	0.00254	0.00%	0.00	Map1b, Mapt
Neuron projection morphogenesis	4 of 11 genes, 36.4%	412 of 25496 genes, 1.6%	0.00336	0.00%	0.00	Map1b, Map1s, Mapt, Map2
Microtubule-based movement	3 of 11 genes, 27.3%	138 of 25496 genes, 0.5%	0.00411	0.00%	0.00	Map4, Map1b, Mapt
Positive regulation of microtubule polymerization or depolymerisation	2 of 11 genes, 18.2%	18 of 25496 genes, 0.1%	0.00428	0.00%	0.00	Map1b, Mapt
Establishment of organelle localization	3 of 11 genes, 27.3%	148 of 25496 genes, 0.6%	0.00507	0.00%	0.00	Map4, Map1b, Mapt
Mitochondrion localization	2 of 11 genes, 18.2%	20 of 25496 genes, 0.1%	0.00531	0.00%	0.00	Map1b, Mapt
Regulation of microtubule polymerization	2 of 11 genes, 18.2%	24 of 25496 genes, 0.1%	0.00771	0.00%	0.00	Map1b, Mapt
Organelle transport along microtubule	2 of 11 genes, 18.2%	24 of 25496 genes, 0.1%	0.00771	0.00%	0.00	Map1b, Mapt
Positive regulation of axon extension	2 of 11 genes, 18.2%	25 of 25496 genes, 0.1%	0.00838	0.00%	0.00	Map1b, Mapt
Cell projection morphogenesis	4 of 11 genes, 36.4%	535 of 25496 genes, 2.1%	0.00934	0.00%	0.00	Map1b, Map1s, Mapt, Map2

Figure 3.19 Comparison of AMPK and NUAK1 neuronal lysate phosphoscreens

An identical experiment to the neuronal lysate phosphoscreen described in Figure 3.18A was carried out using recombinant AMPK instead of NUAK1. The results from these two experiments were compared and common genes were analysed using a gene ontology search.

119

In a parallel experiment to the NUAK1 phosphoscreen, an identical experiment was conducted using recombinant AMPK. By comparing the results from this screen to the NUAK1 screen, a degree of specificity can be determined (Figure 3.19). Clearly many of the proteins common to both the AMPK and NUAK1 screens are regulating microtubule function and cytoskeletal organisation, suggesting there may be redundancy in the AMPK-related kinase family in controlling these functions, especially as the MARK family are known to regulate similar processes (Bright et al., 2009). Comparing the results from this screen to the overall summary of the NUAK1 mass spectrometry experiments, it may suggest that the specific roles of NUAK1 are more focussed on mitosis and metabolism rather than microtubule regulation.

Raw data from the phosphoscreens indicated a lot of proteins with acidic residues having altered phosphorylation levels or protein levels in the NUAK1 wild-types compared to the knockouts (data shown in Appendix 2). Casein kinase 2 (CK2) is a well known upstream kinase of various acidic proteins and it was hypothesised that NUAK1 may be modulating the role of CK2 in some way given the number of acidic proteins that were changed in the mass spectrometry data.
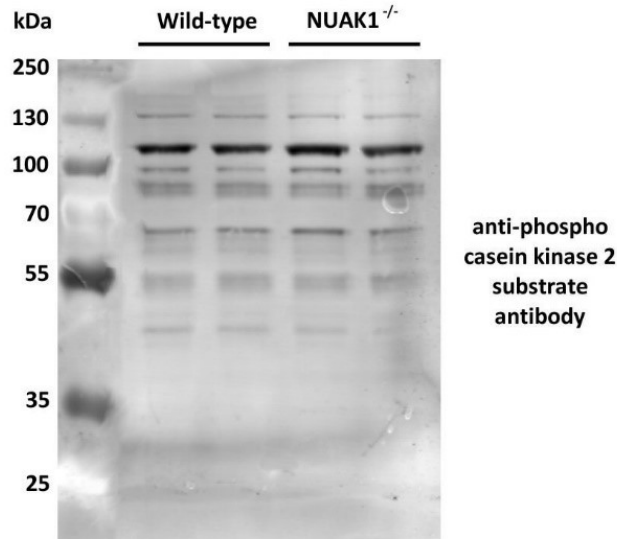
Figure 3.20 Casein kinase 2 substrate phosphorylation is unaffected by NUAK1 knockout in liver

Total tissue lysate from wild-type and homozygous NUAK1 knockout livers were resolved on a 10% SDS-PAGE Tris-Glycine gel and transferred to Immobilon FL PVDF membrane for immunodetection. The membrane was incubated with a phospho-CK2 substrate primary antibody. Various bands were quantified using the LI-COR software and no significant difference in any of the bands was observed (data not shown).

Although the blot was probed with a phospho-CK2 substrate antibody that identifies a generic CK2 recognition motif, it clearly shows there is no obvious change in CK2 substrate phosphorylation (Figure 3.20). If there were large scale changes in CK2 activity it would be reasonable to expect to see some change in phosphorylation using this antibody so it is likely that there is no change in CK2 activity as a result of NUAK1 deletion.

3.3 Discussion

The fields of NUAK1 and AMPK-related kinases in general have been sparsely researched and few reports exist in published literature regarding the role and regulation of these kinases. This presents a challenge and an opportunity simultaneously as there are many possibilities for novel findings but there is also insufficient evidence to support a coherent model of NUAK1 function.

Several findings described in this chapter contradict published reports of NUAK1 regulation and clearly it is difficult to determine the reason for the observed differences and combine

the data to produce a cohesive story. As with any emerging field, more research will be required to establish a consistent picture of the role of NUAK1 in wider signalling pathways.

Only one previous report has investigated the activity of recombinant NUAK1 expressed in *E. coli* (Lizcano et al., 2004). Their data showed that wild-type human recombinant NUAK1 has no intrinsic activity, however in my study a small but measurable amount of activity is seen when the same protein is expressed. The only significant difference in the experimental method that produced these two opposing results was the tag used to purify the expressed protein. The previous study used GST-HA tags, although no details were shown regarding where the tags were located. GST is a large 26 kDa tag and the method did not mention that the tag was cleaved off prior to assaying for activity (Lizcano et al., 2004 – supplementary section). The presence of the large GST tag and data suggesting that the presence of the tag can cause proteins to dimerize in solution (Terpe, 2003) may explain why no catalytic activity was observed. The precise three-dimensional structure of kinases is crucial for their activity and if the active site was obstructed this could lead to a drop in activity. The GST tag may also lead to misfolding or aggregation of the expressed protein which would still be detectable by western blotting but would not have activity. The purification tag used in my study was a His-FLAG tag, both on the N-terminal end of the protein, with a total size of 1.84 kDa. This tag would be much less likely to obstruct any intrinsic activity. To support the evidence in this report that other members of the AMPK-related kinase family may show intrinsic activity in the absence of LKB1, the report that first identified SIK1 expressed a GST tagged form that showed a basal level of activity, presumed to be via autophosphorylation (Wang et al., 1999). This report also supports the hypothesis that some of the AMPK-related kinases may possess intrinsic activity.

The finding that NUAK1 has measurable basal kinase activity without the need for phosphorylation by LKB1 opens up the possibility and requirement for other mechanisms of regulation. The data shown here suggest that although LKB1 is not required for NUAK1 activity, the presence of LKB1 can increase the activity (Figure 3.8 and Figure 3.9). This may suggest that a basal level of NUAK1 is required for some functions but that further phosphorylation by LKB1 could increase its activity in the presence of certain stimuli.

This discovery that LKB1 can still be an activating upstream kinase raises the question of other methods of regulation that can modulate NUAK1 activity in response to relevant stimuli. From the data regarding NUAK1 generated during this study (Appendix 3) and from other data regarding similar AMPK-related kinases (Al-Hakim et al., 2005), it was known that 14-3-3 can bind and potentially regulate NUAK1 activity. The previous study reported that 14-3-3 proteins can bind to the AMPK-related kinases SIK1 and SIK3 (QSK) and increase their activity. Their data also suggested that 14-3-3 binds directly to the T-loop and allows activation by LKB1 (Al-Hakim et al., 2005). To date, there have been no other reports of proteins that can bind directly to the T-loop of AMPK-related kinases and preliminary indications from sequence analysis suggest that 14-3-3 probably binds to NUAK1 in the C-terminal portion of the protein (data not shown), which may mean it regulates the activity differently. Also, data from bacterial expression shows that the conserved threonine residue in the active site probably plays no role in binding 14-3-3 as mutation to alanine did not abolish the binding (Figure 3.2). There is no evidence that 14-3-3s bind to the S600 residue of NUAK1, as binding was still observed with expression of the S600A mutant protein (data not shown). Another function that 14-3-3 may be regulating is subcellular localisation, as numerous reports have demonstrated that the binding of 14-3-3 proteins can control the targeting of proteins within the cell (reviewed in Aitken, 2006). In the case of SIK3, 14-3-3 binding localised the kinase to punctate structures within the cytosol (Al-Hakim et al., 2005). Interestingly, this localisation was not seen in LKB1 deficient HeLa cells, suggesting there may be a co-operative mechanism controlling localisation and activity. 14-3-3 proteins are known to be able to bind two substrate proteins simultaneously and these results led the authors of this report to hypothesise that 14-3-3 may function as a scaffolding complex to allow the interaction of the kinases with other 14-3-3 binding partners.

The results presented in this thesis partially contradict the report on SIK1 and SIK3 because it was observed that 14-3-3s binding to NUAK1 reduced its activity *in vitro* and in cells (Figure 3.3 and Figure 3.8). There are several possible explanations for this observation. Firstly, different AMPK-related kinases may bind 14-3-3 by different mechanisms, leading to diverse structural changes and consequently different effects on kinase activity. Also, different

14-3-3 isoforms may have contrasting effects on their binding partners. The study looking at SIK1 and SIK3 reported interaction with 14-3-3ζ, whereas NUAK1 appears to primarily bind to 14-3-3ε (Appendix 3 and Ballif et al., 2006). Interestingly, looking at the subcellular localisation of NUAK1, there was no difference seen between LKB1 expressing cells and LKB1 null cells (Figure 3.12A and Figure 3.13). This may suggest that LKB1 expression does not influence the localisation of NUAK1 in the same way as SIK1 and SIK3. The localisation of NUAK1 could still be controlled by 14-3-3s and some evidence from this report suggests that it may also be involved in regulating its activity. Basal activity of NUAK1 was reduced in the presence of 14-3-3ε in bacterial cells, indicating that it may be responsible for inactivating and sequestering the kinase in a part of the cell when its activity is not required. The fact that activity was increased to around basal levels in the presence of LKB1 and 14-3-3 (Figure 3.3 and Figure 3.8) points to the possibility that there may be a co-operative mechanism for regulating NUAK1 activity, similar to that reported for SIK1 and SIK3. However, rather than localising LKB1 with its substrate to increase activity, it appears that LKB1 and 14-3-3s may act in an antagonistic manner to regulate NUAK1 activity.

Looking further at the subcellular localisation, it is possible that 14-3-3s and LKB1 act to modulate the activity of NUAK1 at different phases of the cell cycle. The finding that NUAK1 is not maximally phosphorylated (Figure 3.10D) suggests the possibility that by binding of 14-3-3s and phosphorylation by LKB1, the partial basal activity of the kinase could be controlled in response to stimuli. It is possible that the subcellular localisation varies during different phases of the cell cycle, as the cell in Figure 3.12C has just undergone division and all the NUAK1 appears to be diffusely localised in the cytoplasm. This transition may be mediated by association and dissociation of 14-3-3s, as these proteins are known to bind phosphorylated residues and influence localisation (Mackintosh, 2004). NUAK1 is seen to autophosphorylate (Figure 3.11) and some of the residues it phosphorylates may be important for binding 14-3-3s. Further studies using mass spectrometry approaches to identify the autophosphorylation sites would allow these residues to be mutated to assess the effect on 14-3-3 binding. Although no firm evidence is provided in this thesis to support the hypothesis that the localisation of NUAK1 varies with specific cues in the cell cycle, it is an

interesting idea that may support some of the phenotypes observed in NUAK1 knockout cells and animal models.

During this project several attempts were made to express NUAK1 in LKB1 null cell lines such as HeLa and CCL13, but very little protein was detected, despite control proteins being readily expressed (data not shown). Although occasionally it was possible to transfect NUAK1 into LKB1 null cells with some success (Figure 3.13), it is possible that the presence of LKB1 has some effect on the localisation or stablilty of the protein in a cellular environment, hence the low expression observed in LKB1 null cells. Although NUAK1 is capable of autophosphorylation *in vitro* (Figure 3.11), LKB1 may still be responsible for stability and localised activity within mammalian cells.

Contrary to this finding, recombinant LKB1 was not seen to reactivate dephosphorylated NUAK1 *in vitro* (Figure 3.11B). This lack of reactivation could be due to limitations of the assay technique if a small amount of PP2C remained in the assay or if the binding of NUAK1 to the resin somehow interfered with acess to LKB1 to prevent phosphorylation and reactivation. However, it may also suggest that the activity of NUAK1 requires a co-ordinated combination of LKB1, or another upstream kinase, and autophosphorylation to be fully active.

This study also sought to clarify findings of previous reports, particularly the involvement of other potential upstream kinases for NUAK1. A previous report indicated that Akt was capable of phosphorylating NUAK1 on S600 leading to activation (Suzuki et al., 2004b). However, when NUAK1 harbouring a mutation of S600 to alanine was overexpressed in HEK293T cells, no change in the activity was seen (Figure 3.7). It is possible that under basal conditions, S600 might not be phosphorylated so no effect would be observed by simply mutating the residue and it may be more indicative to stimulate the cells with an agonist that would activate the Akt pathway, such as insulin. However, the previous study reported that an overexpression of the S600A mutant in PANC-1 cells completely ablated activity (Suzuki et al., 2004b), which was not seen in my experiment. The previous study measured activity against a GST-tagged SAMS peptide which could explain the variability in observations given that in my hands,

recombinant NUAK1 appears to show better activity against the AMARA and LATS1 peptides (Figure 3.4). The inactivity of K84R and D196A mutants indicate that the predicited structural similarities of NUAK1 to other kinases are correct (Figure 3.7). Similarities such as these may be used to provide some insight into the structure and regulation of NUAK1 when compared to the structure of other similar proteins, such as the MARKs, which are also known to autophosphorylate (Marx et al., 2010).

Although the activity of NUAK1 may share these similarities with other kinases, the finding that neither AMP or salt are capable of activating NUAK1 (Figure 3.10) suggests that there are disparate mechanisms of activation within the family of AMPK-related kinases and if there are any small molecules that are found to activate NUAK1, these may play a role in its subcellular localisation or control of its autophosphorylation. One important issue concerning the regulation of NUAK1 is that there are very few indications of conditions that can activate or inhibit NUAK1 *in vivo.* One report has indicated that phosphorylation of known NUAK1 targets is increased by cell detachment (Zagorska et al., 2010), but no mechanism for this increase was suggested. Establishing phsyiological or pathological conditions that alter NUAK1 activity will be key to understanding its regulation. Various other stresses could be used to establish mechanisms of NUAK1 activation, such as ATP depletion with 2-deoxyglucose, oligomycin or metformin.

As previously mentioned, a major inconsistency in the literature is whether NUAK1 is pro or anti-proliferative. Several reports have implicated it in pro-proliferative mechanisms (Chen et al., 2013a; Kusakai et al., 2004a; Lu et al., 2013) but other reports have indicated the presence of NUAK1 to be anti-proliferative (Humbert et al., 2010). The finding in this report that NUAK1 null MEFs grow significantly faster than wild-type MEFs (Figure 3.15) would support the finding that NUAK1 is anti-proliferative. This could be due to the regulation of LATS1 discussed in Humbert et al. but could also be due to another downstream mechanism, such as downregulating mTOR signalling. To investigate this further it would be interesting to assess S6K and 4E-BP1 phosphorylation. The finding that downregulation of LATS1 is involved in the maintenance of senesence links NUAK1 to key regulators of cell cycle control (Takahashi et al., 2006). However, LATS1 is also involved in the Hippo pathway (Figure 1.10) and NUAK1

reducing expression of LATS1 would have pro-proliferative effects. This opens up the interesting possibility that NUAK1 could have two cell-stage dependent functions. Firstly, it may act as part of the Hippo pathway to control proliferation and organ size and secondly it may act in differentiated cells to maintain senesence.

Interestingly, the quantitative PCR data from the NUAK1 null MEFs show there is a significant upregulation of mitochondrial genes (Figure 3.16). There is no inidication if this is a direct consequence of NUAK1 deletion or if the cell is simply producing more energy in response to proliferative cues created as a result of a different pathway. Further assessment of other pathways in NUAK1 positive and null cells would give a better indication of what pathways were being affected. A previous study had associated some of the downstream functions of NUAK1 to the evidence that inhibition of NUAK1 causes a drop in ATP levels in cells with deregulated Myc expression (Liu et al., 2012). Some data from my study does question this finding, as AMPK activity was found to be unchanged in NUAK1 null MEFs (Figure 3.17). However, the study by Liu and colleagues did suggest it was the deregulation of Myc expression that causes a reliance on NUAK1 activity, so this may indicate that under basal conditions, AMPK activity would remain unchanged when NUAK1 is deleted.

Very few NUAK1 substrates have been identified in the literature and attempts to use mass spectrometry approaches to identify novel interactions has produced a huge amount of data. Crucially, several previously identified NUAK1 interacting partners have appeared in my mass spectrometry screens such as USP9X and MYPT1 (Figure 3.18). A previous study has indicated NUAK1 can bind to to the MYPT1-PP1β complex and regulate the phosphorylation of myosin light chain (Zagorska et al., 2010). The confirmation that NUAK1 can interact with MYPT1 and potentially regulate MLC phosphorylation reveals several possible downstream pathways. MLC phosphorylation has an integral role in the regulation of cell adhesion and polarity in non-muscle cells (Vicente-Manzanares et al., 2009). Complicating the issue, another report has also identified NUAK2, a close homologue of NUAK1, as being able to phosphorylate MYPT1 (Yamamoto et al., 2008). Resolving these interactions and any potential redundancy between the two closely related kinases would be important for understanding this function.

Interestingly, the *C. elegans* orthologue of NUAK1 and NUAK2 (unc-82) has also been shown to be involved in myosin filament organisation (Hoppe et al., 2010). These potential functions are supported by evidence from the mass spectrometry screens, as the main gene ontology functions identified are aspects such as microtubule organisation and mitosis (Figure 3.18). Specifically, some of the other proteins that are identified in the screens include MLC, PP1 and CDC16 which are all involved in cell cycle regulation. As part of the analysis of the mass spectrometry data, it was thought that due to the presence of many acidic peptides, particularly in the neuronal phosphoscreen, that NUAK1 may crosstalk with the CK2 pathway. The finding that a pan-CK2 substrate antibody detects no difference between NUAK1 knockout and wild-type tissues would suggest that NUAK1 does not affect this pathway. However, these findings must be interpreted with caution as it is difficult to know exactly what this antibody recognises. One feature that this highlights is the difficulty of working with such large data sets as it can be unclear exactly what they reveal about the function of a protein of interest.

In summary, the data presented in this chapter shows that NUAK1 has a basal level of activity and the control of its function is likely to regulated by several different mechanisms. It is also shown that NUAK1 is anti-proliferative, at least in growing cells, as its deletion leads to an increase in proliferation. Finally, various data are presented from mass-spectrometry screens which support previous evidence of NUAK1 interactions and provide a useful resource for further investigation of its function.

4 Generation and characterisation of global and liver-specific NUAK1 knockout mice

4.1 Introduction

At the beginning of this project little was known about the *in vivo* role of NUAK1 as most previous studies had focussed on the homology with the AMPK α subunits and activation by LKB1 (Lizcano et al., 2004), or the role of NUAK1 in tumour progression (Kusakai et al., 2004b; Suzuki et al., 2004b). A study aiming to identify new genes involved in mouse brain development uncovered NUAK1 as a potential regulator of ventral body wall closure by generating mice with a global deletion of NUAK1 (Hirano et al., 2006). This study showed that mice lacking NUAK1 display embryonic lethality, due to an omphalocele phenotype, meaning that this approach would be of limited use for studying the *in* vivo role of the kinase. Also, this study did not make the connection that the kinase was NUAK1 displaying homology with the AMPK α subunits, despite the kinase having already been identified and named earlier as part of a project cataloguing the human kinome (Manning et al., 2002). The study identified NUAK1 as having homology to SNF1, but did not relate the findings to other reports on AMPK-related kinases. No other groups have verified the global NUAK1 knockout phenotype and only one publication has demonstrated a conditional NUAK1 knockout phenotype (Inazuka et al., 2012).

During the course of this project, a study was published showing a phenotype in skeletal muscle-specific NUAK1 knockout mice (Inazuka et al., 2012). Despite deleting the kinase in a tissue where it is relatively highly expressed, no morphological or metabolic phenotype was observed under basal conditions (section 1.3.4). A phenotype was only observed when the mice were fed on a high-fat diet, indicating that other conditional knockout phenotypes may be subtle or only observed under challenged conditions.

The use of knockout animal models have historically provided a huge amount of insight into the role of signalling molecules, especially kinases, as the regulatory systems in cells and

tissues can compensate and adapt to gene deletion in a more realistic manner. Knockout mouse models of AMPK, originally focussed on investigating metabolic processes, have also helped reveal its involvement in the control of non-metabolic processes such as cell growth and organization of the cytoskeleton (Viollet et al., 2009). Total gene deletion may not realistically recapitulate pathological states where signalling cascades are over activated or inhibited and therefore phenotypes may be more extreme, however they still provide a useful experimental tool to study the *in vivo* role of signalling cascades.

In this chapter the phenotype of the global NUAK1 knockout mouse is confirmed using a different genetic model to the previously published study. Tissue expression data is also shown and the rationale for deleting NUAK1 in the liver is explained in the context of the LKB1 liver-specific knockout mouse. Phenotyping data is presented for the liver-specific NUAK1 knockout mouse and potential mechanisms are investigated.

4.2 Results

4.2.1 NUAK1 knockout strategy

Embryonic stem cells carrying the CSD knockout first, promoter driven construct were obtained from the trans-NIH Knock-Out Mouse Project (KOMP). These cells were then used to re-derive mice on a C57Bl/6 background which were heterozygous for the construct. The construct was designed such that mice that are homozygous for the construct have global deletion of NUAK1.
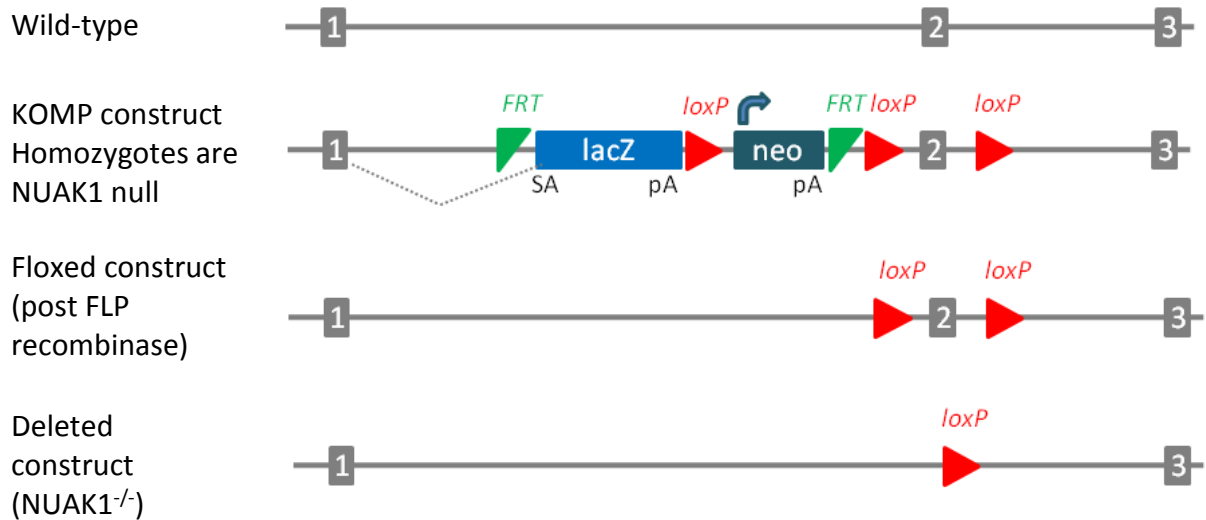
Figure 4.1 The generation of NUAK1 global and conditional knockout mice (adapted from KOMP website)

The construct carries recognition sites for FLP recombinase and loxP sites for production of a floxed construct which can then be conditionally deleted using the cre-lox recombination system. The neomycin insert is available as a selectable marker and is used to culture the embryonic stem cells. The LacZ is available as an expression marker and can be used to track the activation of the gene promoter in histological sections. The selectable markers in the construct prevent NUAK1 expression leading to global deletion of the gene in homozygotes.

Initially mice were bred such that they were heterozygous for the KOMP construct. A genotyping strategy was developed to differentiate between wild-type mice, mice that were heterozygous for the construct and any potential homozygotes. When breeding two heterozygous mice to try and produce homozygotes (global NUAK deletion), in the first few litters no homozygous mice were identified despite the Mendelian frequency predicting one quarter of the mice should be homozygous.

4.2.2 NUAK1 global knockout mice

DNA was extracted from ear biopsies of mice at weaning age (3 – 4 weeks) and used in a PCR reaction to determine the presence of wild-type or recombined construct alleles.
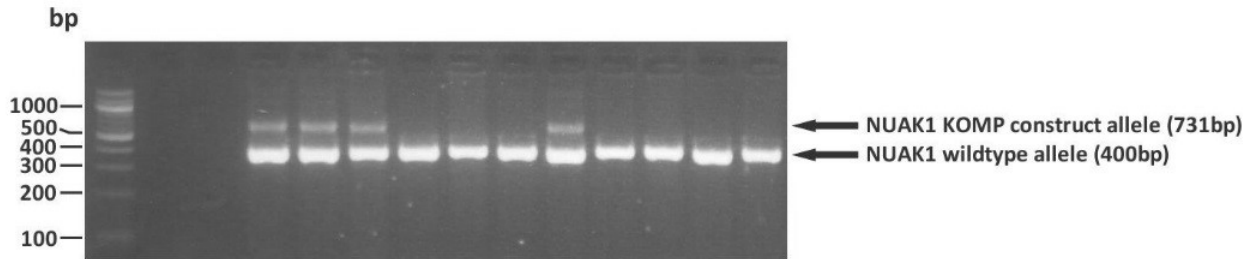
Figure 4.2 NUAK1 construct knockout genotyping

A typical agarose gel of PCR genotyping of offspring from a heterozygous NUAK1 construct cross is shown. Primers were designed against part of exon 2 of NUAK1 and an intronic region, such that two different sized bands would be amplified in the wild-type and construct alleles. The mice with a single smaller band amplified are wild-type and the mice where two bands have been amplified are heterozygous for the KOMP construct.

Note that there are no homozygous mice observed – which would be identified by a single larger band on the gel (Figure 4.2). This suggests that the embryos that are homozygous for the construct are not viable. To confirm if the previously identified embryonic lethality was recapitulated in this model, heterozygous mice carrying the NUAK construct were paired and pregnant mothers were sacrificed at embryonic day 12.5 and embryonic day 15.5 and the embryos harvested. Embryo genotypes were confirmed using the same method as above (data not shown).
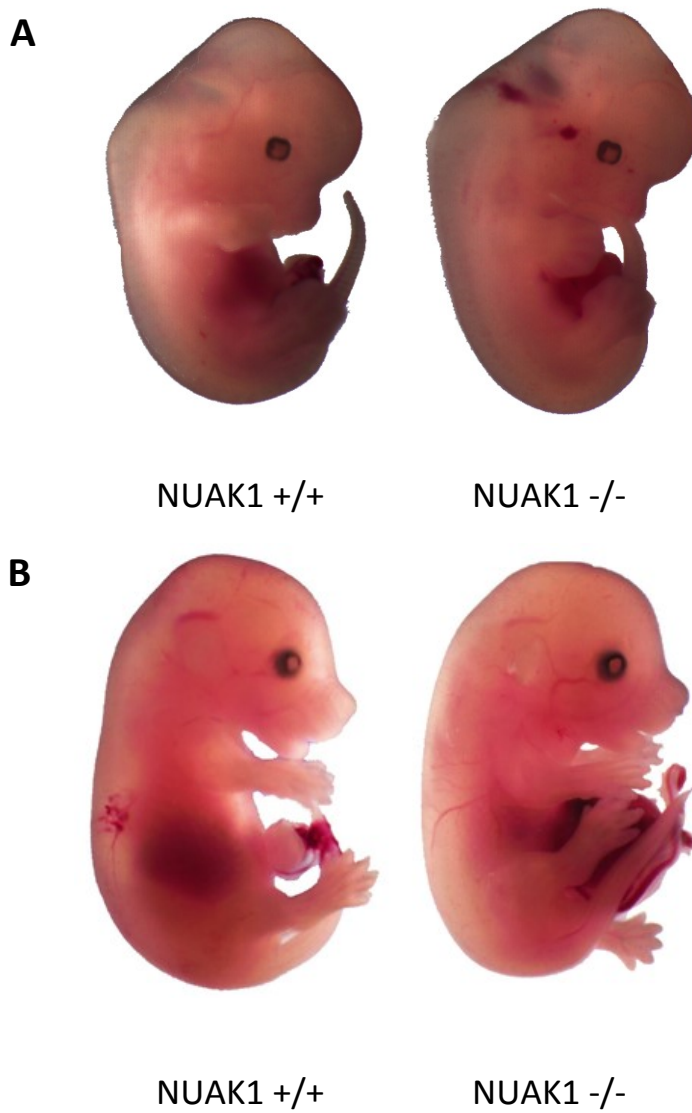
Figure 4.3 NUAK1 global knockouts have an omphalocele phenotype

Mouse embryos from litters deriving from crosses of parent mice that are heterozygous for the knockout construct. **(A)** Embryos from E12.5. The formation of an omphalocele phenotype is just starting to become visible in the NUAK1 knockout. **(B)** Embryos from E15.5. The omphalocele phenotype is very visible in the NUAK1 knockout embryo showing where the abdominal wall has failed to close, leaving key organs in a herniated sac outside the body.
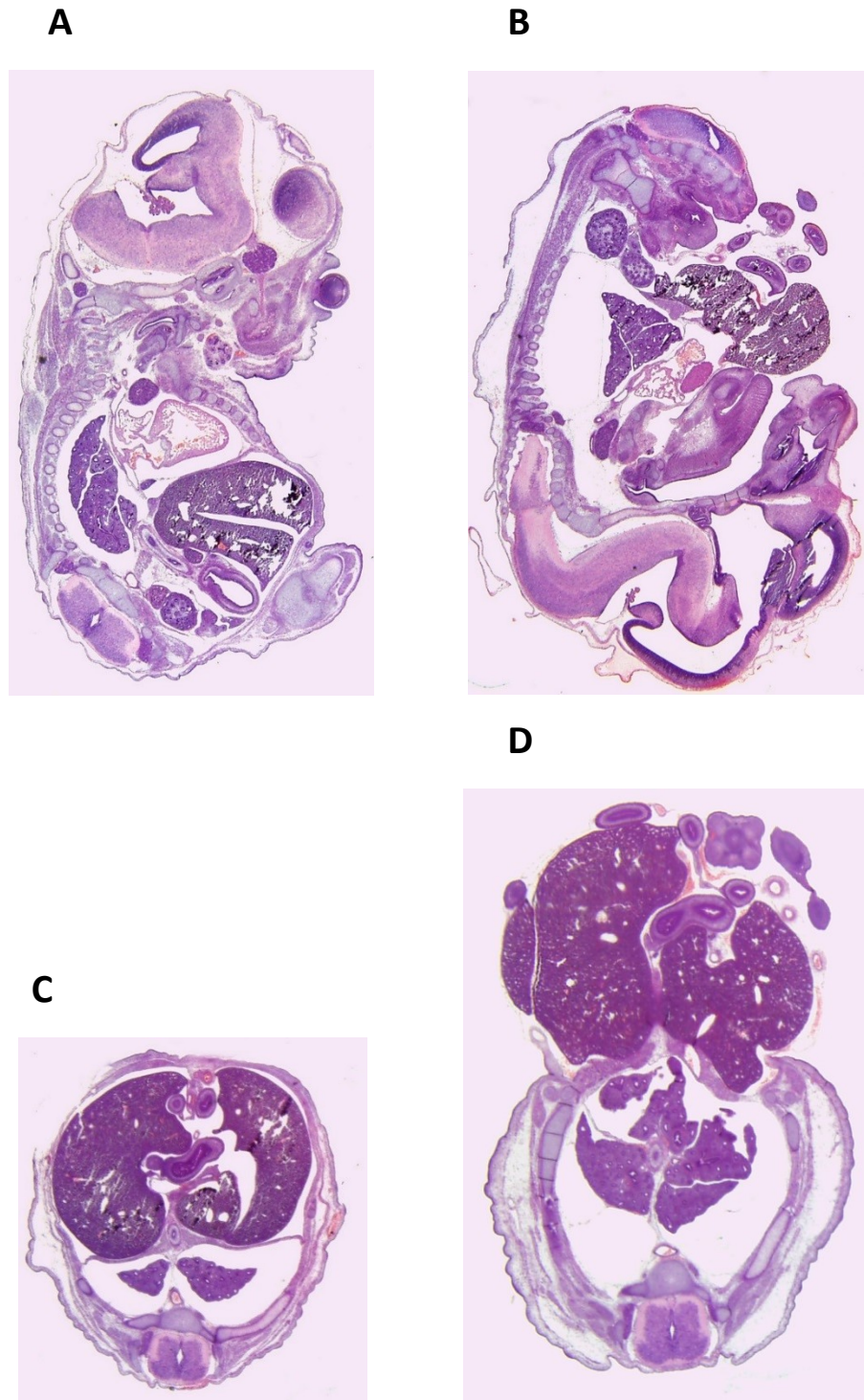
Figure 4.4 NUAK1 global knockouts have defects in abdominal wall closure

E15.5 wild-type and NUAK1 null embryos were harvested and fixed in 4% paraformaldehyde. Embryos were sectioned and stained with haematoxylin and eosin (H&E). Lateral sections from **(A)** wild-type and **(B)** NUAK1 null embryos clearly show the presence of the omphalocele phenotype with large abdominal deformities. Transverse sections from **(C)** wild-type and **(D)** NUAK1 null embryos also show the severity of the omphalocele phenotype because of the lack of ventral body wall closure.

The previous report of NUAK1 knockout used a targeted construct which was inserted into the coding region of exon 1 (Hirano et al., 2006). The KOMP method inserts a large selection cassette between exons 1 and 2 to prevent transcription. Provided both methods result in robust deletion of NUAK1, the resulting phenotype would be expected be the same. By studying wild-type and knockout embryos, it is clear that the same omphalocele phenotype is observed in the KOMP construct model, verifying the previous finding (Figure 4.3). The original global knockout study attributed the phenotype to a defect in the closure of abdominal bands in the midline leading to lack of closure of the ventral body wall (Hirano et al., 2006). Fixing and staining embryos made using the KOMP construct reveals similar defects in ventral body wall closure (Figure 4.4).

4.2.3 Tissue specific NUAK1 knockout mice

Given that the global NUAK1 knockout is embryonically lethal it is impossible to study the effect of NUAK1 deletion in adult tissues without creating a tissue-specific conditional knockout. Choosing a tissue in which to create a conditional knockout depends on a several factors:

- Potential role of the protein in that tissue
- Expression level
- Availability and specificity of recombinase mouse lines for deletion

Several tissue-specific knockout models have produced unexpected phenotypes or minimal phenotypes despite good *in vitro* evidence that the protein would cause a severe phenotype (Viollet et al., 2009). Therefore, there is no guaranteed method for selecting a tissue to target and a decision has to be made on the best available evidence.

To assess the tissue distribution of NUAK1 and to assess subsequent generation of tissue-specific knockouts, a specific antibody is required to recognise the endogenous protein to be able to interpret accurate results from any western blotting. Various commercial antibodies were tested and the specificity and sensitivity of the best available commercial antibody (Cell Signalling) is outlined in Figure 4.5.
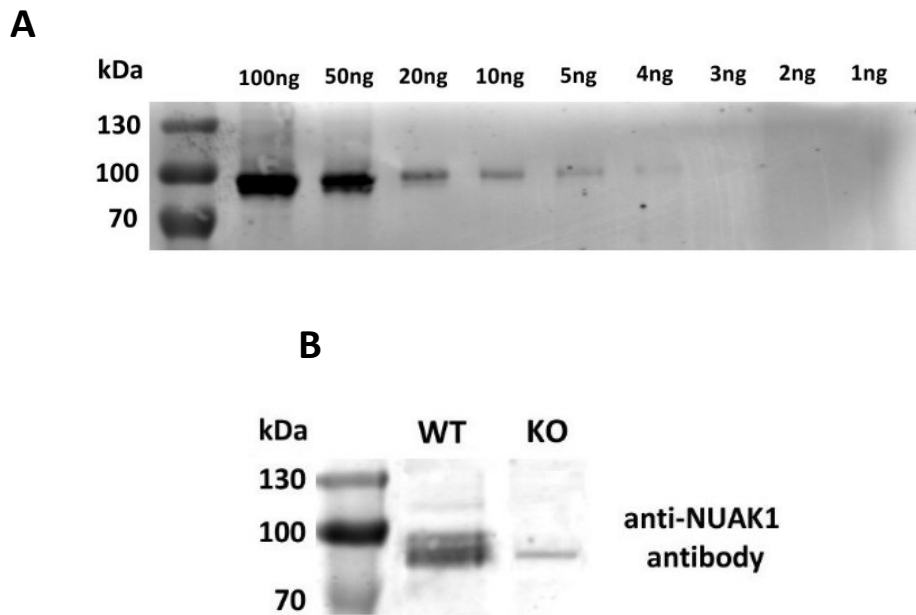
Figure 4.5 Validation of a NUAK1 specific antibody

(A) A serial dilution of wild-type recombinant NUAK1 was resolved on a 10% SDS-PAGE Tris-Glycine gel and transferred to PVDF membrane for immunodetection. The membrane was incubated with anti-NUAK1 primary antibody (Cell Signalling) followed by fluorescently labelled secondary antibody for detection, as before. **(B)** Lysate from wild-type and NUAK1 knockout MEFs was resolved on a 10% SDS-PAGE Tris-Glycine gel, transferred to PVDF membrane and incubated with anti-NUAK1 antibody followed by fluorescently labelled secondary antibody for detection, as before.

The best available antibody clearly recognises recombinant NUAK1 protein and shows almost complete deletion of a band of the correct size when comparing a blot of wild-type and NUAK1 knockout MEF lysates (Figure 4.5). While the antibody may not be particularly sentitive, from these data it can be reasonably assumed that the antibody does specifically recognise NUAK1.
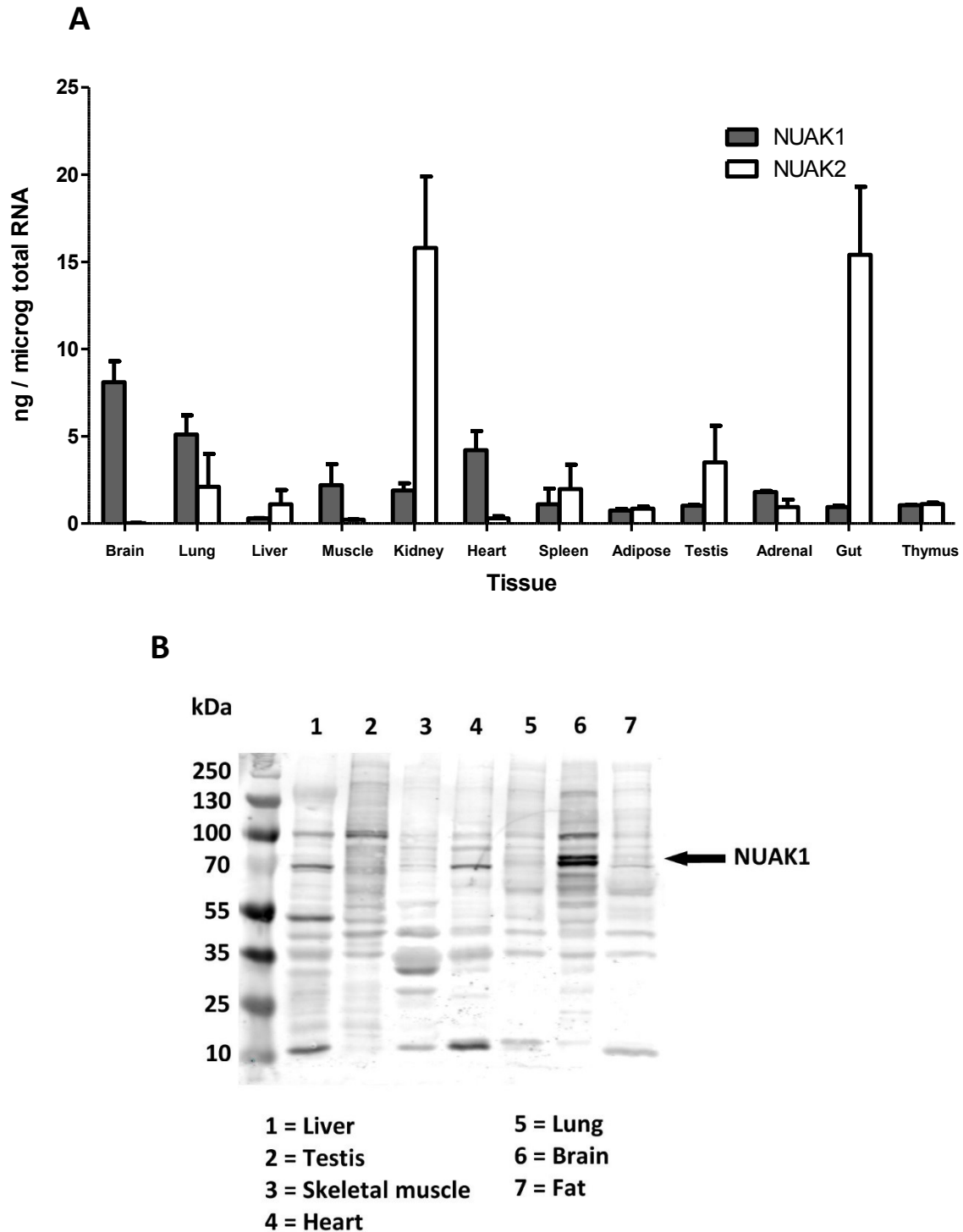
Figure 4.6 Tissue distribution of NUAK1 in adult mice

(A) mRNA derived from different mouse tissues was converted to cDNA and used for quantitative PCR to determine the relative levels of NUAK1 and NUAK2 transcripts in the indicated tissues. **(B)** Equal amounts of different tissue lysates (20µg total lysate) were resolved on a 10% SDS-PAGE Tris-Glycine gel and transferred to PVDF membrane for immunodetection with anti-NUAK1 antibody, followed by fluorescently labelled secondary antibody for detection, as before.

Using the best available antibody there is still some non-specific interaction with other proteins on the blot but the most strongly detected band is of the correct size to correspond to NUAK1. NUAK1 is clearly most highly expressed in brain as shown by the blot and the qPCR data (Figure 4.6). Although no evidence has emerged for a specific neural role for NUAK1, this evidence would support making a conditional knockout in the brain. However, the availability of neural-specific cre recombinase mouse lines is limited. There are several cell-type specific cre lines but none that can delete a gene across a range of neural tissues (Gong et al., 2007). Without further data to narrow down the expression of NUAK1, it is difficult to accurately predict the phenotype of a conditional knockout based on a sub-set of neuronal cells. Of the other tissues analysed, liver was of particular interest because of previous data showing the importance of the upstream kinase, LKB1, in the regulation of bile acid transport and canalicular membrane integrity (Woods et al., 2011). Although the qPCR data indicates that there is very little NUAK1 mRNA in the liver (Figure 4.6A), the blot indicates that there may be a small amount of protein (Figure 4.6B), meaning that there may be a functional role for NUAK1 in the organ. The liver was chosen primarily because of an interest in LKB1 function based on previous data from our laboratory and interest in NUAK1 as a potential mediator of the observed phenotype.

In order to produce conditional knockouts the mice that were heterozygous for the construct were crossed with mice expressing the FLP recombinase under the control of the human β actin promoter (Dymecki, 1996). This cross deletes the LacZ and neomycin cassettes, producing a construct with exon 2 of NUAK1 flanked by loxP sites (Figure 4.1), which can then be deleted by conditional expression of the cre recombinase. To produce liver-specific knockout mice, animals that were homozygous for the loxP flanked exon 2 constructs were crossed with mice carrying the cre recombinase under the control of the albumin promoter which specifically deletes NUAK1 in hepatocytes (Postic et al., 1999).

Mice that carried the FLP recombinase gene were obtained from the Jackson Laboratory and DNA was extracted from mice at weaning age. Genotyping methods were optimised to confirm the presence of the FLP and cre recombinases and the homozygosity of the floxed NUAK1 construct (Figure 4.7). Regions were identified where a single band could be amplified

from both the wild-type allele and the floxed allele but with a size difference such that the two genotypes could be differentiated. Details of the oligonucleotide primers used for PCR genotyping are given in Appendix 1.

Mice that carried the FLP recombinase gene were crossed with heterozygous mice carrying the KOMP NUAK1 construct to obtain mice that were heterozygous for the "floxed" NUAK1 allele (Figure 4.1 and Figure 4.2). The confirmation of deletion of the selection cassette by the FLP recombinase and confirmation of the floxed allele was done by PCR genotyping (Figure 4.7B). Primers were designed against exon 2 of NUAK1 and an exonic region outside the 5' loxP site. This provided two different sized bands in the wild-type and floxed alleles.

Mice carrying cre recombinase under the control of the albumin promoter (alb cre) were obtained from the Jackson Laboratory. Mice carrying the alb cre gene were crossed with homozygous floxed NUAK1 mice to obtain mice with NUAK1 specifically deleted in the liver. The presence of cre recombinase was confirmed by a PCR reaction across an exonic region of the cre which amplified a 100bp band. PCR primers against a ubiquitous housekeeping gene, interleukin-2 (IL2) was used as a positive control (Figure 4.7C).

A

B

C
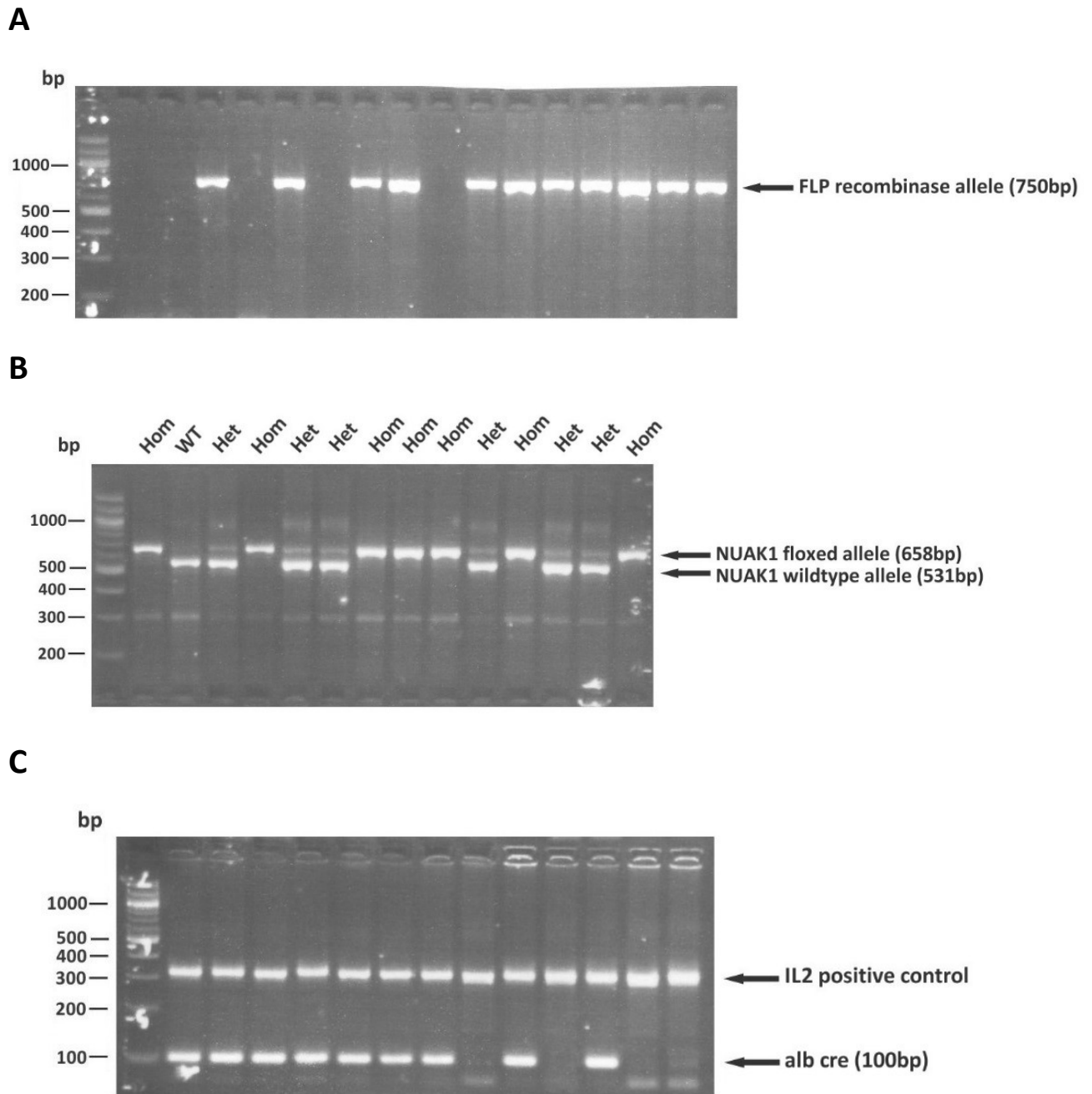
Figure 4.7 Genotyping of conditional knockout mice

(A) The presence of the FLP recombinase gene was confirmed by PCR genotyping. Primers were designed across an exonic region of the FLP gene which amplified a 750bp band. A typical agarose gel of offspring from a heterozygous FLP mice cross is shown. **(B)** A typical agarose gel of a heterozygous floxed NUAK1 cross is shown. Wild-type mice are characterised by a single smaller band (531bp), heterozygous mice are shown by two bands (531bp and 658bp) and homozygous floxed mice are shown by a single larger band (658bp). **(C)** A typical agarose gel of a heterozygous alb cre crossed with a homozygous alb cre is shown. The presence or absence of the cre is shown by the 100bp band.

4.2.4 Young liver-specific NUAK1 knockout mice

Once it had been confirmed by PCR genotyping that the correct transgenic construct was present (Figure 4.7), the knockout in the liver was confirmed by western blotting.
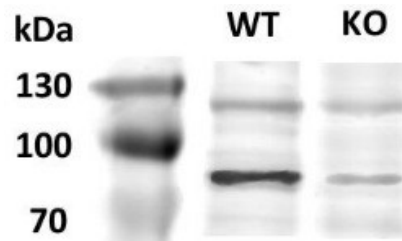
Figure 4.8 Confirmation of liver-specific NUAK1 deletion

Crude lysate from wild-type and NUAK1 knockout livers was resolved on a 10% SDS-PAGE Tris-Glycine gel, transferred to PVDF membrane and incubated with anti-NUAK1 antibody (Cell Signalling). A small amount of NUAK1 protein is present in the knockout liver lysates, most likely because the albumin cre only deletes expression in hepatocytes and the lysates will contain protein from other liver tissues.

Deletion of NUAK1 was confirmed in the liver (Figure 4.8) and because the hepatocyte-specific expression of the alb cre strain is well characterized (Postic et al., 1999) there is minimal chance of any off-target deletion of NUAK1, however no appropriate analyses were carried out to confirm this.

Based on the data from the LKB1 liver-specific knockout mice (Woods et al., 2011), the initial objective was to establish if there was a metabolic phenotype. Mice were maintained under standard conditions and no obvious changes in eating, drinking or breeding behaviour was observed initially. To assess any potential gross morphological changes, a small cohort of mice were sacrificed and basic organ and body weight measurements were taken.
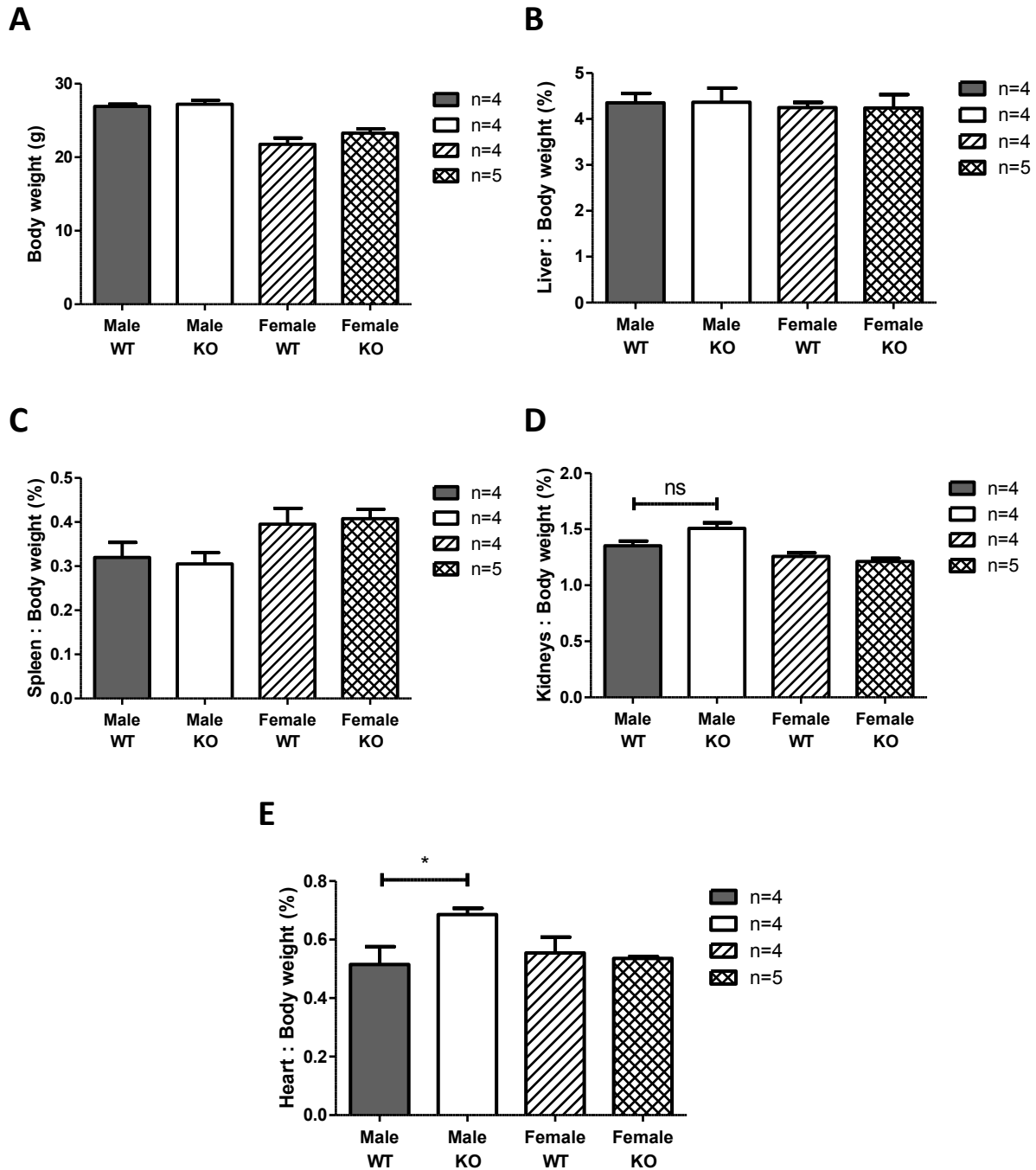
Figure 4.9 Young liver-specific NUAK1 knockout mice appear physiologically normal under basal conditions

(A) Body weights **(B)** Liver weights (normalised to body weight) **(C)** Spleen weights (normalised to body weight) and **(D)** Kidney weight (normalised to body weight). All measurements were taken from 10 – 12 week old liver-specific NUAK1 knockout mice and wild-type littermates. No significant difference ($p>0.05$) was detected for any of these parameters between wild-type and knockout animals using a one-way ANOVA and Bonferroni correction. **(E)** Heart weights (normalised to body weight) from 10 – 12 week old liver-specific NUAK1 knockout mice and wild-type littermates. A small but significant difference ($p<0.05$) is seen in the male mice but not the female mice.

Mice were harvested at a reasonable adult age (10 – 12 weeks) and no significant difference was seen in body weight or liver size. A small but significant difference was seen in male knockout heart size (Figure 4.9).

The body weights of liver-specific NUAK1 knockout animals was unchanged, but there could be a difference in the ratio of fat to lean mass if there were underlying metabolic changes. There is a clear epidemiological link between incidence of liver dysfunction and obesity in human patients and either pathological state can exacerbate the other (Tolman and Dalpiaz, 2007). To assess if there were more subtle changes in body morphology, wild-type and liver-specific NUAK1 mice were analysed using an EchoMRI® machine. This machine uses NMR techniques to create contrast between soft tissues by taking advantage of the differences in relaxation times of the hydrogen proton spins in different environments.
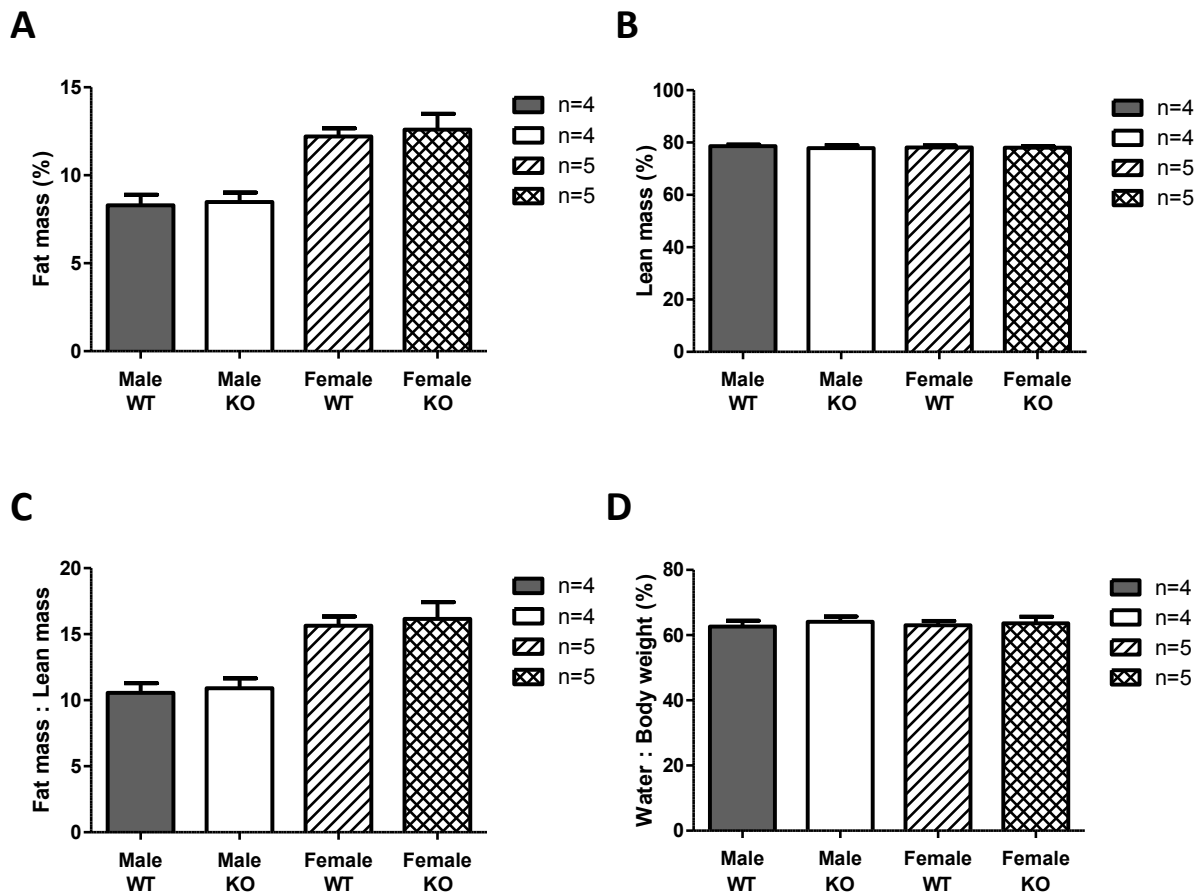
Figure 4.10 Young liver-specific NUAK1 knockout mice have a normal body composition

The body composition of 8 – 10 week old liver-specific NUAK1 knockout mice and their wild-type littermates was assessed using an EchoMRI machine. Plots show mean ± S.E.M. of the indicated number of animals and statistical significance was analysed using the student's t-test to compare the different genotypes within each sex. **(A)** Whole body fat mass measurements. **(B)** Whole body lean mass. **(C)** The ratio between fat mass and lean mass. **(D)** Free water content (normalised to body weight). No significant difference ($p > 0.05$) was detected for any of these parameters between wild-type and knockout animals.

Even after more sensitive analysis, no changes were seen in the body composition of NUAK1 liver-specific knockout mice, suggesting their overall body morphology is normal (Figure 4.10).

Although no changes were observed in whole body morphology, there is a possibility that liver function could be affected in some way that does not manifest itself as a major whole body phenotype. To assess any potential changes in liver structure, wild-type and NUAK1 knockout livers were fixed for histological staining.

WT   **KO**
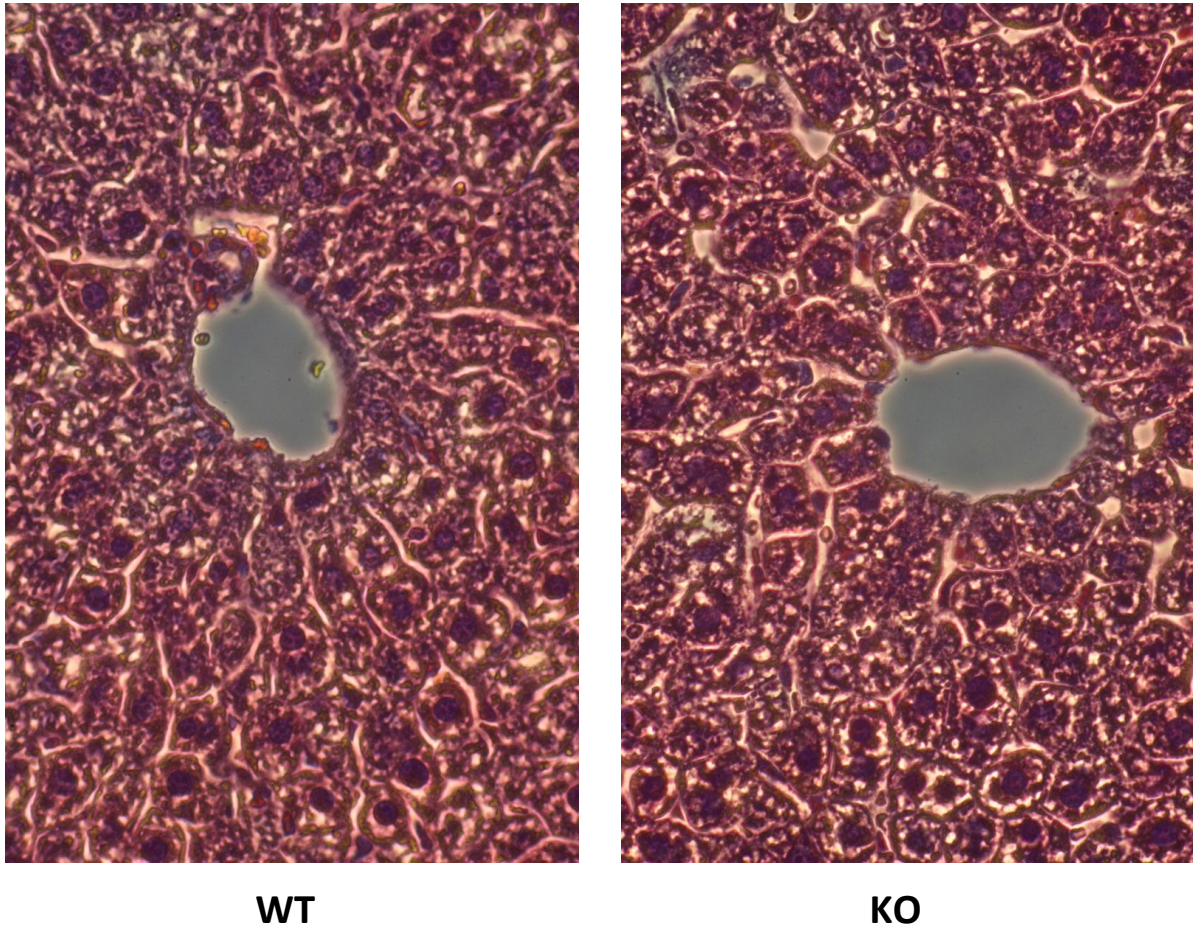
Figure 4.11 Young liver-specific NUAK1 knockout mice have normal liver morphology

The right lobe of livers from wild-type and liver-specific NUAK1 knockout mice were harvested and fixed in 10% formalin. The lobes were sectioned and stained with haematoxylin and eosin (H&E). The sections were imaged and any differences in duct structure, hypertrophy and hyperplasia were observed. Representative images for each genotype are shown and no obvious morphological differences were observed between wild-type and liver-specific NUAK1 knockout mice.

Livers from at least 5 mice of each genotype were assessed with histological staining and no changes in duct structure or cell morphology were observed (Figure 4.11). Compared to LKB1 liver-specific knockout mice, which have a very severe phenotype and die within 2 – 3 weeks of birth (Woods et al., 2011), mice lacking NUAK1 expression in the liver appear structurally normal.

To assess if the liver was functioning correctly, various serum metabolites can be measured to ensure that metabolic processes in the liver are being performed correctly. In cases of liver

damage or dysfunction major changes are seen in some serum metabolites and several of the compounds tested are used as clinical diagnostics of liver disease.
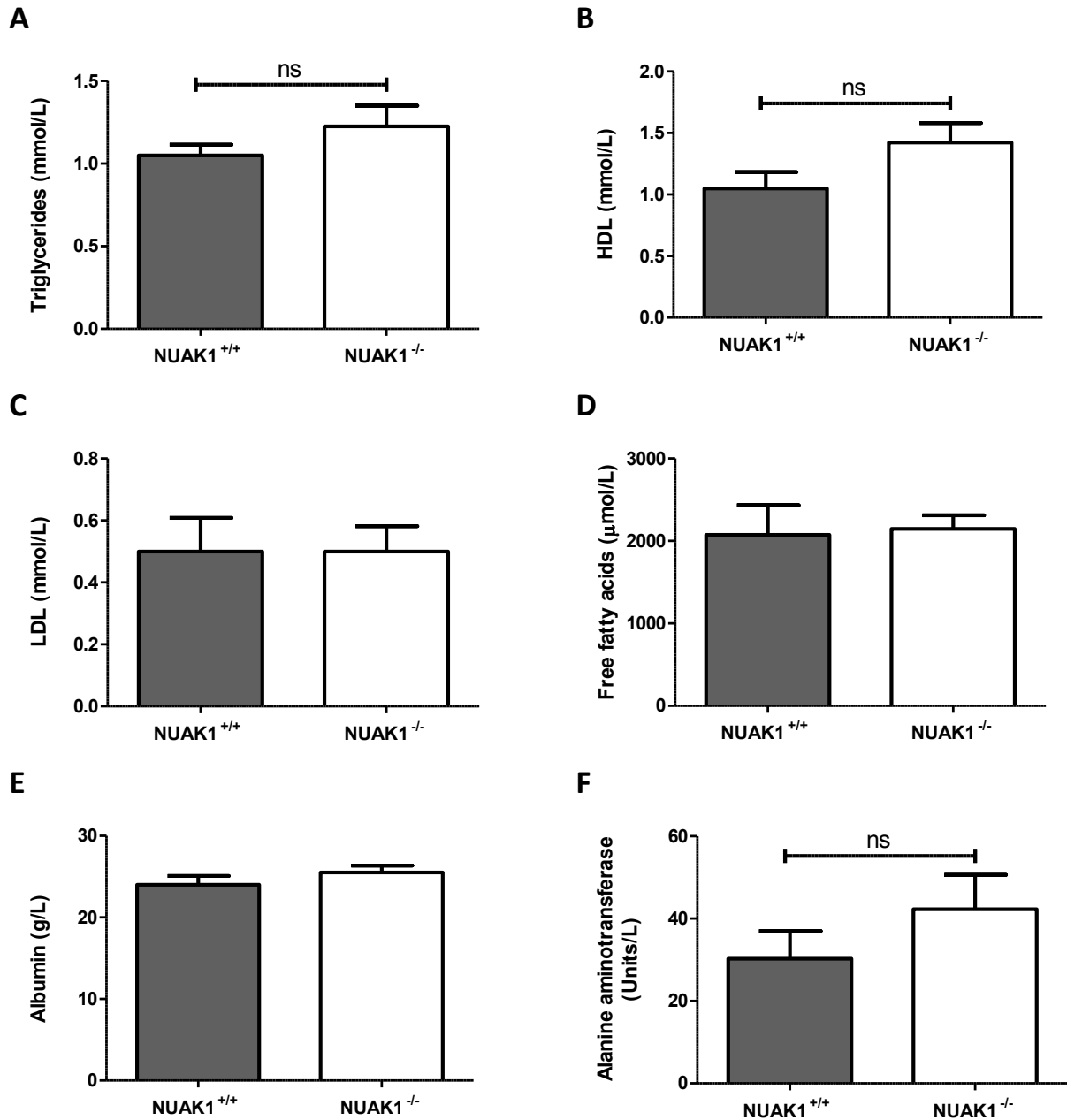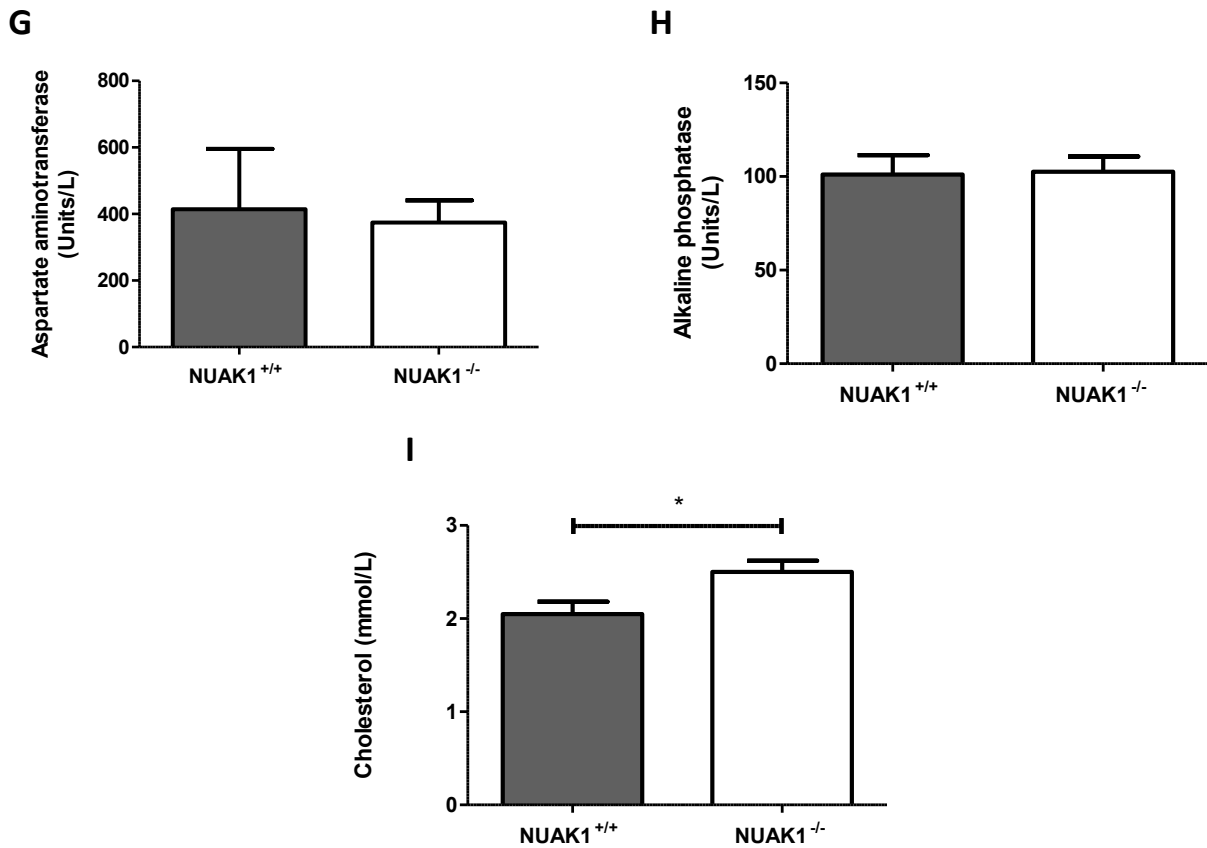
Figure 4.12 Young liver-specific NUAK1 knockout mice show normal serum metabolite levels

Serum was isolated from 10 – 12 week old male wild-type (n=4) and liver-specific NUAK1 knockout (n=4) littermates. The serum was analysed for several indicative metabolites **(A)** Triglycerides **(B)** High density lipoprotein (HDL) **(C)** Low density lipoprotein (LDL) **(D)** Free fatty acids **(E)** Albumin **(F)** Alanine aminotransferase **(G)** Aspartate aminotransferase **(H)** Alkaline phosphatase **(I)** Cholesterol. Plots are all mean ± S.E.M. of samples from 4 mice. In almost all cases no significant difference ($p>0.05$) was observed between knockouts and wild-types when analysed using the student's t-test. A modest but significant increase was observed in cholesterol levels ($p<0.05$) when analysed using a student's t-test.

Across the range of metabolites tested, NUAK1 knockout mice appeared to have normal liver function (Figure 4.12). A small but significant increase in cholesterol was detected but this could be attributed to variation of the assay or the small number of animals used for the test. The slight increase in cholesterol may be indicative of a small degree of liver dysfunction but without other indicators it is difficult to conclusively establish that NUAK1 liver-specific knockout mice have changes in liver metabolism.

In order to study the metabolic profile of these mice further primary hepatocytes were derived from 6 – 8 week old wild-type and liver-specific NUAK1 knockout mice. The hepatocytes were then analysed on the Seahorse Bioscience XF24 Extracellular Flux Analyzer with the assistance of Dr Alicia Garcia (Clinical Sciences Centre). The Seahorse Bioanalyser measures oxygen consumption rate (OCR) and extracellular acidification rate (ECAR) and by using a series of chemicals can measure different mitochondrial parameters. Firstly the basal OCR is measured and by addition of oligomycin, a complex V inhibitor, it is possible to monitor the ATP-linked respiration capacity. Subsequently a mitochondrial uncoupler, carbonyl cyanide p-trifluoromethoxyphenylhydrazone (FCCP) is injected to measure the theoretical maximal OCR. Then antimycin A and rotenone are injected to eliminate all mitochondrial electron transfer and measure the non-mitochondrial portion of energy production. It is designed to detect metabolic changes in cell cultures in real time. If a gene deletion was to cause metabolic changes it would be likely to directly or indirectly affect mitochondrial function and this system is a simple way of measuring several fundamental mitochondrial parameters simultaneously. By adding these chemicals it can measure basal respiration, ATP turnover, proton leak, and spare respiratory capacity. If any of these have changed then it gives a clear indication that functional changes have occurred within the mitochondria.
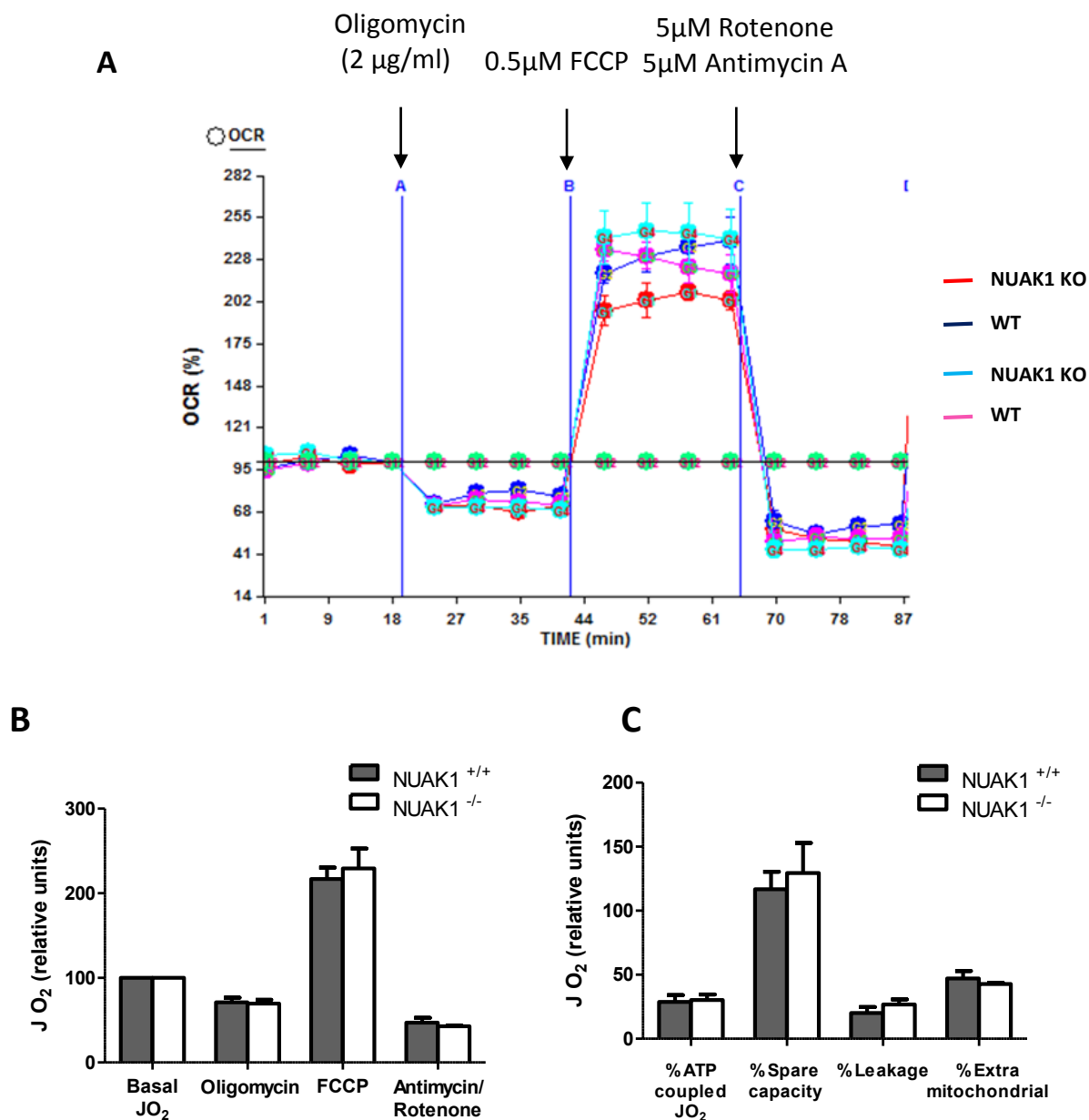
Figure 4.13 NUAK1 knockout hepatocytes from young mice have a normal mitochondrial profile

(A) The normalised oxygen consumption rate profile from the XF24 machine. Two biological replicates were used for each genotype. The different chemicals are injected at the indicated concentrations at the specified points. (B) The 4th point from each data set is taken and the normalised means ± S.E.M. of four repeats from two different animals are plotted. (C) The oxygen consumption rate from each chemical addition can be converted to calculate the percentage of oxygen consumption derived from each source shown. No significant difference ($p>0.05$) was detected between wild-type and NUAK1 knockout hepatocytes when the data was analysed using the student's t-test.

Comparing NUAK1 knockout hepatocytes to their wild-type equivalents it is clear that there is no change in the four parameters measured by the system, indicating that the mitochondria in the liver are functionally normal (Figure 4.13).

Another important metabolic function that is performed in the liver is gluconeogenesis – the generation of glucose from non-carbohydrate carbon sources such as pyruvate. As the mice are housed in a temperature controlled environment and are fed *ad libitum* on an ideal diet, it is possible that under physiologically healthy conditions, gluconeogenesis rarely occurs. Therefore to test if there are changes in the gluconeogenesis pathways, wild-type and NUAK1 knockout hepatocytes were subjected to a hepatic glucose output assay which detects the rate of gluconeogenesis when the cells are only provided with pyruvate as a carbon source. This is measured by replacing the culture medium with basal DMEM containing lactate and pyruvate and measuring the concentration of glucose in the medium over a time course. The glucose concentration is measured using a colorimetric glucose oxidase assay. The protein concentration of the cells is used to normalise the values to produce a rate of glucose production per mg of protein.
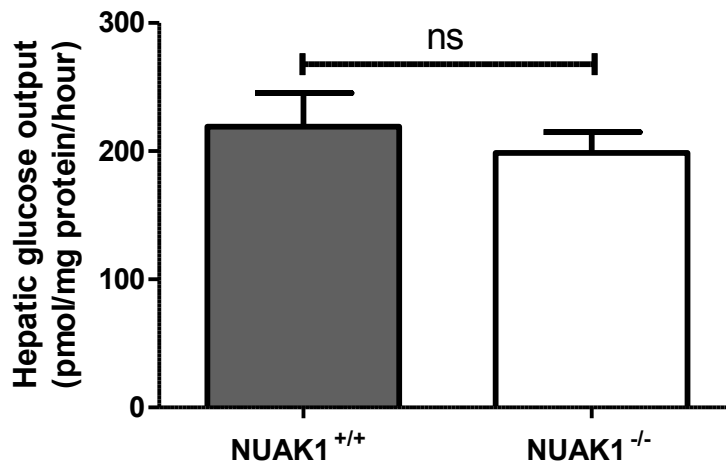
Figure 4.14 NUAK1 knockout hepatocytes from young mice have a normal hepatic glucose output

Hepatic glucose output from wild-type and NUAK1 knockout hepatocytes is shown. Measurements were taken in triplicate from two mice of each genotype. No significant difference ($p>0.05$) was observed when the data was analysed using the student's t-test.

The results of the hepatic glucose output assay show that loss of NUAK1 in the hepatocytes does not affect gluconeogenesis pathways and should not impair the functional role of the liver in maintaining blood glucose levels under conditions of stress (Figure 4.14).

The study that assessed the phenotype of skeletal-muscle specific NUAK1 knockout mice identified a phenotype where NUAK1 deletion protected against high-fat diet induced glucose intolerance (Inazuka et al., 2012). Glucose intolerance is a phenotype normally associated with obesity and early diabetic pathology. The impaired glucose tolerance is caused by insulin insensitivity and indications that NUAK1 may phosphorylate and regulate insulin receptor substrate 1 (IRS1) may suggest that liver-specific NUAK1 knockout mice may have improved glucose tolerance (Inazuka et al., 2012).

Glucose tolerance of liver-specific NUAK1 knockout mice and wild-type littermates was measured by administering an intraperitoneal bolus dose of glucose (1g/kg) to mice that had been fasted overnight. The blood glucose levels were then measured over a period of two hours.

A

B
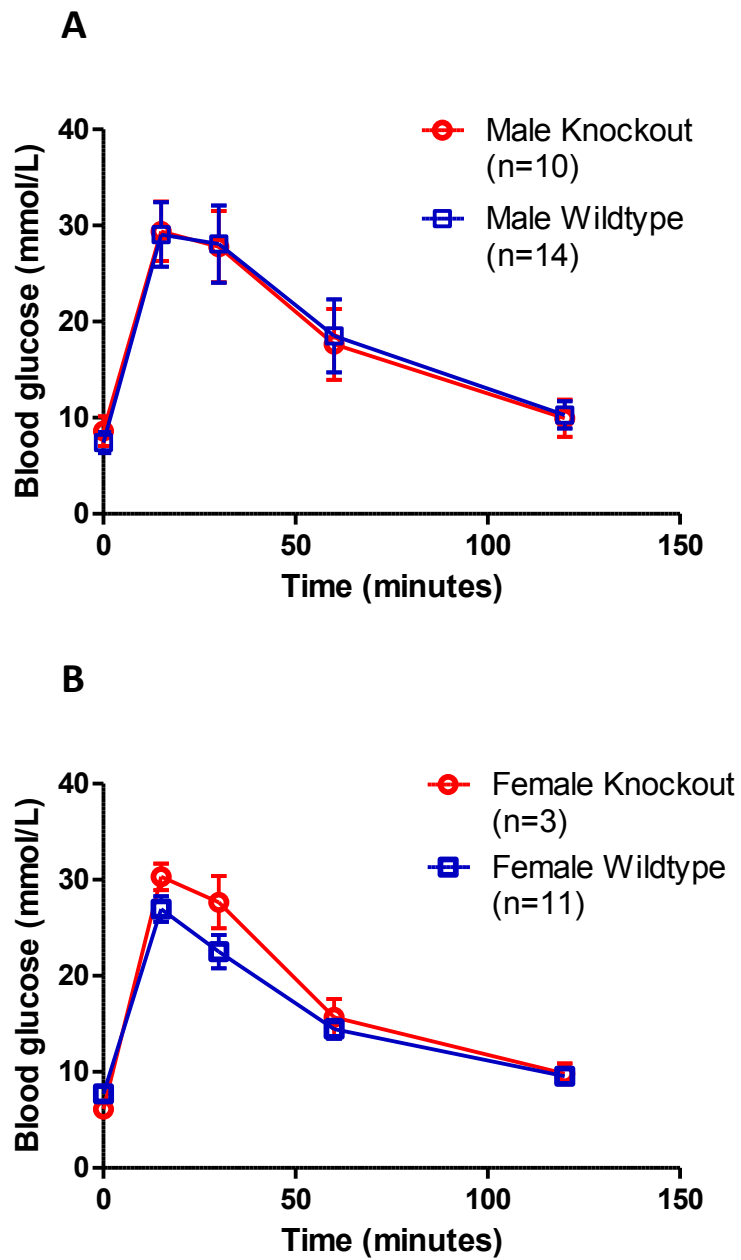
Figure 4.15 Young liver-specific NUAK1 knockout mice have a normal glucose tolerance

Blood glucose levels after intraperitoneal glucose administration is shown in separate plots for **(A)** Males and **(B)** Females. The plots show the mean ± S.E.M. for the indicated number of animals at each time point. The data at each time point were assessed using the student's t-test and no significant difference ($p > 0.05$) was observed.

No variation in glucose tolerance was observed under basal conditions in the NUAK1 liver-specific knockout mice (Figure 4.15). To some extent these data support the muscle-specific NUAK1 knockout study that only saw the reduced glucose intolerance phenotype under stressed conditions (Inazuka et al., 2012).

Given that no major changes were observed in several key metabolic indicators, it was thought that there could be a more subtle phenotype in the liver-specific NUAK1 knockout. To assess this the mice were housed in a Columbus Instruments Comprehensive Lab Animal Monitoring System (CLAMS). This is an automated system that can measure calorimetry, activity, feeding, drinking and sleep detection. The variety of data can indicate if there is a minor change in the metabolic profile of the mice. The first 16 – 20 hours of data from the CLAMS system was disregarded as an acclimatisation period as the animals will often be stressed during the initial period in the apparatus.

The respiratory exchange ratio (RER) is an indicator of the energy source being used to produce ATP in the cell. This is calculated as a ratio between the VO_2 and the VCO_2. The respiratory exchange ratio values are then plotted over a time course.

A

B

C

D

E

F
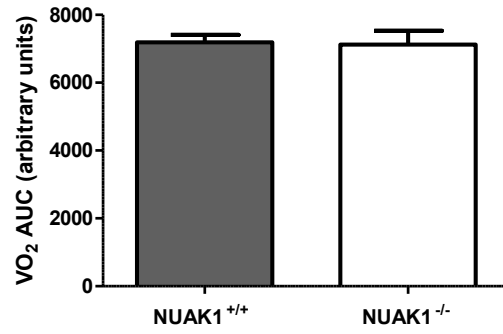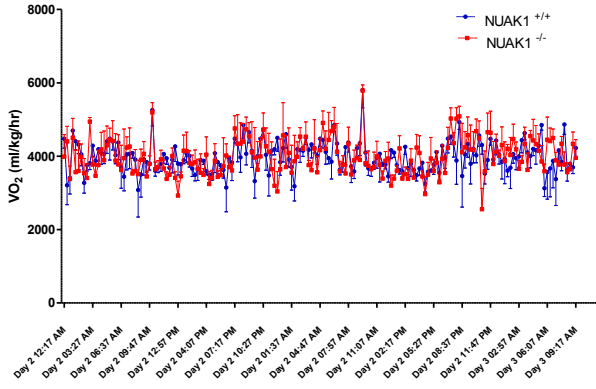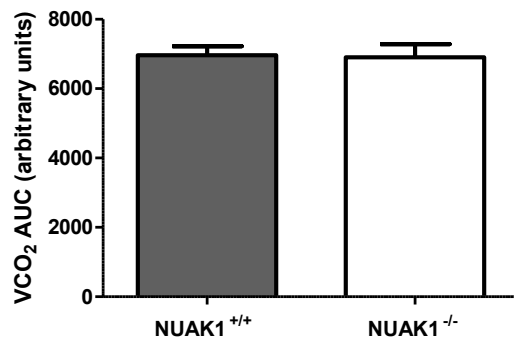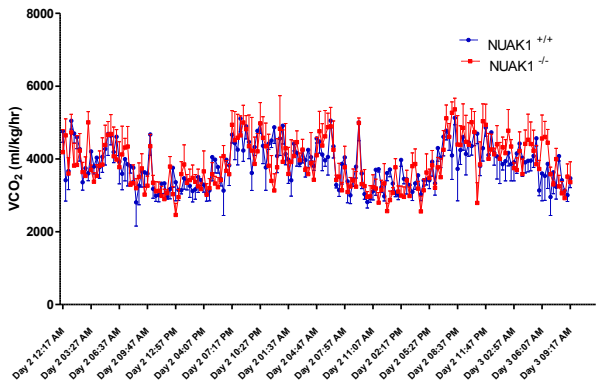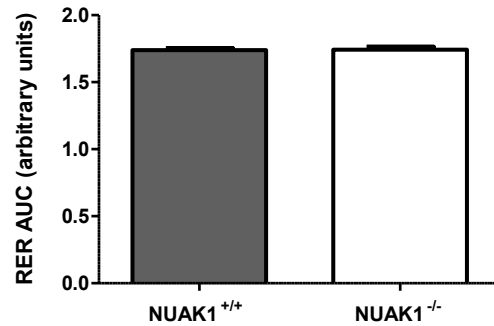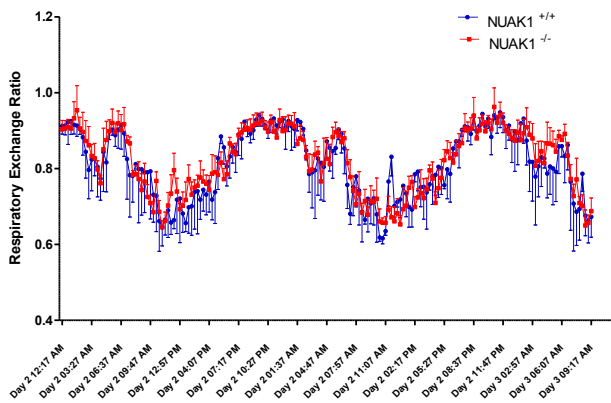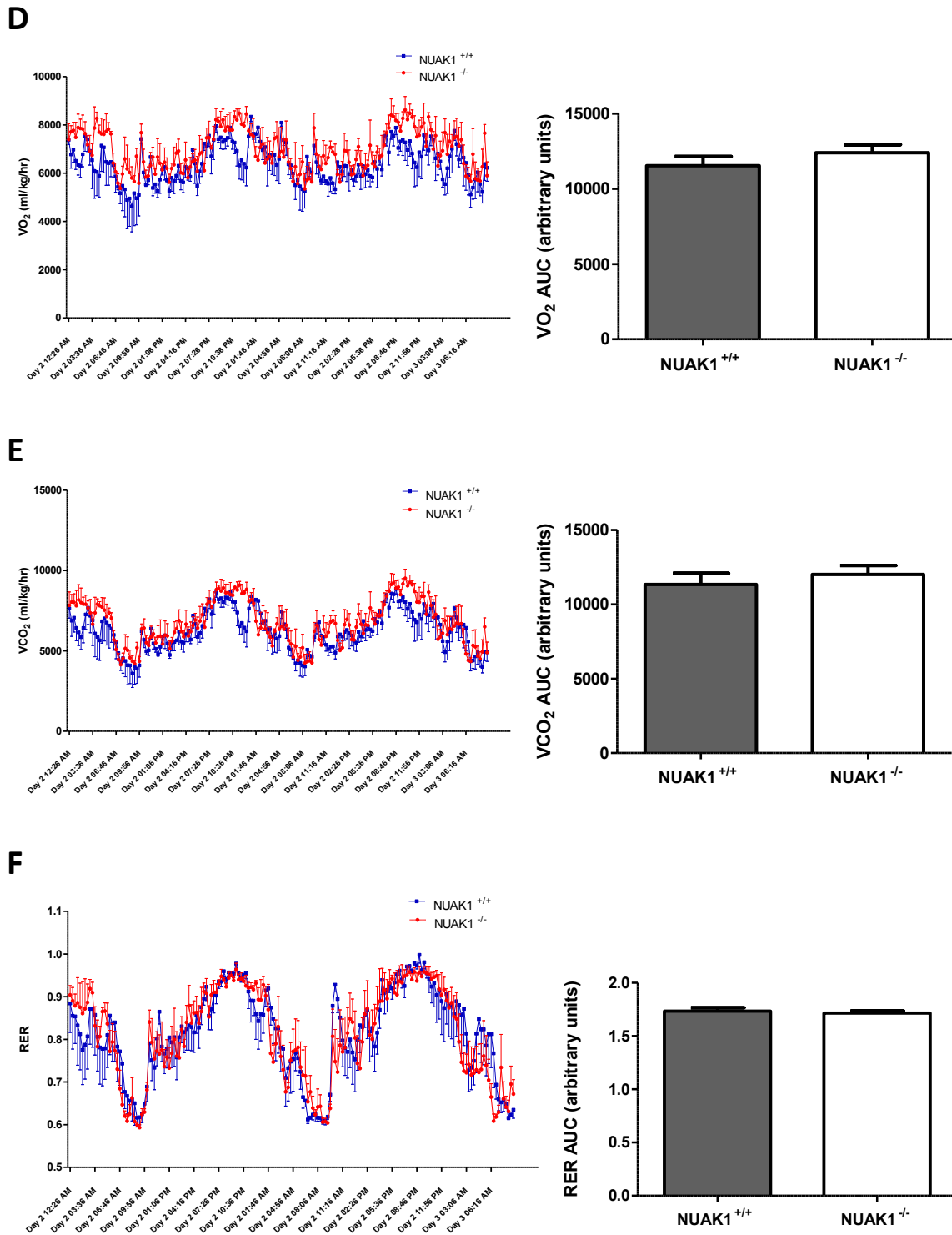
Figure 4.16 Young liver-specific NUAK1 knockout mice have a normal respiratory exchange ratio

O_2, CO_2 and RER plots from the CLAMS system. For each of the time courses, the data has been analysed for statistical significance by integrating the area under the curve and plotting the mean ± S.E.M. of at least of four mice of each genotype. Data is shown for both males **(A)** VO_2, **(B)** VCO_2, **(C)** RER and females **(D)** VO_2, **(E)** VCO_2, **(F)** RER. All these data have then been analysed using the student's t-test and no significance differences ($p>0.05$) were observed.

155

The CLAMS system did not detect any change in VO_2, VCO_2 or RER between wild-type and liver-specific knockout animals, indicating that their metabolic profile and the energy source they are using is normal (Figure 4.16). The CLAMS system is also able to convert the RER measurements into heat production by deriving a calorific value (CV) based on the respiratory exchange ratio. This calorific value is then combined with the VO_2 data to calculate heat according to the following equations:

$$CV = 3.815 + 1.232 \times RER$$

$$Heat = CV \times VO_2$$

The constants for determining the calorific value have been determined from studies investigating oxidation of defined ratios of fat and carbohydrate (Columbus Instruments data sheet).

Any variation in heat production would indicate that the animals are having to burn more calories to maintain homeostatic functions, suggesting possible metabolic dysfunction.

A
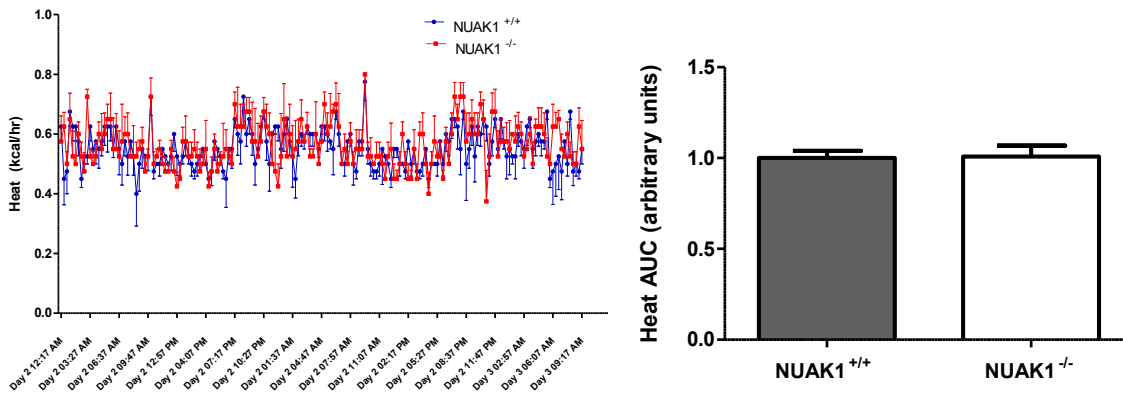
B
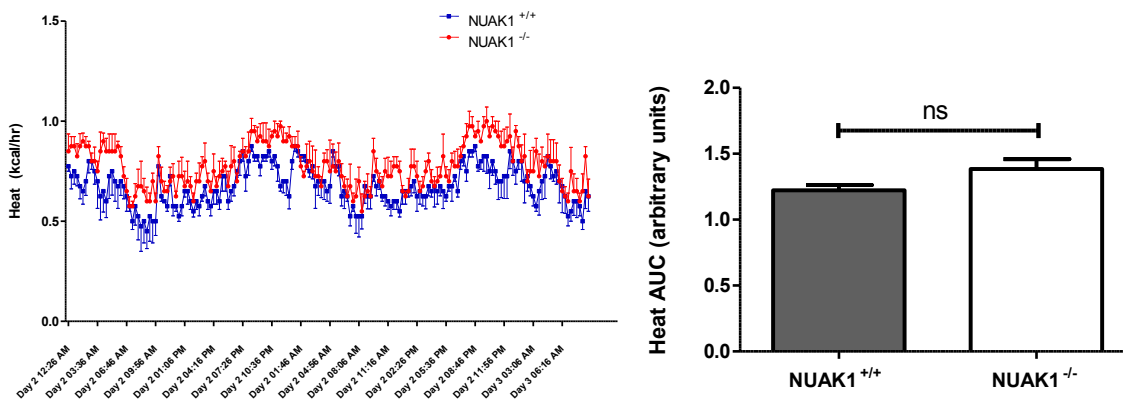
Figure 4.17 Young liver-specific NUAK1 knockout mice burn the same amount of calories as wild-type mice

Heat production was calculated from RER and VO_2 measurements. The time course data is shown alongside integrated area under the curve calculations for statistical comparison. The mean ± S.E.M. was plotted for at least four mice of each genotype. **(A)** Males and **(B)** Females. All these data were analysed using the student's t-test and no significant differences ($p>0.05$) were observed.

These data suggest that there is no variation in the metabolic function in NUAK1 liver-specific knockout mice (Figure 4.16 and Figure 4.17), however the systems controlling metabolism are diverse and multi-factorial and there could be confounding effects that are masking the observation of any phenotype. To ensure that liver-specific NUAK1 knockout mice have the same food consumption and behaviour profile as wild-type mice, their activity and food and water intake were measured.

The CLAMS system is able to monitor total food and water consumption and this has been normalised to the animal's body weight to control for any increase due to greater size. The data is plotted as a time course from the start of when the animals enter the CLAMS system, hence why there may be some disturbances in the early readings.
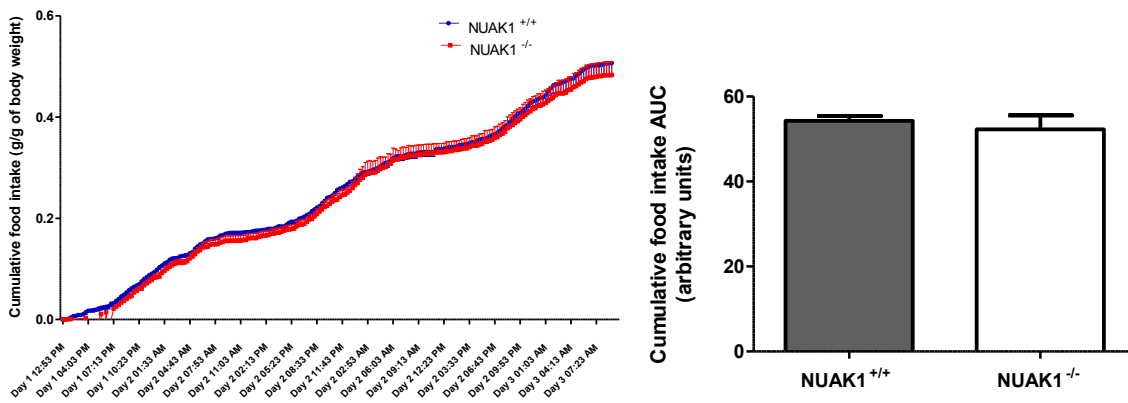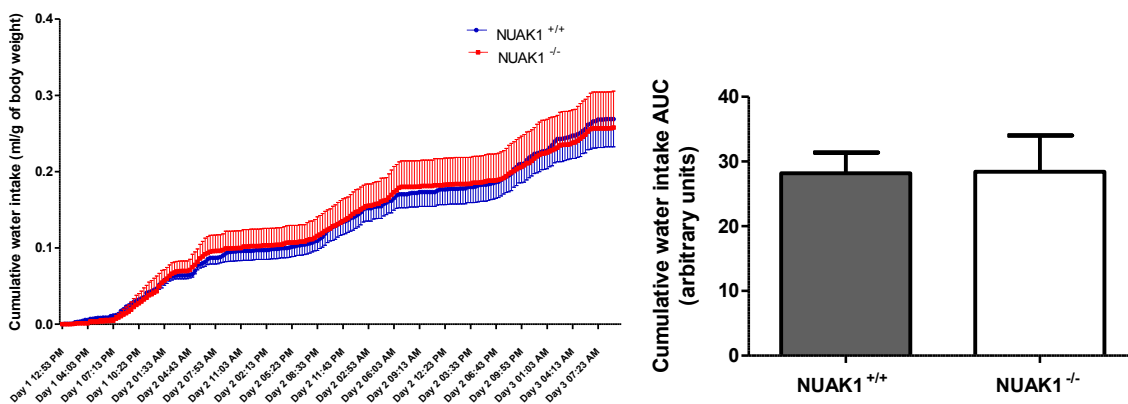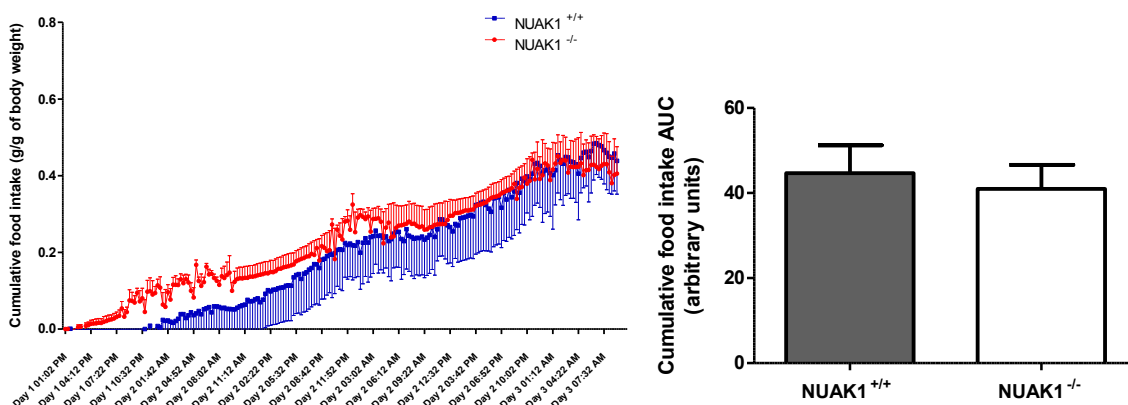
D
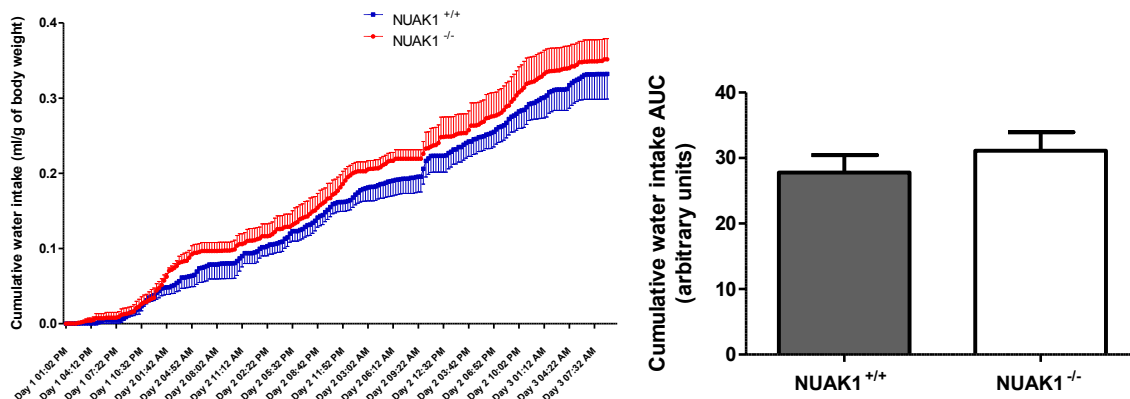
Figure 4.18 Young liver-specific NUAK1 knockout mice have normal food and water consumption

Food and water intake plots from the CLAMS system. The data has been analysed for statistical significance by integrating the area under the curve and plotting the mean ± S.E.M. for each of four mice of each genotype. Data is shown for both males **(A)** Food **(B)** Water and females **(C)** Food **(D)** Water. All these data were analysed using the student's t-test and no significant differences (*p*>0.05) were observed.

There was no change in food or water consumption due to deletion of NUAK1 in the liver (Figure 4.18), so activity measurements were made to assess any potential behavioural differences. The CLAMS system has a mechanism for dual axis detection of animal motion using infrared photocells. These detect counts for each movement that the animal makes so it is possible to track their cumulative movement over the course of the time in the monitoring cages.

A
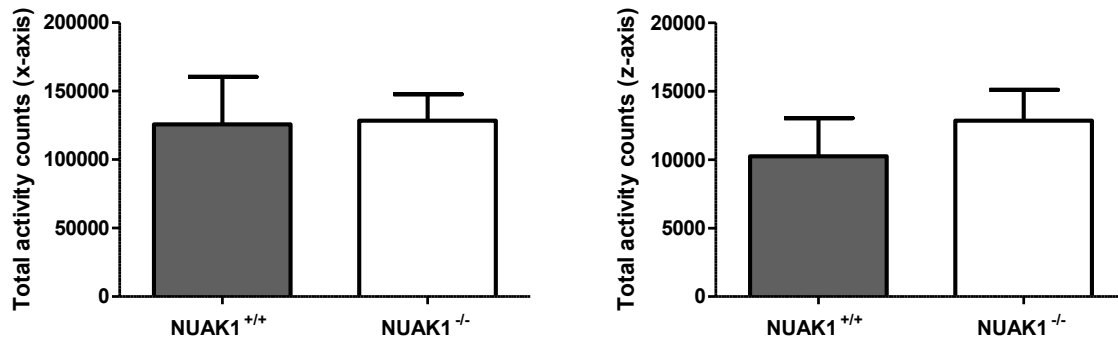
B
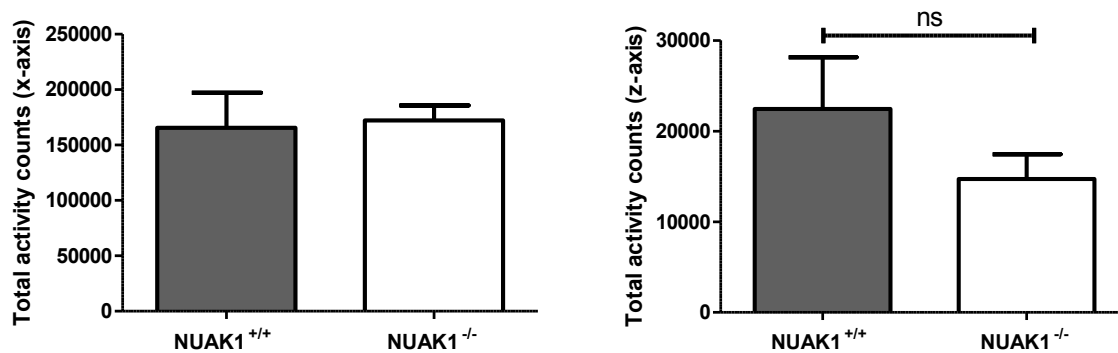
Figure 4.19 Young liver-specific NUAK1 knockout mice have unchanged activity and movement levels

Movement plots from the CLAMS system. The cumulative movement in the x-axis and the z-axis were counted for at least four animals of each sex and genotype. The mean ± S.E.M. was plotted for **(A)** Males and **(B)** Females. All these data were analysed using the student's t-test and no significant differences (*p*>0.05) were observed.

All these data suggest that there is no variation in food and water intake or activity levels that might affect the metabolic measurements of the animals (Figure 4.19). This would also suggest that there are no other feedback mechanisms that are affecting behaviour or eating patterns.

4.2.5 CDE diet treated liver-specific NUAK1 knockout mice

After extensive efforts to discover a phenotype in the liver-specific NUAK1 knockout mice under basal conditions it seemed that they were functionally normal. Following on from reports in the literature that NUAK1 is involved in mediating cell adhesion (Zagorska et al., 2010) and evidence from culturing NUAK1 null MEFs, other studies have also suggested NUAK1 is involved in cell survival during deregulated MYC expression (Liu et al., 2012). Based on these data a decision was made to induce an artificial stress on the livers to observe any potential changes in cell proliferation in response to liver damage. After discussions with collaborators (Stuart Forbes et al., Edinburgh University) the best available diet was a choline-deficient, ethionine supplemented (CDE) diet. Wild-type and liver-specific NUAK1 knockout mice were placed on this diet for a maximum of three weeks with food and water intake and changes in body weight monitored over this time to ensure there was no unnecessary pain, suffering or harm done to the animals.

Although a large degree of liver damage was expected after treatment with the diet, serum metabolites were measured, as before, to assess if there were any variations in response to the diet between wild-type and liver-specific NUAK1 knockout animals.

A

B

C

D

E

F

G

H
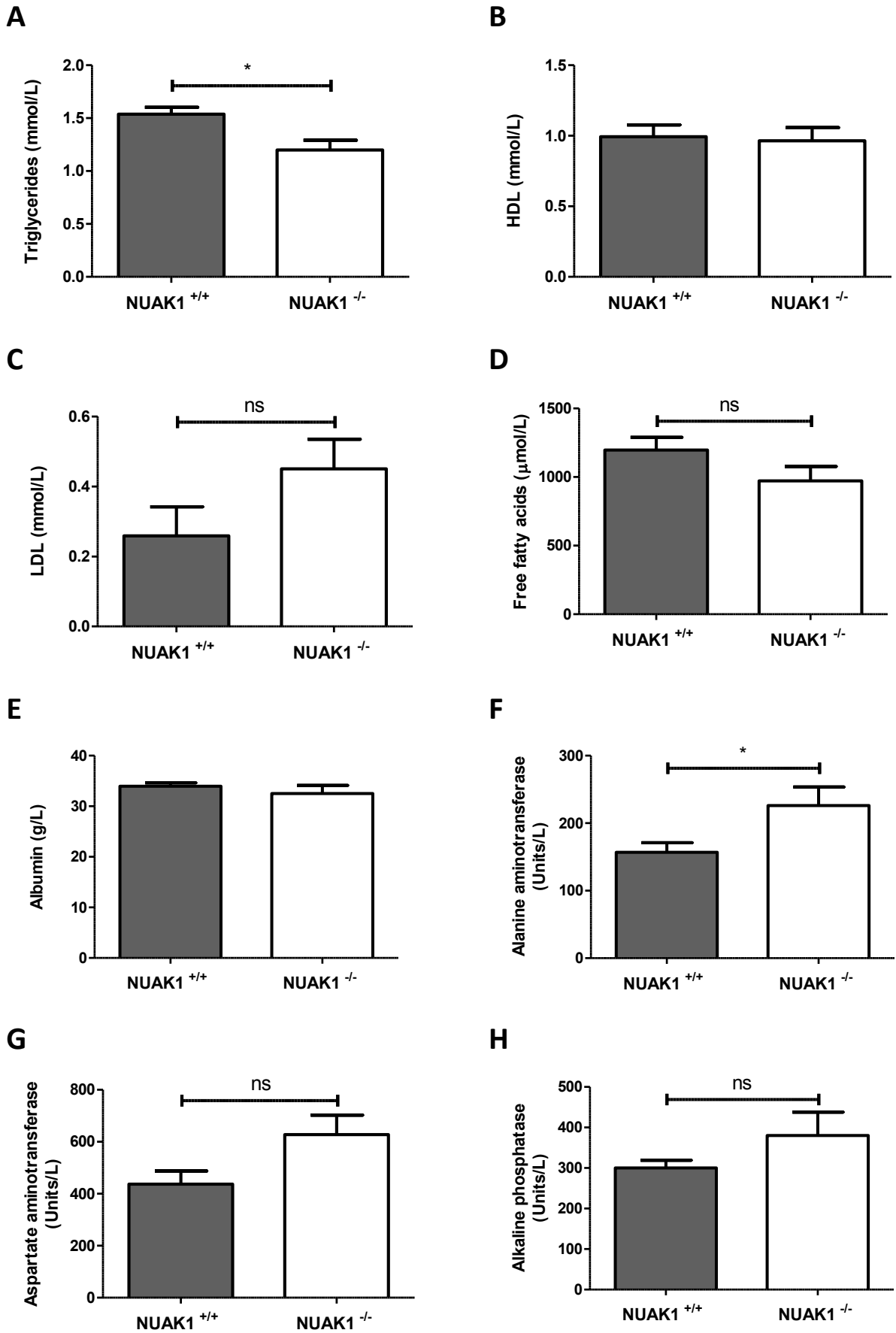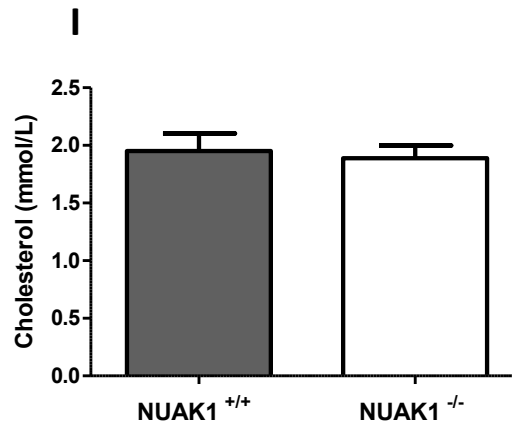
Figure 4.20 Liver-specific NUAK1 knockout mice fed a CDE diet show no difference in serum metabolites

Serum was isolated from 12 – 16 week old male wild-type (n=8) and liver-specific NUAK1 knockout (n=9) littermates that had been fed the same CDE diet for 3 weeks. The serum was analysed for several indicative metabolites **(A)** Triglycerides **(B)** High density lipoprotein (HDL) **(C)** Low density lipoprotein (LDL) **(D)** Free fatty acids **(E)** Albumin **(F)** Alanine aminotransferase **(G)** Aspartate aminotransferase **(H)** Alkaline phosphatase **(I)** Cholesterol. Plots are all mean ± S.E.M. of samples from at least 8 mice. In almost all cases no significant differences ($p > 0.05$) were observed between knockouts and wild-types when analysed using the student's t-test. A modest but significant reduction was observed in triglyceride levels and a significant increase was observed in alanine aminotransferase (ALT) ($p < 0.05$).

Generally the response to the damage induced by the diet was the same between wild-type and liver-specific knockout animals (Figure 4.20). Clearly the livers have been damaged significantly, indicated by a substantial increase in various metabolites compared to untreated animals (Figure 4.12). After feeding on the CDE diet a significant increase in alanine aminotransferase (ALT) levels was observed in liver-specific NUAK1 knockout animals. However, this could be partly due to diurnal variation as small but not clinically significant diurnal variations in ALT levels have been observed in humans (Ruhl and Everhart, 2013). Blood samples were taken at the same time of day so this may not be the cause of the variation, but the levels of rest may vary as some mice become more inactive than others in response to the CDE diet (data not shown).

The main reason for feeding with the CDE diet was to induce cell proliferation in liver stem cells to see if there is a difference in the response to liver damage. To assess this livers from treated animals were fixed and then processed by collaborators at Edinburgh University

(Stuart Forbes et al.). Liver sections were stained with pan-cytokeratin antibodies, a marker of liver progenitor cells (Boulter et al., 2012).

A

WT   KO
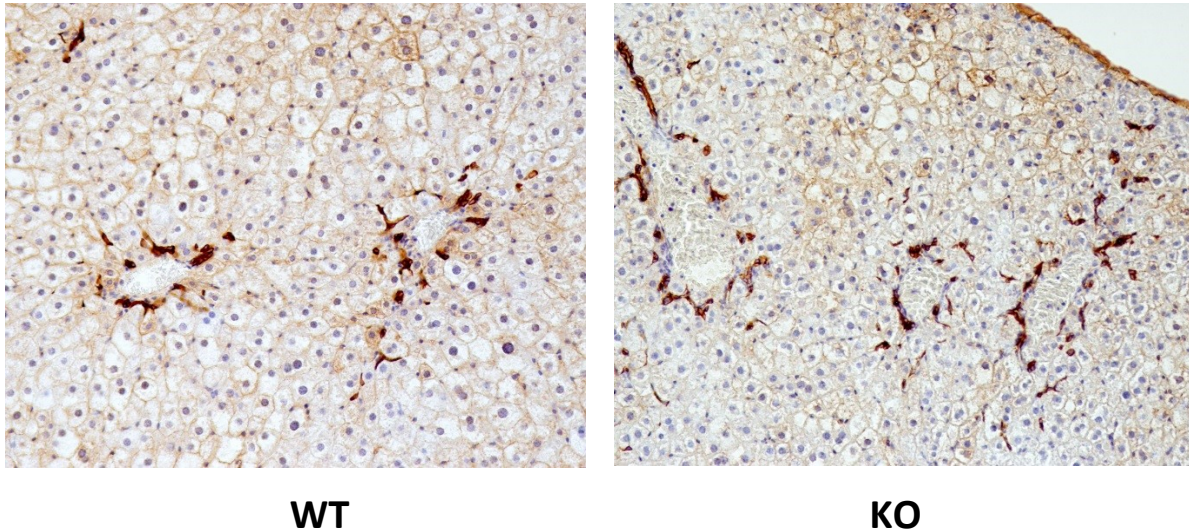
B
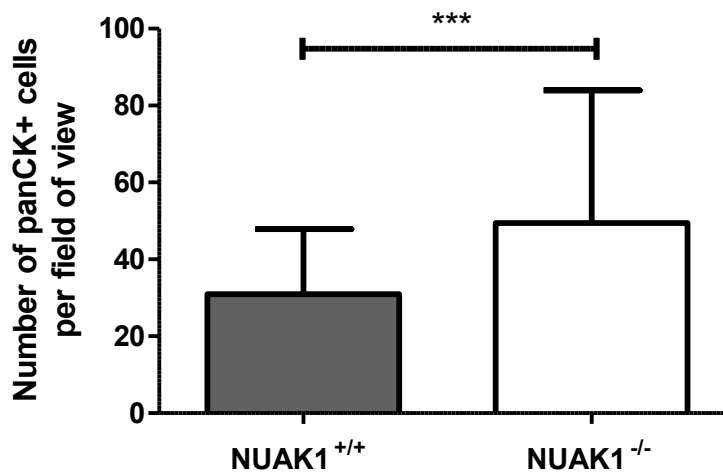
Figure 4.21 Liver-specific NUAK1 knockout mice fed a CDE diet produce more cytokeratin positive liver progenitor cells

The right lobe of livers from wild-type (n=4) and liver-specific NUAK1 knockout mice (n=5) were harvested and fixed in 10% (v/v) formalin. The lobes were sectioned and stained using a pan-cytokeratin (panCK) antibody. **(A)** The sections were imaged and the number of panCK positive cells were counted in each field of view. **(B)** At least 20 fields of view were counted for each of four different mice and the total average for each genotype was determined. A significant difference (*p*<0.001) was observed between the wild-type and NUAK1 liver-specific knockout mice when analysed using a student's t-test.

A significant difference was observed in the ability of the liver-specific NUAK1 mice to respond to acute injury, suggesting that NUAK1 may play a role in the adaptation and response to damage in pathological conditions (Figure 4.21). This could help explain why muscle-specific NUAK1 knockout mice required a stress stimulus to produce a phenotype (Inazuka et al., 2012). However, although the NUAK1 null livers showed a greater proliferation of progenitor cells, there was no improvement in liver function compared to wild-type mice, indicated by serum metabolite measurements (Figure 4.20). This suggests that the damage to the livers is equivalent, however there may be a better response to the insult over a longer time period.

4.2.6 Aged liver-specific NUAK1 knockout mice

To assess if this variation in response to damage was only seen in acute injury or whether variation could be observed over a longer time period, a decision was made to age a cohort of mice to see if any morphological or functional changes were observed as a result of natural damage caused by ageing. Wild-type and liver-specific NUAK1 knockout mice were kept under identical conditions and fed the same chow diet.

Similar metabolic phenotyping analyses were applied to the aged mice to assess if the deletion of NUAK1 in the liver had adversely affected or changed the gradual adaptation to the ageing process in the liver.

The body composition of 50 – 52 week old liver-specific NUAK1 knockout mice and their wild-type littermates was assessed using an EchoMRI instrument and livers were harvested to assess if there was a longer term variation in organ mass due to NUAK1 deletion.
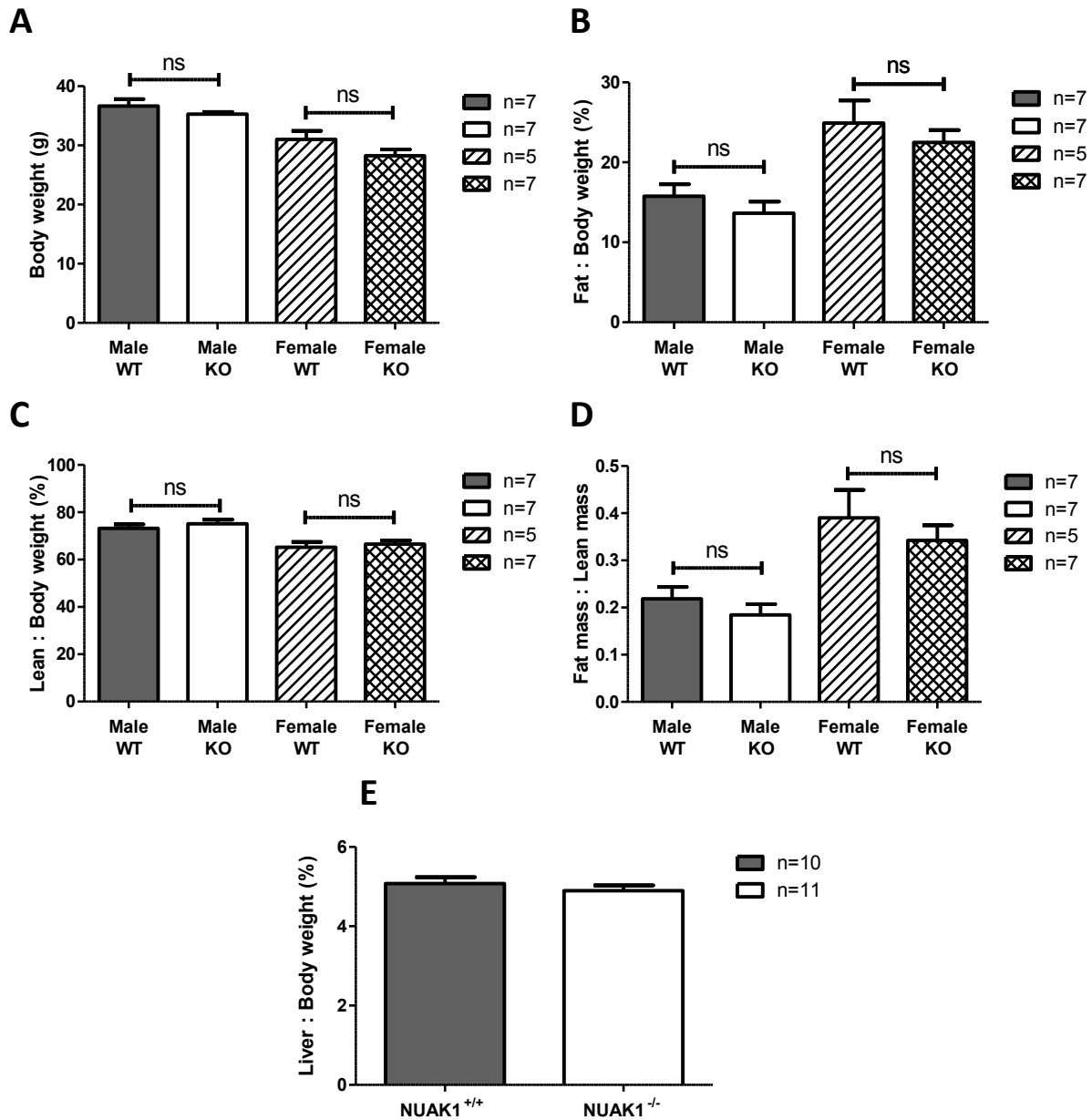
Figure 4.22 Aged liver-specific NUAK1 knockout mice have slightly lower body weight and body fat percentage

(A) Body weight of 50 – 52 week old liver-specific NUAK1 knockout males and females was slightly lower than their wild-type littermates, although not statistically significant. **(B)** Whole body fat mass measurements showed a modest but not significant reduction in both male and female knockout mice. **(C)** Whole body lean mass measurements showed no difference between liver-specific NUAK1 knockouts and wild-type littermates **(D)** The ratio between fat and lean mass showed a substantial but not significant (p>0.05) reduction in both males and females. **(E)** 30 -38 week old male liver-specific NUAK1 knockout mice have no change in liver weight (normalised to body weight) compared to their wild-type littermates. Plots show mean ± S.E.M. of the indicated number of animals and statistical significance was analysed using the student's t-test to compare the different genotypes within each sex.
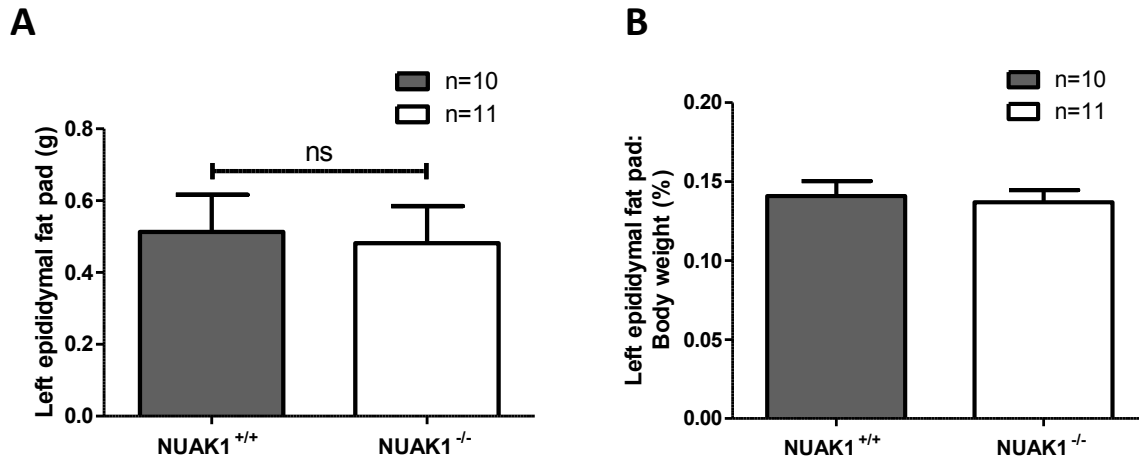
Figure 4.23 Aged liver-specific NUAK1 knockout mice have slightly smaller epididymal fat pads

The epididymal fat pads of 30 – 38 week old male liver-specific NUAK1 knockout mice and their wild-type littermates were harvested. **(A)** Epididymal fat pads of liver-specific NUAK1 knockout males had slightly lower weights compared to their wild-type littermates, although not statistically significant (p>0.05). **(B)** Epididymal fat pad sized normalised to body weight still show a small but not significant reduction in size. Plots show mean ± S.E.M. of the indicated number of animals.

When assessing the overall body morphology of the aged mice it was clear that there was a slight, but not significant reduction in body weight and fat mass in the liver-specific NUAK1 knockout mice (Figure 4.22). Also, when the size of a specific fat pad was measured, a slight reduction was also observed in liver-specific NUAK1 knockout mice (Figure 4.23). Although the number of animals was small, there was a clear change in the fat mass to lean mass ratio (Figure 4.22). The mechanism for this was unclear but it suggested that there are phenotypic differences in response to ageing that were caused by NUAK1 deletion in the liver.

To see if there was any indication that a specific pathway was being affected by loss of NUAK1, serum metabolites were measured as before.
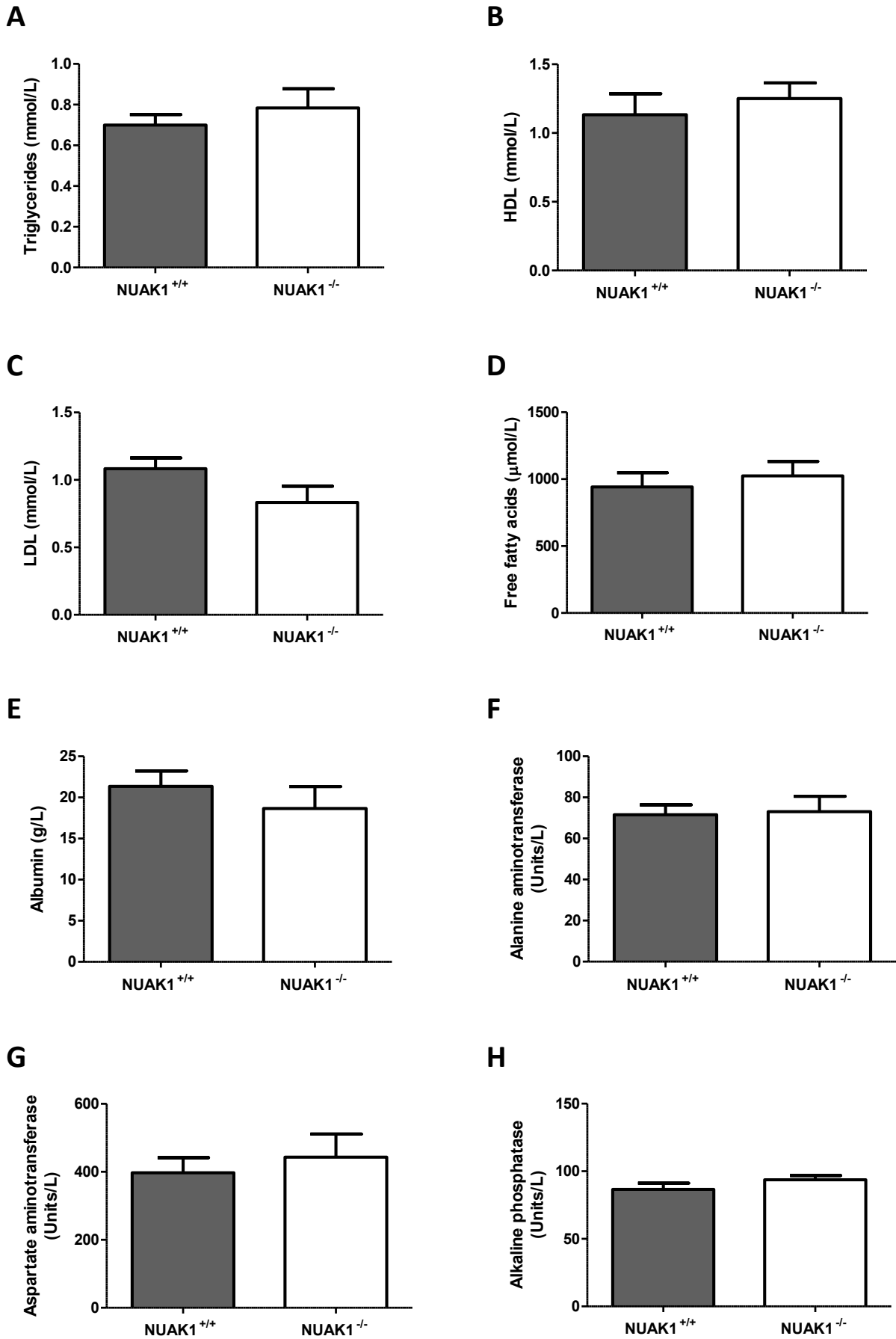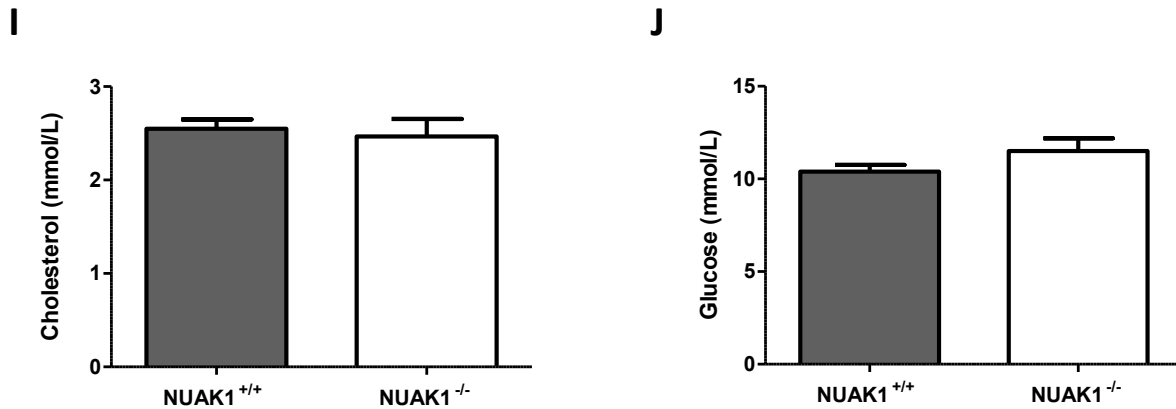
Figure 4.24 Aged liver-specific NUAK1 knockout mice show unchanged serum metabolite levels

Serum was isolated from 50 - 52 week old male wild-type (n=6) and liver-specific NUAK1 knockout (n=5) littermates. The serum was analysed for several indicative metabolites **(A)** Triglycerides **(B)** High density lipoprotein (HDL) **(C)** Low density lipoprotein (LDL) **(D)** Free fatty acids **(E)** Albumin **(F)** Alanine aminotransferase **(G)** Aspartate aminotransferase **(H)** Alkaline phosphatase **(I)** Cholesterol and **(J)** Glucose. Plots are all mean ± S.E.M. of samples from at least 5 mice of each genotype. In all cases no significant differences ($p>0.05$) were observed between knockouts and wild-types when analysed using the student's t-test.

No differences were seen in the serum metabolite profile of aged wild-type mice compared to liver-specific NUAK1 knockout mice (Figure 4.24), providing no evidence to suggest why there is a slight reduction in body weight and fat mass as a result of NUAK1 deletion. Some metabolites showed clear differences across both genotypes compared to the younger mice, for example alanine aminotransferase (see Figure 4.12F and Figure 4.24F). This suggests that the absence of NUAK1 has not affected the adaptation to ageing in these pathways.

Given that there was a modest decrease in body weight and slightly lower body fat percentage in the liver-specific NUAK1 knockouts yet the liver function appeared to be unchanged, it is possible that there was a significant whole body metabolic phenotype that was linked to age-related differences in liver regeneration. To assess any whole body changes in metabolism the CLAMS system was used to measure a variety of important data that can indicate if there is a minor change in the metabolic profile of the mice.

A
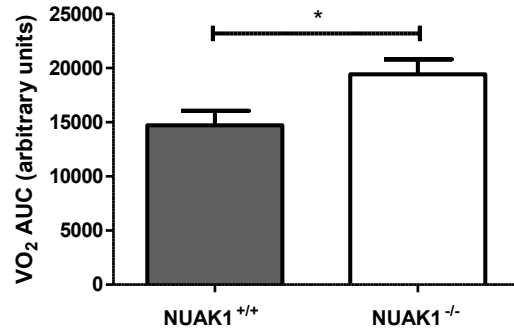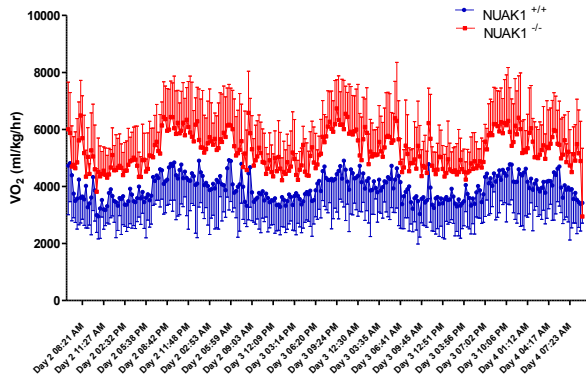
B
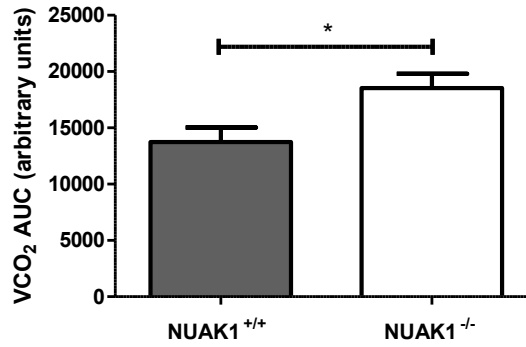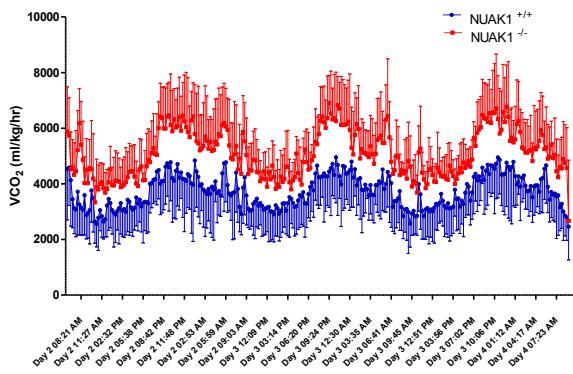
C
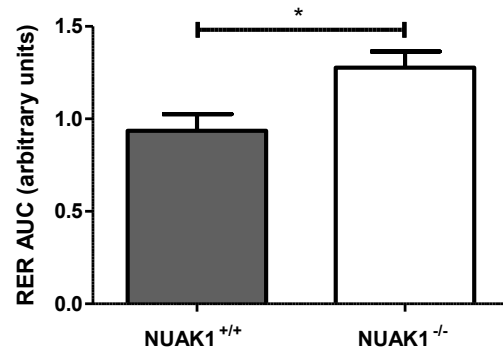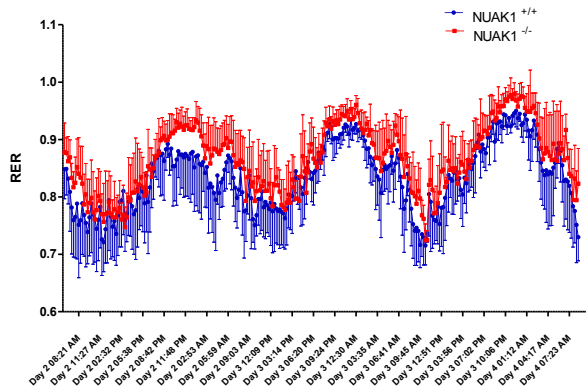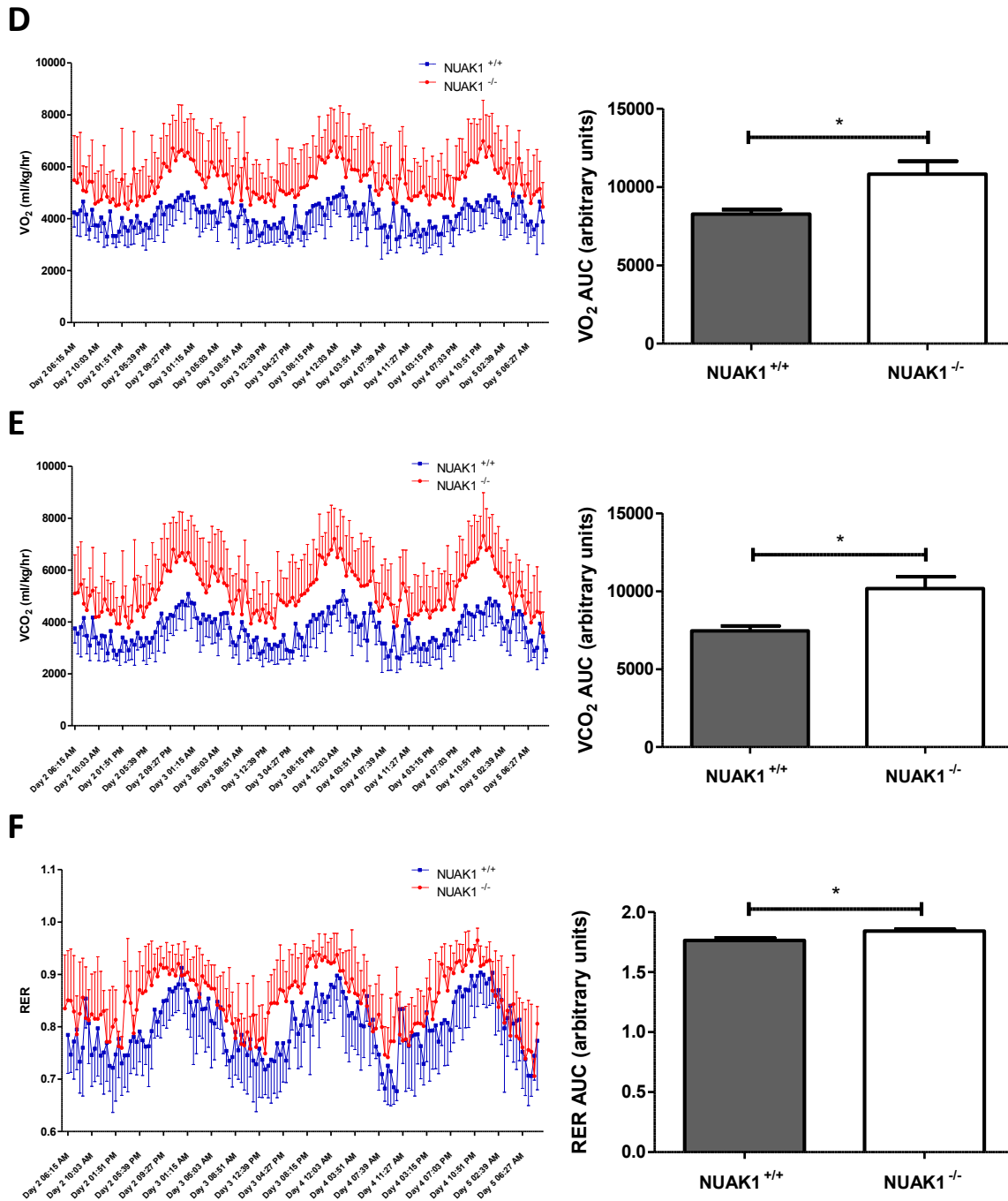
Figure 4.25 Aged liver-specific NUAK1 knockout mice have an increased respiratory exchange ratio

O_2, CO_2 and RER plots from the CLAMS system monitoring 50 - 52 week old mice. For each of the time courses, the data has been analysed for statistical significance by integrating the area under the curve and plotting the mean ± S.E.M. for each of at least five mice of each genotype. Data has been shown for both males **(A)** VO_2, **(B)** VCO_2, **(C)** RER and females **(D)** VO_2, **(E)** VCO_2, **(F)** RER. All these data have then been analysed using the student's t-test and all showed a significant increase ($p<0.05$).

The RER and VO_2 values were used to calculate heat production as an overall readout of the liver-specific NUAK1 knockout animals burning more calories.

A

B
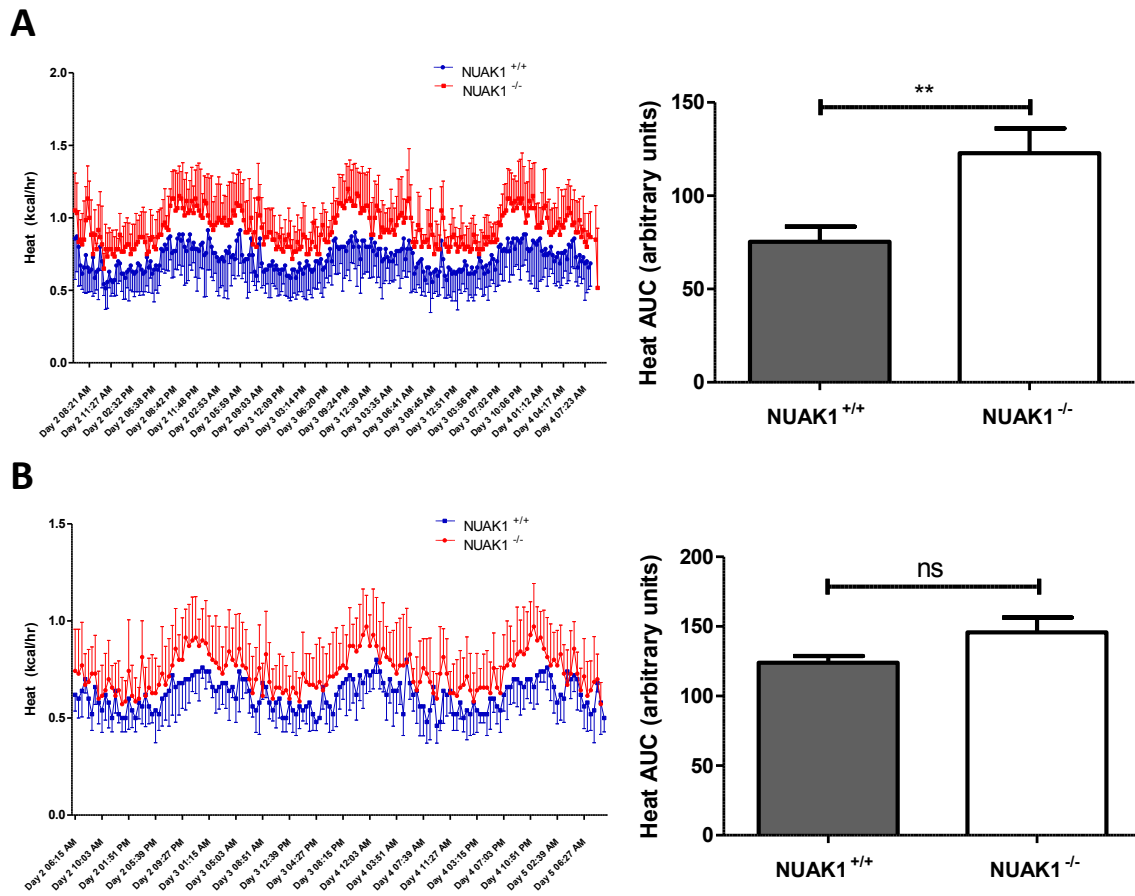
Figure 4.26 Aged liver-specific NUAK1 knockout mice burn more calories than wild-type mice

Heat production was calculated from RER and VO_2 measurements from $50 - 52$ week old mice. The time course data is shown alongside integrated area under the curve calculations for statistical comparison. Readings are shown for **(A)** Males and **(B)** Females. The data has been analysed for statistical significance by integrating the area under the curve and plotting the mean ± S.E.M. for each of at least five mice of each genotype. A significant increase ($p<0.01$) was observed for the males and a small but insignificant increase was observed for the females.

A significant increase was seen in respiratory exchange ratio in both male and female liver-specific NUAK1 knockout mice (Figure 4.25), suggesting a change in their energy source that they are burning more carbohydrate and less fat. Whether this is due to changes in the availability of fat because deposition in fat stores is reduced is unclear. The increase in heat

production also suggests that the liver-specific NUAK1 knockout mice are burning more calories overall, irrespective of the food source (Figure 4.26).

Food and water intake measurements were taken to establish if the knockout mice were eating more to provide the increase in carbohydrates being used for energy. The CLAMS system is able to monitor total food and water consumption and this has been normalised to the animal's body weight to control for any increase due to greater size. The data is plotted as a time course from the start of when the animals enter the CLAMS system, hence why there may be some disturbances in the early readings.

A

B

C

D
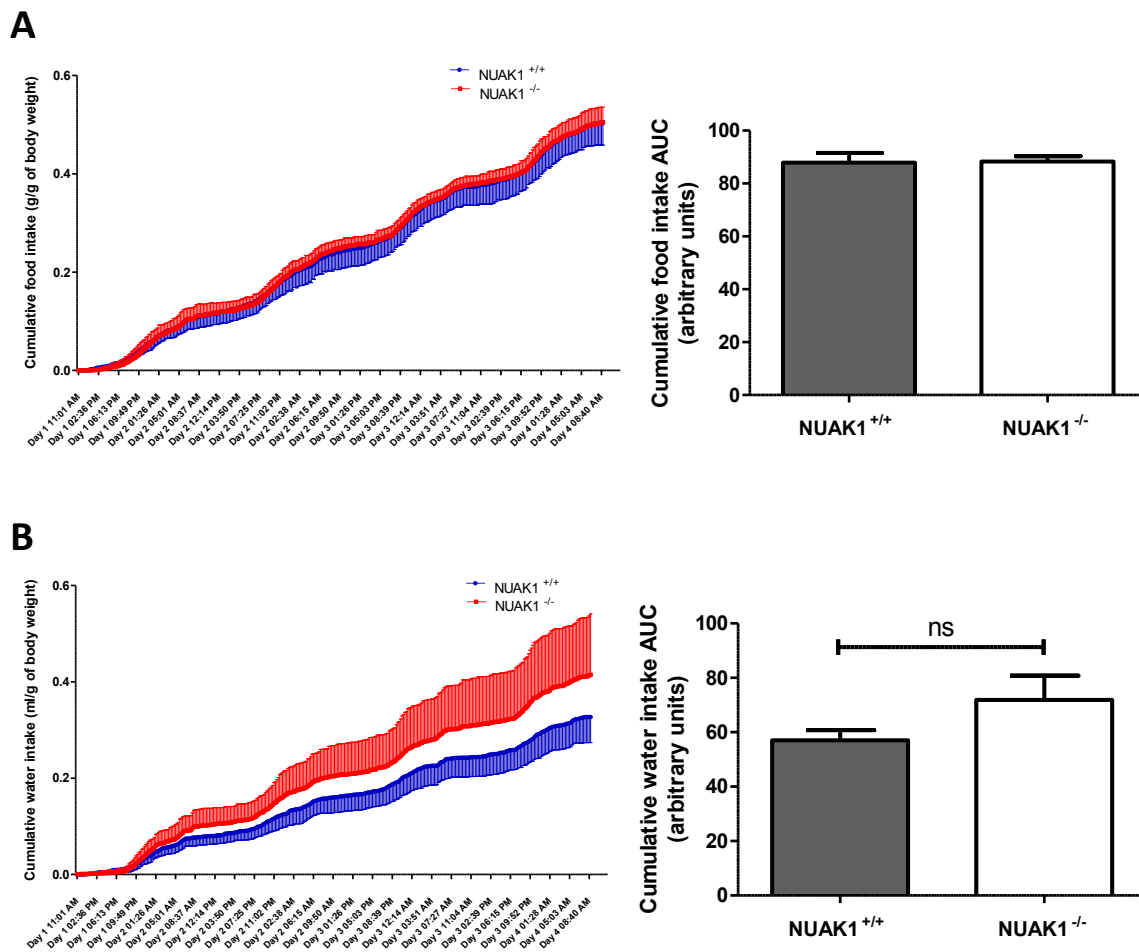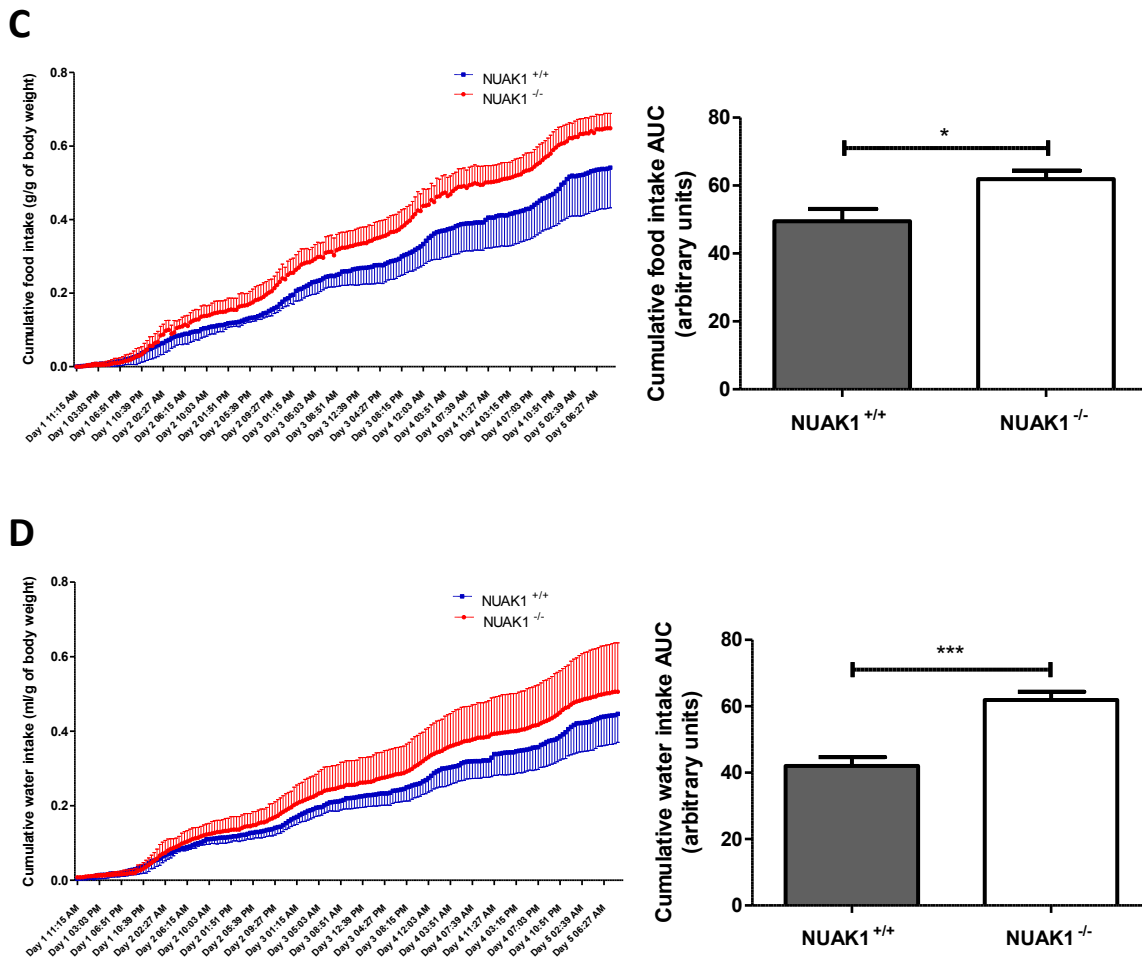
Figure 4.27 Aged liver-specific NUAK1 knockout mice have moderately increased food and water consumption

Food and water consumption plots from the CLAMS system monitoring 50 - 52 week old mice. Data has been shown for both aged males **(A)** Food **(B)** Water and aged females **(C)** Food **(D)** Water. The data has been analysed for statistical significance by integrating the area under the curve and plotting the mean ± S.E.M. for each of at least five mice of each genotype. A modest but not significant increase was observed in water consumption in the male mice. A significant increase ($p<0.05$) was observed in both food and water intake in the female mice.

These data show that the aged liver-specific NUAK1 mice appear to eat and drink slightly more than their wild-type littermates (Figure 4.27), which could account for the increased utilisation of carbohydrates as an energy source but does not entirely fit with the reduced body weight and fat mass measurements (Figure 4.22 and Figure 4.23). The mice appear to be eating more but not gaining weight, so therefore they must somehow be expending the extra energy accounted for in the heat calculations, such that it cannot be laid down in fat

deposits. The activity levels of aged mice were measured to see if the knockout mice were being more active, which would help explain their reduced body weight and body fat percentage.

A
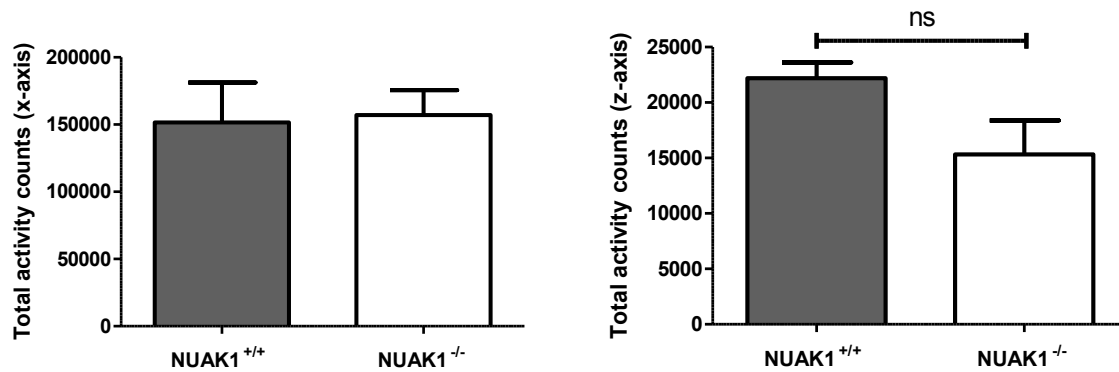
B
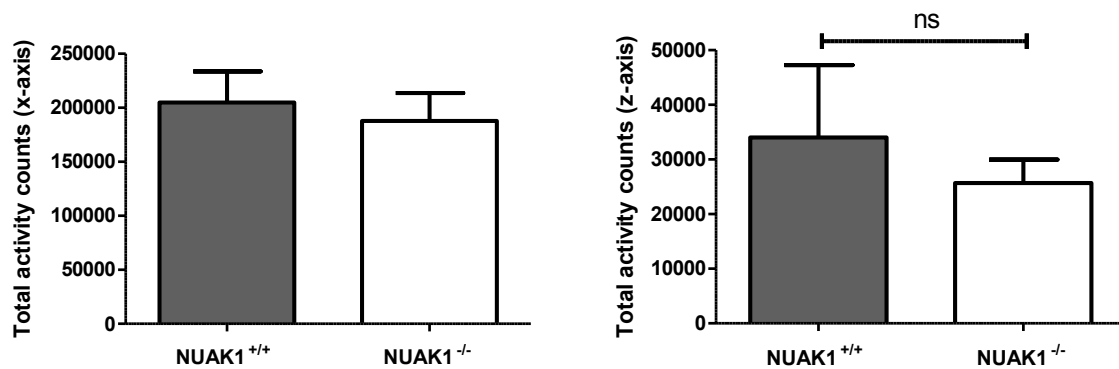
Figure 4.28 Aged liver-specific NUAK1 knockout mice have unchanged activity and movement levels

Movement measurements from the CLAMS system monitoring 50 - 52 week old mice. The cumulative movement in the x-axis and the z-axis were counted for at least five animals of each sex and genotype. The mean ± S.E.M. was plotted for **(A)** Males and **(B)** Females. All these data were analysed using the student's t-test and no significant differences ($p>0.05$) were observed.

Activity levels are unchanged in aged liver-specific NUAK1 knockout mice so burning the extra energy through movement cannot be the reason for their reduced body weight and fat

percentage (Figure 4.28). It is unclear if the reduced body weight and fat percentage confer any health advantage on the liver-specific NUAK1 knockout mice, as survival studies have not been conducted, but in human clinical studies of liver disease, increased body fat is an indicator of increased morbidity and mortality (Tolman and Dalpiaz, 2007). This may indicate that liver-specific NUAK1 knockout mice would be healthier in old age.

Collectively these data show that there is a definite variation in the adaptation of mice to age related changes in liver function depending on the expression of NUAK1. The biochemical basis for this change is unclear but the increase in proliferation of liver stem cells in response to damage may be the underlying reason. It may be that NUAK1 deletion does not directly change liver function but, through a mechanism regulating proliferation, the absence of NUAK1 enhances the ability of the liver to regenerate and maintain healthy bodily function.

4.3 Discussion

To date observations from only one tissue-specific NUAK1 knockout mouse model have been published (Inazuka et al., 2012). Given that the general aim of the field of AMPK and related-kinases is to understand the physiological function of these proteins *in vivo* and establish

potential mechanisms to activate or inhibit these pathways, it is important to understand the role of NUAK1 in different tissues of interest. The data gathered from different tissue-specific knockouts may indicate downstream targets that can be investigated in other experiments and can also provide evidence of physiological functions that may be of clinical interest.

Initial results confirmed the omphalocele phenotype previously reported in NUAK1 global deletion (Figure 4.3) (Hirano et al., 2006). Although no new information was gathered from the knockout embryos, the same lack of closure of the ventral body wall was observed. Lack of closure of the ventral body wall is possibly due to lack of cell outgrowths during development and this observation would fit with previous data suggesting NUAK1 knockout MEFs have fewer outgrowths and are more adherent (Zagorska et al., 2010). One interesting observation is that the ROCKI and ROCKII double knockout mice show the same omphalocele phenotype (Thumkeo et al., 2005). Given that ROCK is known to be an important regulator of MLC phosphorylation (Figure 1.12) (Matsumura, 2005), this provides an interesting link that NUAK1 and ROCK pathways may converge on the same downstream activator that causes the closure of the ventral body wall and potentially other MLC linked functions. It would be interesting to assess if NUAK1 deletion has an impact on the expression or phosphorylation of known members of the ROCK pathway.

Data of tissue distribution of NUAK1 shown in this thesis (Figure 4.6) partially agrees with a previous report that found NUAK1 expressed in heart, kidney, brain, liver, and skeletal muscle (Fisher et al., 2005). This indicates that the antibody used in my experiments is comparable to reagents used in previous studies. From previous reports, changes in NUAK1 expression were primarily involved in mediating cell proliferation phenotypes in cancer (Chang et al., 2012; Chen et al., 2013a; Kusakai et al., 2004a; Lu et al., 2013). The only other indication of a potential phenotype from deleting NUAK1 was the liver-specific knockout of the upstream kinase LKB1, which causes serious metabolic defects (Shaw et al., 2005; Woods et al., 2011).

Initial investigation of a phenotype in the liver-specific NUAK1 knockout mice found there was no obvious whole-body phenotype (Figure 4.9). The slight increase in male knockout mice

heart weight could be the consequence of the small number of animals used for the study or it could be representative of a secondary phenotype as a result of NUAK1 deletion in the liver. There are various examples of liver pathology that can have a secondary effect in the heart and several whole-body changes that can affect both tissues (Naschitz et al., 2000). However, without a further indication of a potential mechanism for this increase in heart size it is difficult to speculate how NUAK1 deletion would cause this. Also, in light of the subsequent observations of a minimal phenotype in young, healthy liver-specific NUAK1 knockout mice it is unlikely that there would be a significant secondary phenotype in the heart. Previous reports have shown in mouse models that inhibition of the Hippo pathway can produce grossly oversized organs (Dong et al., 2007). Evidence shown here would suggest that deletion of NUAK1 does not activate LATS1 or inhibit YAP/TAZ (Figure 1.10) sufficiently to produce a reduction in organ size by modulating the Hippo pathway (Figure 4.10). This is consistent with other indications that the Hippo pathway can define an upper limit for organ size but upregulation of the pathway to inhibit YAP/TAZ would not produce smaller organs (Pan, 2010).

Body composition analysis indicated there were no variations in fat mass or lean mass, indicating that there was unlikely to be a basal metabolic phenotype (Figure 4.10). This may suggest that NUAK1 has no relevant function in mature, differentiated tissues. However, as *in vitro* data and published reports link NUAK1 to regulation of myosin phosphorylation (Zagorska et al., 2010) or senescence regulation (Humbert et al., 2010), these effects may not produce a major phenotype in a young, healthy liver.

The LKB1 liver-specific knockout phenotype is caused by changes in hepatocyte polarity and it was thought that there may be a partial recapitulation of this in NUAK1 deleted livers (Fu et al., 2011; Woods et al., 2011). It is possible that a partial phenotype could be compensated for by other mechanisms in the liver and this would mask any obvious whole-body phenotypes. However, after histological analysis of NUAK1 deleted livers, there were no detectable structural changes compared to wild-type mice (Figure 4.11). No differences were observed in hypertrophy or hyperplasia, indicating that NUAK1 deletion in hepatocytes does not have the same effect of increasing proliferation that was seen in NUAK1 deleted MEFs

(Figure 3.15). This could be due to a number of factors, including possible activation of the Hippo pathway by other mechanisms, which would limit organ size.

After several attempts to establish the presence of a phenotype in the NUAK1 null livers, serum metabolites were analysed for any changes in indicators of liver function. By measuring these metabolites it is possible to get a more sensitive readout of liver function that may not be manifested as a whole-body phenotype. After analysis of several clinically indicative serum metabolites it is clear that NUAK1 liver-specific knockout mice are functionally normal and healthy (Figure 4.12).

All these data indicate that normal liver function was maintained after the deletion of NUAK1, however these observations could mask an underlying change in liver metabolism that is only manifested under conditions of stress. The mice are maintained in tightly controlled environmental conditions and fed on a nutrient rich diet, meaning that they are unlikely to undergo any major metabolic stress during their development. Also, minor metabolic insults may be resolved by redundant pathways such that differences would be masked. By isolating hepatocytes from NUAK1 null livers it is possible to manipulate their metabolic function and determine if there are underlying changes. However, even when the hepatocytes are subjected to a series of mitochondrial stresses, the NUAK1 null cells show no difference in comparison to wild-type cells (Figure 4.13 and Figure 4.14). Hepatic glucose output was significantly increased in LKB1 knockout hepatocytes (Woods et al., 2011), but this was not observed in NUAK deleted livers, suggesting NUAK1 is not an essential downstream target regulating this mechanism.

Although liver function appeared to be maintained in young liver-specific NUAK1 knockout mice, there was potential for a peripheral metabolic phenotype if processes such as insulin signalling were affected. However, no difference was seen in glucose tolerance tests comparing wild-type and liver-specific NUAK1 knockout mice (Figure 4.15). By all overt phenotyping parameters, there appeared to be no functional difference as a result of deleting

NUAK1 in the liver, but to confirm this the CLAMS system was used to measure various metabolic and behavioural parameters to ensure no subtle phenotype was overlooked.

After extensive attempts to phenotype a large number of animals of both sexes, none of the data showed any significant difference across any of the parameters (Figure 4.16 - Figure 4.19). Collectively the CLAMS data shows that deletion of NUAK1 in the liver does not affect the animal's metabolism, eating behaviour or activity levels. Although this is frustrating that there was no manifest phenotype in the young mice, it highlights some of the difficulties of phenotyping animal models with targeted gene deletions. From these data it is highly unlikely that NUAK1 is involved in mediating any of the effects of LKB1 deletion in the liver, adding further credence to the hypothesis that NUAK1 may not be entirely dependent on LKB1 phosphorylation to be active. It also demonstrates how genes that may have a highly significant developmental function, in this case aiding closure of the ventral body wall and maintaining embryo viability, may only have mild or subtle effects in adult tissues.

These data are also comparable to the previous study reporting the effects of NUAK1 deletion in muscle where no basal phenotype was observed (Inazuka et al., 2012). This study did see a significant phenotype when placing the animals on a high fat diet, indicating that the deletion of NUAK1 in adult tissues may only have an effect under stressed conditions. The muscle-specific NUAK1 phenotype in that report was attributed to reduced phosphorylation of IRS1, potentially by NUAK1. However, current data in the literature and *in vitro* findings in my study (Figure 3.18) do not suggest that NUAK1 has any involvement with phosphorylating components of the insulin signalling pathway. Data from this study and others, including the muscle-specific NUAK1 deletion, suggest that NUAK1 primarily targets cytoskeletal components. The current model for how changes in the phosphorylation of cytoskeletal proteins may affect disparate mechanisms such as glucose metabolism is poorly understood. However, it is highly possible that NUAK1 elicits its effects by modulation of cytoskeletal components which then cause secondary phenotypes in other pathways. This may also explain why minimal phenotypes are seen under basal conditions, as cytoskeletal organisation has many redundant mechanisms and minor changes in one component may be compensated for, which may not be possible in pathways such as insulin signalling.

Based on the need for a stress treatment to elicit a phenotype in NUAK1 muscle-specific knockout mice, a similar experiment was conducted in liver knockout mice. The CDE diet was used to induce liver damage. Ethionine addition to rodent diets has been used for decades as a way to induce wide spread damage in many digestive and metabolic tissues (Koch Weser and Popper, 1952). Ethionine acts as a methionine antagonist so interferes with protein transcription and recent studies have modified a choline deficient diet to produce more targeted liver damage, without such severe fat accumulation or necrosis (Akhurst et al., 2001). During the course of the CDE diet feeding, body weights were monitored and showed that the pathology was no more severe in liver-specific NUAK1 mice than wild-type mice (data not shown). Given that there may have been a difference in the NUAK1 null livers ability to respond to the induced damage, metabolite measurements were made as before and no difference was seen, suggesting the change in liver function caused by the diet is similar (Figure 4.20). On harvesting tissues, the apparent level of fat accumulation and weight of the livers were also equivalent across both groups (data not shown).

After CDE diet feeding data suggested there was no significant difference in the change in liver function, but as several studies have previously shown, liver damage diets can be used to induce proliferation of hepatic progenitor cells (oval cells in mice). These cells have been shown to be important in liver regeneration and possibly in the early progression of hepatocellular carcinoma (Boulter et al., 2012; Lee et al., 2006). After analysis of treated livers it was clear that NUAK1 null livers had a much greater proliferation of oval cells (Figure 4.21). The exact mechanisms involved in producing a proliferation response in oval cells is unclear but some research suggests there are cell-cell interactions and cell-matrix interactions within stereotypical niches that produce extra cellular signals, prompting an increase in proliferation (Lorenzini et al., 2010). Whether NUAK1 is part of a network involved in receiving these signals or if it influences the proliferation through a different intrinsic network is unclear. It is possible that NUAK1 exerts this effect through the Hippo pathway as the progenitor cells are more similar to cells during development than senescent adult cells.

Interestingly, this increased proliferation may have two effects. Firstly, if controlled by normal mechanisms it could improve the repair of normal tissues, however there are some indications that increased progenitor cell proliferation can lead to uncontrolled growth and cancer (Lee et al., 2006). If this greater proliferation does contribute to an increased risk of cancer in a NUAK1 deleted model, this also contradicts previous reports of higher NUAK1 expression being associated with cancer progression (Bell et al., 2013; Chen et al., 2013a; Cui et al., 2013; Kusakai et al., 2004a).

After observing a different response in NUAK1 null livers to an acute damage insult, there was potential for a differential response to chronic damage as part of the normal ageing process. Although the aged mice only became available for analysis towards the end of this project, various phenotype measurements indicate that the deletion of NUAK1 does affect the response to ageing.

Firstly, body composition showed that aged NUAK1 null mice were slightly leaner and had a lower overall body fat percentage (Figure 4.22). Although this analysis was not significant, it showed a clear trend and with greater numbers would be likely to show significance. Interestingly, the overall body fat percentage was lower and also the size of an individual fat pad was lower (Figure 4.23), suggesting that the effect may be systemic rather than targeted to an individual tissue or organ. Importantly, liver function was maintained in aged mice after NUAK1 deletion (Figure 4.24), suggesting that the changes in body morphology are not due to dysfunction of the liver.

On assessing the indirect calorimetry measurements from the CLAMS system, the most striking difference was an increase in the respiratory exchange ratio, consistent across both male and female mice (Figure 4.25). The respiratory exchange ratio is a measure of the energy source, with a lower value indicating a higher fat diet and a higher value indicating more carbohydrates are being burned. As all the mice were being fed on identical chow diets, changes in the RER must be due to metabolic differences. Interestingly, a similar study of a transgenic rat model, using identical indirect calorimetry measurements saw an increase in

respiratory exchange ratio (Harasym et al., 2013). This transgenic model was the BHE/cdb rat which has a global loss-of-function mutation in the ATP synthase α-subunit. This study appears to have many other parallels with the observations in aged NUAK1 liver-specific knockout mice. Firstly the rats are leaner and lighter, showing a similar body morphology to the NUAK1 liver knockout mice (Figure 4.22). Crucially there is also no change in circulating lipid levels, suggesting lipid metabolism is unchanged (Figure 4.24) (Harasym et al., 2013). Lastly, both my study and the BHE/cdb rat study observed an increase in food consumption during the CLAMS analysis (Figure 4.27).

Initially, the hypothesis for the phenotype observed in the BHE/cdb rat was that decreased ATP levels would raise the AMP:ATP and ADP:ATP ratios and activate AMPK. Increased AMPK activity would then activate catabolic pathways such as glucose uptake, through GLUT4 signalling, and lipid oxidation, while inhibiting gluconeogenesis (Harasym et al., 2013). However, no increase in AMPK phosphorylation or activation of downstream targets was observed. One explanation that was proposed by Harasym and colleagues was that due to the lack of function of ATP synthase, the cell fails to produce sufficient ATP and to compensate for this the animal increases metabolic flux of carbohydrates, which would account for the increased RER and heat production. Presumably the increased water consumption observed in my study (Figure 4.27) parallels the increase in food consumption to ensure the mice receive adequate hydration.

Several other interesting facets of the biochemical analysis from the BHE/cdb rat study also parallel some findings in relation to NUAK1. Firstly, they observed an increase in expression of mitochondrial proteins such as Cox4, similar to the observed increase in my study of Cox6b expression in NUAK1 null MEFs (Figure 3.16). Also, they saw a downregulation of Akt signalling in liver and soleus muscle, which would be consistent with Akt acting as an upstream kinase of NUAK1 (Suzuki et al., 2004b). However, some *in vitro* data from my study questions this finding (Figure 3.7), so this would require more work to establish if this is a real interaction.

Another encouraging finding that may provide a functional link between the phenotype seen in the BHE/cdb rat and the liver-specific NUAK1 knockout mouse is the fact that several ATP synthase subunits were seen to be differentially phosphorylated in the MEF SILAC experiment (Appendix 2.1). It is possible that NUAK1 could influence the activity of the ATP synthase complex, either directly or indirectly to produce a similar phenotype to the loss-of-function mutation seen in the BHE/cdb rats. A marginal reduction in ATP synthesis would then produce longer term functional changes which could influence whole-body morphology, as seen in the rat model. More work is required to establish if this interaction is real and if NUAK1 can regulate ATP synthase in this way. Also, de-convoluting the primary and secondary phenotypes of this effect would be challenging and require much more *in vitro* confirmation of potential interactions.

Interestingly in the BHE/cdb rat study they also saw improved glucose tolerance so it would be useful to perform glucose tolerance tests in the aged NUAK1 liver-specific knockout mice to test if this improved in line with the other phenotypic similarities seen between the two models. Similarly, the BHE/cdb rat study also saw an upregulation of pyruvate dehydrogenase, so conducting a pyruvate tolerance test would be interesting to establish if this phenotype was similar after NUAK1 deletion. Encouragingly, the ATP-synthase mutated rat study found relatively small changes in muscle insulin signalling, suggesting that the liver is a more important organ than skeletal muscle in modulating the changes in glucose homeostasis (Harasym et al., 2013).

In conclusion, the exact mechanisms regulating the embryonic omphalocele phenotype are unclear but as discussed in section 3.3 there are potentially two divergent mechanisms that NUAK1 could be regulating. Firstly, NUAK1 could be pro-proliferative under developmental conditions by downregulating LATS1 and activating YAP/TAZ as part of the Hippo pathway (Figure 1.10), causing an increase in cell growth and closure of the ventral body wall, potentially explaining the omphalocele phenotype in NUAK1 deleted embryos. However, in differentiated mature tissues, it could be anti-proliferative by downregulating LATS1 and maintaining senescence, thereby reducing the turnover and replacement of cells such as hepatocytes (Humbert et al., 2010). This anti-proliferative effect may also contribute to the

phenotypes observed in liver-specific NUAK1 knockout mice during the normal ageing process, such as reduced fat accumulation. Similarly, during injury or damage, when the stem cells are already up regulated and the organ partially returns to a "developmental" state, the pro-proliferative mechanism could influence an increased response, leading to better repair of damaged tissue but also more possible risk of cancer.

The results from this liver-specific knockout model show that proteins can still have an important physiological function despite there being only a very low level of expression in the tissue of interest (Figure 4.6). This highlights the difficulty of choosing tissues for targeted gene deletion studies and indicates that crucial steps of signalling pathways may be regulated by relatively lowly expressed proteins. Overall the data presented in this chapter provide some interesting insights into the *in vivo* role of NUAK1 and to date represents only the second study of NUAK1 in a tissue-specific knockout model. Although the mice appeared not to have a basal phenotype, there was a significant difference in the response of NUAK1 null livers to damage and ageing. These results may provide useful indications of the processes which NUAK1 is involved in and similarities to other transgenic animal models may provide new avenues for research.

5 Generation and characterisation of heart-specific NUAK1 knockout mice

5.1 Introduction

During the course of this project data was published showing the first reported effect of a NUAK1 tissue-specific knockout (Inazuka et al., 2012). On a high fat diet, skeletal muscle-specific NUAK1 knockout mice had a lower fasting blood glucose level, improved glucose tolerance, higher insulin sensitivity and a higher concentration of muscle glycogen than wild-type mice. This publication and preliminary data from the liver-specific knockout model led to an interest in the possible effect of deleting NUAK1 in cardiac muscle. Given the absence of a significant phenotype in young liver-specific NUAK1 knockout mice a decision was made midway through my project to create another tissue-specific knockout which may produce a significant phenotype. Western blot and quantitative PCR data previously shown confirms that there is significant expression of NUAK1 in heart tissue (Figure 4.6).

To produce heart-specific NUAK1 knockout mice, animals carrying the "floxed" NUAK1 construct (Figure 4.1) were crossed with mice carrying cre recombinase under the control of the α-myosin heavy chain (αMHC) (a gift of Prof. Michael Schneider, National Heart and Lung Institute).

There were communications from the Schneider group and published data to suggest that some αMHC cre mouse lines develop a mild cardiac hypertrophy phenotype in mice that are homozygous for the cre alone after 8 – 10 weeks of age (Buerger et al., 2006). This report indicates that the phenotype was not observed in transgenic lines with lower expression of cre recombinase, suggesting a dose-dependent or threshold of cre expression necessary for the phenotype. For this reason I decided to use mice younger than 10 weeks and both cre-positive and cre-negative controls were used to eliminate any possible effects of the cre-expression alone.

In this chapter the phenotyping data is presented for the heart-specific NUAK1 knockout mouse and a stress treatment is used to assess the effect of the absence of NUAK1 on damage response in a different tissue than the liver.

5.2 Results

5.2.1 Heart-specific NUAK1 knockout mice

DNA was extracted from an ear biopsy taken from mice at weaning age. To establish the homozygosity of the NUAK1 floxed construct, primers were designed against exon 2 of NUAK1 and an exonic region outside the 5' loxP site. Mice carrying cre recombinase under the control of the α-myosin heavy chain promoter (αMHC) were crossed with homozygous floxed NUAK1 mice to obtain mice with NUAK1 specifically deleted in the heart.

A

B
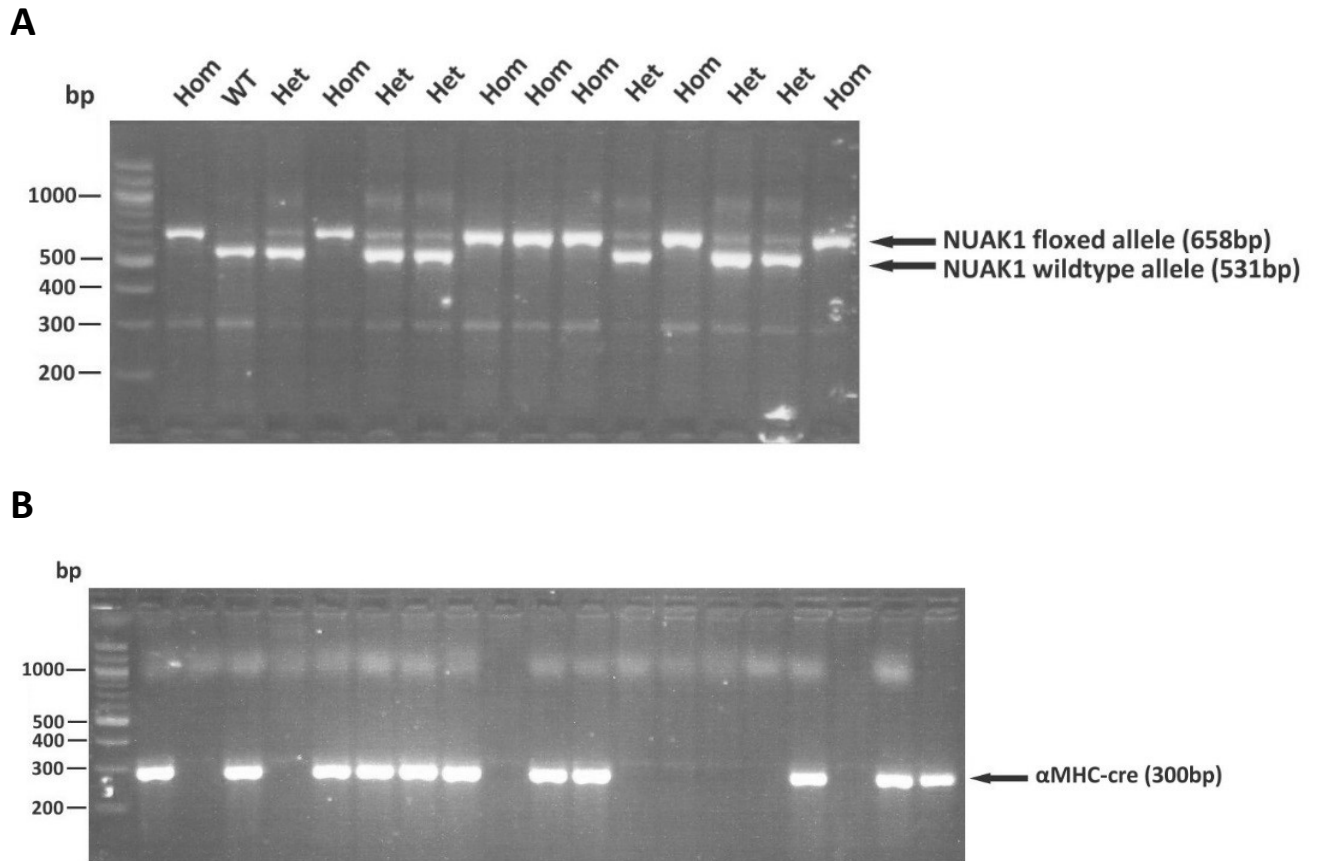
Figure 5.1 Breeding and genotyping of heart-specific NUAK1 knockout

(A) Mice that were homozygous for the floxed NUAK1 construct (Figure 4.1) were confirmed by PCR genotyping. Wild-type mice are characterised by a single smaller band (531bp), heterozygous mice are shown by two bands (531bp and 658bp) and homozygous floxed mice are shown by a single larger band (658bp). **(B)** The presence of αMHC cre recombinase was confirmed by a PCR reaction across an exonic region of the cre which amplified a 300bp band.

The αMHC cre genotyping method amplifies a band from an exonic region of the recombinase gene meaning there is no amplification in wild-type animals and no way to distinguish mice that are heterozygous or homozygous for the cre. As the level of cre expression may affect the phenotype, efforts were made to ensure only heterozygous cre mice were used for breeding, however it was impossible to confirm this by PCR genotyping.

Once the recombination event had been confirmed by PCR genotyping (Figure 5.1), the deletion of the gene was confirmed by western blotting and quantitative PCR.

A
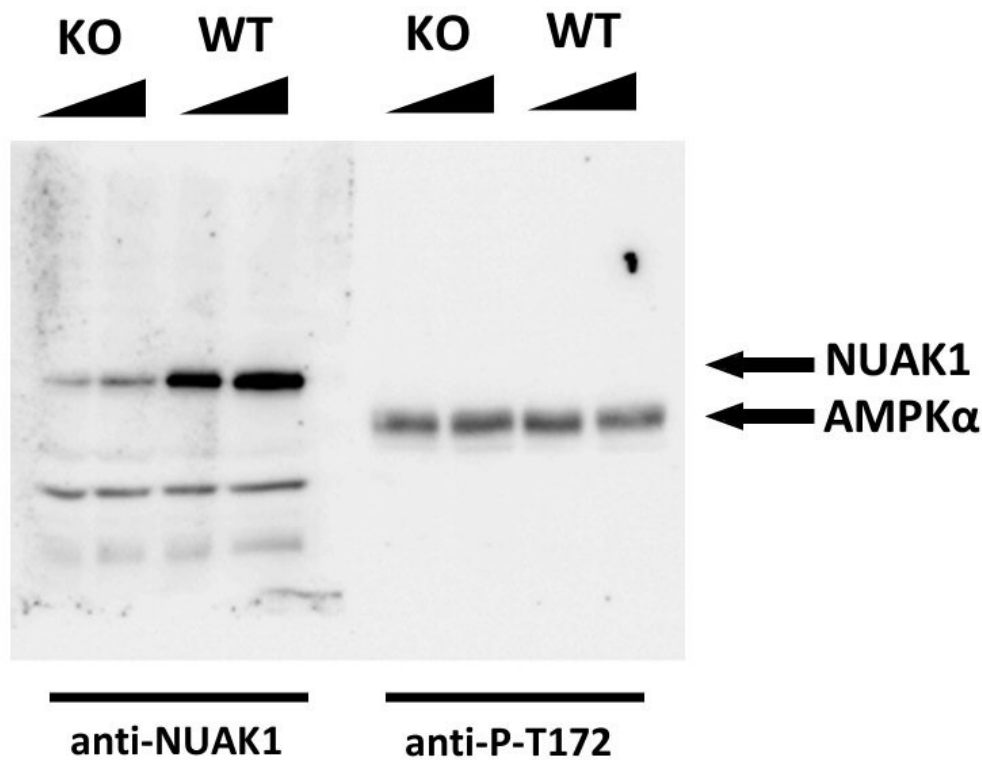
B
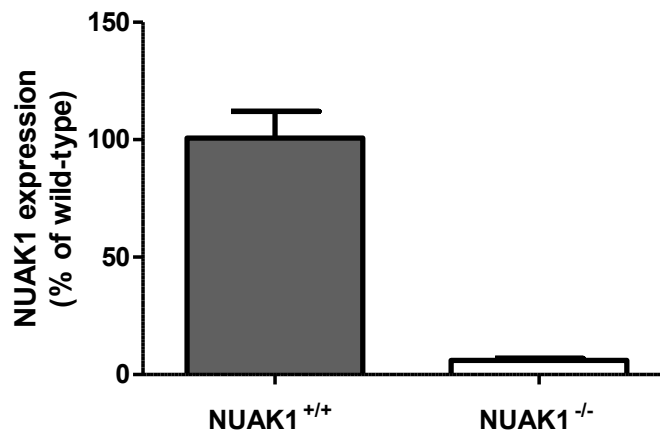
Figure 5.2 Confirmation of NUAK1 deletion in heart tissue by western blot and quantitative PCR analyses

(A) Total tissue lysate from heart-specific NUAK1 knockout and wild-type mice was resolved on a 10% SDS-PAGE Tris-Glycine gel and transferred to PVDF membrane for immunodetection. The membrane was incubated with anti-NUAK1 and anti-AMPK phospho T172 antibodies. **(B)** mRNA purified from whole hearts from wild-type and heart-specific NUAK1 knockout mice was converted to cDNA and used to determine the expression of NUAK1. The values are shown as a fold change against the wild-type value. qPCR values are normalised to GAPDH.

Deletion of the gene was confirmed by western blot and qPCR (Figure 5.2). A small amount of residual protein can be observed in the knockout animals as the αMHC-cre only deletes the specified gene in the cardiac myocytes but the total lysate will contain protein from endothelial tissue, cardiac fibroblasts and other cells still expressing NUAK1. The lack of phospho-T172 staining on the band corresponding to NUAK1 may indicate that there is little activity or is more likely to be a sensitivity issue when being compared alongside AMPK. The phospho-T172 staining of pAMPKα1 in Figure 5.2A acts as a positive control for the antibody and indicates that the activity of AMPK is unchanged in the NUAK1 knockout hearts. Also, the cardiac myocyte-specific expression of the αMHC cre strain is well characterized (Gulick and Robbins, 2009) so there is minimal chance of any off-target deletion of NUAK1, however no appropriate analyses were carried out to confirm this.

Given that the correct recombination events had been confirmed by PCR genotyping, it was possible to start assessing if there was a basal phenotype as a result of the loss of NUAK1. Initially basic body and organ weight measurements were taken to assess any potential gross morphological changes.

A

B

C

D
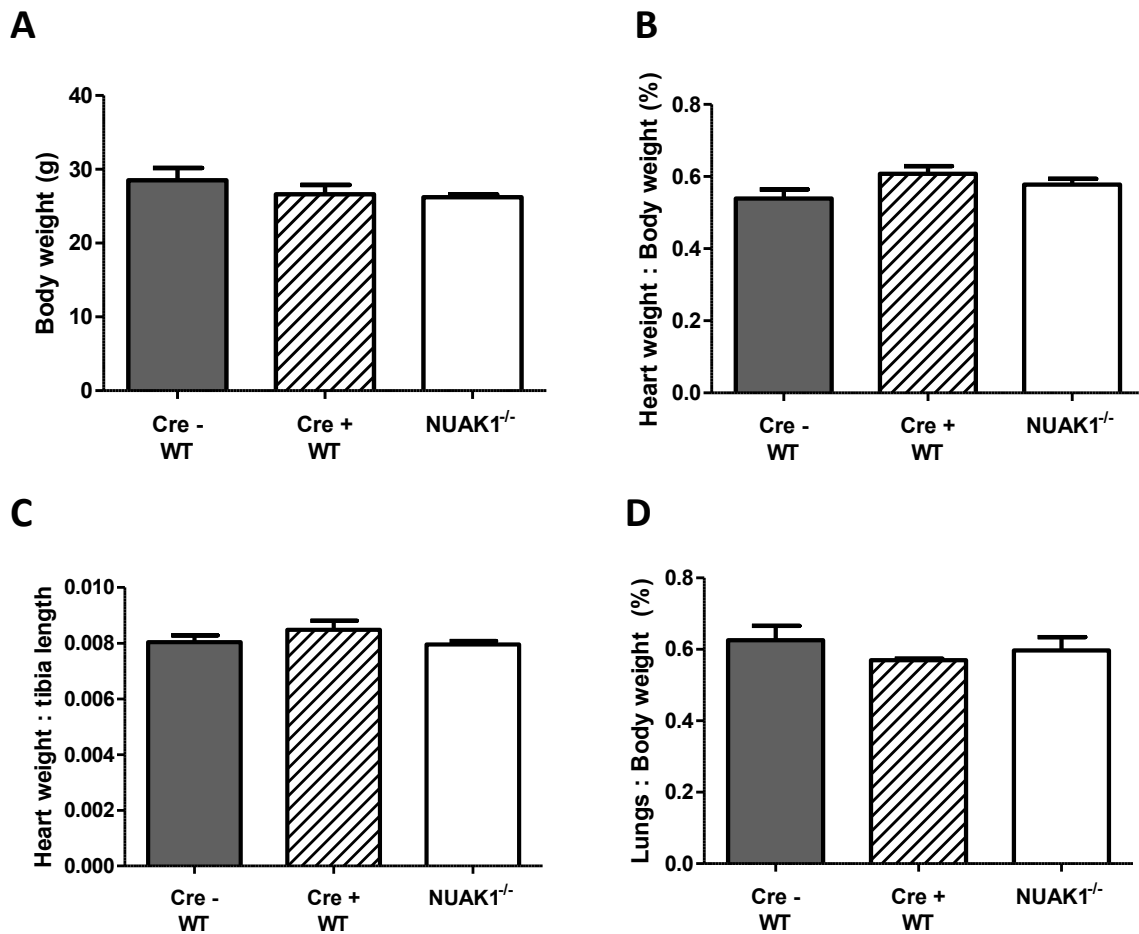
Figure 5.3 Heart-specific NUAK1 knockout mice have no gross morphological changes under basal conditions

Body measurements and organ weights were taken from 7 – 8 week old heart-specific NUAK1 knockout mice, αMHC cre positive and negative control animals. Data is shown for **(A)** Body weight, **(B)** Heart weight normalised to body weight, **(C)** Heart weight normalised to tibia length and **(D)** Lung weight normalised to body weight. In all measurements no significant difference ($p > 0.05$) was observed between cre negative controls, cre positive controls and knockouts when analysed using a one-way ANOVA and Bonferroni correction. Plots are all mean ± S.E.M. of measurements from at least 6 mice of each genotype.

Clearly there is no change in body weight or heart size under basal conditions as a result of NUAK1 deletion (Figure 5.3). Studies have also shown there can be an increase in lung weight in models of chronic heart failure (Kingsbury et al., 2003) so lung weight was measured (and normalised to body weight) to ensure there were no secondary morphological changes as a result of the NUAK1 knockout. No change in lung weight was observed in heart-specific NUAK1 knockout animals.

5.2.2 Echocardiography of heart-specific NUAK1 knockout mice

Many parameters can be measured to assess heart function but factors such as blood pressure and heart rate are difficult to measure over a time course without use of telemetry equipment which requires challenging and risky surgery to implant into the mice. Individual time points can be taken without the need for telemetry but the measurements are generally taken under anaesthetic which affects the heart rate and blood pressure substantially. Also it is more likely that deletion of NUAK1 would affect the structure and morphology of the heart rather than the heart rate because data from my study and previous reports suggest that NUAK1 may elicit its effect by regulating pathways involved in cell proliferation.

In order to further investigate any possible phenotype resulting from the knockout of NUAK1 in cardiac muscle, echocardiography was conducted by a trained, genotype-blinded operator. Echocardiography is a useful tool for measuring various parameters of heart size, muscle thickness and cardiac output. The parameters measured provide the most efficient way of detecting any changes in heart structure. It is possible to detect subtle changes in heart function and, where possible, link these changes to morphological variations.
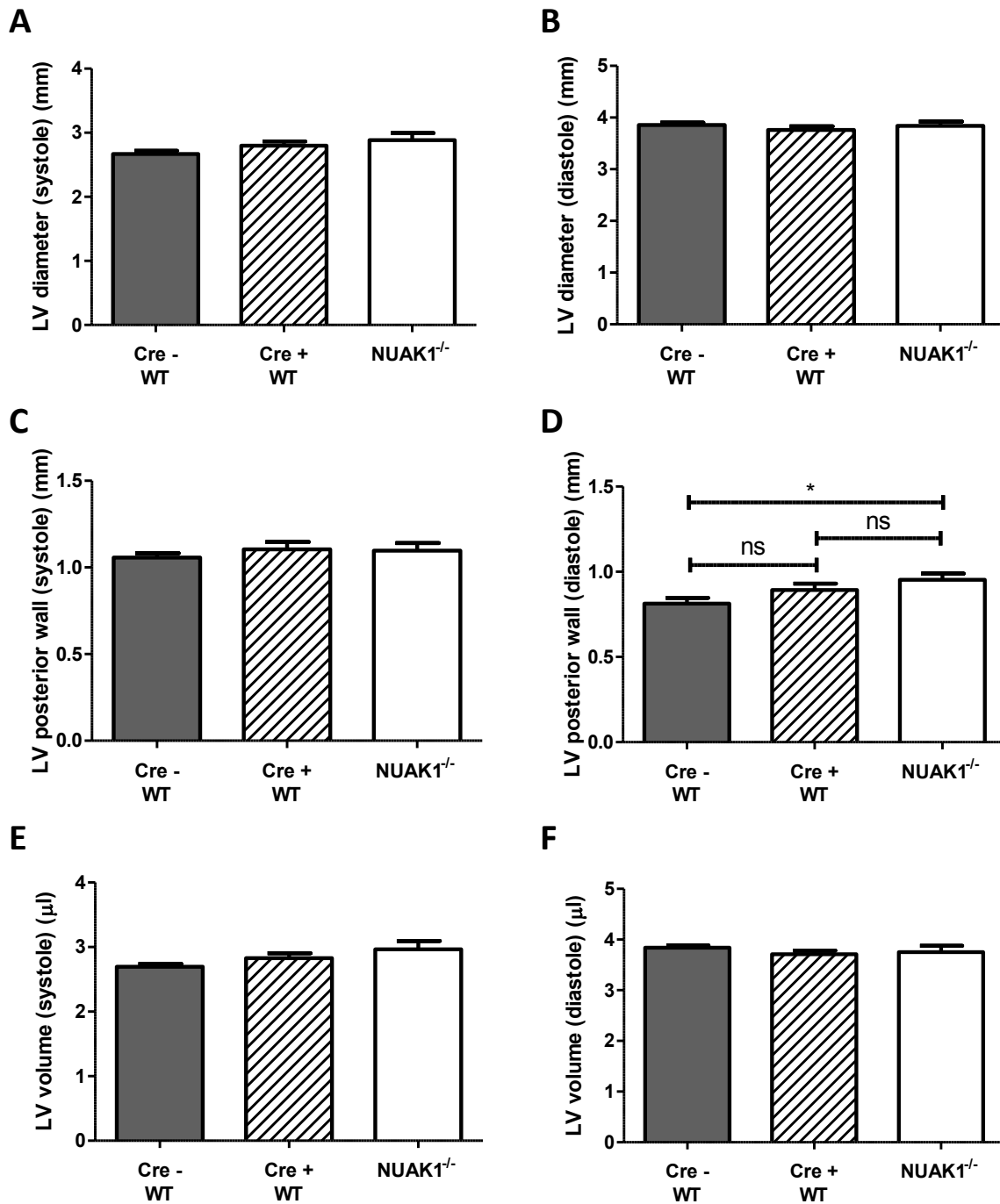
Figure 5.4 Heart-specific NUAK1 knockout mice have no change in left ventricle size, posterior wall thickness and volume

Echocardiography data from 10 – 12 week old heart-specific NUAK1 knockout mice and wild-type littermates. Plots are shown of left ventricle diameter during **(A)** systole and **(B)** diastole. Left ventricular posterior wall thickness during **(C)** systole and **(D)** diastole. Left ventricular volume during **(E)** systole and **(F)** diastole. The significance indicated on the charts represents (* = $p < 0.05$) when analysed using a one-way ANOVA and Bonferroni correction. Plots are all mean ± S.E.M. of repeat measurements from at least 6 mice of each genotype.

Initial measurements of left ventricle wall thickness and volume showed no difference between wild-type and heart-specific NUAK1 knockout mice. The only parameter that showed any difference was left ventricle posterior wall thickness (Figure 5.4). Heart specific NUAK1 knockout mice have slightly thicker left ventricle posterior wall compared to cre negative controls. However there is no difference between cre positive and knockout animals, suggesting this variation is largely an effect of the cre expression.

A

B
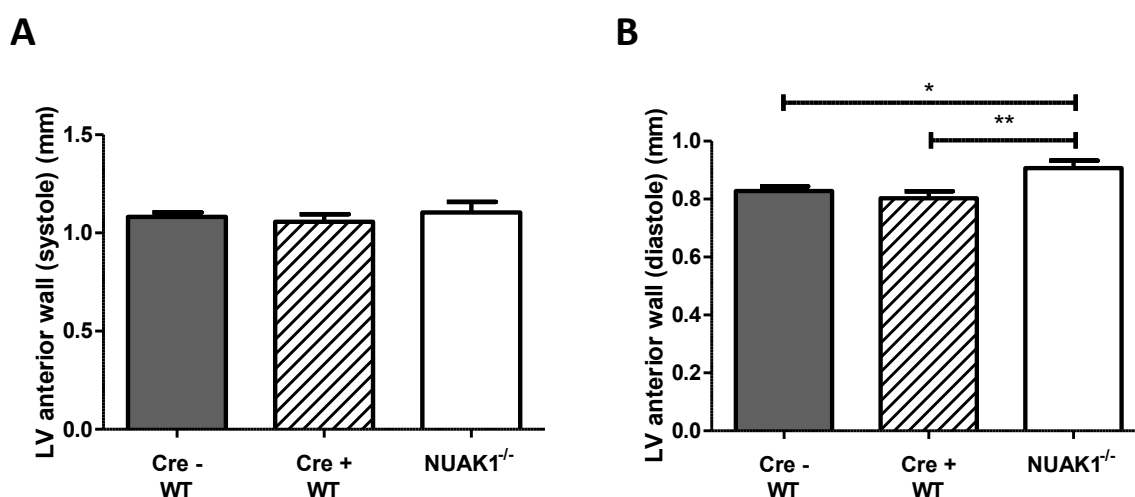
Figure 5.5 Heart-specific NUAK1 knockout mice have increased left ventricular anterior wall thickness during diastole

Echocardiography data from 10 – 12 week old heart-specific NUAK1 knockout mice and wild-type littermates. Plots are shown of left ventricular anterior wall thickness during **(A)** systole and **(B)** diastole. The significance indicated on the charts represents (* = $p<0.05$, ** = $p<0.01$) when analysed using a one-way ANOVA and Bonferroni correction. Plots are all mean ± S.E.M. of repeat measurements from at least 6 mice of each genotype.

Other measurements also show parameters where a difference is seen between knockout animals and cre negative or cre positive mice, suggesting the variation is due to deletion of NUAK1 (Figure 5.5). A significant increase in thickness of the left ventricular anterior wall was measured in knockout animals but only during diastole. Changes in diastolic function may not manifest any phenotype under basal conditions provided the systolic function is maintained. It is likely that systolic function is maintained as the mice appear to have no adverse global phenotype. However, more severe differences in cardiac function may be observed with the influence of an insult aimed at stressing the heart.
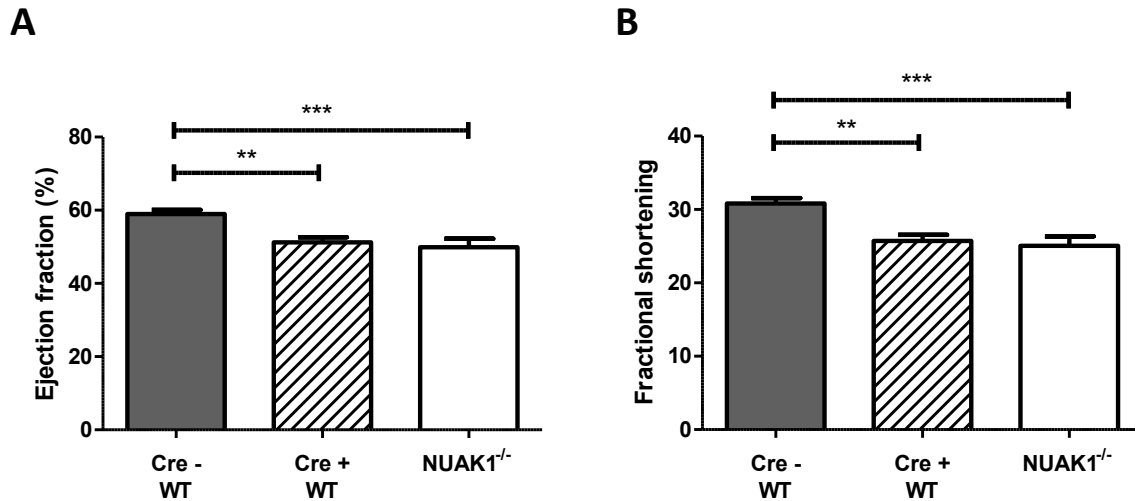
Figure 5.6 αMHC cre mice have a cardiac phenotype independent of NUAK1 knockout

Echocardiography data from 10 – 12 week old heart-specific NUAK1 knockout mice and wild-type littermates. Plots are shown of **(A)** ejection fraction and **(B)** fractional shortening. The significance indicated on the charts represents (** = $p<0.01$, *** = $p<0.001$) when analysed using a one-way ANOVA and Bonferroni correction. Plots are all mean ± S.E.M. of repeat measurements from at least 6 mice of each genotype.

Reports of cardiac dysfunction from the group that provided the αMHC cre mice were confirmed when it was discovered that there were some parameters that varied in cre positive mice, irrespective of whether NUAK1 was deleted. The ejection fraction, which represents the fraction of blood pumped out of the left ventricle during each cardiac cycle, was reduced, indicating that the expression of the cre reduces cardiac function. Fractional shortening, which is a measure of the proportion of the diastolic dimensions that are lost during systole, was also reduced in heart-specific NUAK1 knockout mice. A more significant difference ($p<0.001$ rather than $p<0.01$) was observed between the cre negative controls and the knockouts compared to the cre-positive controls however no significant difference ($p>0.05$) was observed between the cre positive controls, and the heart-specific NUAK1 knockouts, suggesting the phenotype was due to the presence of the αMHC cre (Figure 5.6).

Although all these parameters indicate how the structure of the heart is affected, one of the best overall readouts of cardiac function is the total cardiac output, which takes into account left ventricle size and ejection fraction.
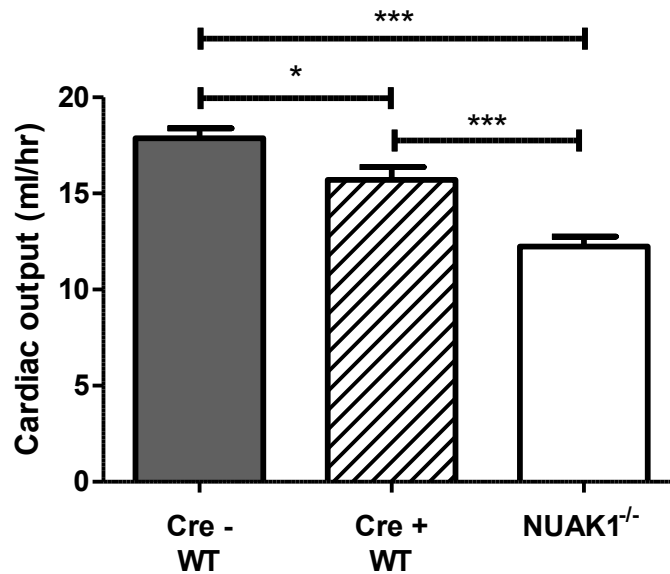
Figure 5.7 Heart-specific NUAK1 knockout mice have decreased cardiac output under basal conditions

Cardiac output data from 10 – 12 week old heart-specific NUAK1 knockout mice and wild-type littermates. A significant difference ($p<0.001$) was observed in cardiac output in heart-specific NUAK1 knockouts when compared to both cre-positive and cre-negative controls. The plot is mean ± S.E.M. of repeat measurements from at least 6 mice of each genotype and analysed using a one-way ANOVA and Bonferroni correction.

A small but significant difference ($p<0.05$) was also observed in comparing the cardiac output between cre-positive and cre-negative controls suggesting that the reduction in cardiac output may not be entirely due to the loss of NUAK1 and that the αMHC cre may have a partial phenotype (Figure 5.7).

Collectively, these data suggest that a certain degree of systolic cardiac function is being lost as a result of cre expression and this is exacerbated by the additional deletion of NUAK1. The mechanism behind this may be difficult to establish as the phenotype of the cre positive mice may confound any mechanism observed in the NUAK1 deleted hearts.

5.2.3 Angiotensin II treatment of heart-specific NUAK1 knockout mice

The phenotype of heart-specific NUAK1 knockout under basal conditions is very mild and the mice seem otherwise phenotypically normal. Many other global and conditional mouse knockout models do not show significant phenotypes without the influence of a stressor (Ayadi et al., 2012). Using a treatment to promote a stress response also creates a more physiologically relevant result as it simulates chronic or acute stresses present in cardiovascular pathologies. Also, given the previous data from the liver-specific NUAK1 knockout model where a difference was only seen in response to damage or aging (Figure 4.21 and Figure 4.26), it is possible that the same will be true in the heart-specific knockout model. A common compound used to promote a stress response in cardiac models is angiotensin II. This is a peptide which causes hypertension via a mechanism of vasoconstriction and sympathetic nervous system stimulation (see section 1.7). Mice were dosed with angiotensin II at a rate of 1.2mg/kg/day using a subcutaneous mini pump. Mice were dosed for a maximum of two weeks whilst food and water intake and changes in body weight were monitored over this time to ensure there was no unnecessary pain, suffering or harm done to the animals. Following this treatment, body and organ weight measurements were taken to assess any potential gross morphological changes.

A

B
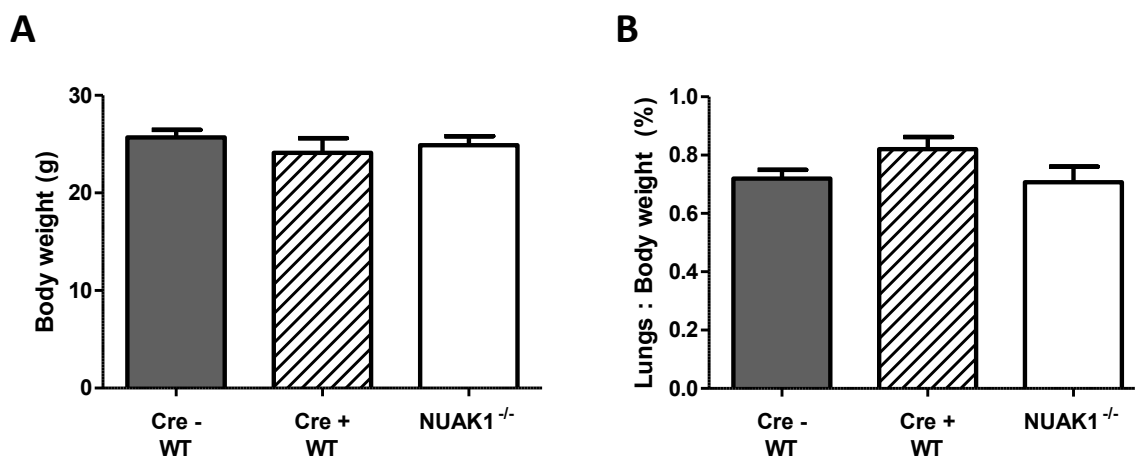
Figure 5.8 Heart-specific NUAK1 knockout does not affect body weight or lung weight after treatment with angiotensin II

8 - 10 week old heart-specific NUAK1 knockout male mice, αMHC cre positive and negative control animals were dosed with 1.2mg/kg/day angiotensin II for 14 days and measurements were taken. Data is shown for **(A)** Body weight and **(B)** Lung weight normalised to body weight. In all measurements no significant difference ($p > 0.05$) was observed between cre negative controls, cre positive controls and knockouts when analysed using a one-way ANOVA and Bonferroni correction. Plots are all mean ± S.E.M. of measurements from at least 5 mice of each genotype.

Clearly there is no change in body weight or lung weight after treatment with angiotensin II when comparing wild-type and heart-specific NUAK1 knockout mice (Figure 5.8). Treatment with angiotensin II raises systemic blood pressure, causing pulmonary hypertension and the lack of change in lung weight suggests there is no genotype dependent variation in the effects of pulmonary hypertension on the lungs of the treated mice. The signalling effects of angiotensin II are wide-ranging and effect a number of different pathways (Nguyen Dinh Cat and Touyz, 2011). The most significant effect is raising blood pressure, which causes a range of adaptations in an attempt to maintain normal blood flow.

The AT_1R receptor is a G protein-coupled receptor that acts as the main signal transducer for angiotensin II. Acute increases in angiotensin II levels leads to positive feedback and increased AT_1R expression, but chronic increases in angiotensin II create a negative feedback loop which downregulates its own receptor (Lassegue et al., 1995). Crucially, many other molecules such as LDL, insulin and nitric oxide can also affect angiotensin II signalling either directly by modulating AT_1R receptor expression or indirectly by regulating vascular tone in the case of

nitric oxide (Mehta and Griendling, 2007). This makes the interpretation of any variation in the effects of angiotensin II difficult to understand.

Hearts were harvested from angiotensin II treated mice to analyse how they adapted to the increased blood pressure and to see if the absence of NUAK1 changes the ability of the heart to adjust to the stress.
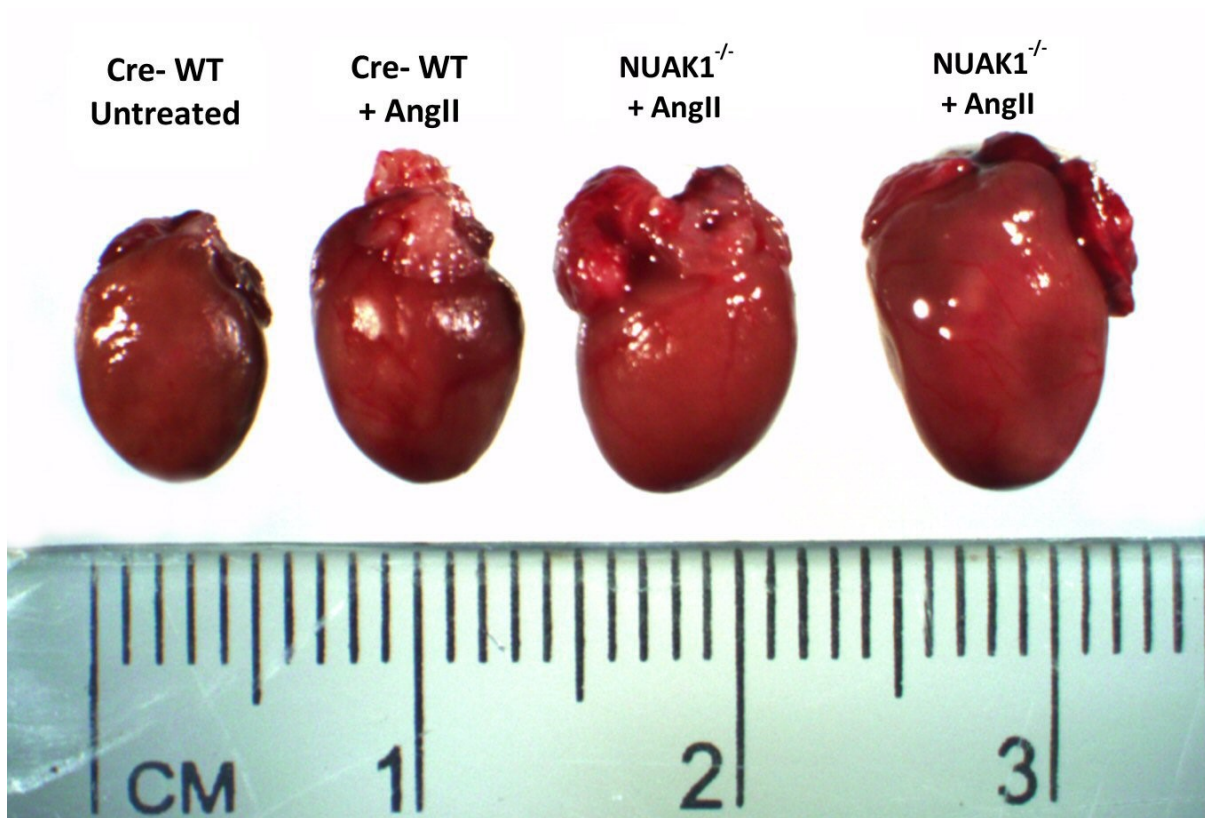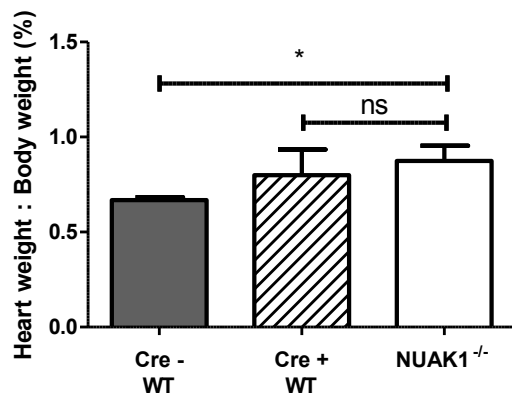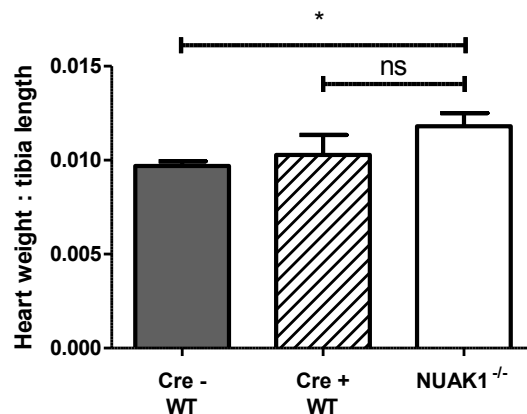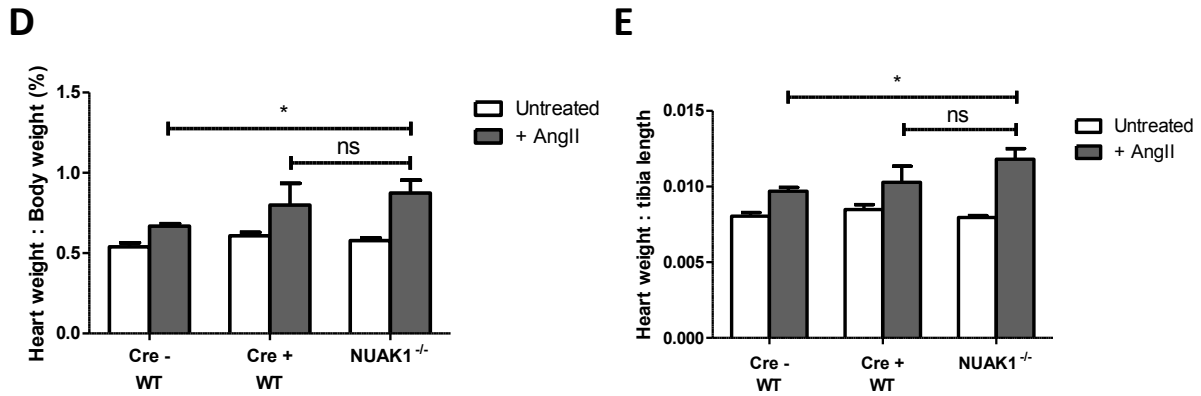
Figure 5.9 Heart-specific NUAK1 knockout mice have a greater increase in heart size and weight after treatment with angiotensin II

8 - 10 week old heart-specific NUAK1 knockout male mice, αMHC cre positive and negative control animals were dosed with 1.2mg/kg/day angiotensin II for 14 days and measurements were taken. **(A)** NUAK1 null hearts shown alongside wild-type cre negative hearts after angiotensin II treatment. **(B)** Heart weight normalised to body weight. **(C)** Heart weight normalised to tibia length. Separate plots also show the heart weight normalised to **(D)** body weight and **(E)** tibia length against the untreated measurements to highlight the proportional size change after treatment with angiotensin II. The significance indicated on the charts represents (* = $p<0.05$) when analysed using a one-way ANOVA and Bonferroni correction. Plots are all mean ± S.E.M. of repeat measurements from at least 5 mice of each genotype.

The data shows that heart-specific NUAK1 mice show a greater increase in heart size after treatment with angiotensin II compared to both other groups (Figure 5.9). Although the increase in weight between hearts from NUAK1 deleted mice versus control cre positive mice is not statistically significant, there is clearly a trend and it is likely that with greater numbers the results would become statistically significant. These data also support the previous indication that there can be a partial phenotype as a result of the αMHC cre expression (Buerger et al., 2006). The lack of NUAK1 expression appears to exacerbate the effect of angiotensin II treatment, leading to a stronger response against the increased blood pressure resulting in a greater increase in heart mass.

To assess if the increase in heart mass was due to hypertrophy or hyperplasia, hearts from angiotensin II treated mice were harvested and fixed for histological staining.

WT **KO**
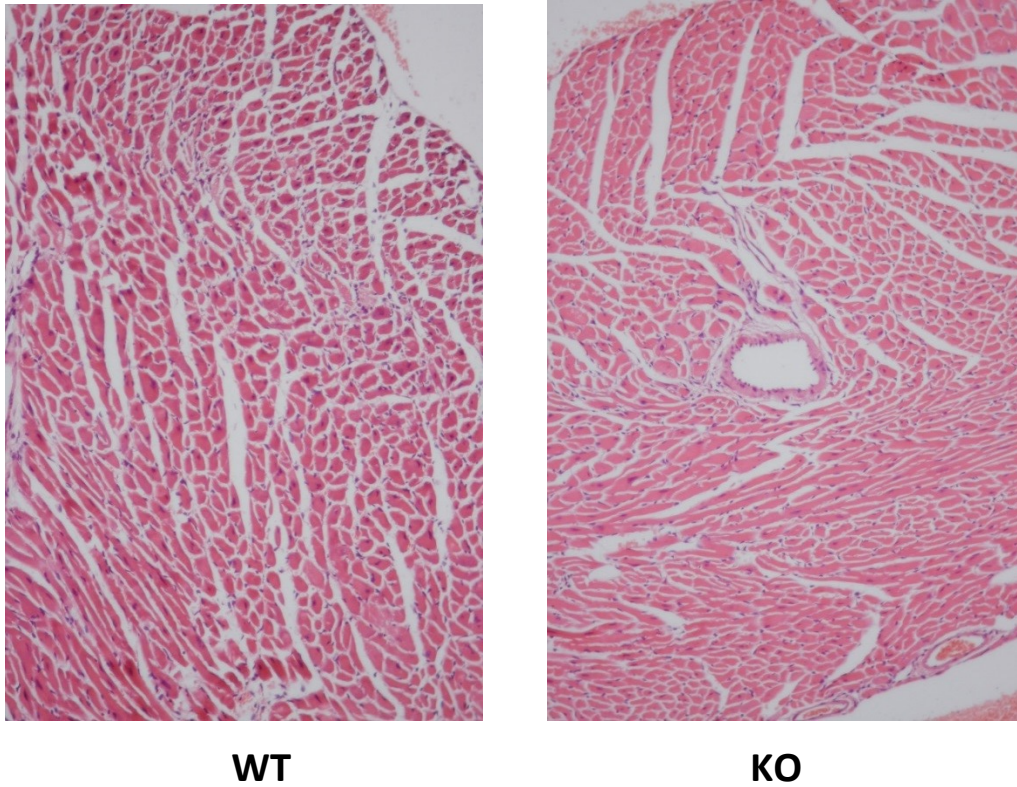
Figure 5.10 Heart-specific NUAK1 knockout mice show no structural differences to wild-type mice after treatment with angiotensin II

Hearts from 8 - 10 week old heart-specific NUAK1 knockout and wild-type mice that have been dosed with 1.2mg/kg/day angiotensin II for 14 days were harvested and fixed in 10% (v/v) formalin. Hearts were sectioned and stained with haematoxylin and eosin (H&E). Representative images are shown for both genotypes. General morphology, cell size and muscle banding were assessed and no change was seen between wild-type and NUAK1 knockout hearts.

The H&E stained hearts showed no obvious difference in cell size or cell number, suggesting that other adaptations in the muscle tissue must have produced the overall change in heart mass. Striated gaps appear in the heart muscle in both wild-type cre negative and heart-specific NUAK1 knockout mice as an indication of where the muscle has stretched to accommodate the higher blood pressure (Figure 5.10). While it is hard to quantify, there appear to be larger striations in wild-type cre negative hearts compared to NUAK1 null hearts. The greater increase in heart mass in NUAK1 deleted hearts may be due to effects on the remodelling process, changing the degree of fibrosis and collagen accumulation in response to stretching and damaging the muscle fibres. To analyse if there is a difference in the degree of fibrosis or glycogen accumulation in the heart muscle after angiotensin II treatment, sections of fixed hearts were stained with Sirius red stain and periodic acid schiff stain.
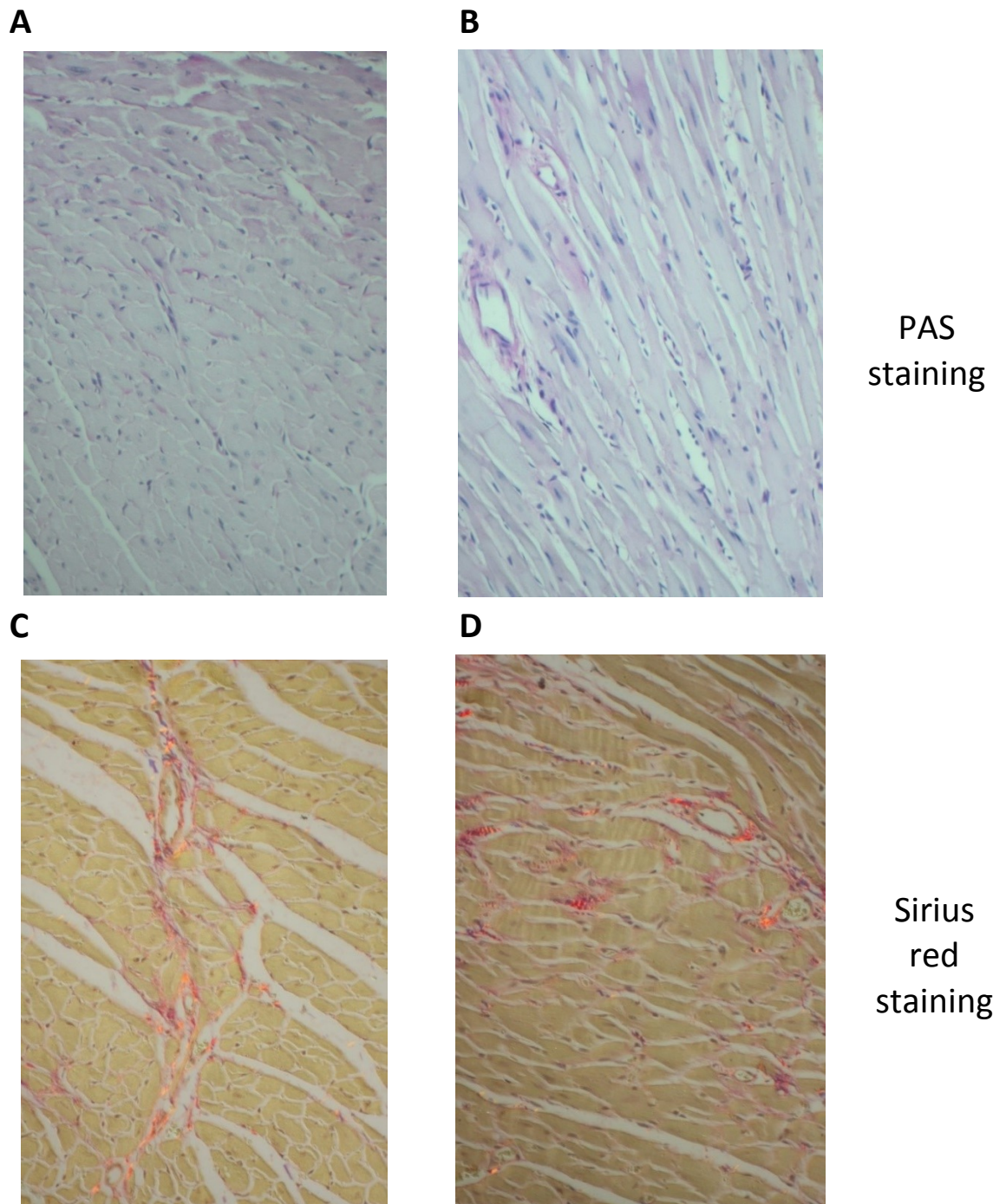
Figure 5.11 Heart-specific NUAK1 knockout mice show no difference in glycogen accumulation or fibrosis after treatment with angiotensin II

Hearts from 8 - 10 week old heart-specific NUAK1 knockout and wild-type mice that have been dosed with 1.2mg/kg/day angiotensin II for 14 days were harvested and fixed in 10% (v/v) formalin. Hearts were and sectioned and stained with the indicated stain. Periodic acid staining (PAS) was used to highlight glycogen accumulation in **(A)** wild-type and **(B)** knockout hearts. Sirius red staining was used to assess collagen fibrosis in **(C)** wild-type and **(D)** knockout hearts. Representative images are shown for both genotypes and no obvious was difference was noted for either stain.

5.2.4 Echocardiography of angiotensin II treated heart-specific NUAK1 knockout mice

The degree of glycogen accumulation and quantity of collagen fibres appears to be similar for both wild-type cre negative and heart-specific NUAK1 knockout mice (Figure 5.11), indicating that the difference in the change in mass is not caused by variations in fibrosis or significant changes in cardiac metabolism. Glycogen was not measured biochemically and this would provide a better indication of overall accumulation within the tissue but histological analysis indicates very little change.

In previous studies using angiotensin II treatment to induce cardiac hypertrophy, various changes in cardiac structure were observed but in some transgenic models and C57Bl/6 controls, these had little effect on cardiac function, suggesting there was compensatory hypertrophy (Harding et al., 2011). Other studies have shown angiotensin II treatment causes no change or marginally decreased left ventricular systolic function with no signs of heart failure (Haudek et al., 2010; Xu et al., 2008; Zhang et al., 2010).

To establish if the greater increase in heart mass has an effect on cardiac function, echocardiography was performed, as before. The echocardiography also measures various parameters of heart structure to try and establish how the loss of NUAK1 leads to a greater increase in heart size.
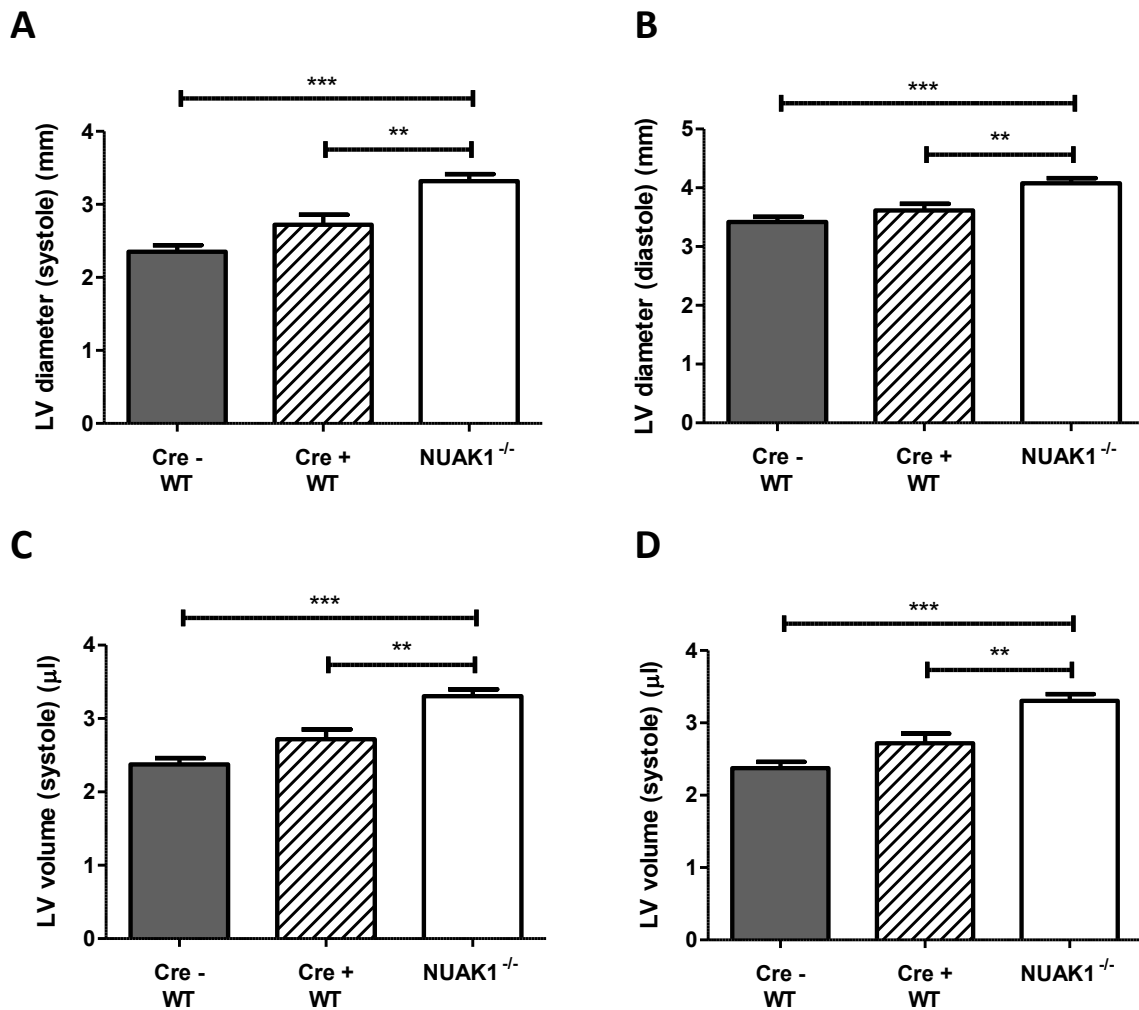
Figure 5.12 Heart-specific NUAK1 knockout mice have more dilated left ventricles and increased left ventricular volume after treatment with angiotensin II

Echocardiography data from 8 - 10 week old heart-specific NUAK1 knockout mice, cre positive and cre negative controls that have been dosed with 1.2mg/kg/day angiotensin II for 14 days. Data is shown for left ventricle diameter during **(A)** systole and **(B)** diastole. Plots are also shown for left ventricle volume during **(C)** systole and **(D)** diastole. The significance indicated on the charts represents (** = $p<0.01$, *** = $p<0.001$) when analysed using a one-way ANOVA and Bonferroni correction. Plots are all mean ± S.E.M. of measurements from at least 5 mice of each genotype.

Crucially an effect was seen in both left ventricle diameter and volume during both systole and diastole, indicating a consistent phenotype in the NUAK1 null hearts (Figure 5.12). In all cases the difference is slightly smaller between the cre positive controls and the knockouts compared to the cre negative mice suggesting there is a partial effect of the cre, but a more significant effect of the NUAK1 deletion.
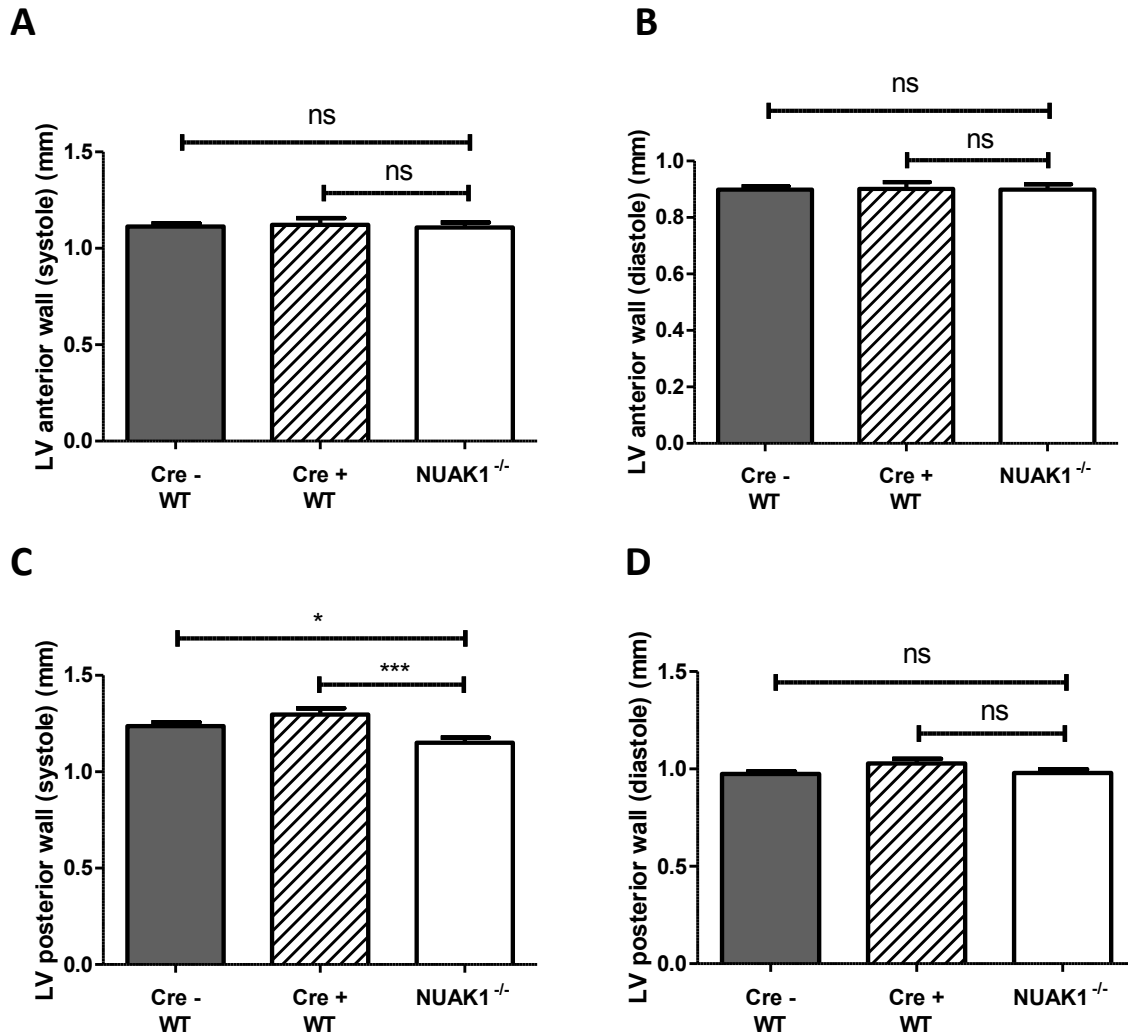
Figure 5.13 Heart-specific NUAK1 knockout mice have narrower posterior walls after treatment with angiotensin II

Echocardiography data from 8 - 10 week old heart-specific NUAK1 knockout mice, cre positive and cre negative controls that have been dosed with 1.2mg/kg/day angiotensin II for 14 days. Data is shown for left ventricle anterior wall thickness during **(A)** systole and **(B)** diastole. Plots are also shown for left ventricle posterior wall thickness during **(C)** systole and **(D)** diastole. The significance indicated on the charts represents (** = $p<0.01$, *** = $p<0.001$) when analysed using a one-way ANOVA and Bonferroni correction. Plots are all mean ± S.E.M. of measurements from at least 5 mice of each genotype.

Although a change was seen in left ventricle diameter and volume, only a small change was seen in one of the wall thickness measurements (Figure 5.13). This indicates that the muscle walls have stretched but have maintained their thickness. Similarly the ventricle walls have not increased in thickness so the left ventricle therefore has a larger volume but no thicker

muscle to contract and pump blood, suggesting there would be a loss of systolic cardiac function.
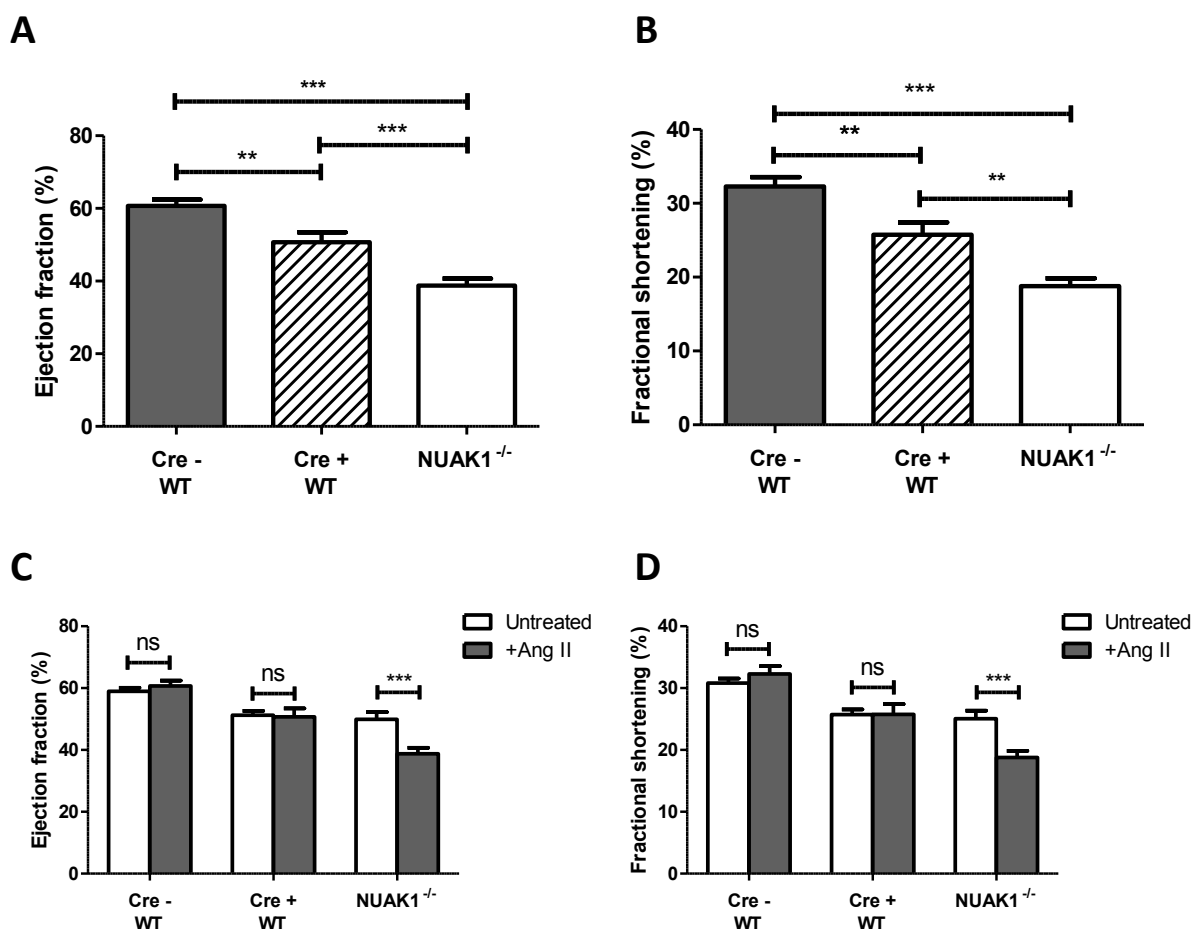
Figure 5.14 Heart-specific NUAK1 knockout mice have lower ejection fraction and fractional shortening after treatment with angiotensin II

Echocardiography data from 8 - 10 week old heart-specific NUAK1 knockout mice, cre positive and cre negative controls that have been dosed with 1.2mg/kg/day angiotensin II for 14 days. Data is shown for **(A)** ejection fraction and **(B)** fractional shortening. Data is shown compared to untreated mice for contrast. This is shown for **(C)** ejection fraction **(D)** fractional shortening The significance indicated on the charts represents (** = $p<0.01$, *** = $p<0.001$) when analysed using a one-way ANOVA and Bonferroni correction. Plots are all mean ± S.E.M. of measurements from at least 5 mice of each genotype.

The ejection fraction and fractional shortening measurements, which are both strong indicators of systolic function, show that only the heart-specific NUAK1 knockout mice showed a significant decrease after angiotensin II treatment (Figure 5.14). Cre positive control mice also showed a decrease in both measurements compared to cre negative controls after angiotensin II treatment but this difference exists in basal conditions (Figure 5.6). This shows

that in wild-type mice, irrespective of cre expression, there is no change in ejection fraction or fractional shortening in response to angiotensin II treatment. Therefore the extra reduction seen in the knockout hearts would suggest this phenotype is due to NUAK1 deletion.
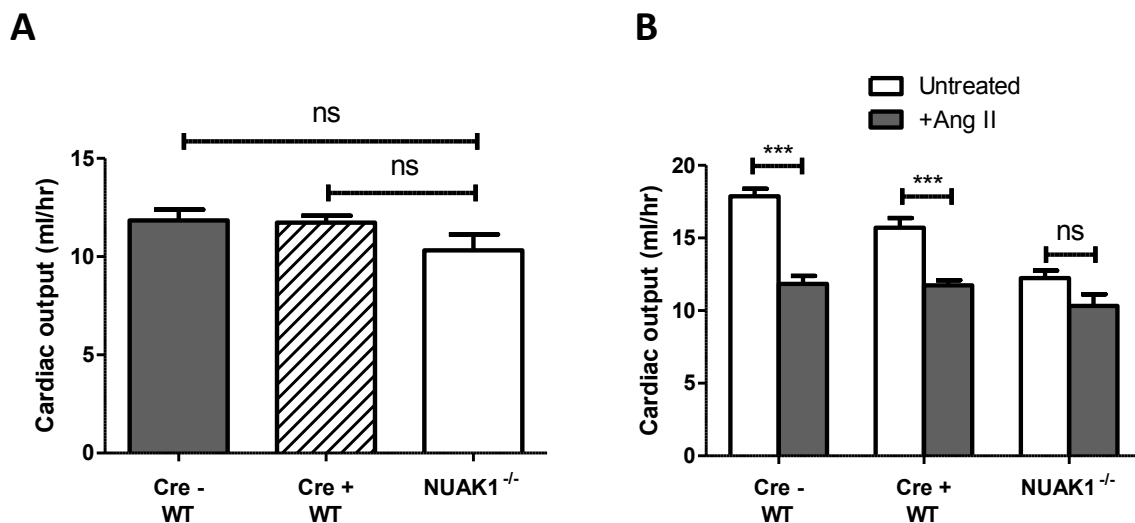
Figure 5.15 Cardiac output in NUAK1 knockout hearts is unchanged compared to wild-types after angiotensin II treatment

Cardiac output data from 8 - 10 week old heart-specific NUAK1 knockout mice, cre positive and cre negative controls that have been dosed with 1.2mg/kg/day angiotensin II for 14 days. **(A)** Data only from angiotensin II treated mice. **(B)** Data from treated mice compared to untreated mice of each genotype. The significance indicated on the charts represents (** = $p<0.01$, *** = $p<0.001$) when analysed using a one-way ANOVA and Bonferroni correction. Plot is mean ± S.E.M. of measurements from at least 5 mice of each genotype.

The cardiac output of NUAK1 mice shows no significant difference to either group of control mice after angiotensin II treatment, eliminating the difference seen under basal conditions (Figure 5.7). Both sets of control mice show significant reductions in cardiac output after angiotensin II treatment, possibly contradicting earlier reports that systolic function is maintained in control mice after treatment (Harding et al., 2011; Haudek et al., 2010). Collectively these data suggest that although heart-specific NUAK1 knockout mice have a basal cardiac phenotype, they are able to maintain cardiac output better than wild-type animals after angiotensin II treatment. However, the reduction in ejection fraction and fractional shortening (Figure 5.14) suggest that there may still be a loss of systolic function after cardiac insult.

5.3 Discussion

In light of the published study into the role of NUAK1 in skeletal muscle (Inazuka et al., 2012) and other data indicating that NUAK1 is highly expressed in heart (Figure 4.6) (Fisher et al., 2005), heart-specific NUAK1 knockout mice were created and characterised.

When confirming the deletion of NUAK1 had taken place correctly, there was a surprising finding that the AMPK phospho-T172 antibody which is known to cross-react with T211 on NUAK1 (Figure 3.5) did not detect any phosphorylation of NUAK1 in the heart (Figure 5.2). This could be due to the kinase not being phosphorylated but is more likely to be a sensitivity issue of the antibody as it is being compared on the same blot to its correct antigen, phosphorylated AMPKα. Despite this lack of cross-reaction with the pT172 antibody, the quantitative PCR data and NUAK1 blot showed a robust reduction in expression, confirming that NUAK1 had been deleted correctly.

Initial phenotyping of the mice showed no difference in heart size and no secondary pathologies affecting the cardiovascular system (Figure 5.3). Consistent with this, there were no observed behavioural or activity changes with the mice. Initial echocardiography results showed no significant difference across most of the parameters measured, however a small difference was seen in left ventricle posterior wall thickness during diastole (Figure 5.4). This difference was very small and only seen when compared to cre negative wild-type, suggesting it may be an effect of the αMHC cre expression. A small difference was also noticed in left ventricle anterior wall thickness during diastole (Figure 5.5), indicating the variation in thickness of the posterior wall may be a real change. However, this could also be partly due to normal variation within the small sample size. Increasing the number of animals tested would be likely to reduce the variation and decrease the significance of these results.

The measurement of systolic function highlighted the previous issues that had been noted about the αMHC cre mice having a cardiac hypertrophy phenotype. Changes were seen in systolic function (ejection fraction and fractional shortening) irrespective of NUAK1 deletion

(Figure 5.6). Although this issue potentially masked the discovery of a phenotype as a result of NUAK1 deletion, it also showed that NUAK1 had no additional effect on reducing systolic function relative to the cre positive mice.

This discovery would suggest that NUAK1 null heart tissue can maintain systolic function to a comparable level as cre positive mice, meaning that any changes in diastolic function may not be detected as healthy circulation should be maintained. Again, in a similar manner to the muscle-specific NUAK1 knockout mice a stress treatment was chosen to test the response of the heart tissue to damage.

After an acute systemic increase in blood pressure caused by angiotensin II treatment, the heart responds by pumping harder to maintain circulation (Tsukamoto et al., 2013). Any variation in heart size or structure in response to this increase, corresponding to genotype, would indicate a difference in the ability of the cardiac myocytes to respond to damage, potentially meaning they would respond differently to pathological stresses.

Initial measurement of body weight and lung weight after angiotensin II treatment detected no change between NUAK1 null hearts and wild-type equivalents (Figure 5.8). This suggested that there was no difference in secondary cardiovascular effects and that there was no change in systemic effects of eating and activity behaviour that might influence body weight. However, significant changes were noted in heart size when normalised to either body weight or tibia length (Figure 5.9). This suggests that the cardiac muscle has responded differently either by increasing cell size, proliferation or by stretching and increasing fibrosis. Again, NUAK1 could be influencing cell proliferation by mechanisms discussed previously, such as the hippo pathway, however no evidence was detected for hyperplasia in H&E stained sections of treated hearts (Figure 5.10). In addition to this, no significant structural changes were noticed in the histological analysis, providing few clues as to the mechanism for the increased heart mass. It is possible that the striations seen in histological analysis, caused by stretching of the heart muscle, are slightly wider in wild-type hearts compared to NUAK1 null hearts (Figure 5.10). This may be mediated by a cell adhesion phenotype, correlating with

other anecdotal data from my studies and a previous report that suggests deletion of NUAK1 causes an increase in cell adhesion (Zagorska et al., 2010).

Echocardiography of the angiotensin II treated mice showed a dilated left ventricular cardiomyopathy phenotype in both wild-type and NUAK1 deleted hearts, but with a larger dilation in the absence of NUAK1 (Figure 5.12). Alongside this, very little change was detected in left ventricular wall thickness, suggesting that the absence of NUAK1 does not increase and may protect against the thinning of the muscle wall as the ventricle dilates (Figure 5.13).

In relation to the resulting cardiac function from these changes in left ventricle size, echocardiography showed that there was a significant decrease in ejection fraction and fractional shortening in NUAK1 null hearts, compared to either cre negative or cre positive wild-types. Interestingly, the knockout mice were the only animals that showed a significant decrease in both these parameters after angiotensin II treatment compared to untreated animals of the same genotype (Figure 5.14C and D). This suggests that the proportion of blood in the left ventricle that is pumped during each heart cycle decreases as a result of NUAK1 loss, indicating a partial loss of systolic function and contractility. However, the cardiac output of NUAK1 knockout mice does not decrease relative to the untreated animals whereas both cre positive and cre negative controls show marked decrease to levels similar to NUAK1 null mice (Figure 5.15). This raises the interesting prospect that the loss of NUAK1 causes a basal reduction in cardiac output, possibly as a result of developmental differences, but then protects against any further reduction as a result of stress treatment or pathology.

Some indications in the literature suggest there may be a possible mechanism for this phenotype. An unbiased human genome wide study to establish gene loci involved in determining muscle strength identified NUAK1 as a potential mediator of this phenotype (Windelinckx et al., 2011). This study identified polymorphisms in the gene but did not indicate if the mutations would cause gain or loss-of-function. It is possible that the identified mutations cause a reduction in NUAK1 activity, leading to a loss of muscle strength. This may explain the basal reduction in cardiac output as the left ventricle walls would be less able to

contract. Interestingly, the muscle strength study also identified PPP1CC (the γ isoform of protein phosphatase 1 catalytic subunit) as another candidate gene, suggesting that there may be links to the previously discussed involvement of NUAK1 in protein phosphatase targeting and organisation of the cytoskeleton through MLC phosphorylation.

The lack of change in cardiac output of heart-specific NUAK1 knockout mice after angiotensin II treatment suggests that their hearts may be capable of contracting better under stress, which would contradict the initial loss of function under basal conditions. However, one very interesting feature that is seen in all of the NUAK1 tissue-specific knockout data presented here and in a previous study (Inazuka et al., 2012), is that they all require a stress treatment to elicit a phenotype. This could indicate an interesting facet of NUAK1 function in that it may have a developmental role, which can be compensated for in deleted tissues, especially when animals are maintained in highly controlled environments, but a separate role in response to ageing or damage. It would be interesting to age a cohort of heart-specific NUAK1 knockout mice and assess if there is a comparable phenotype to the liver-specific knockout mice.

6 Summary and Future Work

This thesis has provided various data that contribute to the study of NUAK1 and the field of AMPK-related kinases. There is a variety of evidence for possible *in vivo* roles and indications of mechanisms from *in vitro* studies that may provide a mechanistic basis for the observed changes. Some of the data shown here supports and strengthens the existing evidence in the literature of a role for NUAK1 in myosin phosphorylation and cell proliferation, however some conflicting evidence still exists which will require more work to resolve.

6.1 *In vitro* observations

Data presented in my thesis shows that NUAK1 has a basal level of activity, both *in vitro* in a bacterial expression system and in cells. This contradicts previous reports but various issues and possible reasons for these differences have been highlighted. The role of 14-3-3s in regulating NUAK1 activity was further explored and data linking it to possible control of phosphorylation by LKB1 was presented. The evidence that NUAK1 has a basal level of activity, without the need for activation by LKB1, is compelling, but has not been replicated by other investigators. However there is a range of evidence in the literature to suggest that there could be basal activity and other regulatory mechanisms in the AMPK-related kinase family. The differences in these observations may be due to regulatory mechanisms that are not yet understood, which confound the activity measurements under different experimental conditions. The subcellular localisation of NUAK1 was investigated but no significant evidence to determine a specific role for the kinase was found. Various data exploring previous reports into the activation of NUAK1 and its similarities to the other related kinases were presented and indications towards novel pathways were provided by mass spectrometry screens.

The data presented here partly supports the previous mechanism which linked NUAK1 to controlling MLC phosphorylation (Zagorska et al., 2010). However certain differences were observed, specifically that 14-3-3 bound directly to NUAK1, an interaction which may affect its activity or localisation, thereby having a different effect on MLC phosphorylation. The observed phenotype of increased cell adhesion fits with this previous model, suggesting that

any differences in the mechanism are likely to be due to differences in experimental techniques or conditions but these may yet be key to understanding the overall physiological role of NUAK1.

Further *in vitro* work will be required to establish the role of binding partners, such as 14-3-3 and the function of the C-terminal part of the protein where autophosphorylation is likely to play a role in regulating NUAK1. Analysis of some of the potential pathways highlighted here such as the regulation of ATP synthase and myosin phosphorylation require further work *in vitro* and in cell based systems to validate. Further mutation and truncation of the protein could reveal insights into the regions important for regulation. As a further project it would be very useful to crystallise and establish the structure of NUAK1 and of the kinase bound to 14-3-3ε. This would provide insight into the activation and regulation of the protein and this understanding could be applied to other AMPK-related kinases to determine if there are any similarities. Little evidence was provided in my study for the role of the ubiquitination in NUAK1 regulation and aspects of this mechanism are still uncertain. Further understanding of the function of NUAK1 binding USP9X and validation of where and how ubiquitin marks are attached to NUAK1 could add another dimension to the localisation and control of the kinase.

The increased growth rate observed in MEFs derived from the NUAK1 global knockout embryos agrees with previous work from our laboratory (Humbert et al., 2010) but conflicts with various reports of NUAK1 overexpression being associated with increased cell growth (Chen et al., 2013a; Cui et al., 2013). The experimental approach of these studies differs significantly from this thesis as they are based on retrospectively screening for changes in cancer models. This approach may lead to different results as several pathways could be affected and the observed phenotype may not solely be due to changes in NUAK1 activity. Also, it is not clear that the increased growth rate observed in NUAK1 null MEFs in this report would correlate with increased growth rate in every *in vivo* environment. However increased proliferation of oval cells in NUAK1 null livers may suggest that this phenotype does apply to certain *in vivo* situations. Interestingly, a study showing increased NUAK1 expression associated with non-small cell lung cancer invasion and metastasis also observed increased cell adhesion following NUAK1 knockdown. Determining how the proliferation of NUAK1 null

cells relates to their adhesion phenotype will be crucial to understanding the *in vivo* significance of this kinase, particularly in relation to cancer. It is possible that NUAK1 knockdown or deletion consistently increases cell adhesion due to changes in myosin phosphorylation, but only increases cell proliferation under certain *in vivo* conditions or under favourable experimental cell culture conditions.

6.2 *In vivo* observations

This thesis presents data from two tissue-specific knockout mouse models of NUAK1, adding to the one previous report that has shown any physiological role for the kinase in adult tissues (Inazuka et al., 2012). As part of my studies the phenotype of global NUAK1 deletion in mice was confirmed and MEFs were produced as a useful *in vitro* tool.

Both the *in vivo* models presented in this thesis support the finding in the previous study that the observed phenotype is mild or insignificant under basal conditions. This could be due to redundancy within the AMPK-related kinase family or other effectors that feed into the pathways that NUAK1 controls. In order to fully understand the effect of changes in NUAK1 expression on pathological conditions, it will be key to understand why the loss of NUAK1 signalling does not produce a basal phenotype and what the various compensatory mechanisms might be.

Thorough phenotyping of young-liver specific NUAK1 knockout mice indicated that the loss of NUAK1 in the liver did not create an overt phenotype under basal conditions. After a stress treatment diet, a greater proliferation of oval cells in NUAK1 null livers provides some evidence of a possible phenotype and links some of my *in vitro* findings to possible *in vivo* mechanisms. Although the aged mice only became available later during my studies, substantial efforts to phenotype NUAK1 liver-specific knockout mice under aged conditions suggested that there was a difference in the response to ageing due to NUAK1 deletion. This interesting phenotype shows some similarities to another animal model and inferences from *in vitro* data in my report may indicate possible mechanisms for this effect. The role of NUAK1

in potentially reducing age-related liver degeneration and metabolic problems suggest that it may be a useful clinical target. However, further understanding of the pathways involved will be necessary to ensure inhibitors or activators are targeting the correct processes.

Data from the heart-specific NUAK1 knockout mice again showed that there was a minimal phenotype under basal conditions, although this was partially confounded by the phenotype of the αMHC cre mice. Structural differences in the heart in response to angiotensin II treatment were observed as a result of NUAK1 deletion but little evidence was uncovered to explain the mechanisms underlying this variation. Taken together, both sets of *in vivo* data may indicate that NUAK1 has a minimal role in adult tissues but could have a more significant role during development or under conditions of proliferation in response to stress. Both stress treatments used in my studies were severe and acute treatments but it would be interesting to establish what response would be seen after mild or chronic stresses were applied to NUAK1 transgenic animal models. Mild and chronic stresses would represent a better recapitulation of pathological states and may reduce confounding or off-target influences from large responses to severe stress.

Results from my animal models indicate more work that could reveal mechanistic insight into the function of NUAK1 as well as provide better evidence for its physiological role. It would be interesting to assess any potential role of the kinase in development by harvesting tissues from animals at earlier time points and measuring any functional changes in tissues of interest. Similarly, useful data would be gained from ageing tissue-specific mouse models and conducting Kaplan-Meier analysis to establish if there was any change in mortality as a result of NUAK1 deletion in a particular tissue. Data from the liver-specific NUAK1 knockout mice would suggest that there may be an improvement in age related degeneration, indicating that the mice may live longer, however this has not been shown conclusively. Also, stress treatments could be applied at different time points to establish the interplay between a potential role in development and a role in response to pathological insult.

Studies have identified human mutations in NUAK1 that could be linked to specific phenotypes (Windelinckx et al., 2011) and further evidence from animal models would provide a better indication of human pathologies to assess for changes in NUAK1. Also, human mutations identified in previous studies could be tested *in vitro* and in cell conditions to understand if they caused a gain or loss-of-function.

6.3 Future directions

One key aspect of NUAK1 regulation, and something that is common across the AMPK and related-kinase field, is the lack of understanding around the protein phosphatases that are responsible for dephosphorylating the kinases *in vivo.* This aspect is of particular interest with regard to NUAK1 as it is known to be able to interact with components of the protein phosphatase system (such as MYPT1), raising the possibility that it may influence its own phosphorylation in a negative feedback loop by activating and targeting protein phosphatase complexes. There is potential for studying this mechanism in other model organisms such as *C. elegans* where preliminary evidence already shows that the NUAK1 orthologue can regulate myosin organisation (Hoppe et al., 2010). Clearly cytoskeletal organisation is complex and multifactorial process and NUAK1 may contribute to a small part of this but identifying the precise interactions will be important for modulating the pathways.

Given that the aged liver-specific NUAK1 knockout mice show a significant metabolic phenotype, it would be of interest to interrogate this system biochemically to establish what changes have occurred and what pathways are influenced. These data may also provide insight into possible pathologies that could be linked to human variation in NUAK1 expression or activity.

A non-specific inhibitor of NUAK1, BX795, has been identified and it would be interesting to treat cells and animal models with this compound to see if reduction in NUAK1 activity would recapitulate the phenotype or function seen in NUAK1 deleted models (Clark et al., 2009).

Evidence from these studies would also provide a better insight for potential pharmacological treatment if NUAK1 is identified as a pathological mediator.

This thesis does not precisely clarify the role of NUAK1 in cell proliferation but various data from my studies suggest reasons for differences observed in previous studies and possible mechanisms that may be regulated by NUAK1. There is substantial interest in the literature surrounding the role of NUAK1 in cancer and future studies may be able to build on the data shown here to clarify this. Useful data could be provided by establishing NUAK1 transgenic mouse models on cancer-prone backgrounds with deregulated Myc expression to study the *in vivo* significance of previous reports into NUAK1 function (Liu et al., 2012). Similarly, other cancer inducing models such as diet treatments could be used to establish the role of NUAK1 as part of *in vivo* pathological systems.

Although this study sheds new insight into some aspects of NUAK1 function, it clearly shows that there is likely to be some redundancy within these mechanisms. Further investigation of other proteins in the AMPK-related kinase family would improve the knowledge of signalling pathways downstream of LKB1 and would provide more evidence for potential drug treatments of these pathways. Also, given the evidence that NUAK1 does not necessarily require LKB1 for activity, this questions similar findings reported for other AMPK-related kinases (Lizcano et al., 2004). As the knowledge of these interlinking pathways is improved, the ability to attenuate and control them pharmacologically will also increase. Expanding the existing knowledge of inhibitors such as BX795 and identifying specific interactions for downstream pathways will be key to understanding the role and regulation of NUAK1 for potential therapeutic treatments.

Appendices

Appendix 1 – Table of oligonucleotides used in this study

The following oligonucleotides were used in this study for the purpose of mutagenesis of the NUAK1 construct in the pRSFDuet-1 vector, genotyping mice or conducting quantitative PCR experiments.

Purpose	Direction	Sequence 5' – 3'
NUAK1 D196A mutagenesis	Forward	TGCAATATTAAGATTGCTGCCTTTGGGCTTTCCAACCTG
	Reverse	CAGGTTGGAAAGCCCAAAGGCAGCAATCTTAATATTGCA
FLP genotyping	Forward	GGTCCAACTGCAGCCCAAGCTTCC
	Reverse	GTGGATCGATCCTACCCCTTGCG
NUAK1 KOMP construct	Forward	GTTGCTATAAAATCCATCCGTAAGGACAAA
	Reverse	GAAACCTGTCTTTCTCGACTACTGGCTTTCAGTAA
NUAK1 conditional construct	Forward	TACGCGCTTTGTAATGGGATGCTCCTGTAATAGGATGTCT
	Reverse	GCTCGTCCTTAATTTTGTCCTTACGGATGGATTTTATAGCAAC
αMHC cre genotyping	Forward	ATGACAGACAGATCCCTCCTATCTCC
	Reverse	CTCATCACTCGTTGCATCGAC
Alb cre genotyping	Forward	GCGGTCTGGCAGTAAAAACTATC
	Reverse	GTGAAACAGCATTGCTGTCACTT
AMPKα1 qPCR	Forward	Qiagen QuantiTect primer pair Prkaa1 (sequence unknown) QT00286923
	Reverse	Qiagen QuantiTect primer pair Prkaa1 (sequence unknown) QT00286923
AMPKα2 qPCR	Forward	Qiagen QuantiTect primer pair Prkaa2 (sequence unknown) QT00140518
	Reverse	Qiagen QuantiTect primer pair Prkaa2 (sequence unknown) QT00262206
AMPKβ1 qPCR	Forward	Qiagen QuantiTect primer pair Prkab1 (sequence unknown) QT00262206
	Reverse	Qiagen QuantiTect primer pair Prkab1 (sequence unknown) QT00140518
AMPKγ1 qPCR	Forward	Qiagen QuantiTect primer pair Phkg1 (sequence unknown) QT00103054
	Reverse	Qiagen QuantiTect primer pair Phkg1 (sequence unknown) QT00103054
Cox6b qPCR	Forward	Qiagen QuantiTect primer pair Cox6b (sequence unknown) QT00096012
	Reverse	Qiagen QuantiTect primer pair Cox6b (sequence unknown) QT00096012
Ndufs4 qPCR	Forward	Qiagen QuantiTect primer pair Ndufs4 (sequence unknown) QT00148799
	Reverse	Qiagen QuantiTect primer pair Ndufs4 (sequence unknown) QT00148799
NUAK1 qPCR	Forward	GTTGCTATAAAATCCATCCGTAAGGACAAA
	Reverse	ACTGATGATATGAGGATGGTTGAGGGATGA
NUAK2 qPCR	Forward	Origene NUAK2 primer pair (sequence unknown) MP209041
	Reverse	Origene NUAK2 primer pair (sequence unknown) MP209041
GAPDH qPCR	Forward	AGGTCGGTGTGAACGGATTTG
	Reverse	TGTAGACCATGTAGTTGAGGTCA

Appendix 2 – Raw data from mass spectrometry screens

The data from the NUAK1 mass spectrometry screens is presented in the form it was produced after searching the MASCOT database. In each case the highest ranking proteins have been screened by the method listed.

Appendix 2.1 – Raw data from MEF SILAC experiment (see Section 2.2.21.1)

The highest ranking proteins have been ordered by the quantitative ratio of peptides detected in the "heavy" compared to the "light" lysates. This ratio is labelled as "H/L Ratio" and 2 was used as a threshold of sufficient increase.

H/L Ratio	Protein	H/L Ratio	Protein
118.46	ATP synthase subunit d, mitochondrial	5.6796	Methylthioribose-1-phosphate isomerase
87.948	Cystatin-B	5.6322	182 kDa tankyrase-1-binding protein
44.817	Calpactin I light chain	5.6043	Inhibitor of nuclear factor kappa-B kinase-interacting protein
43.743	GTPase-interacting protein 2	5.5946	Actin regulatory protein CAP-G
42.235	Cyclin-dependent kinase inhibitor 2A, isoform 3	5.5643	C-type mannose receptor 2
37.467	ATP synthase subunit f, mitochondrial	5.4832	Inosine triphosphate pyrophosphatase
35.81	Acetoacetyl-CoA thiolase	5.301	COP9 homolog
34.675	CD44 antigen	5.1779	Fascin
32.961	Cellular retinol-binding protein	5.1304	Latent-transforming growth factor beta-binding protein 1
32.944	3-ketoacyl-CoA thiolase A, peroxisomal	5.1247	Antioxidant enzyme B166
32.861	Cytochrome b5 outer mitochondrial membrane isoform	5.0896	Post-proline cleaving enzyme
31.89	Peptidyl-tRNA hydrolase 2, mitochondrial	4.9573	Carboxy terminus of Hsp70-interacting protein
31.062	Beta-2-microglobulin	4.9112	Actin cross-linking family 7
27.853	6.8 kDa mitochondrial proteolipid	4.8662	Band 4.1-like protein 2
27.644	Collagen alpha-1(VI) chain	4.7941	Cathepsin Z
27.35	Neuron cytoplasmic protein 9.5	4.787	Asparagine synthetase [glutamine-hydrolyzing]
27.023	Putative uncharacterized protein	4.7718	Formyltetrahydrofolate synthetase
26.814	Cellular retinoic acid-binding protein 1	4.7712	ICD-M
26.071	3,2-trans-enoyl-CoA isomerase, mitochondrial	4.7639	Placental thrombin inhibitor
24.96	UPF0368 protein Cxorf26 homolog	4.5879	Pitrilysin metalloproteinase 1
24.162	Acetyl-Coenzyme A acetyltransferase 3	4.52	Putative uncharacterized protein
23.456	Aspartyl aminopeptidase	4.5077	47 kDa heat shock protein
23.441	6-phosphogluconolactonase	4.5015	Galactokinase 2
22.176	Putative uncharacterized protein	4.4616	Cytosol aminopeptidase
21.808	BPY2-interacting protein 1	4.4166	Tubulin--tyrosine ligase-like protein 12
21.745	Glutathione S-transferase P 1	4.4125	Tpm1 protein
20.69	O-phosphoserine phosphohydrolase	4.4114	Protein G7a
20.112	D4	4.3878	WASH complex subunit FAM21
19.974	UDP-N-acetylhexosamine pyrophosphorylase-like protein 1	4.3617	Diaphorase-1

H/L Ratio	Protein	H/L Ratio	Protein
19.784	Glutathione S-transferase GT8.7	4.3482	Pyrroline-5-carboxylate reductase 3
19.438	26S protease subunit S5 basic	4.3127	Transmembrane emp24 domain-containing protein 5
19.414	ATP synthase subunit b, mitochondrial	4.2903	Thrombospondin 1
18.551	ATP synthase subunit e, mitochondrial	4.2876	Aconitate hydratase, mitochondrial
18.441	E2-induced gene 5 protein homolog	4.2674	UDP-glucose 6-dehydrogenase
18.326	5-methylthioadenosine phosphorylase	4.259	Dynamin-1
18.079	Inosine phosphorylase	4.2321	Tumor protein D52-like 2
17.733	La autoantigen homolog	4.2245	Adenosine 5-phosphotransferase
17.614	Cytochrome b5	4.2162	Complex I-75kD
17.467	Endogenous carboxypeptidase inhibitor	4.1213	Alpha-2 type I collagen
17.367	Glutathione S-transferase Mu 2	4.078	Palladin
17.313	Zyxin	4.0265	CDC47 homolog
17.285	Carboxypeptidase C	3.992	35-alpha calcimedin
17.198	ATP synthase subunit g, mitochondrial	3.9452	Beta-catenin
17.108	D-dopachrome decarboxylase	3.9107	HLA-B-associated transcript 3
16.809	Sepiapterin reductase	3.871	Calponin H2, smooth muscle
16.721	Putative uncharacterized protein	3.8262	E3 ubiquitin-protein ligase UBR3
16.493	Epidermal-type fatty acid-binding protein	3.7362	EH domain-containing protein 1
16.473	AHD-M1	3.6032	Lamina-associated polypeptide 2, isoforms alpha/zeta
16.345	Aldehyde dehydrogenase family 1 member L2	3.6003	Tyrosine-protein phosphatase non-receptor type 23
16.322	Galactokinase	3.5441	Macropain chain Z
16.288	Cytochrome c oxidase polypeptide VIc	3.5367	Aspartate beta-hydroxylase
16.014	60S ribosomal protein L29	3.5231	Dihydropteridine reductase
16.014	Ubiquitin-activating enzyme E1 domain-containing protein 1	3.4956	Dedicator of cytokinesis protein 7
15.967	Atlastin-3	3.4845	Epiplakin
15.915	Prosaposin	3.4821	UDP--Glc:glycoprotein glucosyltransferase
15.211	Low molecular mass protein 19	3.4803	Delta-aminolevulinic acid dehydratase
15.169	Anastellin	3.4389	Alcohol dehydrogenase [NADP+]
14.985	DDAHII	3.4321	GDI-1
14.969	ES1 protein homolog, mitochondrial	3.431	ABP-280-like protein
14.908	Long-chain specific acyl-CoA dehydrogenase, mitochondrial	3.429	Hydroxysteroid (17-beta) dehydrogenase 10
14.698	Aldehyde reductase	3.3969	ADP-ribosylation factor-like protein 10C
14.582	Fibulin-2	3.3754	Anaphase-promoting complex subunit 1
14.504	Complex I-20kD	3.3683	80K-H protein
14.329	Sphingosine-1-phosphate aldolase	3.3592	Copine III
14.258	Sterol-4-alpha-carboxylate 3-dehydrogenase, decarboxylating	3.3278	Heterogeneous nuclear ribonucleoprotein A3
13.886	Beta-type platelet-derived growth factor receptor	3.3039	AFG3-like protein 2
13.837	Ferritin L subunit 1	3.2605	Transportin-3
13.663	Cargo selection protein TIP47	3.2246	Putative uncharacterized protein
13.385	63 kDa membrane protein	3.2031	Aldehyde dehydrogenase family 18 member A1
13.259	E3 ubiquitin-protein ligase NEDD4	3.1754	Lon protease homolog, mitochondrial
13.209	Alpha-mannosidase 2	3.1378	Myosin, heavy polypeptide 10, non-muscle
13.019	Ubiquitin carboxyl-terminal hydrolase	3.1375	Methionine--tRNA ligase
12.883	Adenine nucleotide translocator 1	3.1359	Adenylate cyclase-inhibiting G alpha protein

H/L Ratio	Protein	H/L Ratio	Protein
12.661	Annexin A4	3.1277	Laminin B1 chain
12.503	17-beta-hydroxysteroid dehydrogenase 12	3.0812	Pyrroline-5-carboxylate reductase 2
12.463	65 kDa FK506-binding protein	3.0417	ERT2
12.457	Dihydropyrimidinase-related protein 3	3.0159	C-Jun-amino-terminal kinase-interacting protein 4
12.377	Glutathione S-transferase 5.7	2.9745	Inositol monophosphatase 1
12.343	Cathepsin B	2.9621	Lysyl hydroxylase 3
12.312	Xanthine dehydrogenase	2.9457	ER-Golgi intermediate compartment 53 kDa protein
12.106	52 kDa FK506-binding protein	2.9432	Cadherin-associated Src substrate
12.105	Myb-binding protein 1A	2.9366	Protein transport protein Sec31A
11.79	Perlecan (Heparan sulfate proteoglycan 2)	2.9118	Thimet oligopeptidase
11.732	Actin-depolymerizing factor	2.8566	Protein Gamm1
11.338	Amine oxidase [flavin-containing] A	2.8548	Cathepsin D
11.28	Ferritin heavy chain	2.8484	COP9 signalosome complex subunit 7a
11.24	Thy-1 antigen	2.8297	300 kDa mannose 6-phosphate receptor
11.123	4.1B;Band 4.1-like protein 3	2.8229	Endoplasmic reticulum resident protein 44
10.985	Kinectin	2.8167	Ras-related protein Rab-2A
10.941	Gelsolin	2.7983	Succinyl-CoA ligase [GDP-forming] subunit alpha, mitochondrial
10.868	Bone marrow stromal antigen 2	2.797	SDP3 protein
10.765	Interferon-gamma-inducible protein Mg11	2.7461	Hsc70-interacting protein
10.59	CYPLI	2.7424	Diadenosine tetraphosphate synthetase
10.514	Gem-associated protein 5	2.7331	Ribosome receptor protein
10.506	Glutaminyl-tRNA synthetase	2.7152	Aflatoxin B1 aldehyde reductase member 2
10.446	AGE	2.6943	155 kDa nucleoporin
10.32	Dennd4c protein	2.6869	3-oxoacid-CoA transferase 1
10.292	19 kDa FK506-binding protein	2.6776	Annexin A7
10.288	Cyclin-dependent kinase 4 inhibitor A	2.6641	17 kDa myosin light chain
10.211	Adenine phosphoribosyltransferase	2.6613	33 kDa VAMP-associated protein
10.208	Cholesterol-regulated 39 kDa protein	2.6253	Chromosome-associated protein E
10.192	Protein-tyrosine kinase 7	2.6106	Asparagine--tRNA ligase
10.101	2-amino-3-ketobutyrate coenzyme A ligase, mitochondrial	2.6076	ADP-ribosylation factor-like protein 1
9.8024	14 kDa lectin	2.5982	Sorcin
9.7776	Androgen-regulated short-chain dehydrogenase/reductase 1	2.5842	Tubulin beta-6 chain
9.5464	Acid maltase	2.5758	Formylglycinamide ribotide amidotransferase
9.5436	Fragilis	2.56	Phosphate carrier protein, mitochondrial
9.5412	Sorting nexin-1	2.5521	Complex III subunit 8
9.5241	Glucosamine-6-sulfatase	2.548	PAF acetylhydrolase 30 kDa subunit
9.4823	35 kDa lectin	2.5365	12 kDa FK506-binding protein
9.4811	Loss of heterozygosity 11 chromosomal region 2 gene A protein homolog	2.5347	Aspartate--tRNA ligase
9.339	Calumenin	2.533	Chloride intracellular channel protein 4
9.32	Ribonuclease inhibitor	2.5308	21 kDa polypeptide
9.2627	Imidazoline receptor 1	2.5304	Alpha-actinin cytoskeletal isoform
8.9735	A-kinase anchor protein 12	2.5057	CDC10 protein homolog
8.9681	Translin	2.5004	Neural precursor cell expressed developmentally down-regulated protein 5
8.8691	Adenylosuccinase	2.4946	TES1/TES2

H/L Ratio	Protein	H/L Ratio	Protein
8.6744	Arf-GAP with Rho-GAP domain, ANK repeat and PH domain-containing protein 1	2.4776	Calcium-binding mitochondrial carrier protein Aralar1
8.5512	Cytochrome c oxidase polypeptide IV	2.4749	PAF acetylhydrolase 29 kDa subunit
8.4815	Interferon-stimulated protein 15	2.44	Putative uncharacterized protein Myo9a
8.4497	Endometrial progesterone-induced protein	2.4375	Tripeptidyl aminopeptidase
8.4083	Ankyrin-2	2.4358	Fibrous sheath component 2
8.3811	NSFL1 cofactor p47	2.4232	Septin-9
8.3505	Tubulin beta-2B chain	2.4097	67 kDa calelectrin
8.3209	HCNPpp	2.4096	Rho GTPase-activating protein 1
8.2784	Dihydropyrimidinase-related protein 2	2.4011	High density lipoprotein-binding protein
8.2337	p23	2.3805	5-aminoimidazole-4-carboxamide ribonucleotide formyltransferase
8.2304	Complex I-B14.5b	2.3711	A kinase (PRKA) anchor protein 2
8.2144	Inverted formin-2	2.3695	DnaJ homolog subfamily C member 2
8.1087	Putative uncharacterized protein Col6a3	2.3485	Citrate synthase, mitochondrial
8.0475	BAT2 domain-containing protein 1	2.34	Elongation factor 1-alpha 1
8.0437	Glutathione S-transferase omega-1	2.3276	Septin-11
7.9589	Microsomal signal peptidase 25 kDa subunit	2.3245	Isocitrate dehydrogenase 3 (NAD+) beta
7.9245	Ubiquitin conjugation factor E4 B	2.2946	15S Mg(2+)-ATPase p97 subunit
7.9011	Pyridoxal-dependent decarboxylase domain-containing protein 1	2.2821	11S regulator complex subunit alpha
7.7396	Myosin regulatory light chain 12B	2.2774	cAMP-dependent protein kinase catalytic subunit alpha
7.7071	Cavin-1	2.2748	Cytosolic NADP-isocitrate dehydrogenase
7.6894	Apoptosis regulator BAX	2.2475	SEC23-interacting protein
7.5652	Proline synthase co-transcribed bacterial homolog protein	2.2326	Ras-related protein Rab-18
7.5018	Alpha-tropomyosin	2.2252	Anchorin CII
7.4569	ADH-C2	2.1884	11S regulator complex subunit beta
7.3865	Alpha-2-macroglobulin receptor	2.163	ACC-alpha
7.2854	Procollagen-proline,2-oxoglutarate-4-dioxygenase subunit alpha-1	2.141	Spectrin alpha 2
7.2348	[Acyl-carrier-protein] S-acetyltransferase	2.1387	LIM and senescent cell antigen-like domains 1, isoform CRA_c
7.2067	Phosphoenolpyruvate carboxykinase [GTP], mitochondrial	2.128	Coronin-1B
7.1812	Glucocorticoid-attenuated response gene 16 protein	2.1224	Archain
7.1387	Annexin A1	2.1085	ERT1
6.9973	High mobility group protein 2	2.0955	Rab3 GTPase-activating protein 150 kDa subunit
6.9588	Synaptic vesicle membrane protein VAT-1 homolog	2.0832	Reticulon-3
6.9217	2,3-epoxysqualene--lanosterol cyclase	2.0818	Endopeptidase Clp
6.8851	Protein FAM129A	2.0808	Cytoplasmic FMR1-interacting protein 1
6.7669	Complex I-MLRQ	2.0578	Elongin 15 kDa subunit
6.7154	Eukaryotic translation initiation factor 2A	2.0542	GTP-binding protein MMR1
6.587	Dipeptidyl peptidase 9	2.0433	ATP synthase subunit O, mitochondrial
6.5257	Alpha-1 type I collagen	2.0424	Isopentenyl pyrophosphate isomerase 1
6.4314	Acetoacetyl-CoA synthetase	2.0364	Minichromosome maintenance deficient 5, cell division cycle 46 (S. cerevisiae)
6.4029	MCG140951	2.0353	Major vault protein

H/L Ratio	Protein	H/L Ratio	Protein
6.2763	Esterase 10	2.0311	Complex III subunit 1
6.2219	Cytochrome c oxidase polypeptide II	2.0243	Epithelial protein lost in neoplasm
6.1564	Ubiquitin-conjugating enzyme E2 variant 1	2.0229	Ras suppressor protein 1
6.1439	Thrombospondin-2	2.019	Deubiquitinating enzyme 5
6.0721	Alpha-N-acetylglucosaminidase	2.017	MEK-binding partner 1
6.0714	ADP-ribosylation factor 4	2.013	Protein LSM12 homolog
5.9181	Cellular myosin heavy chain, type A	2.0115	GTP-binding protein SAR1a
5.9124	Erythrocyte band 7 integral membrane protein	2.0112	Dynein cytoplasmic 1 intermediate chain 2
5.9021	14-3-3 protein eta	2.0052	Neurite outgrowth inhibitor
5.8577	Parathymosin		

Appendix 2.2 – Raw data from NUAK1 neuronal phosphoscreen (see Section 2.2.21.2

The highest ranking proteins have been ordered by the quantitative ratio of phosphopeptides detected in the 1µg experiment compared to the 5µg experiment. This ratio is labelled as "Phospho Ratio" and 2 was used as a threshold of sufficient increase.

Phospho Ratio	Protein	Phospho Ratio	Protein
10.4492	Voltage-dependent N-type calcium channel subunit alpha-1B	2.4492	Neuromodulin
7.5605	NUAK family SNF1-like kinase 1	2.4489	Heterogeneous nuclear ribonucleoproteins C1/C2
7.5566	U4/U6 small nuclear ribonucleoprotein Prp3	2.4386	Rho GTPase-activating protein 33
7.2565	Myotubularin-related protein 7	2.4382	Protein RUFY3
7.1870	NUAK family SNF1-like kinase 1	2.4311	Calnexin
7.1460	Transcription factor 20	2.4281	CTP synthase 1
7.1373	Rho GTPase-activating protein 10	2.4277	Microtubule-associated protein tau
7.1373	T-complex protein 1 subunit gamma	2.4231	Microtubule-associated protein 1B
6.5426	Syntaxin-binding protein 1	2.4220	Heat shock protein HSP 90-beta
6.0902	Transcriptional activator protein Pur-beta	2.4187	Myristoylated alanine-rich C-kinase substrate
5.9394	Heterogeneous nuclear ribonucleoproteins C1/C2	2.4119	Ankyrin-2
5.7815	Cadherin-12	2.4103	Transmembrane protein 55B
5.5190	Protein PRRC2A	2.4007	Protein-methionine sulfoxide oxidase MICAL3
5.3145	Disks large-associated protein 4	2.3977	60S ribosomal protein L14
5.3092	Amyloid beta A4 precursor protein-binding family A member 2	2.3952	Coronin-1A
5.2943	Serine/arginine repetitive matrix protein 1	2.3883	Cyclin-dependent kinase 16
5.2035	Coatomer subunit gamma-1	2.3858	BTB/POZ domain-containing protein KCTD4
5.1072	Serine/threonine-protein phosphatase 6 regulatory subunit 2	2.3851	Drebrin
5.0852	Heat shock protein HSP 90-beta	2.3815	Dystrophin
5.0482	Heat shock protein HSP 90-alpha	2.3803	Phosphatidylinositol 4-kinase beta
4.9492	Peripheral-type benzodiazepine receptor-associated protein 1	2.3728	Microtubule-associated protein 2
4.8865	THUMP domain-containing protein 1	2.3609	Ankyrin-2
4.8786	PC4 and SFRS1-interacting protein	2.3547	Myristoylated alanine-rich C-kinase substrate

Phospho Ratio	Protein	Phospho Ratio	Protein
4.7987	B-cell CLL/lymphoma 9 protein	2.3456	Ubiquitin carboxyl-terminal hydrolase 10
4.7039	Protein IWS1 homolog	2.3454	LIM domain-containing protein 2
4.6766	Heat shock protein HSP 90-alpha	2.3429	Gamma-tubulin complex component 3
4.6766	WASH complex subunit 7	2.3391	Heat shock protein HSP 90-beta
4.5338	Vacuolar protein sorting-associated protein 4B	2.3376	Pyridoxal-dependent decarboxylase domain-containing protein 1
4.5053	Translocation protein SEC62	2.3367	NCK-interacting protein with SH3 domain
4.4163	Dematin	2.3335	Protein phosphatase 1 regulatory subunit 1A
4.3980	Band 4.1-like protein 1	2.3259	CTTNBP2 N-terminal-like protein
4.3544	Dual specificity mitogen-activated protein kinase kinase 2	2.3254	Protein TANC2
4.2874	Heat shock protein HSP 90-alpha	2.3234	Catenin beta-1
4.2830	Microtubule-associated protein 1B	2.3188	SLIT-ROBO Rho GTPase-activating protein 2
4.0329	tRNA pseudouridine(38/39) synthase	2.3061	Neuronal membrane glycoprotein M6-a
3.9165	Heat shock protein HSP 90-alpha	2.3033	Adenomatous polyposis coli protein
3.9029	Myristoylated alanine-rich C-kinase substrate	2.2899	Calmodulin-regulated spectrin-associated protein 1
3.8958	Dihydropyrimidinase-related protein 2	2.2879	Catenin alpha-2
3.8682	T-complex protein 1 subunit gamma	2.2868	Reticulon-4
3.6936	Myristoylated alanine-rich C-kinase substrate	2.2829	Connector enhancer of kinase suppressor of ras 2
3.6863	Pinin	2.2801	Microtubule-associated protein 2
3.6714	MARCKS-related protein	2.2646	CREB-regulated transcription coactivator 1
3.6055	Obscurin	2.2597	Cyclic AMP-dependent transcription factor ATF-2
3.5733	Cutaneous T-cell lymphoma-associated antigen 5 homolog	2.2484	Serine/arginine repetitive matrix protein 2
3.5690	Dematin	2.2450	Soluble lamin-associated protein of 75 kDa
3.5665	Interleukin enhancer-binding factor 3	2.2389	Heat shock protein HSP 90-beta
3.5562	Traf2 and NCK-interacting protein kinase	2.2385	Myristoylated alanine-rich C-kinase substrate
3.5428	Microtubule-associated protein tau	2.2384	Protein phosphatase 1H
3.4887	Small glutamine-rich tetratricopeptide repeat-containing protein alpha	2.2378	Hepatoma-derived growth factor
3.4582	Myosin-9	2.2362	Serine/threonine-protein kinase PAK 1
3.4504	Myosin-9	2.2344	Ran-binding protein 3
3.4358	MARCKS-related protein	2.2221	Connector enhancer of kinase suppressor of ras 2
3.4028	Ras-related protein Rab-31	2.2184	Monocarboxylate transporter 1
3.3524	Heat shock protein HSP 90-beta	2.2129	Zinc finger Ran-binding domain-containing protein 2
3.3350	MARCKS-related protein	2.2122	Ataxin-2-like protein
3.3169	Splicing factor 45	2.2091	Kinesin light chain 1
3.3103	Unconventional myosin-Va	2.2074	MARCKS-related protein
3.2969	Inositol 1,4,5-trisphosphate receptor type 1	2.2073	Nestin
3.2832	Actin-binding LIM protein 1	2.2056	G protein-regulated inducer of neurite outgrowth 1
3.2812	Serine/arginine repetitive matrix protein 4	2.2047	Microtubule-associated protein 2
3.2573	Microtubule-associated protein 2	2.2044	Coiled-coil domain-containing protein 85A
3.2108	Numb-like protein	2.1995	CREB-regulated transcription coactivator 1
3.1912	Heat shock protein HSP 90-alpha	2.1983	Microtubule-actin cross-linking factor 1
3.1458	Microtubule-associated protein 2	2.1927	Heat shock protein HSP 90-beta

Phospho Ratio	Protein	Phospho Ratio	Protein
3.1133	Ankyrin-2	2.1895	Syntaxin-1A
3.1115	Microtubule-associated protein tau	2.1885	Phosphoglucomutase-1
3.0983	Band 4.1-like protein 1	2.1848	Dihydropyrimidinase-related protein 3
3.0926	Ankyrin-2	2.1790	RNA-binding protein 39
3.0805	Zinc finger CCCH domain-containing protein 18	2.1790	Hepatoma-derived growth factor-related protein 2
3.0736	Heat shock protein HSP 90-alpha	2.1737	Spectrin beta chain, non-erythrocytic 1
3.0388	Sphingosine kinase 2	2.1718	Calnexin
3.0171	Protein phosphatase 1 regulatory subunit 12A	2.1629	Gamma-adducin
3.0148	E3 ubiquitin-protein ligase HECW2	2.1616	Uncharacterized protein KIAA0930 homolog
2.9793	HIV Tat-specific factor 1 homolog	2.1597	CLK4-associating serine/arginine rich protein
2.9447	SLIT-ROBO Rho GTPase-activating protein 2	2.1594	Calnexin
2.9247	S-phase kinase-associated protein 1	2.1579	Neural cell adhesion molecule 1
2.9144	Arginine-glutamic acid dipeptide repeats protein	2.1575	Protein piccolo
2.9044	Guanine nucleotide-binding protein G(I)/G(S)/G(O) subunit gamma-3	2.1551	Nuclear ubiquitous casein and cyclin-dependent kinase substrate 1
2.8968	Probable phospholipid-transporting ATPase IA	2.1507	Calmodulin-regulated spectrin-associated protein 2
2.8855	Hydroxymethylglutaryl-CoA synthase, cytoplasmic	2.1493	SUZ domain-containing protein 1
2.8603	Microtubule-associated protein tau	2.1492	cAMP-specific 3',5'-cyclic phosphodiesterase 4D
2.8547	RNA polymerase-associated protein LEO1	2.1434	Interleukin enhancer-binding factor 3
2.8490	Ubiquitin-conjugating enzyme E2 E3	2.1394	Target of Myb protein 1
2.8312	Synapsin-2	2.1378	Reticulon-4
2.7790	Apoptotic chromatin condensation inducer in the nucleus	2.1350	Serine/arginine repetitive matrix protein 2
2.7631	Transmembrane protein 55B	2.1345	Serine/arginine repetitive matrix protein 2
2.7619	Coilin	2.1343	Centrosome and spindle pole associated protein 1
2.7591	T-box brain protein 1	2.1301	La-related protein 1
2.7527	Sickle tail protein	2.1271	Epidermal growth factor receptor substrate 15-like 1
2.7527	Serine/threonine-protein kinase PRP4 homolog	2.1234	Heat shock protein HSP 90-alpha
2.7456	Protein phosphatase 1 regulatory subunit 7	2.1221	Microtubule-associated protein 1B
2.7303	Microtubule-associated protein 1B	2.1221	Pinin
2.7268	Probable E3 ubiquitin-protein ligase MYCBP2	2.1181	Ral GTPase-activating protein subunit beta
2.7210	Ankyrin-2	2.1163	Band 4.1-like protein 1
2.7157	Serine/arginine repetitive matrix protein 2	2.1159	Eukaryotic translation initiation factor 4 gamma 1
2.6917	Activating transcription factor 7-interacting protein 1	2.1131	Activating transcription factor 7-interacting protein 2
2.6863	MARCKS-related protein	2.1124	Brain acid soluble protein 1
2.6837	Stathmin	2.1099	N-alpha-acetyltransferase 25, NatB auxiliary subunit
2.6794	Dihydropyrimidinase-related protein 5	2.1096	Coiled-coil domain-containing protein 85A
2.6678	Serine/arginine repetitive matrix protein 2	2.1090	Uncharacterized protein KIAA1211
2.6650	Hepatoma-derived growth factor	2.1018	Protein SOGA1
2.6611	Unconventional myosin-Va	2.1018	Treacle protein
2.6599	Neuralized-like protein 4	2.0987	Shootin-1

Phospho Ratio	Protein	Phospho Ratio	Protein
2.6584	Ras-related protein Rab-31	2.0977	A-kinase anchor protein 5
2.6465	26S proteasome non-ATPase regulatory subunit 1	2.0949	Vacuolar protein sorting-associated protein 26B
2.6395	Neural cell adhesion molecule 1	2.0896	Serine/arginine repetitive matrix protein 2
2.6221	Inactive phospholipase C-like protein 2	2.0840	Interferon regulatory factor 2-binding protein-like
2.6154	Protein IWS1 homolog	2.0835	Brain acid soluble protein 1
2.6142	Nuclear ubiquitous casein and cyclin-dependent kinase substrate 1	2.0833	Ras-related protein R-Ras2
2.6062	Brain acid soluble protein 1	2.0625	Myotubularin-related protein 3
2.5896	Myristoylated alanine-rich C-kinase substrate	2.0613	Elongation factor 1-delta
2.5876	Band 4.1-like protein 4A	2.0596	Phosphoribosyl pyrophosphate synthase-associated protein 2
2.5867	Synergin gamma	2.0594	Microtubule-associated protein 4
2.5858	Adenomatous polyposis coli protein	2.0558	Serine/threonine-protein kinase LMTK3
2.5717	182 kDa tankyrase-1-binding protein	2.0552	Tumor suppressor p53-binding protein 1
2.5704	cAMP-dependent protein kinase catalytic subunit beta	2.0518	E3 ubiquitin-protein ligase HECW1
2.5682	Elongation factor 1-delta	2.0484	G-protein-signaling modulator 1
2.5635	Microtubule-associated protein 2	2.0467	Protein LSM12 homolog
2.5275	TBC1 domain family member 24	2.0429	Serine/arginine repetitive matrix protein 1
2.5236	Heat shock protein HSP 90-beta	2.0421	Putative RNA-binding protein 15B
2.5235	Dedicator of cytokinesis protein 7	2.0365	Glutamate receptor-interacting protein 1
2.5201	Mitogen-activated protein kinase kinase kinase kinase 4	2.0350	Reticulon-4
2.5200	Protein TANC2	2.0344	Ankyrin-2
2.5121	Calcium/calmodulin-dependent protein kinase kinase 2	2.0307	Reticulon-4
2.4950	Reticulon-4	2.0302	Microtubule-associated protein 1B
2.4912	Beta-adducin	2.0187	Abnormal spindle-like microcephaly-associated protein homolog
2.4878	Guanine nucleotide-binding protein G(I)/G(S)/G(O) subunit gamma-2	2.0179	Alstrom syndrome protein 1 homolog
2.4816	Pre-mRNA-splicing factor CWC22 homolog	2.0162	G protein-regulated inducer of neurite outgrowth 1
2.4815	Heat shock protein HSP 90-beta	2.0147	Protein kinase C epsilon type
2.4805	Rho guanine nucleotide exchange factor 12	2.0124	Sodium/calcium exchanger 1
2.4796	Regulating synaptic membrane exocytosis protein 2	2.0099	Serine/arginine repetitive matrix protein 2
2.4718	Heat shock protein HSP 90-beta	2.0083	Transcription intermediary factor 1-alpha
2.4496	MARCKS-related protein	2.0065	Dedicator of cytokinesis protein 7

Appendix 2.3 – Raw data from NUAK1 SILAC IP (see Section 2.2.21.3)

The highest ranking proteins have been ordered by the number of unique peptide hits that varied between the "heavy" immunoprecipitate and the "light" immunoprecipitate.

Rank	Protein	Rank	Protein
1	AMPK-related protein kinase 5;NUAK family SNF	69	Activator interaction domain-containing protein 2
2	Myosin phosphatase-targeting subunit 1;Protein phosphatase 1 regulatory subunit	70	ER lumen protein retaining receptor 2
3	14-3-3 protein epsilon	71	4F2 cell-surface antigen heavy chain
4	14-3-3 protein eta	72	Calcium-binding protein ERC-55
5	ATP synthase subunit alpha, mitochondrial	73	CTCL tumor antigen se20-10
6	Damage-specific DNA-binding protein 1	74	Solute carrier family 35 member E1
7	Putative uncharacterized protein CWC22	75	One-twenty two protein 1
8	14-3-3 protein gamma	76	Medium tumor antigen-associated 61 kDa protein
9	14-3-3 protein zeta/delta	77	DDB1- and CUL4-associated factor 1
10	Deubiquitinating enzyme 7	78	Histone H1.3
11	Coatomer subunit gamma-2	79	Ribonucleases P/MRP protein subunit POP1
12	DNA-directed RNA polymerase II 140 kDa polypeptide	80	Ser/Arg-related nuclear matrix protein
13	Heterogeneous nuclear ribonucleoprotein K	81	Fas ligand-associated factor 1
14	SAPS domain family member 3	82	EEF1A protein
15	Protein phosphatase 1 regulatory subunit 22	83	DNA polymerase delta subunit 3
16	Importin-9	84	FAST kinase domain-containing protein 5
17	Emerin	85	Cleavage and polyadenylation specificity factor 100 kDa subunit
18	DnaJ homolog subfamily A member 1	86	NF-X1-type zinc finger protein NFXL1
19	F-box and WD repeats protein beta-TrCP2	87	NMDA receptor-regulated protein 2
20	CUL4- and DDB1-associated WDR protein 2	88	Chorea-acanthocytosis protein
21	Putative uncharacterized protein HCFC1	89	cDNA FLJ77771, highly similar to Homo sapiens replication initiator 1, mRNA
22	Adapter-related protein complex 3 subunit beta-1	90	Zinc finger protein 3
23	Protein clk-2 homolog	91	CT-ZFP48
24	Importin subunit beta-1	92	Protein FAM83H
25	Deubiquitinating enzyme FAF-X	93	Importin subunit beta-3
26	Breakpoint cluster region protein 2	94	cDNA FLJ11352 fis, clone HEMBA1000020, highly similar to Tubulin beta-2C chain
27	Serine/threonine-protein phosphatase PP1-beta catalytic subunit	95	cDNA FLJ56823, highly similar to Protein-glutamine gamma-glutamyltransferase E (EC 2.3.2.13)
28	Proteasome (Prosome, macropain) 26S subunit, non-ATPase, 6, isoform CRA_b	96	Delta transcription factor
29	Deubiquitinating enzyme 11	97	ATP-dependent metalloprotease FtsH1

Rank	Protein	Rank	Protein
30	300 kDa nuclear matrix antigen	98	ATP-dependent RNA helicase DDX18
31	Protein phosphatase 1 myosin-binding subunit of 85 kDa	99	Glutaminyl-peptide cyclotransferase-like protein
32	O-GlcNAc transferase subunit p110	100	60S ribosomal protein L37a
33	140 kDa nuclear and cell adhesion-related phosphoprotein	101	cDNA FLJ16129 fis, clone BRACE2039823, highly similar to CDP-diacylglycerol--inositol3-phosphatidyltransferase (EC 2.7.8.11)
34	TRM1-like protein	102	PAI1 RNA-binding protein 1
35	Swd2	103	Mitochondrial 20 kDa outer membrane protein
36	hSGT2	104	cDNA FLJ56334, highly similar to SEC13-related protein
37	60S ribosomal protein L17	105	Binder of OVCA1-1
38	Fanconi anemia group I protein	106	Histone H3.3
39	Protein phosphatase 1C catalytic subunit	107	60S ribosomal protein L30
40	BMP2-induced 3-kb gene protein	108	28S ribosomal protein S23
41	GCUNC-45	109	28 kDa heat shock protein
42	APOBEC1-binding protein 2	110	Cell division cycle 5-like protein
43	Protein SCO1 homolog, mitochondrial	111	Zinc finger protein 598
44	Adenine nucleotide translocator 1	112	ElaC homolog protein 2
45	RING finger protein 219	113	Conventional kinesin heavy chain
46	Dolichyl-diphosphooligosaccharide--protein glycosyltransferase 48 kDa subunit	114	Testis-expressed sequence 10 protein
47	6-phosphofructokinase, liver type	115	3D3/LYRIC
48	Long-chain fatty acid transport protein 4	116	Nucleolar protein 1
49	cDNA FLJ58665, highly similar to Serine/threonine-protein phosphatase 2A 55 kDa regulatory subunit B alpha isoform	117	Putative uncharacterized protein DKFZp686M24262
50	Cullin-associated and neddylation-dissociated protein 1	118	HBV pre-S2 trans-regulated protein 2
51	AIR carboxylase	119	Flavoprotein subunit of complex II
52	Pre-mRNA-splicing factor SRP75	120	DNA-directed RNA polymerase, mitochondrial
53	80 kDa nuclear cap-binding protein	121	Heterogeneous nuclear ribonucleoprotein U-like protein 2
54	RNA-binding motif protein 34	122	DEAH box protein 36
55	Cytoplasmic dynein 1 intermediate chain 2	123	UPF0488 protein C8orf33
56	MAP7 domain-containing protein 2	124	cDNA FLJ76962, highly similar to Homo sapiens nucleolar protein 5A (56kDa with KKE/D repeat) (NOL5A), mRNA
57	aarF domain-containing protein kinase 3	125	Bromodomain and WD repeat-containing protein 2
58	14-3-3 protein beta/alpha	126	Coiled-coil domain-containing protein 8
59	Met-induced mitochondrial protein	127	Novel nuclear protein 1
60	HCLS1-associated protein X-1	128	BCL-6 corepressor-like protein 1
61	H/ACA ribonucleoprotein complex non-core subunit NAF1	129	28S ribosomal protein S31, mitochondrial

Rank	Protein	Rank	Protein
62	NAP-1-related protein	130	Zinc finger CCHC domain-containing protein 10
63	cAMP-dependent protein kinase catalytic subunit alpha	131	Conserved ERA-like GTPase
64	Ran-binding protein 10	132	60 kDa chaperonin
65	Condensin-2 complex subunit D3	133	Histone H1.2
66	E3RSIkappaB	134	Histone H1
67	Macropain chain Z	135	Histone H1.4
68	ARM protein lost in epithelial cancers on chromosome X 3		

Appendix 3 – Original identification of NUAK1 and 14-3-3ε binding

FLAG tagged NUAK1 was transfected into HEK293T cells and immunoprecipitated with M2-FLAG resin and eluted with FLAG peptide. The eluted protein was further purified by size exclusion on the SMART system, resolved on a 10% SDS-PAGE Tris-Glycine gel and silver stained.
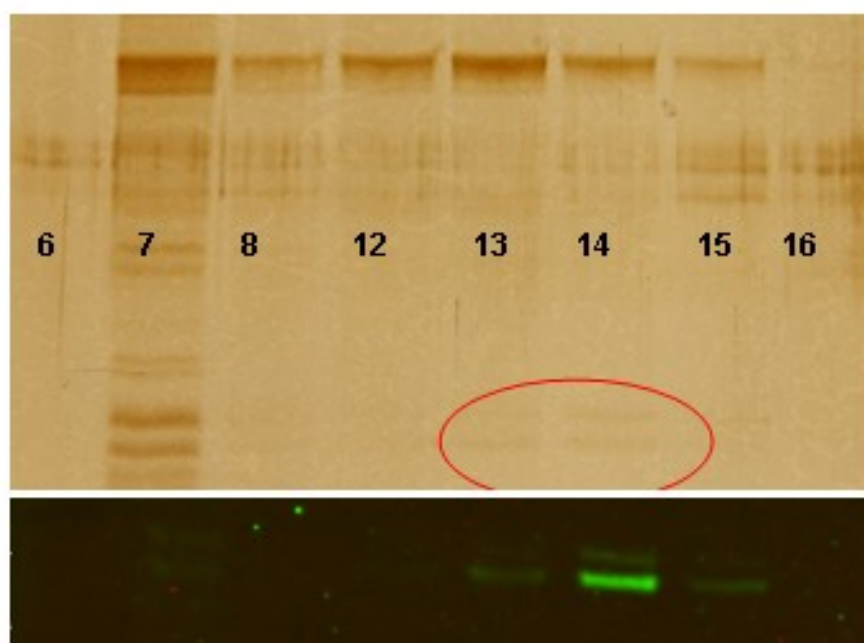
An equivalent gel was transferred to Immobilon FL PVDF membrane for immunoblotting with anti-pan-14-3-3 antibody and is shown superimposed over the same fractions below the gel. The indicated bands were dissected from the gel and analysed by mass spectrometry.

IPI00000816 (100%), 29,175.0 Da
YWHAE 14-3-3 protein epsilon
9 unique peptides, 10 unique spectra, 14 total spectra, 96/255 amino acids (38% coverage)

```
MDDREDLVYQ  AKLAEQAERY  DEMVESMKKV  AGMDVELTVE  ERNLLSVAYK
NVIGARRASW  RIISSIEQKE  ENKGGEDKLK  MIREYRQMVE  TELKLICCDI
LDVLDKHLIP  AANTGESKVF  YYKMKGDYHR  YLAEFATGND  RKEAAENSLV
AYKAASDIAM  TELPPTHPIR  LGLALNFSVF  YYEILNSPDR  ACRLAKAAFD
DAIAELDTLS  EESYKDSTLI  MQLLRDNLTL  WTSDMQGDGE  EQNKEALQDV
EDENQ
```

The protein that co-purified with NUAK1 was identified specifically as 14-3-3ε. One peptide for another isoform of 14-3-3 was detected but it was confidently identified as the primarily the epsilon isoform.

References

Aitken, A. (2006). 14-3-3 proteins: a historic overview. Semin Cancer Biol *16*, 162-172.

Akhurst, B., Croager, E.J., Farley-Roche, C.A., Ong, J.K., Dumble, M.L., Knight, B., and Yeoh, G.C. (2001). A modified choline-deficient, ethionine-supplemented diet protocol effectively induces oval cells in mouse liver. Hepatology *34*, 519-522.

Al-Hakim, A.K., Goransson, O., Deak, M., Toth, R., Campbell, D.G., Morrice, N.A., Prescott, A.R., and Alessi, D.R. (2005). 14-3-3 cooperates with LKB1 to regulate the activity and localization of QSK and SIK. J Cell Sci *118*, 5661-5673.

Al-Hakim, A.K., Zagorska, A., Chapman, L., Deak, M., Peggie, M., and Alessi, D.R. (2008). Control of AMPK-related kinases by USP9X and atypical Lys(29)/Lys(33)-linked polyubiquitin chains. Biochem J *411*, 249-260.

Alessi, D., MacDougall, L.K., Sola, M.M., Ikebe, M., and Cohen, P. (1992). The control of protein phosphatase-1 by targetting subunits. The major myosin phosphatase in avian smooth muscle is a novel form of protein phosphatase-1. Eur J Biochem *210*, 1023-1035.

Alessi, D.R., Sakamoto, K., and Bayascas, J.R. (2006). LKB1-dependent signaling pathways. Annu Rev Biochem *75*, 137-163.

Anderson, K.A., and Kane, C.D. (1998). Ca2+/calmodulin-dependent protein kinase IV and calcium signaling. Biometals *11*, 331-343.

Andersson, U., Filipsson, K., Abbott, C.R., Woods, A., Smith, K., Bloom, S.R., Carling, D., and Small, C.J. (2004). AMP-activated protein kinase plays a role in the control of food intake. J Biol Chem *279*, 12005-12008.

Ayadi, A., Birling, M.C., Bottomley, J., Bussell, J., Fuchs, H., Fray, M., Gailus-Durner, V., Greenaway, S., Houghton, R., Karp, N.*, et al.* (2012). Mouse large-scale phenotyping initiatives: overview of the European Mouse Disease Clinic (EUMODIC) and of the Wellcome Trust Sanger Institute Mouse Genetics Project. Mamm Genome *23*, 600-610.

Baas, A.F., Kuipers, J., van der Wel, N.N., Batlle, E., Koerten, H.K., Peters, P.J., and Clevers, H.C. (2004). Complete polarization of single intestinal epithelial cells upon activation of LKB1 by STRAD. Cell *116*, 457-466.

Bachmann, M., Hennemann, H., Xing, P.X., Hoffmann, I., and Moroy, T. (2004). The oncogenic serine/threonine kinase Pim-1 phosphorylates and inhibits the activity of Cdc25C-associated kinase 1 (C-TAK1): a novel role for Pim-1 at the G2/M cell cycle checkpoint. J Biol Chem *279*, 48319-48328.

Ballif, B.A., Cao, Z., Schwartz, D., Carraway, K.L., 3rd, and Gygi, S.P. (2006). Identification of 14-3-3epsilon substrates from embryonic murine brain. J Proteome Res *5*, 2372-2379.

Banko, M.R., Allen, J.J., Schaffer, B.E., Wilker, E.W., Tsou, P., White, J.L., Villen, J., Wang, B., Kim, S.R., Sakamoto, K.*, et al.* (2011). Chemical genetic screen for AMPKalpha2 substrates uncovers a network of proteins involved in mitosis. Mol Cell *44*, 878-892.

Bardeesy, N., Sinha, M., Hezel, A.F., Signoretti, S., Hathaway, N.A., Sharpless, N.E., Loda, M., Carrasco, D.R., and DePinho, R.A. (2002). Loss of the Lkb1 tumour suppressor provokes intestinal polyposis but resistance to transformation. Nature *419*, 162-167.

Barnes, A.P., Lilley, B.N., Pan, Y.A., Plummer, L.J., Powell, A.W., Raines, A.N., Sanes, J.R., and Polleux, F. (2007). LKB1 and SAD kinases define a pathway required for the polarization of cortical neurons. Cell *129*, 549-563.

Barnes, K., Ingram, J.C., Porras, O.H., Barros, L.F., Hudson, E.R., Fryer, L.G., Foufelle, F., Carling, D., Hardie, D.G., and Baldwin, S.A. (2002). Activation of GLUT1 by metabolic and osmotic stress: potential involvement of AMP-activated protein kinase (AMPK). J Cell Sci *115*, 2433-2442.

Beghini, A., Magnani, I., Roversi, G., Piepoli, T., Di Terlizzi, S., Moroni, R.F., Pollo, B., Fuhrman Conti, A.M., Cowell, J.K., Finocchiaro, G.*, et al.* (2003). The neural progenitor-restricted isoform of the MARK4 gene in 19q13.2 is upregulated in human gliomas and overexpressed in a subset of glioblastoma cell lines. Oncogene *22*, 2581-2591.

Bell, R.E., Khaled, M., Netanely, D., Schubert, S., Golan, T., Buxbaum, A., Janas, M.M., Postolsky, B., Goldberg, M.S., Shamir, R.*, et al.* (2013). Transcription Factor/microRNA Axis Blocks Melanoma Invasion Program by miR-211 Targeting NUAK1. J Invest Dermatol.

Bessone, S., Vidal, F., Le Bouc, Y., Epelbaum, J., Bluet-Pajot, M.T., and Darmon, M. (1999). EMK protein kinase-null mice: dwarfism and hypofertility associated with alterations in the somatotrope and prolactin pathways. Dev Biol *214*, 87-101.

Bettencourt-Dias, M., Giet, R., Sinka, R., Mazumdar, A., Lock, W.G., Balloux, F., Zafiropoulos, P.J., Yamaguchi, S., Winter, S., Carthew, R.W.*, et al.* (2004). Genome-wide survey of protein kinases required for cell cycle progression. Nature *432*, 980-987.

Boudeau, J., Baas, A.F., Deak, M., Morrice, N.A., Kieloch, A., Schutkowski, M., Prescott, A.R., Clevers, H.C., and Alessi, D.R. (2003). MO25alpha/beta interact with STRADalpha/beta enhancing their ability to bind, activate and localize LKB1 in the cytoplasm. EMBO J *22*, 5102-5114.

Boudeau, J., Scott, J.W., Resta, N., Deak, M., Kieloch, A., Komander, D., Hardie, D.G., Prescott, A.R., van Aalten, D.M., and Alessi, D.R. (2004). Analysis of the LKB1-STRAD-MO25 complex. J Cell Sci *117*, 6365-6375.

Boulter, L., Govaere, O., Bird, T.G., Radulescu, S., Ramachandran, P., Pellicoro, A., Ridgway, R.A., Seo, S.S., Spee, B., Van Rooijen, N.*, et al.* (2012). Macrophage-derived Wnt opposes Notch signaling to specify hepatic progenitor cell fate in chronic liver disease. Nat Med *18*, 572-579.

Brajenovic, M., Joberty, G., Kuster, B., Bouwmeester, T., and Drewes, G. (2004). Comprehensive proteomic analysis of human Par protein complexes reveals an interconnected protein network. J Biol Chem *279*, 12804-12811.

Brewer, S., and Williams, T. (2004a). Finally, a sense of closure? Animal models of human ventral body wall defects. Bioessays *26*, 1307-1321.

Brewer, S., and Williams, T. (2004b). Loss of AP-2alpha impacts multiple aspects of ventral body wall development and closure. Dev Biol *267*, 399-417.

Bright, N.J., Carling, D., and Thornton, C. (2008). Investigating the regulation of brain-specific kinases 1 and 2 by phosphorylation. J Biol Chem *283*, 14946-14954.

Bright, N.J., Thornton, C., and Carling, D. (2009). The regulation and function of mammalian AMPK-related kinases. Acta Physiol (Oxf) *196*, 15-26.

Buerger, A., Rozhitskaya, O., Sherwood, M.C., Dorfman, A.L., Bisping, E., Abel, E.D., Pu, W.T., Izumo, S., and Jay, P.Y. (2006). Dilated cardiomyopathy resulting from high-level myocardial expression of Cre-recombinase. J Card Fail *12*, 392-398.

Calle, E.E., Rodriguez, C., Walker-Thurmond, K., and Thun, M.J. (2003). Overweight, obesity, and mortality from cancer in a prospectively studied cohort of U.S. adults. N Engl J Med *348*, 1625-1638.

Canto, C., and Auwerx, J. (2010). AMP-activated protein kinase and its downstream transcriptional pathways. Cell Mol Life Sci *67*, 3407-3423.

Carey, R.M., and Siragy, H.M. (2003). Newly recognized components of the renin-angiotensin system: potential roles in cardiovascular and renal regulation. Endocr Rev *24*, 261-271.

Carling, D. (2004). The AMP-activated protein kinase cascade--a unifying system for energy control. Trends Biochem Sci *29*, 18-24.

Carling, D., Clarke, P.R., Zammit, V.A., and Hardie, D.G. (1989). Purification and characterization of the AMP-activated protein kinase. Copurification of acetyl-CoA carboxylase kinase and 3-hydroxy-3-methylglutaryl-CoA reductase kinase activities. Eur J Biochem *186*, 129-136.

Carling, D., and Hardie, D.G. (1989). The substrate and sequence specificity of the AMP-activated protein kinase. Phosphorylation of glycogen synthase and phosphorylase kinase. Biochim Biophys Acta *1012*, 81-86.

Carling, D., Thornton, C., Woods, A., and Sanders, M.J. (2012). AMP-activated protein kinase: new regulation, new roles? Biochem J *445*, 11-27.

Carninci, P., Kasukawa, T., Katayama, S., Gough, J., Frith, M.C., Maeda, N., Oyama, R., Ravasi, T., Lenhard, B., Wells, C.*, et al.* (2005). The transcriptional landscape of the mammalian genome. Science *309*, 1559-1563.

Caron, E., Ghosh, S., Matsuoka, Y., Ashton-Beaucage, D., Therrien, M., Lemieux, S., Perreault, C., Roux, P.P., and Kitano, H. (2010). A comprehensive map of the mTOR signaling network. Mol Syst Biol *6*, 453.

Carvajal, K., Zarrinpashneh, E., Szarszoi, O., Joubert, F., Athea, Y., Mateo, P., Gillet, B., Vaulont, S., Viollet, B., Bigard, X.*, et al.* (2007). Dual cardiac contractile effects of the alpha2-AMPK deletion in low-flow ischemia and reperfusion. Am J Physiol Heart Circ Physiol *292*, H3136-3147.

Carvajal, L.A., and Manfredi, J.J. (2013). Another fork in the road--life or death decisions by the tumour suppressor p53. EMBO Rep *14*, 414-421.

Casado, P., Rodriguez-Prados, J.C., Cosulich, S.C., Guichard, S., Vanhaesebroeck, B., Joel, S., and Cutillas, P.R. (2013). Kinase-substrate enrichment analysis provides insights into the heterogeneity of signaling pathway activation in leukemia cells. Sci Signal *6*, rs6.

Chajes, V., Cambot, M., Moreau, K., Lenoir, G.M., and Joulin, V. (2006). Acetyl-CoA carboxylase alpha is essential to breast cancer cell survival. Cancer Res *66*, 5287-5294.

Chang, X.Z., Yu, J., Liu, H.Y., Dong, R.H., and Cao, X.C. (2012). ARK5 is associated with the invasive and metastatic potential of human breast cancer cells. J Cancer Res Clin Oncol *138*, 247-254.

Chen, P., Li, K., Liang, Y., Li, L., and Zhu, X. (2013a). High NUAK1 expression correlates with poor prognosis and involved in NSCLC cells migration and invasion. Exp Lung Res *39*, 9-17.

Chen, Y.M., Wang, Q.J., Hu, H.S., Yu, P.C., Zhu, J., Drewes, G., Piwnica-Worms, H., and Luo, Z.G. (2006). Microtubule affinity-regulating kinase 2 functions downstream of the PAR-3/PAR-6/atypical PKC complex in regulating hippocampal neuronal polarity. Proc Natl Acad Sci U S A *103*, 8534-8539.

Chen, Z., Shen, X., Shen, F., Zhong, W., Wu, H., Liu, S., and Lai, J. (2013b). TAK1 activates AMPK-dependent cell death pathway in hydrogen peroxide-treated cardiomyocytes, inhibited by heat shock protein-70. Mol Cell Biochem *377*, 35-44.

Cheng, S.W., Fryer, L.G., Carling, D., and Shepherd, P.R. (2004). Thr2446 is a novel mammalian target of rapamycin (mTOR) phosphorylation site regulated by nutrient status. J Biol Chem *279*, 15719-15722.

Clark, K., Plater, L., Peggie, M., and Cohen, P. (2009). Use of the pharmacological inhibitor BX795 to study the regulation and physiological roles of TBK1 and IkappaB kinase epsilon: a distinct upstream kinase mediates Ser-172 phosphorylation and activation. J Biol Chem *284*, 14136-14146.

Clarke, P.R., and Hardie, D.G. (1990). Regulation of HMG-CoA reductase: identification of the site phosphorylated by the AMP-activated protein kinase in vitro and in intact rat liver. EMBO J *9*, 2439-2446.

Courchet, J., Lewis, T.L., Jr., Lee, S., Courchet, V., Liou, D.Y., Aizawa, S., and Polleux, F. (2013). Terminal Axon Branching Is Regulated by the LKB1-NUAK1 Kinase Pathway via Presynaptic Mitochondrial Capture. Cell *153*, 1510-1525.

Crump, J.G., Zhen, M., Jin, Y., and Bargmann, C.I. (2001). The SAD-1 kinase regulates presynaptic vesicle clustering and axon termination. Neuron *29*, 115-129.

Cui, J., Yu, Y., Lu, G.F., Liu, C., Liu, X., Xu, Y.X., and Zheng, P.Y. (2013). Overexpression of ARK5 is associated with poor prognosis in hepatocellular carcinoma. Tumour Biol *34*, 1913-1918.

Dai, D.F., and Rabinovitch, P. (2011). Mitochondrial oxidative stress mediates induction of autophagy and hypertrophy in angiotensin-II treated mouse hearts. Autophagy *7*, 917-918.

Dale, S., Wilson, W.A., Edelman, A.M., and Hardie, D.G. (1995). Similar substrate recognition motifs for mammalian AMP-activated protein kinase, higher plant HMG-CoA reductase kinase-A, yeast SNF1, and mammalian calmodulin-dependent protein kinase I. FEBS Lett *361*, 191-195.

Dantas, A.P., and Sandberg, K. (2005). Regulation of ACE2 and ANG-(1-7) in the aorta: new insights into the renin-angiotensin system in the control of vascular function. Am J Physiol Heart Circ Physiol *289*, H980-981.

Davies, S.P., Carling, D., and Hardie, D.G. (1989). Tissue distribution of the AMP-activated protein kinase, and lack of activation by cyclic-AMP-dependent protein kinase, studied using a specific and sensitive peptide assay. Eur J Biochem *186*, 123-128.

Davies, S.P., Helps, N.R., Cohen, P.T., and Hardie, D.G. (1995). 5'-AMP inhibits dephosphorylation, as well as promoting phosphorylation, of the AMP-activated protein kinase. Studies using bacterially expressed human protein phosphatase-2C alpha and native bovine protein phosphatase-2AC. FEBS Lett *377*, 421-425.

Denison, F.C., Hiscock, N.J., Carling, D., and Woods, A. (2009). Characterization of an alternative splice variant of LKB1. J Biol Chem *284*, 67-76.

Denison, F.C., Smith, L.B., Muckett, P.J., O'Hara, L., Carling, D., and Woods, A. (2011). LKB1 is an essential regulator of spermatozoa release during spermiation in the mammalian testis. PLoS One *6*, e28306.

Dentin, R., Liu, Y., Koo, S.H., Hedrick, S., Vargas, T., Heredia, J., Yates, J., 3rd, and Montminy, M. (2007). Insulin modulates gluconeogenesis by inhibition of the coactivator TORC2. Nature *449*, 366-369.

Dong, J., Feldmann, G., Huang, J., Wu, S., Zhang, N., Comerford, S.A., Gayyed, M.F., Anders, R.A., Maitra, A., and Pan, D. (2007). Elucidation of a universal size-control mechanism in Drosophila and mammals. Cell *130*, 1120-1133.

Drewes, G., Ebneth, A., Preuss, U., Mandelkow, E.M., and Mandelkow, E. (1997). MARK, a novel family of protein kinases that phosphorylate microtubule-associated proteins and trigger microtubule disruption. Cell *89*, 297-308.

Dunker, N., and Krieglstein, K. (2002). Tgfbeta2 -/- Tgfbeta3 -/- double knockout mice display severe midline fusion defects and early embryonic lethality. Anat Embryol (Berl) *206*, 73-83.

Dyck, J.R., and Lopaschuk, G.D. (2006). AMPK alterations in cardiac physiology and pathology: enemy or ally? J Physiol *574*, 95-112.

Dymecki, S.M. (1996). Flp recombinase promotes site-specific DNA recombination in embryonic stem cells and transgenic mice. Proc Natl Acad Sci U S A *93*, 6191-6196.

Egan, D.F., Shackelford, D.B., Mihaylova, M.M., Gelino, S., Kohnz, R.A., Mair, W., Vasquez, D.S., Joshi, A., Gwinn, D.M., Taylor, R.*, et al.* (2011). Phosphorylation of ULK1 (hATG1) by AMP-activated protein kinase connects energy sensing to mitophagy. Science *331*, 456-461.

El-Serag, H.B. (2004). Hepatocellular carcinoma: recent trends in the United States. Gastroenterology *127*, S27-34.

El-Serag, H.B. (2011). Hepatocellular carcinoma. N Engl J Med *365*, 1118-1127.

El-Serag, H.B., Hampel, H., and Javadi, F. (2006). The association between diabetes and hepatocellular carcinoma: a systematic review of epidemiologic evidence. Clin Gastroenterol Hepatol *4*, 369-380.

El-Serag, H.B., and Mason, A.C. (1999). Rising incidence of hepatocellular carcinoma in the United States. N Engl J Med *340*, 745-750.

Ferrario, C.M. (2011). ACE2: more of Ang-(1-7) or less Ang II? Curr Opin Nephrol Hypertens *20*, 1-6.

Fickert, P., Stoger, U., Fuchsbichler, A., Moustafa, T., Marschall, H.U., Weiglein, A.H., Tsybrovskyy, O., Jaeschke, H., Zatloukal, K., Denk, H.*, et al.* (2007). A new xenobiotic-induced mouse model of sclerosing cholangitis and biliary fibrosis. Am J Pathol *171*, 525-536.

Fisher, J.S., Ju, J.S., Oppelt, P.J., Smith, J.L., Suzuki, A., and Esumi, H. (2005). Muscle contractions, AICAR, and insulin cause phosphorylation of an AMPK-related kinase. Am J Physiol Endocrinol Metab *289*, E986-992.

Foretz, M., Carling, D., Guichard, C., Ferre, P., and Foufelle, F. (1998). AMP-activated protein kinase inhibits the glucose-activated expression of fatty acid synthase gene in rat hepatocytes. J Biol Chem *273*, 14767-14771.

Frigo, D.E., Howe, M.K., Wittmann, B.M., Brunner, A.M., Cushman, I., Wang, Q., Brown, M., Means, A.R., and McDonnell, D.P. (2011). CaM kinase kinase beta-mediated activation of the growth regulatory kinase AMPK is required for androgen-dependent migration of prostate cancer cells. Cancer Res *71*, 528-537.

Fu, D., Lippincott-Schwartz, J., and Arias, I.M. (2011). Cellular mechanism of bile acid-accelerated hepatocyte polarity. Small GTPases *2*, 314-317.

Fu, D., Wakabayashi, Y., Ido, Y., Lippincott-Schwartz, J., and Arias, I.M. (2010). Regulation of bile canalicular network formation and maintenance by AMP-activated protein kinase and LKB1. J Cell Sci *123*, 3294-3302.

Fujimoto, T., Yurimoto, S., Hatano, N., Nozaki, N., Sueyoshi, N., Kameshita, I., Mizutani, A., Mikoshiba, K., Kobayashi, R., and Tokumitsu, H. (2008). Activation of SAD kinase by Ca2+/calmodulin-dependent protein kinase kinase. Biochemistry *47*, 4151-4159.

Gamblin, T.C., Berry, R.W., and Binder, L.I. (2003). Tau polymerization: role of the amino terminus. Biochemistry *42*, 2252-2257.

Gong, S., Doughty, M., Harbaugh, C.R., Cummins, A., Hatten, M.E., Heintz, N., and Gerfen, C.R. (2007). Targeting Cre recombinase to specific neuron populations with bacterial artificial chromosome constructs. J Neurosci *27*, 9817-9823.

Goransson, O., Deak, M., Wullschleger, S., Morrice, N.A., Prescott, A.R., and Alessi, D.R. (2006). Regulation of the polarity kinases PAR-1/MARK by 14-3-3 interaction and phosphorylation. J Cell Sci *119*, 4059-4070.

Gowans, G.J., Hawley, S.A., Ross, F.A., and Hardie, D.G. (2013). AMP is a true physiological regulator of AMP-activated protein kinase by both allosteric activation and enhancing net phosphorylation. Cell Metab *18*, 556-566.

Grady, E.F., Sechi, L.A., Griffin, C.A., Schambelan, M., and Kalinyak, J.E. (1991). Expression of AT2 receptors in the developing rat fetus. J Clin Invest *88*, 921-933.

Gulick, J., and Robbins, J. (2009). Cell-type-specific transgenesis in the mouse. Methods Mol Biol *561*, 91-104.

Gwinn, D.M., Shackelford, D.B., Egan, D.F., Mihaylova, M.M., Mery, A., Vasquez, D.S., Turk, B.E., and Shaw, R.J. (2008). AMPK phosphorylation of raptor mediates a metabolic checkpoint. Mol Cell *30*, 214-226.

Habets, D.D., Coumans, W.A., El Hasnaoui, M., Zarrinpashneh, E., Bertrand, L., Viollet, B., Kiens, B., Jensen, T.E., Richter, E.A., Bonen, A.*, et al.* (2009). Crucial role for LKB1 to AMPKalpha2 axis in the regulation of CD36-mediated long-chain fatty acid uptake into cardiomyocytes. Biochim Biophys Acta *1791*, 212-219.

Harasym, A.C., Thrush, A.B., Harper, M.E., Wright, D.C., and Chan, C.B. (2013). Enhanced glucose homeostasis in BHE/cdb rats with mutated ATP synthase. Mitochondrion *13*, 320-329.

Hardie, D.G. (2007). AMPK and SNF1: Snuffing Out Stress. Cell Metab *6*, 339-340.

Hardie, D.G. (2008). AMPK: a key regulator of energy balance in the single cell and the whole organism. Int J Obes (Lond) *32 Suppl 4*, S7-12.

Hardie, D.G., Ross, F.A., and Hawley, S.A. (2012). AMPK: a nutrient and energy sensor that maintains energy homeostasis. Nat Rev Mol Cell Biol *13*, 251-262.

Harding, P., Yang, X.P., He, Q., and Lapointe, M.C. (2011). Lack of microsomal prostaglandin E synthase-1 reduces cardiac function following angiotensin II infusion. Am J Physiol Heart Circ Physiol *300*, H1053-1061.

Hartshorne, D.J., Ito, M., and Erdodi, F. (2004). Role of protein phosphatase type 1 in contractile functions: myosin phosphatase. J Biol Chem *279*, 37211-37214.

Haudek, S.B., Cheng, J., Du, J., Wang, Y., Hermosillo-Rodriguez, J., Trial, J., Taffet, G.E., and Entman, M.L. (2010). Monocytic fibroblast precursors mediate fibrosis in angiotensin-II-induced cardiac hypertrophy. J Mol Cell Cardiol *49*, 499-507.

Hawley, S.A., Boudeau, J., Reid, J.L., Mustard, K.J., Udd, L., Makela, T.P., Alessi, D.R., and Hardie, D.G. (2003). Complexes between the LKB1 tumor suppressor, STRAD alpha/beta and MO25 alpha/beta are upstream kinases in the AMP-activated protein kinase cascade. J Biol *2*, 28.

Hawley, S.A., Davison, M., Woods, A., Davies, S.P., Beri, R.K., Carling, D., and Hardie, D.G. (1996). Characterization of the AMP-activated protein kinase kinase from rat liver and identification of threonine 172 as the major site at which it phosphorylates AMP-activated protein kinase. J Biol Chem *271*, 27879-27887.

Hawley, S.A., Pan, D.A., Mustard, K.J., Ross, L., Bain, J., Edelman, A.M., Frenguelli, B.G., and Hardie, D.G. (2005). Calmodulin-dependent protein kinase kinase-beta is an alternative upstream kinase for AMP-activated protein kinase. Cell Metab *2*, 9-19.

Hemminki, A., Markie, D., Tomlinson, I., Avizienyte, E., Roth, S., Loukola, A., Bignell, G., Warren, W., Aminoff, M., Hoglund, P.*, et al.* (1998). A serine/threonine kinase gene defective in Peutz-Jeghers syndrome. Nature *391*, 184-187.

Hemminki, A., Tomlinson, I., Markie, D., Jarvinen, H., Sistonen, P., Bjorkqvist, A.M., Knuutila, S., Salovaara, R., Bodmer, W., Shibata, D.*, et al.* (1997). Localization of a susceptibility locus for Peutz-Jeghers syndrome to 19p using comparative genomic hybridization and targeted linkage analysis. Nat Genet *15*, 87-90.

Hezel, A.F., Gurumurthy, S., Granot, Z., Swisa, A., Chu, G.C., Bailey, G., Dor, Y., Bardeesy, N., and Depinho, R.A. (2008). Pancreatic LKB1 deletion leads to acinar polarity defects and cystic neoplasms. Mol Cell Biol *28*, 2414-2425.

Higuchi, S., Ohtsu, H., Suzuki, H., Shirai, H., Frank, G.D., and Eguchi, S. (2007). Angiotensin II signal transduction through the AT1 receptor: novel insights into mechanisms and pathophysiology. Clin Sci (Lond) *112*, 417-428.

Hirano, M., Kiyonari, H., Inoue, A., Furushima, K., Murata, T., Suda, Y., and Aizawa, S. (2006). A new serine/threonine protein kinase, Omphk1, essential to ventral body wall formation. Dev Dyn *235*, 2229-2237.

Hoppe, P.E., Chau, J., Flanagan, K.A., Reedy, A.R., and Schriefer, L.A. (2010). Caenorhabditis elegans unc-82 encodes a serine/threonine kinase important for myosin filament organization in muscle during growth. Genetics *184*, 79-90.

Horike, N., Takemori, H., Katoh, Y., Doi, J., Min, L., Asano, T., Sun, X.J., Yamamoto, H., Kasayama, S., Muraoka, M., *et al.* (2003). Adipose-specific expression, phosphorylation of Ser794 in insulin receptor substrate-1, and activation in diabetic animals of salt-inducible kinase-2. J Biol Chem *278*, 18440-18447.

Horiuchi, M., Akishita, M., and Dzau, V.J. (1999). Recent progress in angiotensin II type 2 receptor research in the cardiovascular system. Hypertension *33*, 613-621.

Horiuchi, M., Iwanami, J., and Mogi, M. (2012). Regulation of angiotensin II receptors beyond the classical pathway. Clin Sci (Lond) *123*, 193-203.

Hou, X., Liu, J.E., Liu, W., Liu, C.Y., Liu, Z.Y., and Sun, Z.Y. (2011). A new role of NUAK1: directly phosphorylating p53 and regulating cell proliferation. Oncogene *30*, 2933-2942.

Humbert, N., Navaratnam, N., Augert, A., Da Costa, M., Martien, S., Wang, J., Martinez, D., Abbadie, C., Carling, D., de Launoit, Y., *et al.* (2010). Regulation of ploidy and senescence by the AMPK-related kinase NUAK1. EMBO J *29*, 376-386.

Hurley, R.L., Anderson, K.A., Franzone, J.M., Kemp, B.E., Means, A.R., and Witters, L.A. (2005). The Ca2+/calmodulin-dependent protein kinase kinases are AMP-activated protein kinase kinases. J Biol Chem *280*, 29060-29066.

Hurov, J., and Piwnica-Worms, H. (2007). The Par-1/MARK family of protein kinases: from polarity to metabolism. Cell Cycle *6*, 1966-1969.

Hurov, J.B., Stappenbeck, T.S., Zmasek, C.M., White, L.S., Ranganath, S.H., Russell, J.H., Chan, A.C., Murphy, K.M., and Piwnica-Worms, H. (2001). Immune system dysfunction and autoimmune disease in mice lacking Emk (Par-1) protein kinase. Mol Cell Biol *21*, 3206-3219.

Hurov, J.B., Watkins, J.L., and Piwnica-Worms, H. (2004). Atypical PKC phosphorylates PAR-1 kinases to regulate localization and activity. Curr Biol *14*, 736-741.

Hutchison, M., Berman, K.S., and Cobb, M.H. (1998). Isolation of TAO1, a protein kinase that activates MEKs in stress-activated protein kinase cascades. J Biol Chem *273*, 28625-28632.

Ikebe, M., Inagaki, M., Naka, M., and Hidaka, H. (1988). Correlation of conformation and phosphorylation and dephosphorylation of smooth muscle myosin. J Biol Chem *263*, 10698-10704.

Ikeda, Y., Sato, K., Pimentel, D.R., Sam, F., Shaw, R.J., Dyck, J.R., and Walsh, K. (2009). Cardiac-specific deletion of LKB1 leads to hypertrophy and dysfunction. J Biol Chem *284*, 35839-35849.

Inazuka, F., Sugiyama, N., Tomita, M., Abe, T., Shioi, G., and Esumi, H. (2012). Muscle-specific knock-out of NUAK family SNF1-like kinase 1 (NUAK1) prevents high fat diet-induced glucose intolerance. J Biol Chem *287*, 16379-16389.

Inoki, K., Li, Y., Xu, T., and Guan, K.L. (2003). Rheb GTPase is a direct target of TSC2 GAP activity and regulates mTOR signaling. Genes Dev *17*, 1829-1834.

Inoue, E., Mochida, S., Takagi, H., Higa, S., Deguchi-Tawarada, M., Takao-Rikitsu, E., Inoue, M., Yao, I., Takeuchi, K., Kitajima, I.*, et al.* (2006). SAD: a presynaptic kinase associated with synaptic vesicles and the active zone cytomatrix that regulates neurotransmitter release. Neuron *50*, 261-275.

Jager, S., Handschin, C., St-Pierre, J., and Spiegelman, B.M. (2007). AMP-activated protein kinase (AMPK) action in skeletal muscle via direct phosphorylation of PGC-1alpha. Proc Natl Acad Sci U S A *104*, 12017-12022.

Jakobsen, S.N., Hardie, D.G., Morrice, N., and Tornqvist, H.E. (2001). 5'-AMP-activated protein kinase phosphorylates IRS-1 on Ser-789 in mouse C2C12 myotubes in response to 5-aminoimidazole-4-carboxamide riboside. J Biol Chem *276*, 46912-46916.

Jaleel, M., McBride, A., Lizcano, J.M., Deak, M., Toth, R., Morrice, N.A., and Alessi, D.R. (2005). Identification of the sucrose non-fermenting related kinase SNRK, as a novel LKB1 substrate. FEBS Lett *579*, 1417-1423.

Jaleel, M., Villa, F., Deak, M., Toth, R., Prescott, A.R., Van Aalten, D.M., and Alessi, D.R. (2006). The ubiquitin-associated domain of AMPK-related kinases regulates conformation and LKB1-mediated phosphorylation and activation. Biochem J *394*, 545-555.

Jenne, D.E., Reimann, H., Nezu, J., Friedel, W., Loff, S., Jeschke, R., Muller, O., Back, W., and Zimmer, M. (1998). Peutz-Jeghers syndrome is caused by mutations in a novel serine threonine kinase. Nat Genet *18*, 38-43.

Jeon, S., Kim, Y.S., Park, J., and Bae, C.D. (2005). Microtubule affinity-regulating kinase 1 (MARK1) is activated by electroconvulsive shock in the rat hippocampus. J Neurochem *95*, 1608-1618.

Jishage, K., Nezu, J., Kawase, Y., Iwata, T., Watanabe, M., Miyoshi, A., Ose, A., Habu, K., Kake, T., Kamada, N.*, et al.* (2002). Role of Lkb1, the causative gene of Peutz-Jegher's syndrome, in embryogenesis and polyposis. Proc Natl Acad Sci U S A *99*, 8903-8908.

Jorgensen, S.B., Nielsen, J.N., Birk, J.B., Olsen, G.S., Viollet, B., Andreelli, F., Schjerling, P., Vaulont, S., Hardie, D.G., Hansen, B.F.*, et al.* (2004). The alpha2-5'AMP-activated protein kinase is a site 2 glycogen synthase kinase in skeletal muscle and is responsive to glucose loading. Diabetes *53*, 3074-3081.

Kahn, B.B., Alquier, T., Carling, D., and Hardie, D.G. (2005). AMP-activated protein kinase: ancient energy gauge provides clues to modern understanding of metabolism. Cell Metab *1*, 15-25.

Kanagawa, S.L., Begleiter, M.L., Ostlie, D.J., Holcomb, G., Drake, W., and Butler, M.G. (2002). Omphalocele in three generations with autosomal dominant transmission. J Med Genet *39*, 184-185.

Katajisto, P., Vallenius, T., Vaahtomeri, K., Ekman, N., Udd, L., Tiainen, M., and Makela, T.P. (2007). The LKB1 tumor suppressor kinase in human disease. Biochim Biophys Acta *1775*, 63-75.

Kato, T., Satoh, S., Okabe, H., Kitahara, O., Ono, K., Kihara, C., Tanaka, T., Tsunoda, T., Yamaoka, Y., Nakamura, Y.*, et al.* (2001). Isolation of a novel human gene, MARKL1, homologous to MARK3 and its involvement in hepatocellular carcinogenesis. Neoplasia *3*, 4-9.

Kemphues, K.J., Priess, J.R., Morton, D.G., and Cheng, N.S. (1988). Identification of genes required for cytoplasmic localization in early C. elegans embryos. Cell *52*, 311-320.

Kimura, K., Ito, M., Amano, M., Chihara, K., Fukata, Y., Nakafuku, M., Yamamori, B., Feng, J., Nakano, T., Okawa, K.*, et al.* (1996). Regulation of myosin phosphatase by Rho and Rho-associated kinase (Rho-kinase). Science *273*, 245-248.

Kingsbury, M.P., Huang, W., Donnelly, J.L., Jackson, E., Needham, E., Turner, M.A., and Sheridan, D.J. (2003). Structural remodelling of lungs in chronic heart failure. Basic Res Cardiol *98*, 295-303.

Kishi, T., Hirooka, Y., Masumoto, A., Ito, K., Kimura, Y., Inokuchi, K., Tagawa, T., Shimokawa, H., Takeshita, A., and Sunagawa, K. (2005). Rho-kinase inhibitor improves increased vascular resistance and impaired vasodilation of the forearm in patients with heart failure. Circulation *111*, 2741-2747.

Koch Weser, D., and Popper, H. (1952). Hepatic fibrosis produced by chronic ethionine feeding. Proc Soc Exp Biol Med *79*, 34-37.

Kohli, S., Ahuja, S., and Rani, V. (2011). Transcription factors in heart: promising therapeutic targets in cardiac hypertrophy. Curr Cardiol Rev *7*, 262-271.

Koo, S.H., Flechner, L., Qi, L., Zhang, X., Screaton, R.A., Jeffries, S., Hedrick, S., Xu, W., Boussouar, F., Brindle, P.*, et al.* (2005). The CREB coactivator TORC2 is a key regulator of fasting glucose metabolism. Nature *437*, 1109-1111.

Kusakabe, M., and Nishida, E. (2004). The polarity-inducing kinase Par-1 controls Xenopus gastrulation in cooperation with 14-3-3 and aPKC. EMBO J *23*, 4190-4201.

Kusakai, G., Suzuki, A., Ogura, T., Kaminishi, M., and Esumi, H. (2004a). Strong association of ARK5 with tumor invasion and metastasis. J Exp Clin Cancer Res *23*, 263-268.

Kusakai, G., Suzuki, A., Ogura, T., Miyamoto, S., Ochiai, A., Kaminishi, M., and Esumi, H. (2004b). ARK5 expression in colorectal cancer and its implications for tumor progression. Am J Pathol *164*, 987-995.

Lassegue, B., Alexander, R.W., Nickenig, G., Clark, M., Murphy, T.J., and Griendling, K.K. (1995). Angiotensin II down-regulates the vascular smooth muscle AT1 receptor by transcriptional and post-transcriptional mechanisms: evidence for homologous and heterologous regulation. Mol Pharmacol *48*, 601-609.

Lee, J.H., Koh, H., Kim, M., Kim, Y., Lee, S.Y., Karess, R.E., Lee, S.H., Shong, M., Kim, J.M., Kim, J.*, et al.* (2007). Energy-dependent regulation of cell structure by AMP-activated protein kinase. Nature *447*, 1017-1020.

Lee, J.S., Heo, J., Libbrecht, L., Chu, I.S., Kaposi-Novak, P., Calvisi, D.F., Mikaelyan, A., Roberts, L.R., Demetris, A.J., Sun, Z*., et al.* (2006). A novel prognostic subtype of human hepatocellular carcinoma derived from hepatic progenitor cells. Nat Med *12*, 410-416.

Lemarie, C.A., and Schiffrin, E.L. (2010). The angiotensin II type 2 receptor in cardiovascular disease. J Renin Angiotensin Aldosterone Syst *11*, 19-31.

Li, J., Hu, X., Selvakumar, P., Russell, R.R., 3rd, Cushman, S.W., Holman, G.D., and Young, L.H. (2004). Role of the nitric oxide pathway in AMPK-mediated glucose uptake and GLUT4 translocation in heart muscle. Am J Physiol Endocrinol Metab *287*, E834-841.

Li, Y., Xu, S., Mihaylova, M.M., Zheng, B., Hou, X., Jiang, B., Park, O., Luo, Z., Lefai, E., Shyy, J.Y*., et al.* (2011). AMPK phosphorylates and inhibits SREBP activity to attenuate hepatic steatosis and atherosclerosis in diet-induced insulin-resistant mice. Cell Metab *13*, 376-388.

Liu, L., Ulbrich, J., Muller, J., Wustefeld, T., Aeberhard, L., Kress, T.R., Muthalagu, N., Rycak, L., Rudalska, R., Moll, R*., et al.* (2012). Deregulated MYC expression induces dependence upon AMPK-related kinase 5. Nature *483*, 608-612.

Lizcano, J.M., Goransson, O., Toth, R., Deak, M., Morrice, N.A., Boudeau, J., Hawley, S.A., Udd, L., Makela, T.P., Hardie, D.G*., et al.* (2004). LKB1 is a master kinase that activates 13 kinases of the AMPK subfamily, including MARK/PAR-1. EMBO J *23*, 833-843.

Lorenzini, S., Bird, T.G., Boulter, L., Bellamy, C., Samuel, K., Aucott, R., Clayton, E., Andreone, P., Bernardi, M., Golding, M*., et al.* (2010). Characterisation of a stereotypical cellular and extracellular adult liver progenitor cell niche in rodents and diseased human liver. Gut *59*, 645-654.

Lu, S., Niu, N., Guo, H., Tang, J., Guo, W., Liu, Z., Shi, L., Sun, T., Zhou, F., Li, H*., et al.* (2013). ARK5 promotes glioma cell invasion, and its elevated expression is correlated with poor clinical outcome. Eur J Cancer *49*, 752-763.

Mackintosh, C. (2004). Dynamic interactions between 14-3-3 proteins and phosphoproteins regulate diverse cellular processes. Biochem J *381*, 329-342.

Magnus, I.A., Roe, D.A., and Bhutani, L.K. (1969). Factors affecting the induction of porphyria in the laboratory rat. Biochemical and photobiological studies using diethyl 1,4-dihydro-2,4,6-trimethyl-pyridine-3,5-dicarboxylate (DDC) as a porphyrogenic agent. J Invest Dermatol *53*, 400-413.

Mamidi, A., Inui, M., Manfrin, A., Soligo, S., Enzo, E., Aragona, M., Cordenonsi, M., Wessely, O., Dupont, S., and Piccolo, S. (2012). Signaling crosstalk between TGFbeta and Dishevelled/Par1b. Cell Death Differ *19*, 1689-1697.

Manley, N.R., Barrow, J.R., Zhang, T., and Capecchi, M.R. (2001). Hoxb2 and hoxb4 act together to specify ventral body wall formation. Dev Biol *237*, 130-144.

Manning, G., Whyte, D.B., Martinez, R., Hunter, T., and Sudarsanam, S. (2002). The protein kinase complement of the human genome. Science *298*, 1912-1934.

Marsin, A.S., Bertrand, L., Rider, M.H., Deprez, J., Beauloye, C., Vincent, M.F., Van den Berghe, G., Carling, D., and Hue, L. (2000). Phosphorylation and activation of heart PFK-2 by AMPK has a role in the stimulation of glycolysis during ischaemia. Curr Biol *10*, 1247-1255.

Marx, A., Nugoor, C., Panneerselvam, S., and Mandelkow, E. (2010). Structure and function of polarity-inducing kinase family MARK/Par-1 within the branch of AMPK/Snf1-related kinases. FASEB J *24*, 1637-1648.

Massie, C.E., Lynch, A., Ramos-Montoya, A., Boren, J., Stark, R., Fazli, L., Warren, A., Scott, H., Madhu, B., Sharma, N.*, et al.* (2011). The androgen receptor fuels prostate cancer by regulating central metabolism and biosynthesis. EMBO J *30*, 2719-2733.

Matsumura, F. (2005). Regulation of myosin II during cytokinesis in higher eukaryotes. Trends Cell Biol *15*, 371-377.

McDermott-Roe, C., Ye, J., Ahmed, R., Sun, X.M., Serafin, A., Ware, J., Bottolo, L., Muckett, P., Canas, X., Zhang, J.*, et al.* (2011). Endonuclease G is a novel determinant of cardiac hypertrophy and mitochondrial function. Nature *478*, 114-118.

Mehta, P.K., and Griendling, K.K. (2007). Angiotensin II cell signaling: physiological and pathological effects in the cardiovascular system. Am J Physiol Cell Physiol *292*, C82-97.

Merrill, G.F., Kurth, E.J., Hardie, D.G., and Winder, W.W. (1997). AICA riboside increases AMP-activated protein kinase, fatty acid oxidation, and glucose uptake in rat muscle. Am J Physiol *273*, E1107-1112.

Mihaylova, M.M., and Shaw, R.J. (2011). The AMPK signalling pathway coordinates cell growth, autophagy and metabolism. Nat Cell Biol *13*, 1016-1023.

Minguez, B., Tovar, V., Chiang, D., Villanueva, A., and Llovet, J.M. (2009). Pathogenesis of hepatocellular carcinoma and molecular therapies. Curr Opin Gastroenterol *25*, 186-194.

Minokoshi, Y., Alquier, T., Furukawa, N., Kim, Y.B., Lee, A., Xue, B., Mu, J., Foufelle, F., Ferre, P., Birnbaum, M.J.*, et al.* (2004). AMP-kinase regulates food intake by responding to hormonal and nutrient signals in the hypothalamus. Nature *428*, 569-574.

Miyoshi, H., Nakau, M., Ishikawa, T.O., Seldin, M.F., Oshima, M., and Taketo, M.M. (2002). Gastrointestinal hamartomatous polyposis in Lkb1 heterozygous knockout mice. Cancer Res *62*, 2261-2266.

Momcilovic, M., Hong, S.P., and Carlson, M. (2006). Mammalian TAK1 activates Snf1 protein kinase in yeast and phosphorylates AMP-activated protein kinase in vitro. J Biol Chem *281*, 25336-25343.

Moreno-Moral, A., Mancini, M., D'Amati, G., Camici, P., and Petretto, E. (2013). Transcriptional Network Analysis for the Regulation of Left Ventricular Hypertrophy and Microvascular Remodeling. J Cardiovasc Transl Res.

Morrison, D.K. (2009). The 14-3-3 proteins: integrators of diverse signaling cues that impact cell fate and cancer development. Trends Cell Biol *19*, 16-23.

Moussavi, R.S., Kelley, C.A., and Adelstein, R.S. (1993). Phosphorylation of vertebrate nonmuscle and smooth muscle myosin heavy chains and light chains. Mol Cell Biochem *127-128*, 219-227.

Muller, J., Ory, S., Copeland, T., Piwnica-Worms, H., and Morrison, D.K. (2001). C-TAK1 regulates Ras signaling by phosphorylating the MAPK scaffold, KSR1. Mol Cell *8*, 983-993.

Murphy, J.M., Korzhnev, D.M., Ceccarelli, D.F., Briant, D.J., Zarrine-Afsar, A., Sicheri, F., Kay, L.E., and Pawson, T. (2007). Conformational instability of the MARK3 UBA domain compromises ubiquitin recognition and promotes interaction with the adjacent kinase domain. Proc Natl Acad Sci U S A *104*, 14336-14341.

Nakada, D., Saunders, T.L., and Morrison, S.J. (2010). Lkb1 regulates cell cycle and energy metabolism in haematopoietic stem cells. Nature *468*, 653-658.

Nakau, M., Miyoshi, H., Seldin, M.F., Imamura, M., Oshima, M., and Taketo, M.M. (2002). Hepatocellular carcinoma caused by loss of heterozygosity in Lkb1 gene knockout mice. Cancer Res *62*, 4549-4553.

Naschitz, J.E., Slobodin, G., Lewis, R.J., Zuckerman, E., and Yeshurun, D. (2000). Heart diseases affecting the liver and liver diseases affecting the heart. Am Heart J *140*, 111-120.

Neumann, D., Woods, A., Carling, D., Wallimann, T., and Schlattner, U. (2003). Mammalian AMP-activated protein kinase: functional, heterotrimeric complexes by co-expression of subunits in Escherichia coli. Protein Expr Purif *30*, 230-237.

Nguyen Dinh Cat, A., and Touyz, R.M. (2011). A new look at the renin-angiotensin system--focusing on the vascular system. Peptides *32*, 2141-2150.

Nie, J., Liu, X., Lilley, B.N., Zhang, H., Pan, Y.A., Kimball, S.R., Zhang, J., Zhang, W., Wang, L., Jefferson, L.S.*, et al.* (2013). SAD-A kinase controls islet beta-cell size and function as a mediator of mTORC1 signaling. Proc Natl Acad Sci U S A.

Nishimura, I., Yang, Y., and Lu, B. (2004). PAR-1 kinase plays an initiator role in a temporally ordered phosphorylation process that confers tau toxicity in Drosophila. Cell *116*, 671-682.

O'Neill, H.M., Maarbjerg, S.J., Crane, J.D., Jeppesen, J., Jorgensen, S.B., Schertzer, J.D., Shyroka, O., Kiens, B., van Denderen, B.J., Tarnopolsky, M.A.*, et al.* (2011). AMP-activated protein kinase (AMPK) beta1beta2 muscle null mice reveal an essential role for AMPK in maintaining mitochondrial content and glucose uptake during exercise. Proc Natl Acad Sci U S A *108*, 16092-16097.

Oakhill, J.S., Steel, R., Chen, Z.P., Scott, J.W., Ling, N., Tam, S., and Kemp, B.E. (2011). AMPK is a direct adenylate charge-regulated protein kinase. Science *332*, 1433-1435.

Ohmura, T., Shioi, G., Hirano, M., and Aizawa, S. (2012). Neural tube defects by NUAK1 and NUAK2 double mutation. Dev Dyn *241*, 1350-1364.

Okazaki, Y., Furuno, M., Kasukawa, T., Adachi, J., Bono, H., Kondo, S., Nikaido, I., Osato, N., Saito, R., Suzuki, H.*, et al.* (2002). Analysis of the mouse transcriptome based on functional annotation of 60,770 full-length cDNAs. Nature *420*, 563-573.

Ossipova, O., Dhawan, S., Sokol, S., and Green, J.B. (2005). Distinct PAR-1 proteins function in different branches of Wnt signaling during vertebrate development. Dev Cell *8*, 829-841.

Owen, M.R., Doran, E., and Halestrap, A.P. (2000). Evidence that metformin exerts its anti-diabetic effects through inhibition of complex 1 of the mitochondrial respiratory chain. Biochem J *348 Pt 3*, 607-614.

Pan, D. (2010). The hippo signaling pathway in development and cancer. Dev Cell *19*, 491-505.

Park, I.J., Lee, Y.K., Hwang, J.T., Kwon, D.Y., Ha, J., and Park, O.J. (2009). Green tea catechin controls apoptosis in colon cancer cells by attenuation of H2O2-stimulated COX-2 expression via the AMPK signaling pathway at low-dose H2O2. Ann N Y Acad Sci *1171*, 538-544.

Peng, C.Y., Graves, P.R., Ogg, S., Thoma, R.S., Byrnes, M.J., 3rd, Wu, Z., Stephenson, M.T., and Piwnica-Worms, H. (1998). C-TAK1 protein kinase phosphorylates human Cdc25C on serine 216 and promotes 14-3-3 protein binding. Cell Growth Differ *9*, 197-208.

Petroulakis, E., Mamane, Y., Le Bacquer, O., Shahbazian, D., and Sonenberg, N. (2006). mTOR signaling: implications for cancer and anticancer therapy. Br J Cancer *94*, 195-199.

Pizer, E.S., Lax, S.F., Kuhajda, F.P., Pasternack, G.R., and Kurman, R.J. (1998). Fatty acid synthase expression in endometrial carcinoma: correlation with cell proliferation and hormone receptors. Cancer *83*, 528-537.

Popov, S., Silveira, A., Wagsater, D., Takemori, H., Oguro, R., Matsumoto, S., Sugimoto, K., Kamide, K., Hirose, T., Satoh, M.*, et al.* (2011). Salt-inducible kinase 1 influences Na(+),K(+)-ATPase activity in vascular smooth muscle cells and associates with variations in blood pressure. J Hypertens *29*, 2395-2403.

Postic, C., Shiota, M., Niswender, K.D., Jetton, T.L., Chen, Y., Moates, J.M., Shelton, K.D., Lindner, J., Cherrington, A.D., and Magnuson, M.A. (1999). Dual roles for glucokinase in glucose homeostasis as determined by liver and pancreatic beta cell-specific gene knock-outs using Cre recombinase. J Biol Chem *274*, 305-315.

Qin, Z. (2008). Newly developed angiotensin II-infused experimental models in vascular biology. Regul Pept *150*, 1-6.

Ross, H., Armstrong, C.G., and Cohen, P. (2002). A non-radioactive method for the assay of many serine/threonine-specific protein kinases. Biochem J *366*, 977-981.

Rossi, D.J., Ylikorkala, A., Korsisaari, N., Salovaara, R., Luukko, K., Launonen, V., Henkemeyer, M., Ristimaki, A., Aaltonen, L.A., and Makela, T.P. (2002). Induction of cyclooxygenase-2 in a mouse model of Peutz-Jeghers polyposis. Proc Natl Acad Sci U S A *99*, 12327-12332.

Ruhl, C.E., and Everhart, J.E. (2013). Diurnal variation in serum alanine aminotransferase activity in the US population. J Clin Gastroenterol *47*, 165-173.

Sakamoto, K., Goransson, O., Hardie, D.G., and Alessi, D.R. (2004). Activity of LKB1 and AMPK-related kinases in skeletal muscle: effects of contraction, phenformin, and AICAR. Am J Physiol Endocrinol Metab *287*, E310-317.

Sakamoto, K., Zarrinpashneh, E., Budas, G.R., Pouleur, A.C., Dutta, A., Prescott, A.R., Vanoverschelde, J.L., Ashworth, A., Jovanovic, A., Alessi, D.R.*, et al.* (2006). Deficiency of LKB1 in heart prevents ischemia-mediated activation of AMPKalpha2 but not AMPKalpha1. Am J Physiol Endocrinol Metab *290*, E780-788.

Sanders, M.J., Grondin, P.O., Hegarty, B.D., Snowden, M.A., and Carling, D. (2007). Investigating the mechanism for AMP activation of the AMP-activated protein kinase cascade. Biochem J *403*, 139-148.

Santos, R.A., Simoes e Silva, A.C., Maric, C., Silva, D.M., Machado, R.P., de Buhr, I., Heringer-Walther, S., Pinheiro, S.V., Lopes, M.T., Bader, M.*, et al.* (2003). Angiotensin-(1-7) is an endogenous ligand for the G protein-coupled receptor Mas. Proc Natl Acad Sci U S A *100*, 8258-8263.

Sato, S., Sanjo, H., Takeda, K., Ninomiya-Tsuji, J., Yamamoto, M., Kawai, T., Matsumoto, K., Takeuchi, O., and Akira, S. (2005). Essential function for the kinase TAK1 in innate and adaptive immune responses. Nat Immunol *6*, 1087-1095.

Savoia, C., Burger, D., Nishigaki, N., Montezano, A., and Touyz, R.M. (2011). Angiotensin II and the vascular phenotype in hypertension. Expert Rev Mol Med *13*, e11.

Scholey, J.M., Taylor, K.A., and Kendrick-Jones, J. (1980). Regulation of non-muscle myosin assembly by calmodulin-dependent light chain kinase. Nature *287*, 233-235.

Screaton, R.A., Conkright, M.D., Katoh, Y., Best, J.L., Canettieri, G., Jeffries, S., Guzman, E., Niessen, S., Yates, J.R., 3rd, Takemori, H.*, et al.* (2004). The CREB coactivator TORC2 functions as a calcium- and cAMP-sensitive coincidence detector. Cell *119*, 61-74.

Shaw, R.J., Lamia, K.A., Vasquez, D., Koo, S.H., Bardeesy, N., Depinho, R.A., Montminy, M., and Cantley, L.C. (2005). The kinase LKB1 mediates glucose homeostasis in liver and therapeutic effects of metformin. Science *310*, 1642-1646.

Shen, Y., and Cao, D. (2012). Hepatocellular carcinoma stem cells: origins and roles in hepatocarcinogenesis and disease progression. Front Biosci (Elite Ed) *4*, 1157-1169.

Shield, M.A., Haugen, H.S., Clegg, C.H., and Hauschka, S.D. (1996). E-box sites and a proximal regulatory region of the muscle creatine kinase gene differentially regulate expression in diverse skeletal muscles and cardiac muscle of transgenic mice. Mol Cell Biol *16*, 5058-5068.

Shinozuka, H., Lombardi, B., Sell, S., and Iammarino, R.M. (1978). Early histological and functional alterations of ethionine liver carcinogenesis in rats fed a choline-deficient diet. Cancer Res *38*, 1092-1098.

Singhirunnusorn, P., Suzuki, S., Kawasaki, N., Saiki, I., and Sakurai, H. (2005). Critical roles of threonine 187 phosphorylation in cellular stress-induced rapid and transient activation of transforming growth factor-beta-activated kinase 1 (TAK1) in a signaling complex containing TAK1-binding protein TAB1 and TAB2. J Biol Chem *280*, 7359-7368.

Sjostrom, M., Stenstrom, K., Eneling, K., Zwiller, J., Katz, A.I., Takemori, H., and Bertorello, A.M. (2007). SIK1 is part of a cell sodium-sensing network that regulates active sodium transport through a calcium-dependent process. Proc Natl Acad Sci U S A *104*, 16922-16927.

Stahmann, N., Woods, A., Carling, D., and Heller, R. (2006). Thrombin activates AMP-activated protein kinase in endothelial cells via a pathway involving Ca2+/calmodulin-dependent protein kinase kinase beta. Mol Cell Biol *26*, 5933-5945.

Stamer, K., Vogel, R., Thies, E., Mandelkow, E., and Mandelkow, E.M. (2002). Tau blocks traffic of organelles, neurofilaments, and APP vesicles in neurons and enhances oxidative stress. J Cell Biol *156*, 1051-1063.

Stoothoff, W.H., and Johnson, G.V. (2005). Tau phosphorylation: physiological and pathological consequences. Biochim Biophys Acta *1739*, 280-297.

Stopka, T., and Skoultchi, A.I. (2003). The ISWI ATPase Snf2h is required for early mouse development. Proc Natl Acad Sci U S A *100*, 14097-14102.

Su, J.Y., Erikson, E., and Maller, J.L. (1996). Cloning and characterization of a novel serine/threonine protein kinase expressed in early Xenopus embryos. J Biol Chem *271*, 14430-14437.

Sun, T.Q., Lu, B., Feng, J.J., Reinhard, C., Jan, Y.N., Fantl, W.J., and Williams, L.T. (2001). PAR-1 is a Dishevelled-associated kinase and a positive regulator of Wnt signalling. Nat Cell Biol *3*, 628-636.

Suter, M., Riek, U., Tuerk, R., Schlattner, U., Wallimann, T., and Neumann, D. (2006). Dissecting the role of 5'-AMP for allosteric stimulation, activation, and deactivation of AMP-activated protein kinase. J Biol Chem *281*, 32207-32216.

Suzuki, A., Iida, S., Kato-Uranishi, M., Tajima, E., Zhan, F., Hanamura, I., Huang, Y., Ogura, T., Takahashi, S., Ueda, R.*, et al.* (2005). ARK5 is transcriptionally regulated by the Large-MAF family and mediates IGF-1-induced cell invasion in multiple myeloma: ARK5 as a new molecular determinant of malignant multiple myeloma. Oncogene *24*, 6936-6944.

Suzuki, A., Kusakai, G., Kishimoto, A., Lu, J., Ogura, T., and Esumi, H. (2003a). ARK5 suppresses the cell death induced by nutrient starvation and death receptors via inhibition of caspase 8 activation, but not by chemotherapeutic agents or UV irradiation. Oncogene *22*, 6177-6182.

Suzuki, A., Kusakai, G., Kishimoto, A., Lu, J., Ogura, T., Lavin, M.F., and Esumi, H. (2003b). Identification of a novel protein kinase mediating Akt survival signaling to the ATM protein. J Biol Chem *278*, 48-53.

Suzuki, A., Kusakai, G., Kishimoto, A., Shimojo, Y., Miyamoto, S., Ogura, T., Ochiai, A., and Esumi, H. (2004a). Regulation of caspase-6 and FLIP by the AMPK family member ARK5. Oncogene *23*, 7067-7075.

Suzuki, A., Lu, J., Kusakai, G., Kishimoto, A., Ogura, T., and Esumi, H. (2004b). ARK5 is a tumor invasion-associated factor downstream of Akt signaling. Mol Cell Biol *24*, 3526-3535.

Suzuki, A., Ogura, T., and Esumi, H. (2006). NDR2 acts as the upstream kinase of ARK5 during insulin-like growth factor-1 signaling. J Biol Chem *281*, 13915-13921.

Takahashi, A., Ohtani, N., Yamakoshi, K., Iida, S., Tahara, H., Nakayama, K., Nakayama, K.I., Ide, T., Saya, H., and Hara, E. (2006). Mitogenic signalling and the p16INK4a-Rb pathway cooperate to enforce irreversible cellular senescence. Nat Cell Biol *8*, 1291-1297.

Takemori, H., Katoh, Y., Horike, N., Doi, J., and Okamoto, M. (2002). ACTH-induced nucleocytoplasmic translocation of salt-inducible kinase. Implication in the protein kinase A-activated gene transcription in mouse adrenocortical tumor cells. J Biol Chem *277*, 42334-42343.

Tamas, P., Hawley, S.A., Clarke, R.G., Mustard, K.J., Green, K., Hardie, D.G., and Cantrell, D.A. (2006). Regulation of the energy sensor AMP-activated protein kinase by antigen receptor and Ca2+ in T lymphocytes. J Exp Med *203*, 1665-1670.

Terpe, K. (2003). Overview of tag protein fusions: from molecular and biochemical fundamentals to commercial systems. Appl Microbiol Biotechnol *60*, 523-533.

Thumkeo, D., Shimizu, Y., Sakamoto, S., Yamada, S., and Narumiya, S. (2005). ROCK-I and ROCK-II cooperatively regulate closure of eyelid and ventral body wall in mouse embryo. Genes Cells *10*, 825-834.

Tiainen, M., Ylikorkala, A., and Makela, T.P. (1999). Growth suppression by Lkb1 is mediated by a G(1) cell cycle arrest. Proc Natl Acad Sci U S A *96*, 9248-9251.

Timm, T., Balusamy, K., Li, X., Biernat, J., Mandelkow, E., and Mandelkow, E.M. (2008). Glycogen synthase kinase (GSK) 3beta directly phosphorylates Serine 212 in the regulatory loop and inhibits microtubule affinity-regulating kinase (MARK) 2. J Biol Chem *283*, 18873-18882.

Tolman, K.G., and Dalpiaz, A.S. (2007). Treatment of non-alcoholic fatty liver disease. Ther Clin Risk Manag *3*, 1153-1163.

Totsukawa, G., Yamakita, Y., Yamashiro, S., Hartshorne, D.J., Sasaki, Y., and Matsumura, F. (2000). Distinct roles of ROCK (Rho-kinase) and MLCK in spatial regulation of MLC phosphorylation for assembly of stress fibers and focal adhesions in 3T3 fibroblasts. J Cell Biol *150*, 797-806.

Tousoulis, D., Androulakis, E., Papageorgiou, N., Miliou, A., Chatzistamatiou, E., Oikonomou, E., Moustakas, G., Kallikazaros, I., and Stefanadis, C. (2013). Genetic predisposition to left ventricular hypertrophy and the potential involvement of cystatin-C in untreated hypertension. Am J Hypertens *26*, 683-690.

Towler, M.C., Fogarty, S., Hawley, S.A., Pan, D.A., Martin, D.M., Morrice, N.A., McCarthy, A., Galardo, M.N., Meroni, S.B., Cigorraga, S.B.*, et al.* (2008). A novel short splice variant of the tumour suppressor LKB1 is required for spermiogenesis. Biochem J *416*, 1-14.

Treebak, J.T., Frosig, C., Pehmoller, C., Chen, S., Maarbjerg, S.J., Brandt, N., MacKintosh, C., Zierath, J.R., Hardie, D.G., Kiens, B.*, et al.* (2009). Potential role of TBC1D4 in enhanced post-exercise insulin action in human skeletal muscle. Diabetologia *52*, 891-900.

Tsukamoto, Y., Mano, T., Sakata, Y., Ohtani, T., Takeda, Y., Tamaki, S., Omori, Y., Ikeya, Y., Saito, Y., Ishii, R.*, et al.* (2013). A Novel Heart Failure Mice Model of Hypertensive Heart Disease by Angiotensin II Infusion, Nephrectomy, and Salt Loading. Am J Physiol Heart Circ Physiol.

Uboha, N.V., Flajolet, M., Nairn, A.C., and Picciotto, M.R. (2007). A calcium- and calmodulin-dependent kinase Ialpha/microtubule affinity regulating kinase 2 signaling cascade mediates calcium-dependent neurite outgrowth. J Neurosci *27*, 4413-4423.

Vicente-Manzanares, M., Ma, X., Adelstein, R.S., and Horwitz, A.R. (2009). Non-muscle myosin II takes centre stage in cell adhesion and migration. Nat Rev Mol Cell Biol *10*, 778-790.

Villanueva, A., Newell, P., Chiang, D.Y., Friedman, S.L., and Llovet, J.M. (2007). Genomics and signaling pathways in hepatocellular carcinoma. Semin Liver Dis *27*, 55-76.

Viollet, B., Athea, Y., Mounier, R., Guigas, B., Zarrinpashneh, E., Horman, S., Lantier, L., Hebrard, S., Devin-Leclerc, J., Beauloye, C.*, et al.* (2009). AMPK: Lessons from transgenic and knockout animals. Front Biosci (Landmark Ed) *14*, 19-44.

Wang, B., Wang, X.B., Chen, L.Y., Huang, L., and Dong, R.Z. (2013). Belinostat-induced apoptosis and growth inhibition in pancreatic cancer cells involve activation of TAK1-AMPK signaling axis. Biochem Biophys Res Commun *437*, 1-6.

Wang, Z., Takemori, H., Halder, S.K., Nonaka, Y., and Okamoto, M. (1999). Cloning of a novel kinase (SIK) of the SNF1/AMPK family from high salt diet-treated rat adrenal. FEBS Lett *453*, 135-139.

Weiner, M.W. (2013). Dementia in 2012: Further insights into Alzheimer disease pathogenesis. Nat Rev Neurol *9*, 65-66.

Windelinckx, A., De Mars, G., Huygens, W., Peeters, M.W., Vincent, B., Wijmenga, C., Lambrechts, D., Aerssens, J., Vlietinck, R., Beunen, G.*, et al.* (2011). Identification and prioritization of NUAK1 and PPP1CC as positional candidate loci for skeletal muscle strength phenotypes. Physiol Genomics *43*, 981-992.

Winder, W.W., Holmes, B.F., Rubink, D.S., Jensen, E.B., Chen, M., and Holloszy, J.O. (2000). Activation of AMP-activated protein kinase increases mitochondrial enzymes in skeletal muscle. J Appl Physiol *88*, 2219-2226.

Woods, A., Dickerson, K., Heath, R., Hong, S.P., Momcilovic, M., Johnstone, S.R., Carlson, M., and Carling, D. (2005). Ca2+/calmodulin-dependent protein kinase kinase-beta acts upstream of AMP-activated protein kinase in mammalian cells. Cell Metab *2*, 21-33.

Woods, A., Heslegrave, A.J., Muckett, P.J., Levene, A.P., Clements, M., Mobberley, M., Ryder, T.A., Abu-Hayyeh, S., Williamson, C., Goldin, R.D.*, et al.* (2011). LKB1 is required for hepatic bile acid transport and canalicular membrane integrity in mice. Biochem J *434*, 49-60.

Woods, A., Johnstone, S.R., Dickerson, K., Leiper, F.C., Fryer, L.G., Neumann, D., Schlattner, U., Wallimann, T., Carlson, M., and Carling, D. (2003). LKB1 is the upstream kinase in the AMP-activated protein kinase cascade. Curr Biol *13*, 2004-2008.

Xia, Y., Zhang, Z., Kruse, U., Vogt, P.K., and Li, J. (2000). The new serine-threonine kinase, Qik, is a target of the Qin oncogene. Biochem Biophys Res Commun *276*, 564-570.

Xiang, X., Saha, A.K., Wen, R., Ruderman, N.B., and Luo, Z. (2004). AMP-activated protein kinase activators can inhibit the growth of prostate cancer cells by multiple mechanisms. Biochem Biophys Res Commun *321*, 161-167.

Xiao, B., Sanders, M.J., Underwood, E., Heath, R., Mayer, F.V., Carmena, D., Jing, C., Walker, P.A., Eccleston, J.F., Haire, L.F.*, et al.* (2011). Structure of mammalian AMPK and its regulation by ADP. Nature *472*, 230-233.

Xie, M., Zhang, D., Dyck, J.R., Li, Y., Zhang, H., Morishima, M., Mann, D.L., Taffet, G.E., Baldini, A., Khoury, D.S.*, et al.* (2006). A pivotal role for endogenous TGF-beta-activated kinase-1 in the LKB1/AMP-activated protein kinase energy-sensor pathway. Proc Natl Acad Sci U S A *103*, 17378-17383.

Xu, Z., Okamoto, H., Akino, M., Onozuka, H., Matsui, Y., and Tsutsui, H. (2008). Pravastatin attenuates left ventricular remodeling and diastolic dysfunction in angiotensin II-induced hypertensive mice. J Cardiovasc Pharmacol *51*, 62-70.

Yamada, R., Mizutani-Koseki, Y., Koseki, H., and Takahashi, N. (2004). Requirement for Mab21l2 during development of murine retina and ventral body wall. Dev Biol *274*, 295-307.

Yamamoto, H., Takashima, S., Shintani, Y., Yamazaki, S., Seguchi, O., Nakano, A., Higo, S., Kato, H., Liao, Y., Asano, Y.*, et al.* (2008). Identification of a novel substrate for TNFalpha-induced kinase NUAK2. Biochem Biophys Res Commun *365*, 541-547.

Yang, Y., Atasoy, D., Su, H.H., and Sternson, S.M. (2011). Hunger states switch a flip-flop memory circuit via a synaptic AMPK-dependent positive feedback loop. Cell *146*, 992-1003.

Yatsenko, S.A., Mendoza-Londono, R., Belmont, J.W., and Shaffer, L.G. (2003). Omphalocele in trisomy 3q: further delineation of phenotype. Clin Genet *64*, 404-413.

Ylikorkala, A., Rossi, D.J., Korsisaari, N., Luukko, K., Alitalo, K., Henkemeyer, M., and Makela, T.P. (2001). Vascular abnormalities and deregulation of VEGF in Lkb1-deficient mice. Science *293*, 1323-1326.

Zagorska, A., Deak, M., Campbell, D.G., Banerjee, S., Hirano, M., Aizawa, S., Prescott, A.R., and Alessi, D.R. (2010). New roles for the LKB1-NUAK pathway in controlling myosin phosphatase complexes and cell adhesion. Sci Signal *3*, ra25.

Zaidi, A., and Sharma, S. (2013). Exercise and heart disease: from athletes and arrhythmias to hypertrophic cardiomyopathy and congenital heart disease. Future Cardiol *9*, 119-136.

Zeqiraj, E., Filippi, B.M., Deak, M., Alessi, D.R., and van Aalten, D.M. (2009). Structure of the LKB1-STRAD-MO25 complex reveals an allosteric mechanism of kinase activation. Science *326*, 1707-1711.

Zhang, B.B., Zhou, G., and Li, C. (2009). AMPK: an emerging drug target for diabetes and the metabolic syndrome. Cell Metab *9*, 407-416.

Zhang, R., Zhang, Y.Y., Huang, X.R., Wu, Y., Chung, A.C., Wu, E.X., Szalai, A.J., Wong, B.C., Lau, C.P., and Lan, H.Y. (2010). C-reactive protein promotes cardiac fibrosis and inflammation in angiotensin II-induced hypertensive cardiac disease. Hypertension *55*, 953-960.

Zhou, G., Sebhat, I.K., and Zhang, B.B. (2009). AMPK activators--potential therapeutics for metabolic and other diseases. Acta Physiol (Oxf) *196*, 175-190.